frontiers | Research Topics

Molecular mechanism of vascular remodelling and target organ damage

Edited by
Jia Qi, Qingxun Hu, Jintao Wang, Haineng Xu and Yanggang Yuan

Published in
Frontiers in Cardiovascular Medicine

ISSN 1664-8714
ISBN 978-2-8325-2520-3
DOI 10.3389/978-2-8325-2520-3

About Frontiers

Frontiers is more than just an open access publisher of scholarly articles: it is a pioneering approach to the world of academia, radically improving the way scholarly research is managed. The grand vision of Frontiers is a world where all people have an equal opportunity to seek, share and generate knowledge. Frontiers provides immediate and permanent online open access to all its publications, but this alone is not enough to realize our grand goals.

Frontiers journal series

The Frontiers journal series is a multi-tier and interdisciplinary set of open-access, online journals, promising a paradigm shift from the current review, selection and dissemination processes in academic publishing. All Frontiers journals are driven by researchers for researchers; therefore, they constitute a service to the scholarly community. At the same time, the *Frontiers journal series* operates on a revolutionary invention, the tiered publishing system, initially addressing specific communities of scholars, and gradually climbing up to broader public understanding, thus serving the interests of the lay society, too.

Dedication to quality

Each Frontiers article is a landmark of the highest quality, thanks to genuinely collaborative interactions between authors and review editors, who include some of the world's best academicians. Research must be certified by peers before entering a stream of knowledge that may eventually reach the public - and shape society; therefore, Frontiers only applies the most rigorous and unbiased reviews. Frontiers revolutionizes research publishing by freely delivering the most outstanding research, evaluated with no bias from both the academic and social point of view. By applying the most advanced information technologies, Frontiers is catapulting scholarly publishing into a new generation.

What are Frontiers Research Topics?

Frontiers Research Topics are very popular trademarks of the *Frontiers journals series*: they are collections of at least ten articles, all centered on a particular subject. With their unique mix of varied contributions from Original Research to Review Articles, Frontiers Research Topics unify the most influential researchers, the latest key findings and historical advances in a hot research area.

Find out more on how to host your own Frontiers Research Topic or contribute to one as an author by contacting the Frontiers editorial office: frontiersin.org/about/contact

Molecular mechanism of vascular remodelling and target organ damage

Topic editors

Jia Qi — Shanghai Jiao Tong University, China
Qingxun Hu — Shanghai University, China
Jintao Wang — National Heart, Lung, and Blood Institute (NIH), United States
Haineng Xu — University of Pennsylvania, United States
Yanggang Yuan — Nanjing Medical University, China

Citation

Qi, J., Hu, Q., Wang, J., Xu, H., Yuan, Y., eds. (2023). *Molecular mechanism of vascular remodelling and target organ damage*. Lausanne: Frontiers Media SA. doi: 10.3389/978-2-8325-2520-3

Table of contents

05 Deciphering the Intercellular Communication Between Immune Cells and Altered Vascular Smooth Muscle Cell Phenotypes in Aortic Aneurysm From Single-Cell Transcriptome Data
Genmao Cao, Zhengchao Lu, Ruiyuan Gu, Xuezhen Xuan, Ruijing Zhang, Jie Hu and Honglin Dong

20 Short-Term Prognostic Efficacy of mGPS and LCS in Patients With Acute Heart Failure
Jing Wang, Ling Xie, Ping Lyu, Feng Zhou, Hong-Li Cai, Rong-Xing Qi and Qing Zhang

26 Evaluation of anthracycline-induced subclinical LV dysfunction by using myocardial composite index and two-dimension speckle tracking echocardiography technique
Jiabao Zhu, Shuhui Xie, Hanzhen Ji, Xingxing Gu and Jing Wu

34 Impact of borderline pulmonary hypertension due to left heart failure on mortality in a multicenter registry study: A 3-year survivorship analysis
Yangyi Lin, Lingpin Pang, Shian Huang, Jieyan Shen, Weifeng Wu, Fangming Tang, Weiqing Su, Xiulong Zhu, Jingzhi Sun, Ruilin Quan, Tao Yang, Huijun Han and Jianguo He

44 Ablation of cardiomyocyte-derived BDNF during development causes myocardial degeneration and heart failure in the adult mouse heart
Lilin Li, Hongyan Guo, Binglin Lai, Chunbao Liang, Hongyi Chen, Yilin Chen, Weimin Guo, Ziqiang Yuan, Ruijin Huang, Zhaohua Zeng, Liying Liang, Hui Zhao, Xin Zheng, Yanmei Li, Qin Pu, Xufeng Qi and Dongqing Cai

67 Investigation of the protective mechanism of leonurine against acute myocardial ischemia by an integrated metabolomics and network pharmacology strategy
Weiwei Rong, Jiejia Li, Lifeng Wang, Shanshan Luo, Tulu Liang, Xunjia Qian, Xiaodan Zhang, Qinbei Zhou, Yizhun Zhu and Qing Zhu

81 Robust therapeutic effects on COVID-19 of novel small molecules: Alleviation of SARS-CoV-2 S protein induction of ACE2/TMPRSS2, NOX2/ROS, and MCP-1
Ji Youn Youn, Jian Wang, Qian Li, Kai Huang and Hua Cai

90 Proteomics and bioinformatics analysis of cardiovascular related proteins in offspring exposed to gestational diabetes mellitus
Hai-Tao Pan, Yi-Meng Xiong, Hong-Dan Zhu, Xiao-Liang Shi, Bin Yu, Hai-Gang Ding, Ren-Jie Xu, Jin-Long Ding, Tao Zhang and Juan Zhang

101 Hydrogen sulfide against preeclampsia exposure-induced oxidative mitochondrial damage in HTR-8/SVneo cells
Xianli Wang, Shaokun Yu, Yuting Jian, Hongmin Pan, Jiannan Guo, Jian Wu and Wei Guo

112 Polymorphisms of the apolipoprotein E gene affect response to atorvastatin therapy in acute ischemic stroke
QianQian Bi, XiaoYu Zhou, YanQin Lu, Wang Fu, YongPeng Wang, Feng Wang and Jue Wang

121 Prevalence and possible factors of cognitive frailty in the elderly with hypertension and diabetes
Shourong Lu, Qiao Xu, Jie Yu, Ying Yang, Zhuo Wang, Bingshan Zhang, Shuqiang Wang, Xiaorong Chen, Yunyun Zhang, Xiaowei Zhu and Kan Hong

127 Vascular dysfunction in HFpEF: Potential role in the development, maintenance, and progression of the disease
Andrea Saavedra-Alvarez, Katherine V. Pereyra, Camilo Toledo, Rodrigo Iturriaga and Rodrigo Del Rio

135 Endovascular treatment for acute M2 occlusion stroke within 6 hours-a retrospective real-world evidence
Yi Xu, Wang Fu, Yongpeng Wang, Qianqian Bi, Qiwei Wang, Lu Yang, Quanbin Zhang and Feng Wang

143 Mitochondrial dynamics in vascular remodeling and target-organ damage
Tong Zhu, Qingxun Hu, Yanggang Yuan, Huijuan Yao, Jian Zhang and Jia Qi

frontiers | Frontiers in Cardiovascular Medicine

ORIGINAL RESEARCH
published: 28 June 2022
doi: 10.3389/fcvm.2022.936287

Deciphering the Intercellular Communication Between Immune Cells and Altered Vascular Smooth Muscle Cell Phenotypes in Aortic Aneurysm From Single-Cell Transcriptome Data

*Genmao Cao[1], Zhengchao Lu[1], Ruiyuan Gu[1], Xuezhen Xuan[1], Ruijing Zhang[2], Jie Hu[1] and Honglin Dong[1]**

[1] Department of Vascular Surgery, The Second Hospital of Shanxi Medical University, Taiyuan, China, [2] Department of Nephrology, The Second Hospital of Shanxi Medical University, Taiyuan, China

OPEN ACCESS

Edited by:
Jia Qi,
Shanghai Jiao Tong University, China

Reviewed by:
YuFeng Zhang,
Nanjing University of Chinese Medicine, China
Qing Zhu,
Nantong University, China

***Correspondence:**
Honglin Dong
honglindong@sxmu.edu.cn

Specialty section:
This article was submitted to General Cardiovascular Medicine, a section of the journal Frontiers in Cardiovascular Medicine

Received: 05 May 2022
Accepted: 06 June 2022
Published: 28 June 2022

Citation:
Cao G, Lu Z, Gu R, Xuan X, Zhang R, Hu J and Dong H (2022) Deciphering the Intercellular Communication Between Immune Cells and Altered Vascular Smooth Muscle Cell Phenotypes in Aortic Aneurysm From Single-Cell Transcriptome Data. Front. Cardiovasc. Med. 9:936287. doi: 10.3389/fcvm.2022.936287

Background: Vascular smooth muscle cell (VSMC) phenotype switching has been preliminarily found in aortic aneurysms. However, two major questions were raised: (1) What factors drive phenotypic switching of VSMCs in aortic aneurysms? (2) What role does VSMC phenotype transformation play in aortic aneurysms? We speculated that the interaction between infiltrated immune cells and VSMCs played a pivotal role in aortic aneurysm expansion.

Materials and Methods: We obtained single-cell transcriptome data GSE155468 that incorporate eight aortic aneurysm samples and three normal aorta samples. A standard single-cell analysis procedure was performed by Seurat (v3.1.2) for identifying the general cell components. Subsequently, VSMCs were extracted separately and re-clustered for identifying switched VSMC phenotypes. VSMC phenotype annotation was relied on the definitions of specific VSMC phenotypes in published articles. Vital VSMC phenotypes were validated by immunofluorescence. Next, identified immune cells and annotated vital VSMC phenotypes were extracted for analyzing the intercellular communication. R package CellChat (v1.1.3) was used for investigating the communication strength, signaling pathways, and communication patterns between various VSMC phenotypes and immune cells.

Result: A total of 42,611 cells were identified as CD4 + T cells, CD8 + T cells, VSMC, monocytes, macrophages, fibroblasts, endothelial cells, and B cells. VSMCs were further classified into contractile VSMCs, secreting VSMCs, macrophage-like VSMCs, mesenchymal-like VSMCs, adipocyte-like VSMCs, and T-cell-like VSMCs. Intercellular communication analysis was performed between immune cells (macrophages, B cells, CD4 + T cells, CD8 + T cells) and immune related VSMCs (macrophage-like VSMCs, mesenchymal-like VSMCs, T-cell-like VSMCs, contractile VSMCs). Among selected cell populations, 27 significant signaling pathways with 61 ligand–receptor pairs were identified. Macrophages and macrophage-like VSMCs both assume the roles of a signaling sender and receiver, showing the highest communication capability. T cells

acted more as senders, while B cells acted as receivers in the communication network. T-cell-like VSMCs and contractile VSMCs were used as senders, while mesenchymal-like VSMCs played a poor role in the communication network. Signaling macrophage migration inhibitory factor (MIF), galectin, and C-X-C motif chemokine ligand (CXCL) showed high information flow of intercellular communication, while signaling complement and chemerin were completely turned on in aortic aneurysms. MIF and galectin promoted VSMC switch into macrophage-like phenotypes, CXCL, and galectin promoted VSMCs transform into T-cell-like phenotypes. MIF, galectin, CXCL, complement, and chemerin all mediated the migration and recruitment of immune cells into aortic aneurysms.

Conclusion: The sophisticated intercellular communication network existed between immune cells and immune-related VSMCs and changed as the aortic aneurysm progressed. Signaling MIF, galectin, CXCL, chemerin, and complement made a significant contribution to aortic aneurysm progression through activating immune cells and promoting immune cell migration, which could serve as the potential target for the treatment of aortic aneurysms.

Keywords: aortic aneurysm, immune cells, VSMC phenotype switching, intercellular communication, single-cell transcriptome

HIGHLIGHTS

- MIF signaling from T cells promoted the transformation of contractile VSMCs to macrophage-like VSMCs; MIF signaling from VSMCs recruited immune cells (especially B cells) into aortic aneurysms.
- GALECTIN signaling presented the immunomodulatory capacity of macrophage-like VSMCs and macrophages and promoted the formation of macrophage-like VSMCs and T-cell-like VSMCs.
- CXCL signaling promoted VSMC switch into T-cell-like phenotypes and mediated immune cell migration into aortic aneurysms.
- COMPLEMENT and CHEMERIN signaling were turned on in aortic aneurysms, which promoted macrophage migration, thereby aggravating aortic inflammation.

INTRODUCTION

Aortic aneurysm refers to permanent localized dilation of the aorta (expansion ratio > 150% or diameter > 3 cm) (1). Although aortic aneurysms are usually asymptomatic and are diagnosed on physical examination, ruptured aortic aneurysms have a mortality rate of more than 80 percent. Therefore, medical intervention for aortic aneurysm is necessary. Currently, the effective treatments for aortic aneurysm are open surgery repair (OSR) and endovascular aneurysm repair (EVAR), whose indication is an aneurysm diameter over 5.5 cm (2). The application of OSR and EVAR is limited by a large number of complications and a large financial burden. OSR causes significant physical harm to patients, especially for thoracic aortic aneurysm (TAA). However, currently, there is no effective pharmacotherapy for aortic aneurysm, which is due to the misunderstanding of the pathogenesis of aortic aneurysm. Early studies have suggested that the pathological features of aortic aneurysms include loss or apoptosis of VSMCs (3), immune cell infiltration (lymphocytes, neutrophils, dendritic cells, macrophages) (4), extracellular matrix remodeling (5), atherosclerosis (6), and intraluminal thrombus (7). However, none of the clinical drug trials based on these conventional mechanisms has shown the ability to reduce AAA expansion, including MMP inhibitors (doxycycline) (8), antiatherosclerotic drugs (fenofibrate, statins) (9, 10), and antithrombotic drugs (ticagrelor). The failure of these clinical trials suggests that the pathophysiological mechanisms of aortic aneurysm remain poorly studied.

Previous studies indicated that the lack of contractile force caused by VSMC apoptosis or VSMC loss was one of the direct causes of aortic dilatation. Subsequently, emerging studies found that VSMCs in aortic aneurysms underwent phenotypic transformation. Part of VSMCs lost the expression of specific contractile protein and transformed into intermediate state cells which could further transform into macrophage-like VSMCs (expressing macrophage markers MAC2 and CD68) under conditional stimulation (11). Phenotypic transformation of VSMCs is regulated by growth factor (such as connective tissue growth factor, CTGF) (12), non-coding RNA (such as miR-143/145) (13), transcription factor (such as Kruppel-like factor 4, KLF4) (14), and environmental factor (such as lactate) (15).

However, no studies have shown the effect of changes in aortic aneurysm cell composition on phenotypic transformation of VSMCs. We are interested in how VSMCs function and interact with surrounding cells as they undergo phenotypic transformation. The infiltrating immune cells in aortic aneurysms include neutrophils, macrophages, B cells, and T cells, which maintain a chronic inflammatory environment

in the aorta. Since the transformed VSMCs also exhibited immune-related phenotypes, we speculated that immune cells interacted with VSMCs during the phenotypic transformation of VSMCs. The interaction of immune cells with target cells depends on a series of receptor–ligand binding, which is a precondition for the activation of immune cells. For example, the interaction between antigen-presenting cells (APC) and T cells depends on the binding of MHC-CD3 and costimulatory receptor CD28-B7. Therefore, we believe that on the one hand, immune cells promote the transformation of VSMCs to immune-related phenotypes; on the other hand, immune-related VSMCs strengthen the function of immune cells and recruit immune cells to infiltrate into the aorta, promoting aortic aneurysm growth. Therefore, the present study investigated the interaction pattern between immune-related VSMC and immune cells in aortic aneurysms, as well as the involved signaling pathway and ligand–receptor pairs, which could be the potential target for the treatment of aortic aneurysms.

MATERIALS AND METHODS

Data Source and Data Pre-processing

Single-cell sequencing data for eight human aortic aneurysm samples (four males, four females) and three human normal aorta samples (one male, two females) were obtained from GSE155468 (16). Patients in dataset GSE155468 aged from 56 to 78 years and the maximum aneurysm diameter ranged from 4.9 cm to 5.8 cm. Of note, 10 of 11 patients were non-Hispanic, nine of 11 patients were white, and 10 of 11 patients had hypertension. Aortic aneurysm samples and normal aorta samples were merged for creating two Seurat objects, respectively, through using Seurat R package (version 3.1.2) (17). Subsequently, data integration was performed between the aortic aneurysm Seurat object and the normal aorta Seurat object through identifying anchors between the two datasets. Cells with less than 200 genes or more than a 10% mitochondria content and genes with less than 10 cells were removed. The count matrix was normalized and scaled by "NormalizeData" function and "ScaleData" function in Seurat, respectively.

General Cell Type Identification and Vascular Smooth Muscle Cell Phenotype Identification

Top 2000 highly variable genes (HVGs) were calculated through "FindVariableFeatures" function in Seurat, and top 20 principal components were calculated by "RunPCA" function according to the top 2000 HVGs. The t-distributed stochastic neighbor embedding (t-SNE) algorithm with a solution of 0.6 was used for clustering and visualization of all cell clusters. The automatic cell annotation algorithm "SingleR" annotated all cell clusters by using databases "HumanPrimaryCellAtlasData" and "BlueprintEncodeData" as the reference. Background knowledge pertaining to the cellular components of normal aortas and aortic aneurysms was used to assist cell annotation. VSMCs identified by the aforementioned steps were separately extracted, and HVGs and top 20 principal components were recalculated for re-clustering. Because VSMC phenotype transformation is a new concept proposed in recent years and its identification relies on the expression of specific marker genes, SingleR does not work on VSMC phenotypic annotation. In order to recognize marker genes, we calculated differently expressed genes through "FindAllMarkers" function in Seurat. The threshold of log fold-change was set as 0.25, and the Wilcoxon rank sum test was used to test the significance of differences.

Mice Aortic Aneurysm Model Construction

Male C57/BL6 mice (8–10 weeks old, 25–30 g) were obtained from the Experimental Animal Centre, Shanxi Medical University, China. The mice were anesthetized using ether inhalation. Then, abdominal organs were exposed *via* a median abdominal incision. The abdominal aorta was exposed through reversing colons and intestines. The abdominal aorta was isolated from the inferior vena cava under an optical microscope. Gelatin sponge (1 mm × 1 mm × 5 mm) was soaked in elastase solution (100 mg/ml) and was then covered on the surface of the aorta for 20 min. Subsequently, the abdominal cavity was irrigated with normal saline at 37°C for three times. The muscle layer and skin layer were sutured, respectively. After surgery, the mice recovered on a 37°C warm pad. A feed of 0.2% (v/v) 3-aminopropionitrile fumarate (BAPN) was given to mice to help aortic aneurysm formation. After 21 days, aortic aneurysm was obtained for immunofluorescence staining.

Immunofluorescence Staining

Briefly, the mice aortic aneurysm was irrigated with normal saline, fixed in 4% paraformaldehyde, and dehydrated in graded ethanol. The sections were immersed in ethylenediaminetetraacetic acid (EDTA) antigen retrieval buffer, and endogenous peroxidase was blocked by 3% H_2O_2. After blocking with 3% bovine serum albumin (BSA), the sections were incubated with αSMA antibody (Santa Cruz, sc-32251, 1:200), CD68 antibody (Santa Cruz, sc-20060, 1:200), CD3D antibody (Abcam, ab213362, 1:200), and CD34 antibody (Santa Cruz, sc-7324, 1:200) overnight at 4°C. Secondary antibody was incubated for 50 min at room temperature.

Analysis of General Intercellular Communication Between Immune Cells and Immune-Related Vascular Smooth Muscle Cells

R package "CellChat" (version 1.1.3) is the latest algorithm that infers intercellular communication from gene expression levels from single-cell transcriptome data (18). Immune cells (incorporating macrophages, CD4 + T cells, CD8 + T cells, and B cells), contractile VSMCs, and immune-related VSMC phenotypes (including mesenchymal-like VSMC, T-cell-like VSMC, and macrophage-like VSMC) were extracted for intercellular communication analysis. The gene expression profile of extracted cells was input for identifying differentially overexpressed ligands and receptors of each cell population.

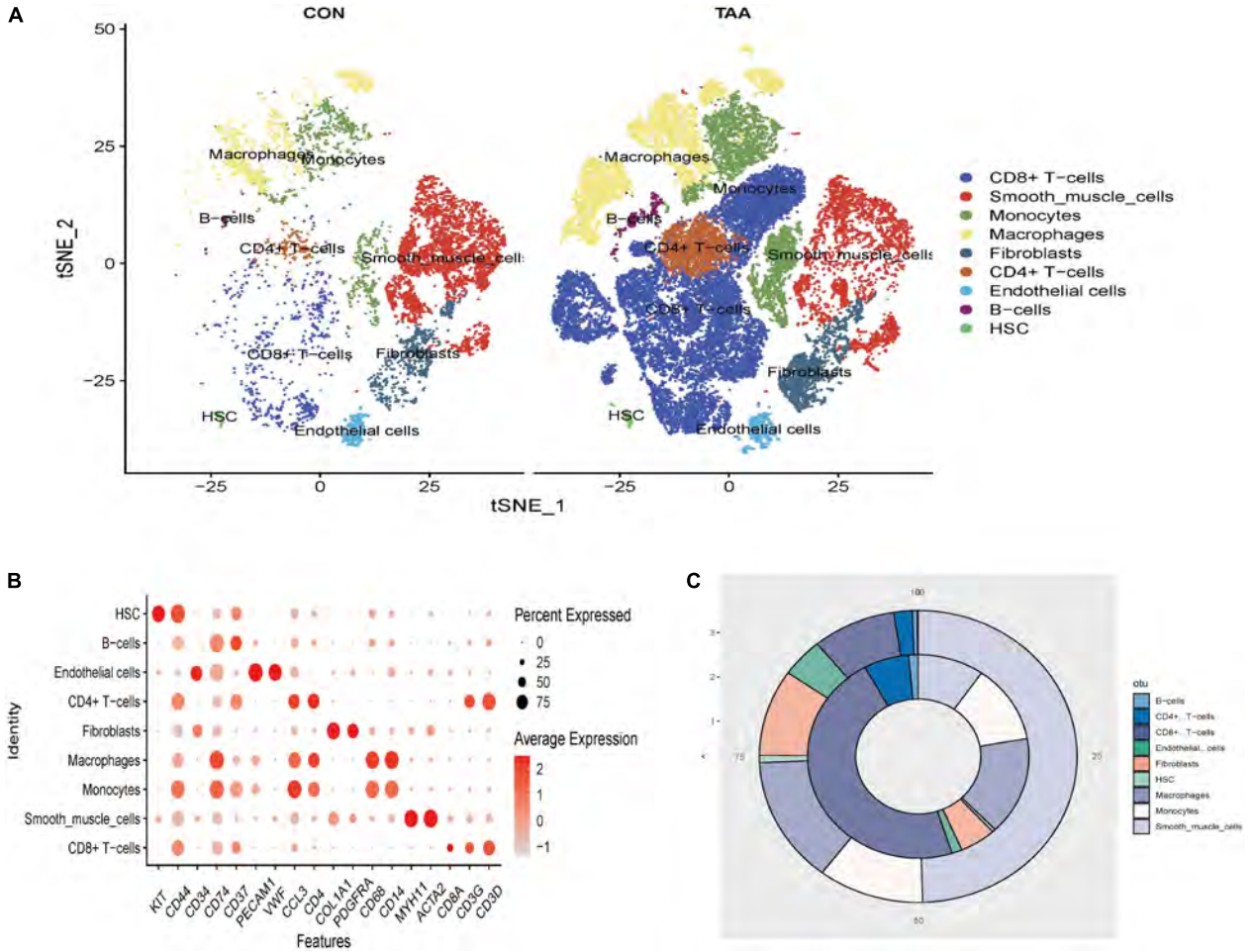

FIGURE 1 | Clustering all cells filtrated from GSE155468. The t-distributed stochastic neighbor embedding (t-SNE) plot of the aligned gene expression of cells from the normal aorta and aortic aneurysms, respectively, showing the distribution of nine cell identities **(A)**. The expression level and expression percentage of marker genes are illustrated on the dot plot **(B)**. The change of proportion of identified cell types was shown in a donut chart **(C)**. The proportion of adipocyte-like VSMCs, mesenchymal-like VSMCs, macrophage-like VSMCs, and T-cell-like VSMCs significantly increased in aortic aneurysms (inner donut), and the proportion of contractile VSMCs dramatically decreased in the normal aorta (outer donut).

"CellChat" first calculated a probability value of each ligand–receptor interaction, and then the communication probability of each signaling pathway was calculated by summarizing the probability of its subordinate ligand–receptor pairs. The communication probability refers to communication strength. Statistically significant interactions were counted if p-value < 0.05. Finally, the number of significant interactions and communication strength were visualized by circ plot.

Identification of Vital Signaling Pathways and Ligand–Receptor Pairs in the Communication Network

"CellChat" allows researchers to visualize each signaling pathway or ligand–receptor pair between cell groups of interest. Immune cells were considered as source cells and VSMCs as target cells, and then their positions were switched. For vital signaling pathways, the hierarchy plot was first applied for visualizing the network structure among source cells and target cells. Heatmap was plotted for picturing communication probabilities between all cell pairs. Network centrality analysis was performed to investigate the role each cell population played in the signaling pathway. The roles incorporate "Sender," "Receiver," "Mediator," and "Influencer." The contribution of significant ligand–receptor pairs to the signaling pathway in the communication network was analyzed by calculating the relative ratio of communication strength of single ligand–receptor pair to that of the whole signaling pathway.

Recognition of Communication Patterns

Except for investigating individual pathways, "CellChat" also allows exploring how multiple cell groups and signaling pathways act in concert to function. To achieve this, "CellChat" outputs the so-called incoming/outgoing communication patterns for uncovering the coordination relationship between cell groups

and signaling pathways. In addition, "CellChat" could recognize the similarity between signaling pathways and group similar signaling pathways into groups.

Exploring Changes of Signaling Pathways and Communication Patterns Between the Aortic Aneurysm and Normal Aorta

Selected cell types from the aortic aneurysm and normal aorta were used for constructing two CellChat objects, respectively. The information flow value of each signaling pathway was first calculated by summarizing all communication probabilities of the signaling pathway. Significant signaling pathways were sorted according to differences in their relative information flow ratio in the inferred networks between the aortic aneurysm and normal aorta. The alterations of incoming/outgoing communication strength were illustrated in two-dimensional diagrams.

Quantitative Polymerase Chain Reaction

qPCR was used to quantify vital ligands and receptors in signaling MIF, galectin, CXCL, chemerin, and complement. Total RNA was extracted from mice aortic aneurysm tissues using the Tiangen RNA Simple Total RNA Kit (DP419, Tiangen). Subsequently, 1 μg of total RNA was reverse-transcribed using PrimeScript RT Master Mix (RR036A, Takara). Amplification was performed using SYBR Green Premix (RR420A, Takara). NADPH was used as the internal reference for mRNA qPCR. The independent sample *t*-test was used to validate any significant differences of relative expression levels between the aortic aneurysm and normal aorta. *P*-values < 0.05 were considered statistically significant. Primers used in this work are listed in **Supplementary Data Sheet 1**.

RESULTS

Identified Cell Types and Vascular Smooth Muscle Cell Phenotypes in Aortic Aneurysms

A total of 42,611 cells with 20,551 genes remained after unqualified cells and genes were filtrated. Top 2000 HVGs were calculated for clustering (see **Supplementary Data Sheet 2**). The unsupervised clustering algorithm clustered 42,611 cells into 25 cell populations. Marker genes of each cell cluster could be seen in **Supplementary Data Sheet 3**. Then the automated reference-based annotation algorithm "SingleR" annotated 25 cell populations as cell types incorporating CD4 + T cells, CD8 + T cells, VSMCs, monocytes, macrophages, fibroblasts, endothelial cells, B cells, and hematopoietic stem cells (HSC) (**Figures 1A,B**). The percentage of CD4 + T cells, CD8 + T cells, B cells, monocytes, and macrophages increased in aortic aneurysms, while the proportion of VSMCs and fibroblasts significantly decreased (**Figure 1C**).

Subsequently, all VSMCs were separately extracted and re-clustered into 16 VSMC clusters (**Figure 2A**). Marker genes of each VSMC cluster could be seen in **Supplementary Data Sheet 4**. According to the canonical definition of each specific VSMC phenotype (19), we identified six VSMC phenotypes incorporating contractile VSMCs (ACTA2 + MYH11+), secreting VSMCs (ACTA2 + MYH11 + COL1A1 + COL1A2+), mesenchymal-like VSMCs (ACTA2 + MYH11 + CD34 + PDGFRA +), adipocyte-like VSMCs (ACTA2 + MYH11 + FABP4 + EBF2+), macrophage-like VSMCs (ACTA2 + MYH11 + CD14 + CD68+), and T-cell-like VSMCs (ACTA2 + MYH11 + CD3D + CD3G+) (**Figures 2B,C**). The percentage of secreting VSMCs, mesenchymal-like VSMCs, adipocyte-like VSMCs, macrophage-like VSMCs, and T-cell-like VSMCs significantly increased in aortic aneurysms, whereas contractile VSMCs were reduced (**Figure 2D**).

Successful Validation of Immune-Related Vascular Smooth Muscle Cell Phenotypes in the Mice Model of Aortic Aneurysms

According to published articles, mesenchymal-like VSMCs were prone to switch into several phenotypes such as macrophage-like VSMCs (20). Therefore, we consider mesenchymal-like VSMCs, macrophage-like VSMCs, and T-cell-like VSMCs as immune-related VSMCs. In order to confirm the presence of immune-related VSMC phenotypes in aortic aneurysms, we constructed mice models of aortic aneurysms through periaortic elastase induction. After 21 days, no mice died during the modeling process, and all six mice were successfully modeled (see **Supplementary Figure 1**). Aortic aneurysm tissues were obtained for double immunofluorescence staining. Macrophage-like VSMCs (αSMA + CD68+) were observed in the tunica media of aortic aneurysms but were not fund in the normal aorta (**Figure 3A**). T-cell-like VSMCs (αSMA + CD3D+) existed in the tunica media of aortic aneurysm but not in the normal aorta (**Figure 3B**). Mesenchymal-like VSMCs appeared in both of the aortic aneurysm and normal aorta but demonstrated a much greater proportion in aortic aneurysms (**Figure 3C**).

Overview of Intercellular Communication Between Immune Cells and Immune-Related Vascular Smooth Muscle Cells

The overall communication number and weight between immune cells and immune-related VSMCs were quantified and visualized (**Figures 4A,B**). Among all immune cells, macrophages showed the highest numbers and strengths of interaction with each VSMC phenotypes, especially macrophage-like VSMCs and T-cell-like VSMCs (**Figure 4C**). CD4 + T cells and CD8 + T cells both demonstrated a strong communication number and strength with macrophage-like VSMCs but weaker communication with other VSMC phenotypes. Nevertheless, B cells showed a weak intercellular communication with all VSMC phenotypes. In brief, macrophages possess the strongest intercellular communication with all VSMC phenotypes.

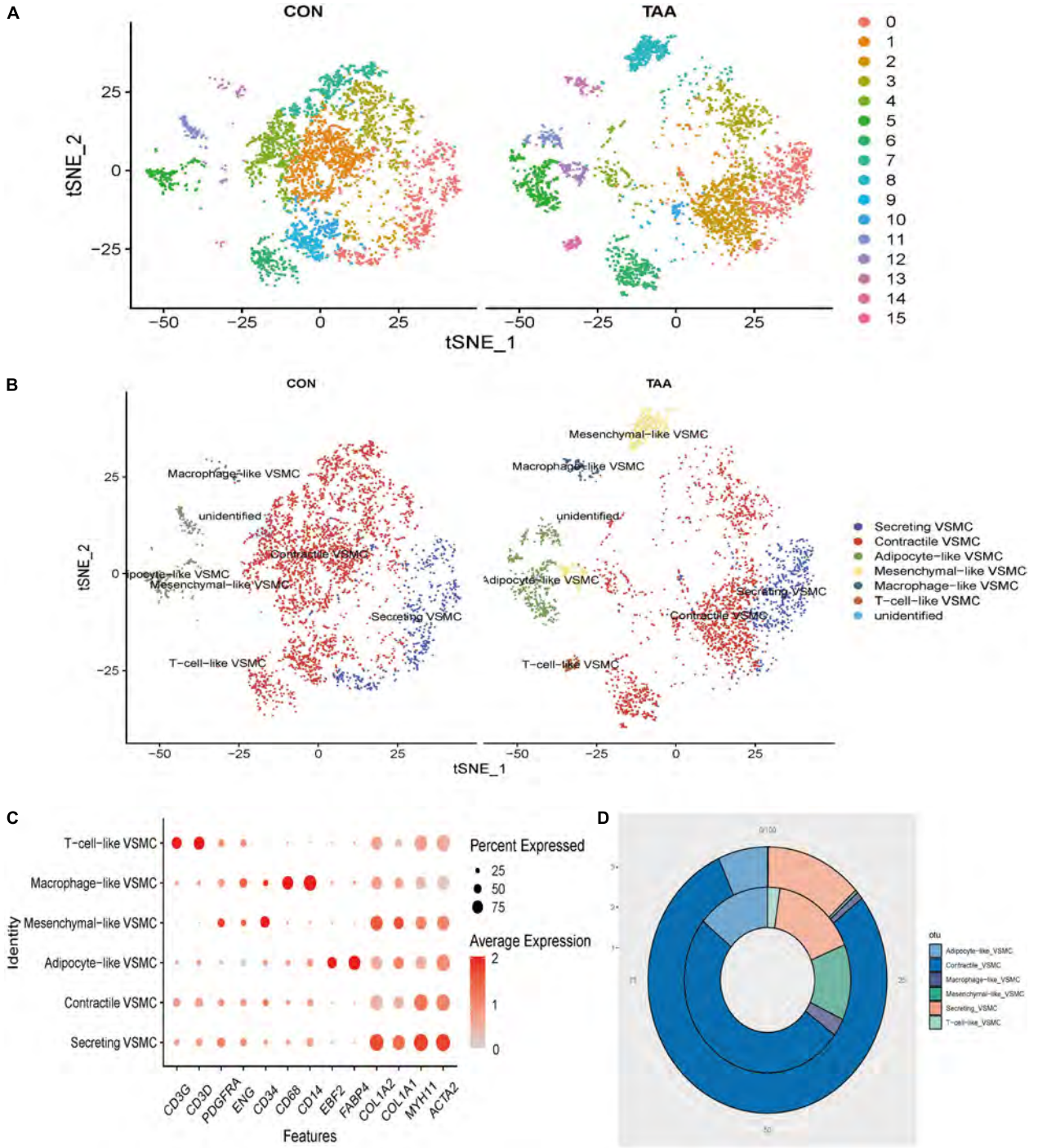

FIGURE 2 | Reanalysis of VSMC subtypes. t-SNE of identified 16 cell clusters **(A)**, which were then annotated as six VSMC phenotypes **(B)**. The expression level and expression percentage of specific marker genes were illustrated on the dot plot **(C)**. The proportion of monocyte, B cells, T cells, and macrophages was increased in aortic aneurysms (inner donut), while the proportion of smooth muscle cells, fibroblasts, and HSC was higher in the normal aorta (outer donut) **(D)**.

We subsequently investigated the role of cells in the communication network (**Figure 4D**). Macrophages and macrophage-like VSMCs both assume the roles of senders and receivers, and they showed the highest communication capability. CD8 + T cells and CD4 + T cells acted more as a sender, rather than a receiver. B cells act primarily as a receiver in the communication network. T-cell-like VSMCs and contractile VSMCs acted as a sender in the communication network,

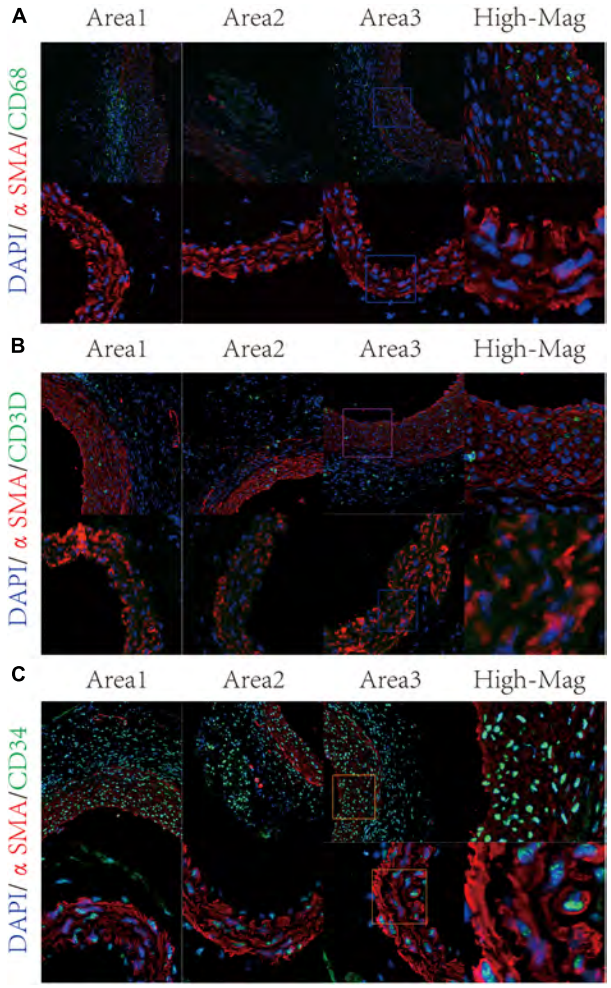

FIGURE 3 | Validation of VSMC subtypes through immunofluorescence staining. Macrophage-like VSMC was labeled by αSMA and CD68 **(A)**. T-cell-like VSMC was labeled by αSMA and CD3D **(B)**; mesenchymal-like VSMC was labeled by αSMA and CD34 **(C)**.

whereas mesenchymal-like VSMCs play a poor role in the communication network.

Significant Signaling Pathways and Ligand–Receptor Pairs Between Immune Cells and Immune-Related Vascular Smooth Muscle Cells

A total of 61 significant ligand–receptor pairs were identified among immune cells and VSMC phenotypes, which were grouped into 27 signaling pathways incorporating but not limited to MIF, galectin, CXCL, growth arrest-specific gene (GAS), pleiotrophin (PTN), visfatin, CC chemokine ligand (CCL), annexin, and secreted phosphoprotein 1 (SPP1) (see **Supplementary Data Sheet 5**). We understand this mechanism in terms of the sender/target and signaling pathway, respectively. We first set immune cells as the senders and set VSMCs as the receivers because we speculated that signaling from immune cells to VSMCs promotes phenotype transformation of VSMCs (**Supplementary Figure 2A**). We found that macrophages sent the most complex signaling pathways, while macrophage-like VSMCs received the most kinds of signaling pathways. Among these significant signaling pathways, MIF–(CD74 + CD44) pairs mediated the strongest communication probability from CD4 + T cells and CD8 + T cells to macrophage-like VSMCs. NAMPT–(ITGA5 + ITGB1) showed the highest communication force from macrophages and B cells to macrophage-like VSMCs. In addition, galectin signaling (LGALS9-CD44/CD45) also played a pivotal role in the communication from macrophages to T-cell-like VSMCs and macrophage-like VSMCs. In conclusion, the formation of macrophage-like VSMCs is associated with MIF, NAMPT, and galectin signaling, and the formation of T-cell-like VSMCs is associated with galectin signaling.

Subsequently, immune cells were set as the receivers and VSMCs were set as the senders because we reckon that signaling from VSMCs to immune cells could explain how immune-related VSMC phenotypes aggravate aortic aneurysm progression (**Supplementary Figure 2B**). We found that macrophage-like VSMCs were characterized by the maximum number of the signaling pathways sent, and macrophages received the maximum signaling pathways. Through PTN, galectin, and CXCL signaling, macrophage-like VSMCs could communicate with all immune cells, indicating the potential role of modulating immune response. Additionally, CXCL12–CXCR4 pair also connected T-cell-like VSMCs and mesenchymal-like VSMCs with all immune cells. We also noticed the high communication probability of MIF signaling from contractile VSMCs, T-cell-like VSMCs, and macrophage-like VSMCs to B cells, which may be associated with B cell infiltration in aortic aneurysms.

Among 27 significant signaling pathways, MIF, galectin, and CXCL were the signaling pathways with the highest communication strength (see **Supplementary Data Sheet 6**) and seem to play a significant role in immune regulation. Thus, we showed all detailed intercellular communication mediated by them and the role each cell played in these pathways. The MIF pathway mediated intercellular communication among multiple distinct cells and formed a sophisticated communication network (**Figures 5A,B**). The hierarchy plot indicated that macrophage-like VSMCs and immune cells were the primary target of the MIF pathway. CD8 + T cells and CD4 + T cells were the principal secreting cells, and importantly, macrophages merely secreted MIF. CD8 + T cells obtained the highest mediator score, which indicated that CD8 + T cells act as a gatekeeper to control the communication flow in the inferred MIF signaling network (**Figure 5C**). Of note, macrophage-like VSMCs acquired the highest influencer score, indicating that macrophage-like VSMCs possess a high capacity of the influencing information flow. Ligand MIF primarily combined with receptors CD74, CD44, and CXCR4 (**Figures 5D,E**).

Distinct from the redundant and complex signaling structures of MIF, galectin signaling demonstrated its simple inferred network structure. Only two cell groups, macrophages and macrophage-like VSMCs, acted as the sender cells, while all cells were the receivers (especially CD4 + T cells and CD8 + T cells) (**Supplementary Figures 3A,B**). Macrophages also took on the

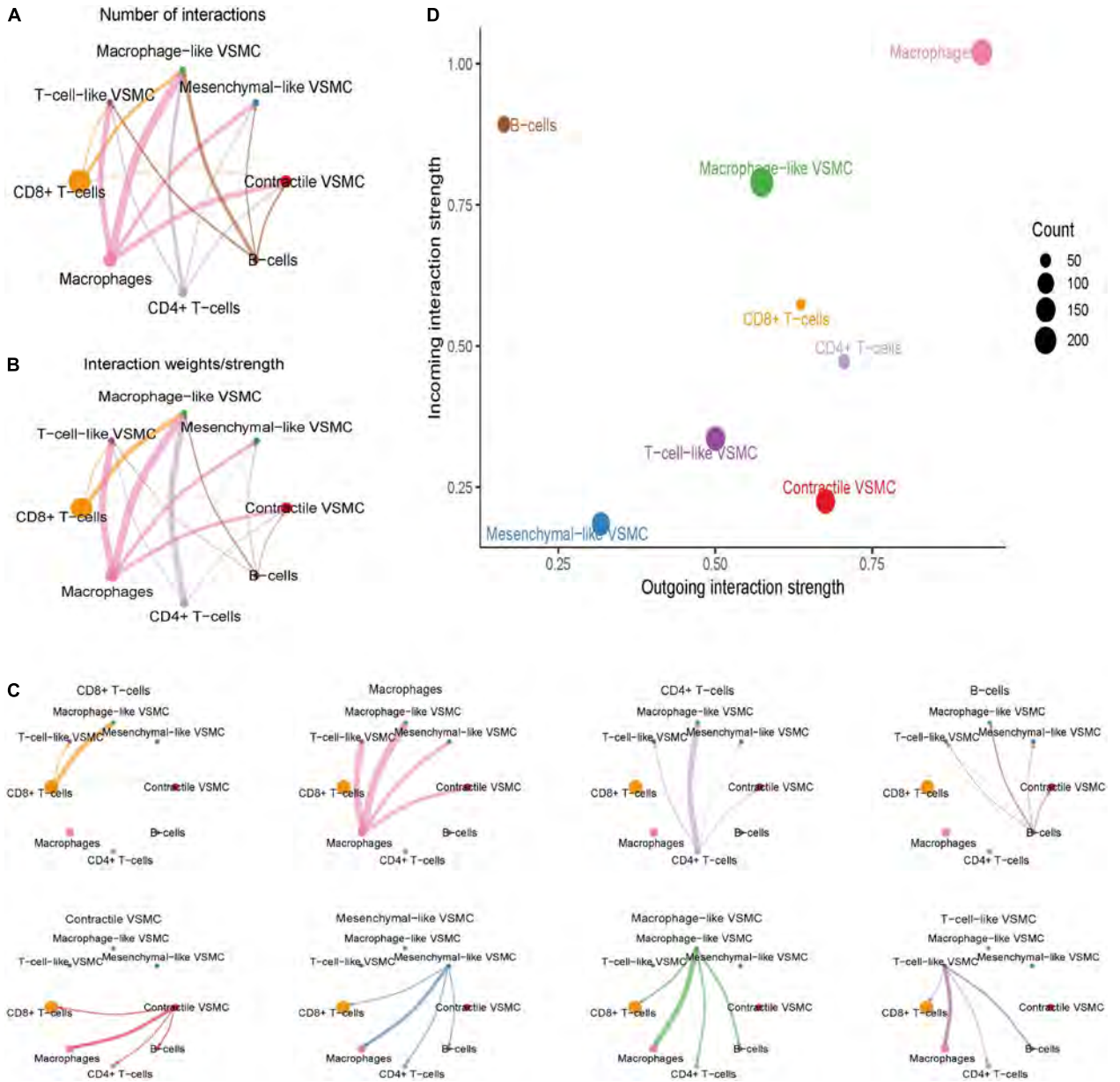

FIGURE 4 | Global cell–cell communication between immune cells and selected VSMC phenotypes. The overall intercellular interaction number **(A)** and weight **(B)** were visualized in the network. The line width represents the intensity. Subsequently, the communication intensity from each immune cell type to all VSMC phenotypes or from each VSMC phenotype to all immune cell types was visualized, respectively **(C)**. The incoming and outgoing communication capacity of each cell type **(D)**.

role of a mediator and influencer (**Supplementary Figure 3C**). Of note, only one ligand (LGALS9) was paired with three receptors (CD44, CD45, and HAVCR2), and LGALS9–CD44 pairs seem to make the greatest contribution (**Supplementary Figures 3D,E**).

The senders of CXCL signaling were macrophages, mesenchymal-like VSMCs, T-cell-like VSMCs, and macrophage-like VSMCs, while the receivers were mainly T-cell-like VSMCs, CD4 + T cells, CD8 + T cells, and B cells (**Supplementary Figures 4A–C**). CXCL singling was mainly mediated by CXCL12–CXCR4 and CXCL16–CXCR6 pairs (**Supplementary Figure 4D**). Macrophages and immune-related VSMCs (mesenchymal-like, T-cell-like, and macrophage-like VSMCs) secreted CXCL12/16 that were then received by T cells, B cells, and T-cell-like VSMCs. T-cell-like VSMCs were also characterized by playing a mediator role. The level of CXCL12/16 in macrophage-like VSMCs is as high as that in macrophages, while the level of CXCR4/6 is similar between T cells and T-cell-like VSMCs, which indicated the

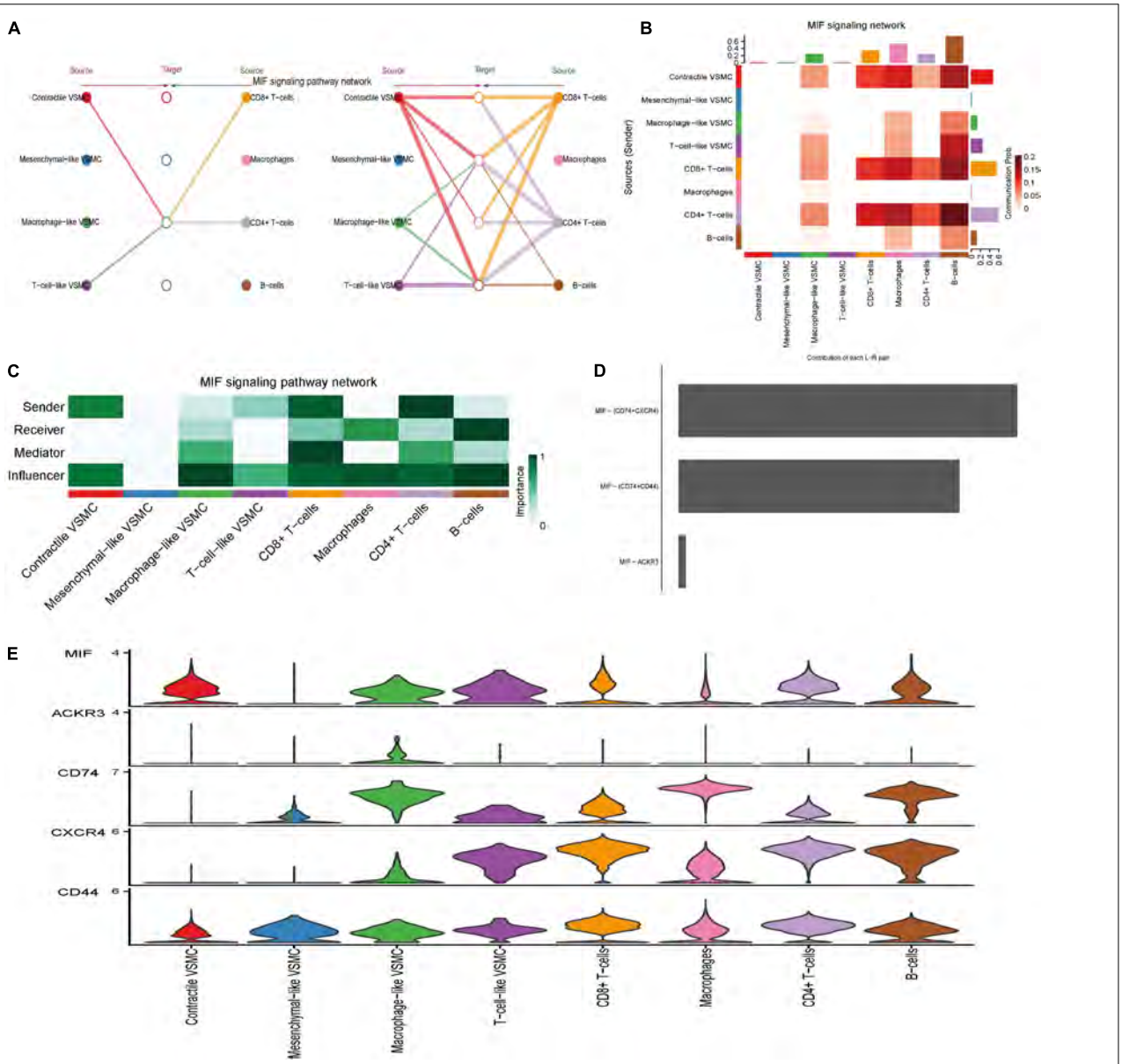

FIGURE 5 | MIF signaling pathway-mediated intercellular communication intensity is shown in the hierarchy plot **(A)** and heatmap **(B)**. Network center score showed the role each cell type played, including sender, receiver, mediator, and influencer **(C)**. Contribution of each ligand–receptor pair to MIF signaling **(D)**. Expression level of every ligand and receptor gene in each cell type **(E)**.

functional similarity between macrophages and macrophage-like VSMCs and similarity between T cells and T-cell-like VSMCs (**Supplementary Figure 4E**).

Coordinated Communication Patterns

In addition to investigating the role of individual signaling pathways in intercellular pathways, it is of great significance to explore how cells and significant pathways work in concert. The outgoing communication patterns were first studied, in which all cells were considered as secreting cells (**Supplementary Figure 5A**). The analysis revealed that contractile VSMCs, mesenchymal-like VSMCs, and macrophage-like VSMCs shared the pattern #1 that incorporated signaling pathways such as GAS, PTN, tumor necrosis factor-like weak inducer of apoptosis (TWEAK), platelet-derived growth factors (PDGF), and fibroblast growth factor (FGF). Outgoing signaling of macrophages and B cells were characterized by pattern #2 including but not limited to galectin. CXCL, visfatin, SPP1, progranulin (GRN), epidermal growth factor (EGF), and tumor necrosis factor (TNF). Meanwhile, CD4 + T cells and CD8 + T cells both concentrated on outgoing communication pattern #3, driven by pathways including MIF, transforming growth factor beta (TGFb), interferon-II (IFN-II), protease-activated receptors (PARs), and CD40. On the other hand, when considered

as target cells/receivers, contractile VSMCs, mesenchymal-like VSMCs, and T-cell-like VSMCs showed the same pattern #1 that included PTN, visfatin, SPP1, TWEAK, GRN, and PDGF (**Supplementary Figure 5B**). Macrophage-like VSMCs and macrophages demonstrated the immune-related incoming pattern #2 such as CCL, annexin, IFN-II, CD40, and complement, indicating their functional similarity in the immune signaling pathway. In brief, through analyzing communication patterns, we learned that distinct cell groups could share mostly overlapping signaling pathways, such as the similarity between macrophage-like VSMCs and macrophages.

Alterations of Intercellular Communication Patterns Between the Normal Aorta and Aortic Aneurysm

The aforementioned analysis investigated the intercellular communication from a global perspective. Furthermore, the changes in communication patterns between the normal aorta and aortic aneurysm samples could interpret the relationship between intercellular communication and aortic aneurysm progression. Altogether, the number of significant interactions between selected VSMC phenotypes and immune cells was more numerous in aortic aneurysms than in the normal aorta (472 vs. 357) (**Figure 6A**). However, the average interaction strength was reduced in aortic aneurysms compared with the normal aorta (**Figure 6B**).

Second, we compared the information flow between the aortic aneurysm and normal aorta (**Figure 6C**). In aortic aneurysms, relative information flow of signaling chemerin, FGF, complement, TWEAK, hepatocyte growth factor (HGF), TNF, CXCL, IFN-II, CCL, and SPP1 were elevated and signaling chemerin and complement were completely turned on, whereas the relative information flow of signaling galectin, insulin-like growth factor (IGF), colony-stimulating factor (CSF), PDGF, TGFb, EGF, MIF, and GAS were decreased and signaling (C-X3-C motif chemokine) CX3C, B-cell activating factor (BAFF), and angiopoietin-like protein (ANGPTL) were completely turned off in aortic aneurysms. Therefore, we speculated that signaling chemerin and complement play a pivotal role in promoting VSMC phenotype switching in aortic aneurysms. We visualized signaling chemerin and complement by heatmap (**Figures 6D,E**). In complement signaling, macrophage-like VSMCs acted as a sender, and the message was received by macrophages. For macrophage-like VSMCs, complement signaling can be regarded as the autocrine signaling pathway to a certain extent. Regarding to chemerin signaling (RARRES2-CMKLR1), contractile VSMCs and mesenchymal-like VSMCs seem to have the highest communication strength as a signaling source, and macrophage-like VSMCs and VSMCs received signaling. As CMKLR1 mediates the migration of macrophages and dendritic and NK cells (21), we speculated that chemerin signaling from VSMCs could active immune cell migration and aggravating aortic aneurysm progression.

We also compared the intensity of incoming and outgoing communication of each cell population between the aortic aneurysm and normal aorta, which was projected in a two-dimensional plot (**Figure 6F**). In brief, the incoming communication strength of macrophage-like VSMCs and T-cell-like VSMCs significantly increased, whereas that of mesenchymal-like VSMCs and contractile VSMCs significantly decreased. On the other hand, the outgoing communication strength of T-cell-like VSMCs and contractile VSMCs was dramatically enhanced, while that of macrophage-like VSMCs, mesenchymal-like VSMCs, and B cells was reduced.

Finally, we compared the difference in incoming signaling patterns and outgoing signaling patterns between the aortic aneurysm and normal aorta. Although the overall outgoing signaling was significantly decreased in macrophage-like VSMCs, the intensity of CXCL, FGF, chemerin, complement, and PROS increased (**Supplementary Figure 6A**). According to incoming signaling, GAS, annexin, chemerin, CD40, PROS, and ANGPT were significantly elevated (**Supplementary Figure 6B**). Of note, the overall outgoing signaling and incoming signaling of T-cell-like VSMCs both dramatically increased, including a variety of pathways.

Validation of Expression Levels of Vital Signaling Pathways in Aortic Aneurysm

Quantitative polymerase chain reaction was performed for quantifying relative expression of significant ligand–receptor pairs of signaling MIF, galectin, CXCL, chemerin, and complement (**Figure 7**). For MIF signaling, the expression level of all ligand and receptors were upregulated: MIF = 2.142 ($p < 0.05$), CD74 = 23.82 ($p < 0.05$), CD44 = 8.476 ($p < 0.05$), and CXCR4 = 4.398 ($P < 0.001$). For galectin signaling, all ligands and receptors were overexpressed LGALS9 = 6.739 ($P < 0.05$), CD44 = 8.476 ($p < 0.05$), CD45 = 9.463 ($p < 0.001$). For CXCL signaling, the ligand–receptor pairs were overexpressed: CXCL12 = 14.28 ($p < 0.05$) and CXCR4 = 3.101 ($p < 0.05$). However, for chemerin signaling, the ligand RARRES2 showed a non-significant upregulation: RARRES2 = 1.560 ($p = 0.113$) and CMKLR1 = 12.17 ($p < 0.001$). Finally, the C3-C3AR pair in complement signaling was also overexpressed, C3 = 6.174 ($p < 0.0001$) and C3AR = 17.28 ($p < 0.0001$).

DISCUSSION

In the healthy mature artery, VSMCs present a terminally differentiated and quiescent state termed as contractile VSMCs, which are characterized by little capacity of proliferation and migration but high capacity of contraction (22). Contractile VSMCs exist in the tunica media and contractile to confront the expansion force when large amounts of blood are pumped from the heart into the aorta, whereas once as injury occurred or the external environment changed, contractile VSMC loss its contractile markers such as ACTA2 and MYH11 and switched into an intermediate state. VSMCs in the intermediate state could transform into distinct phenotypes by receiving distinct stimulation (20). Some VSMC phenotypes, such as macrophage-like VSMCs, showed the inherent characteristics of immune cells such as phagocytosis and secreting chemokines (23). Therefore, it is natural to doubt whether an intimate communication exists

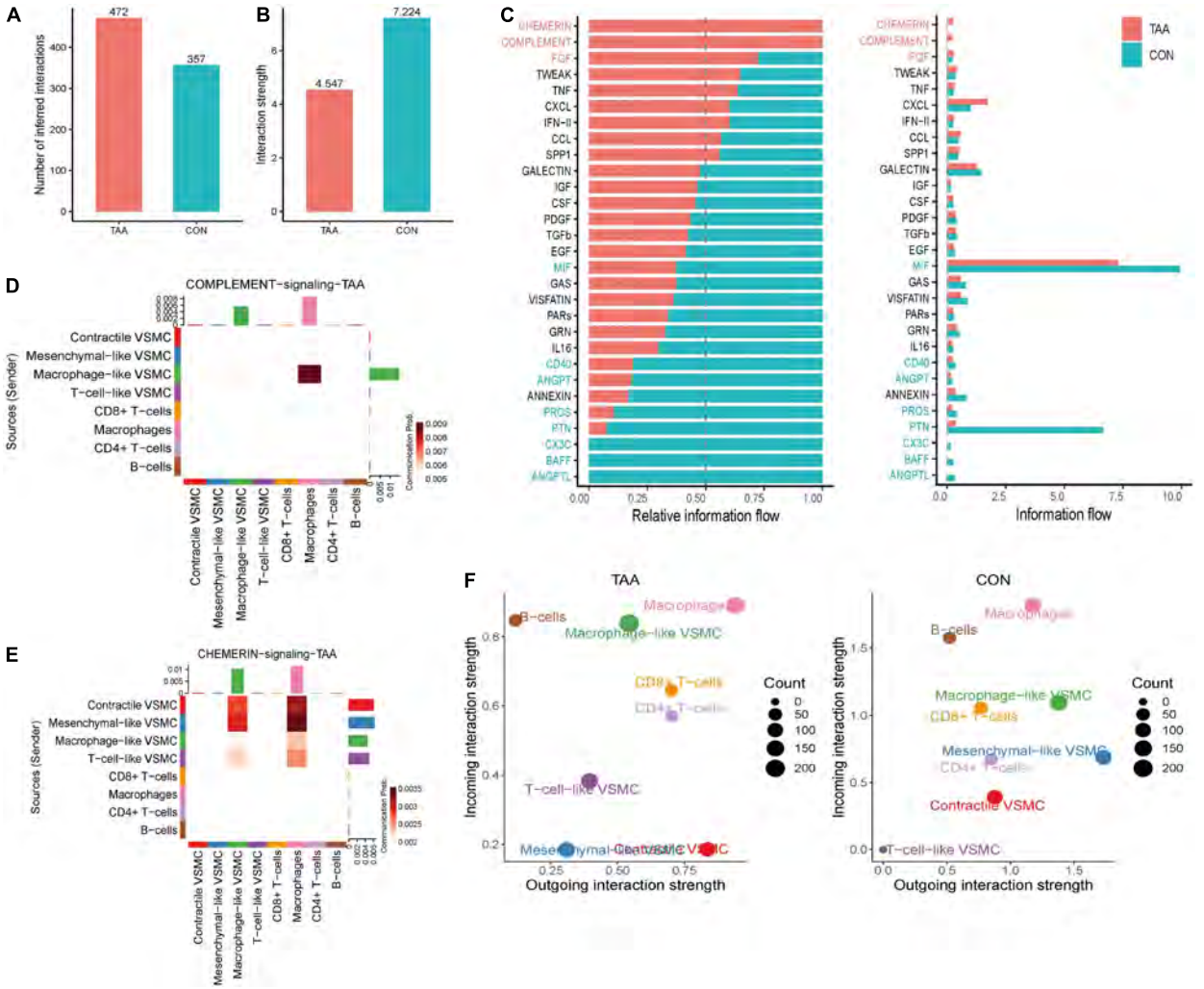

FIGURE 6 | Alterations of intercellular communication patterns between the aortic aneurysm and normal aorta. The number of interactions increased **(A)**, but the mean interaction strength decreased in aortic aneurysms **(B)**. Relative information flow of the significant signaling pathway in the normal aorta and aortic aneurysm **(C)**. Sources and targets of signaling complement **(D)** and chemerin **(E)**. Alteration of incoming/outgoing communication ability of each cell type between the aortic aneurysm and normal aorta **(F)**.

between immune cells and VSMCs. The present study aimed to address the concern.

We found that the communication intensity between macrophages and VSMCs was the highest among all immune cells, while macrophage-like VSMCs showed the highest intercellular communication with immune cells. Similarly, the communication intensity between macrophages and macrophage-like VSMCs is also noticeable. It suggests that macrophages and macrophage-like VSMCs and their interaction may play a pivotal role in the progression of aortic aneurysms.

When analyzing communication between immune cells and VSMCs, we set two directions: from immune cells to VSMCs and from VSMCs to immune cells. We raised a hypothesis that signaling from immune cells to VSMCs acts as a trigger activating VSMC switching into immune-related phenotypes. On the other hand, signaling from immune-related VSMCs to immune cells exerts a chemotaxis function that attracts more immune cells to migrate to aorta lesions. In the whole analysis results, many signaling pathways showed special importance, but we considered MIF, galectin, CXCL, chemerin, and complement to be the most important.

Among all the significant signaling pathways identified from immune cells to VSMCs, MIF signaling was the one that shines the brightest. MIF was characterized by the highest information flow. We found that MIF–(CD44-CD74) pairs mediated signaling from CD4 + T cells and CD8 + T cells to macrophage-like VSMCs. On the other hand, MIF–(CD74 + CXCR4) mediated signal transmission from contractile VSMCs, T-cell-like VSMCs, and macrophage-like VSMCs to B cells Numerous studies have shown that MIF possesses the function of recruiting and activating macrophages through combining with CD74 and CXCR2 (24–26) and promote normal cells to acquire an

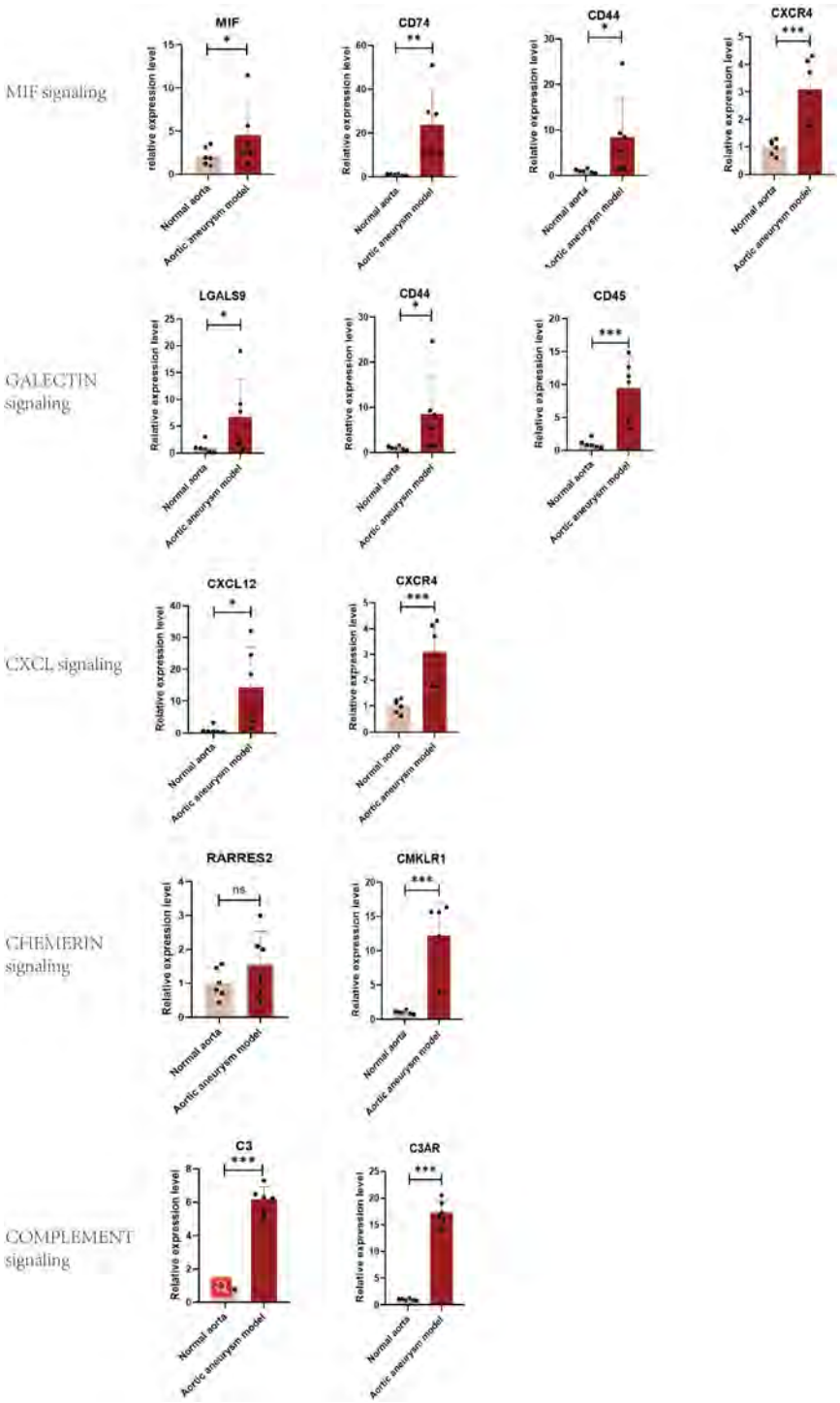

FIGURE 7 | Validation of the expression level of significant ligand–receptor pairs of signaling MIF, galectin, CXCL, chemerin, and complement by qPCR. *$P < 0.05$, **$P < 0.001$, ***$P < 0.0001$.

inflammatory phenotype by interacting with the receptor CD74 (27). MIF binds to CD74 + CXCR4, which promotes B-cell migration (28). Therefore, in aortic aneurysms, MIF from T cells plays a role in promoting the transformation of VSMCs to macrophage-like VSMCs, while MIF from VSMCs recruits immune cells (especially B cells) into aortic aneurysms. As previous studies showed that galectin 9–CD44 interaction is in favor of stability and function of adaptive regulatory T

cells (29), galectin 9–CD45 inhibits naive B-cell activation (30), and can inhibit CD4 + T-cell expansion and suppress Th1 effector function (31). Hence, we speculate that macrophage-like VSMCs and macrophages both exert an immunomodulatory capacity through the galectin signaling pathway. The recipients of CXCL signals are mainly T cells, B cells, and T-cell-like VSMCs. Previous studies have shown that T and B cells infiltrated in abdominal aortic aneurysms are CXCR4-positive and are recruited by CXCL12-positive stromal cells (32). CXCL16-CXCR6 also mediates the recruitment of lymphocytes and peripheral blood mononuclear cells (33, 34). Therefore, in aortic aneurysms, mesenchymal-like, macrophage-like, and T-cell-like VSMC can recruit circulating lymphocytes through the CXCL signaling pathway, exacerbating the aortic immune response. Furthermore, CXCL may promote VSMC switch into T-cell-like phenotypes since T-cell-like VSMC is the main receiver of CXCL signaling.

Signaling complement and chemerin did not exist in the normal aorta but were turned on in aortic aneurysm. In complement signaling, macrophage-like VSMCs secreted C3 and then C3 combined with receptors in macrophages and macrophage-like VSMCs including C3AR1, ITGAM, ITGAX, and ITGB2. ITGAM (integrin αM), a surface marker in mononuclear macrophages, is also termed as CD11b. ITGAM acts as an adhesion molecule and mediated the migration of circulating monocytes/macrophages; thus, ITGAM deficiency could ameliorate aortic aneurysm expansion (35). Similarly, C2AR1, ITGAX (CD11c), and ITGB2 (CD18) also promote the infiltration of macrophages in immune-mediated disease (36–38). Hence, complement signaling exerts a harmful effect that promotes aortic aneurysm expansion through mediating macrophage infiltration and migration. Regarding chemerin signaling, all VSMC phenotypes secreted chemerin (encoded by RARRES2), and then chemerin was received by chemerin chemokine-like receptor 1 (CMKLR1) in macrophages. Chemerin–CMKLR1 pair stimulated macrophage transformation to the M1 (proinflammatory) subtype *via* the p-Akt/CEBPα axis (39) and mediated the migration of macrophages and dendritic cells (40). Collectively, signaling complement and chemerin mainly promoted macrophage migration, thereby aggravating aortic inflammation.

CONCLUSION

Extensive intercellular communications exist between multiple VSMC phenotypes and immune cells, as macrophages and macrophage-like VSMCs mediated the highest communication intensity.

Signaling MIF, galectin, and CXCL showed high information flow of intercellular communication, while signaling complement and chemerin were completely turned on in aortic aneurysms. MIF and galectin promoted VSMC switch into macrophage-like phenotypes, and CXCL and galectin promoted VSMC transform into T-cell-like phenotypes. MIF, galectin, CXCL, complement, and chemerin all mediated the migration and recruitment of immune cells into aortic aneurysms.

DATA AVAILABILITY STATEMENT

The original contributions presented in the study are included in the article/**Supplementary Material**, further inquiries can be directed to the corresponding author.

ETHICS STATEMENT

The animal study was reviewed and approved by Ethics Committee of the Second Hospital of Shanxi Medical University.

AUTHOR CONTRIBUTIONS

GC and HD designed the study and wrote the manuscript. GC and ZL conducted the data analysis. GC, RG, and XX completed the animal experiment. RZ and HD revised the manuscript and figures. HD supervised the whole study. All authors contributed to the article and approved the submitted version.

FUNDING

This study was supported by the Scientific Research Project of Shanxi Provincial Health Commission (Grant No. 2022053) and National Natural Science Foundation of China (Grant No. 81870354).

SUPPLEMENTARY MATERIAL

The Supplementary Material for this article can be found online at: https://www.frontiersin.org/articles/10.3389/fcvm.2022.936287/full#supplementary-material

Supplementary Figure 1 | Successful construction of mice model of aortic aneurysm.

Supplementary Figure 2 | The significant signaling (ligand-receptor pairs) from immune cells to VSMC subtypes **(A)** and from VSMC phenotypes to immune cells **(B)**.

Supplementary Figure 3 | GALECTIN signaling pathway mediated intercellular communication intensity was showed in hierarchy plot **(A)** and heatmap **(B)**. Network center score showed the role each cell type played, including sender, receiver, mediator, and influencer **(C)**. Contribution of each ligand-receptor pair to GALECTIN signaling **(D)**. Expression level of every ligand and receptor gene of GALECTIN signaling in each cell type **(E)**.

Supplementary Figure 4 | CXCL signaling pathway mediated intercellular communication intensity was showed in hierarchy plot **(A)** and heatmap **(B)**. Network center score showed the role each cell type played, including sender, receiver, mediator, and influencer **(C)**. Contribution of each ligand-receptor pair to CXCL signaling **(D)**. Expression level of every ligand and receptor gene of CXCL signaling in each cell type **(E)**.

Supplementary Figure 5 | The outgoing communication patterns **(A)** and incoming communication patterns **(B)** of each cell type was visualized by river plot.

Supplementary Figure 6 | Alteration of outgoing communication ability **(A)** and incoming communication ability **(B)** of every significant signaling pathway in each cell type between normal aorta and aortic aneurysm.

REFERENCES

1. Owens DK, Davidson KW, Krist AH, Barry MJ, Cabana M, Caughey AB, et al. Screening for abdominal aortic aneurysm: US preventive services task force recommendation statement. *JAMA*. (2019) 322:2211–8. doi: 10.1001/jama.2019.18928
2. Bradbury AW, Davies AH, Dhesi JK, Hammond CJ, Hampshire M, Jellett K, et al. Recommendations on the use of open surgical and endovascular aneurysm repair for the management of unruptured abdominal aortic aneurysm from the guideline development committee appointed by the UK National Institute for Health and Care Excellence. *Eur J Vasc Endovasc Surg.* (2021) 61:877–80. doi: 10.1016/j.ejvs.2021.01.047
3. Henderson EL, Geng YJ, Sukhova GK, Whittemore AD, Knox J, Libby P. Death of smooth muscle cells and expression of mediators of apoptosis by T lymphocytes in human abdominal aortic aneurysms. *Circulation.* (1999) 99:96–104. doi: 10.1161/01.cir.99.1.96
4. Pearce WH, Koch AE. Cellular components and features of immune response in abdominal aortic aneurysms. *Ann N Y Acad Sci.* (1996) 800:175–85. doi: 10.1111/j.1749-6632.1996.tb33308.x
5. Wills A, Thompson MM, Crowther M, Sayers RD, Bell PR. Pathogenesis of abdominal aortic aneurysms–cellular and biochemical mechanisms. *Eur J Vasc Endovasc Surg.* (1996) 12:391–400. doi: 10.1016/s1078-5884(96)80002-5
6. Golledge J, Norman PE. Atherosclerosis and abdominal aortic aneurysm: cause, response, or common risk factors?. *Arterioscler Thromb Vasc Biol.* (2010) 30:1075–7. doi: 10.1161/atvbaha.110.206573
7. Touat Z, Ollivier V, Dai J, Huisse MG, Bezeaud A, Sebbag U, et al. Renewal of mural thrombus releases plasma markers and is involved in aortic abdominal aneurysm evolution. *Am J Pathol.* (2006) 168:1022–30. doi: 10.2353/ajpath.2006.050868
8. Meijer CA, Stijnen T, Wasser MN, Hamming JF, van Bockel JH, Lindeman JH. Doxycycline for stabilization of abdominal aortic aneurysms: a randomized trial. *Ann Intern Med.* (2013) 159:815–23. doi: 10.7326/0003-4819-159-12-201312170-00007
9. Pinchbeck JL, Moxon JV, Rowbotham SE, Bourke M, Lazzaroni S, Morton SK, et al. Randomized placebo-controlled trial assessing the effect of 24-week fenofibrate therapy on circulating markers of abdominal aortic aneurysm: outcomes from the FAME -2 trial. *J Am Heart Assoc.* (2018) 7:e009866. doi: 10.1161/JAHA.118.009866
10. Twine CP, Williams IM. Systematic review and meta-analysis of the effects of statin therapy on abdominal aortic aneurysms. *Br J Surg.* (2011) 98:346–53. doi: 10.1002/bjs.7343
11. Rong JX, Shapiro M, Trogan E, Fisher EA. Transdifferentiation of mouse aortic smooth muscle cells to a macrophage-like state after cholesterol loading. *Proc Natl Acad Sci USA.* (2003) 100:13531–6. doi: 10.1073/pnas.1735526100
12. Branchetti E, Poggio P, Sainger R, Shang E, Grau JB, Jackson BM, et al. Oxidative stress modulates vascular smooth muscle cell phenotype *via* CTGF in thoracic aortic aneurysm. *Cardiovasc Res.* (2013) 100:316–24. doi: 10.1093/cvr/cvt205
13. Vengrenyuk Y, Nishi H, Long X, Ouimet M, Savji N, Martinez FO, et al. Cholesterol loading reprograms the microRNA-143/145-myocardin axis to convert aortic smooth muscle cells to a dysfunctional macrophage-like phenotype. *Arterioscler Thromb Vasc Biol.* (2015) 35:535–46. doi: 10.1161/ATVBAHA.114.304029
14. Yoshida T, Yamashita M, Hayashi M. Kruppel-like factor 4 contributes to high phosphate-induced phenotypic switching of vascular smooth muscle cells into osteogenic cells. *J Biol Chem.* (2012) 287:25706–14. doi: 10.1074/jbc.M112.361360
15. Yang L, Gao L, Nickel T, Yang J, Zhou J, Gilbertsen A, et al. Lactate promotes synthetic phenotype in vascular smooth muscle cells. *Circ Res.* (2017) 121:1251–62. doi: 10.1161/CIRCRESAHA.117.311819
16. Li Y, Ren P, Dawson A, Vasquez HG, Ageedi W, Zhang C, et al. Single-cell transcriptome analysis reveals dynamic cell populations and differential gene expression patterns in control and aneurysmal human aortic tissue. *Circulation.* (2020) 142:1374–88. doi: 10.1161/circulationaha.120.046528
17. Stuart T, Butler A, Hoffman P, Hafemeister C, Papalexi E, Mauck WM III, et al. Comprehensive integration of single-cell data. *Cell.* (2019) 177:1888–902.e21. doi: 10.1016/j.cell.2019.05.031
18. Jin S, Guerrero-Juarez CF, Zhang L, Chang I, Ramos R, Kuan CH, et al. Inference and analysis of cell-cell communication using CellChat. *Nat Commun.* (2021) 12:1088. doi: 10.1038/s41467-021-21246-9
19. Yap C, Mieremet A, de Vries CJM, Micha D, de Waard V. Six shades of vascular smooth muscle cells illuminated by KLF4 (Kruppel-Like Factor 4). *Arterioscler Thromb Vasc Biol.* (2021) 41:2693–707. doi: 10.1161/ATVBAHA.121.316600
20. Chen PY, Qin L, Li G, Malagon-Lopez J, Wang Z, Bergaya S, et al. Smooth muscle cell reprogramming in aortic aneurysms. *Cell Stem Cell.* (2020) 26:542–57.e11. doi: 10.1016/j.stem.2020.02.013
21. Shin WJ, Zabel BA, Pachynski RK. Mechanisms and functions of chemerin in cancer: potential roles in therapeutic intervention. *Front Immunol.* (2018) 9:2772. doi: 10.3389/fimmu.2018.02772
22. Inamoto S, Kwartler CS, Lafont AL, Liang YY, Fadulu VT, Duraisamy S, et al. TGFBR2 mutations alter smooth muscle cell phenotype and predispose to thoracic aortic aneurysms and dissections. *Cardiovasc Res.* (2010) 88:520–9. doi: 10.1093/cvr/cvq230
23. Bennett MR, Sinha S, Owens GK. Vascular smooth muscle cells in atherosclerosis. *Circ Res.* (2016) 118:692–702. doi: 10.1161/CIRCRESAHA.115.306361
24. Tilstam PV, Schulte W, Holowka T, Kim BS, Nouws J, Sauler M, et al. MIF but not MIF-2 recruits inflammatory macrophages in an experimental polymicrobial sepsis model. *J Clin Invest.* (2021) 131:e127171. doi: 10.1172/jci127171
25. Klemke L, Oliveira T. De, Witt D, Winkler N, Bohnenberger H, Bucala R, et al. Hsp90-stabilized MIF supports tumor progression *via* macrophage recruitment and angiogenesis in colorectal cancer. *Cell Death Dis.* (2021) 12:155. doi: 10.1038/s41419-021-03426-z
26. Kim BS, Tilstam PV, Arnke K, Leng L, Ruhl T, Piecychna M, et al. Differential regulation of macrophage activation by the MIF cytokine superfamily members MIF and MIF-2 in adipose tissue during endotoxemia. *FASEB J.* (2020) 34:4219–33. doi: 10.1096/fj.201901511R
27. Song H, Zhu Z, Zhou Y, Du N, Song T, Liang H, et al. MIF/CD74 axis participates in inflammatory activation of Schwann cells following sciatic nerve injury. *J Mol Histol.* (2019) 50:355–67. doi: 10.1007/s10735-019-09832-0
28. Klasen C, Ohl K, Sternkopf M, Shachar I, Schmitz C, Heussen N, et al. MIF promotes B cell chemotaxis through the receptors CXCR4 and CD74 and ZAP-70 signaling. *J Immunol.* (2014) 192:5273–84. doi: 10.4049/jimmunol.1302209
29. Wu C, Thalhamer T, Franca RF, Xiao S, Wang C, Hotta C, et al. Galectin-9-CD44 interaction enhances stability and function of adaptive regulatory T cells. *Immunity.* (2014) 41:270–82. doi: 10.1016/j.immuni.2014.06.011
30. Giovannone N, Liang J, Antonopoulos A, Geddes Sweeney J, King SL, Pochebit SM, et al. Galectin-9 suppresses B cell receptor signaling and is regulated by I-branching of N-glycans. *Nat Commun.* (2018) 9:3287. doi: 10.1038/s41467-018-05770-9
31. Pang N, Alimu X, Chen R, Muhashi M, Ma J, Chen G, et al. Activated Galectin-9/Tim3 promotes Treg and suppresses Th1 effector function in chronic lymphocytic leukemia. *FASEB J.* (2021) 35:e21556. doi: 10.1096/fj.202100013R
32. Ocaña E, Pérez-Requena J, Bohórquez JC, Brieva JA, Rodríguez C. Chemokine receptor expression on infiltrating lymphocytes from abdominal aortic aneurysms: role of CXCR4-CXCL12 in lymphoid recruitment. *Atherosclerosis.* (2008) 200:264–70. doi: 10.1016/j.atherosclerosis.2007.12.043
33. Linke B, Meyer Dos Santos S, Picard-Willems B, Keese M, Harder S, Geisslinger G, et al. CXCL16/CXCR6-mediated adhesion of human peripheral blood mononuclear cells to inflamed endothelium. *Cytokine.* (2019) 122:154081. doi: 10.1016/j.cyto.2017.06.008
34. Günther C, Carballido-Perrig N, Kaesler S, Carballido JM, Biedermann T. CXCL16 and CXCR6 are upregulated in psoriasis and mediate cutaneous recruitment of human CD8+ T cells. *J Invest Dermatol.* (2012) 132:626–34. doi: 10.1038/jid.2011.371
35. Zhou M, Wang X, Shi Y, Ding Y, Li X, Xie T, et al. Deficiency of ITGAM attenuates experimental abdominal aortic aneurysm in mice. *J Am Heart Assoc.* (2021) 10:e019900. doi: 10.1161/jaha.120.019900
36. Liu L, Zhao Q, Kong M, Mao L, Yang Y, Xu Y. Myocardin-related transcription factor A regulates integrin beta 2 transcription to promote macrophage infiltration and cardiac hypertrophy in mice. *Cardiovasc Res.* (2022) 118:844–58. doi: 10.1093/cvr/cvab110

37. Wu H, Gower RM, Wang H, Perrard XY, Ma R, Bullard DC, et al. Functional role of CD11c+ monocytes in atherogenesis associated with hypercholesterolemia. *Circulation.* (2009) 119:2708–17. doi: 10.1161/circulationaha.108.823740
38. Dick J, Gan PY, Kitching AR, Holdsworth SR. The C3aR promotes macrophage infiltration and regulates ANCA production but does not affect glomerular injury in experimental anti-myeloperoxidase glomerulonephritis. *PLoS One.* (2018) 13:e0190655. doi: 10.1371/journal.pone.0190655
39. Ji ZS, Jiang H, Xie Y, Wei QP, Yin XF, Ye JH, et al. Chemerin promotes the pathogenesis of preeclampsia by activating CMKLR1/p-Akt/CEBPα axis and inducing M1 macrophage polarization. *Cell Biol Toxicol.* (2021). [Online ahead of print.]. doi: 10.1007/s10565-021-09636-7
40. Fischer TF, Czerniak AS, Weiß T, Schoeder CT, Wolf P, Seitz O, et al. Ligand-binding and -scavenging of the chemerin receptor GPR1. *Cell Mol Life Sci.* (2021) 78:6265–81. doi: 10.1007/s00018-021-03894-8

Conflict of Interest: The authors declare that the research was conducted in the absence of any commercial or financial relationships that could be construed as a potential conflict of interest.

frontiers | Frontiers in Cardiovascular Medicine

ORIGINAL RESEARCH
published: 05 July 2022
doi: 10.3389/fcvm.2022.944424

Short-Term Prognostic Efficacy of mGPS and LCS in Patients With Acute Heart Failure

Jing Wang[1†], *Ling Xie*[1†], *Ping Lyu*[1], *Feng Zhou*[2], *Hong-Li Cai*[3], *Rong-Xing Qi*[4*] and *Qing Zhang*[3*]

[1] Department of Cardiology, Affiliated Hospital 2 of Nantong University, Nantong, China, [2] Department of Clinical Laboratory, Affiliated Hospital 2 of Nantong University, Nantong, China, [3] Department of General Practice, Affiliated Hospital 2 of Nantong University, Nantong, China, [4] Department of Image, Affiliated Hospital 2 of Nantong University, Nantong, China

Aim: Systemic inflammation plays an important role in the occurrence and development of acute heart failure. The modified Glasgow Prognostic Score (mGPS) and "lymphocyte C-reactive protein score" (LCS) are used to assess the inflammation levels in cancer patients. The purpose of this study was to assess the prognostic value of these two inflammation-related scoring systems in patients with acute heart failure.

Methods: Two hundred and fifty patients with acute heart failure were enrolled in this study. The mGPS and LCS scores were recorded after admission. All patients were divided into 2 groups: the death group and the survival group according to the 3-month follow-up results. The predictive values of mGPS and LCS were assessed using receiver-operating characteristic (ROC) analyses. Univariate and multivariate logistic analyses were used to evaluate the relationships between variables and endpoint.

Results: The levels of mGPS and LCS in the death group were significantly higher than those in the survival group ($P<0.05$). The areas under the ROC curve of the mGPS and LCS for predicting death were 0.695 (95%CI: 0.567∼0.823) and 0.736 (95%CI: 0.616∼0.856), respectively. Multivariate analysis demonstrated that both LCS, LVEF and serum direct bilirubin were independent predictors of all-cause death, excluding mGPS.

Conclusions: Compared with mGPS, LCS is independently associated with short-term outcomes in patients with acute heart failure. LCS was a clinically promising and feasible prognostic scoring system for patients with acute heart failure.

Keywords: acute heart failure, inflammation, LCS, mGPS, prognosis

OPEN ACCESS

Edited by:
Jia Qi,
Shanghai Jiao Tong University, China

Reviewed by:
Zhang Jinlong,
Yancheng First Peoples' Hospital, China
Xuelian Wang,
Shanghai General Hospital, China

***Correspondence:**
Qing Zhang
zzhangqing32@sina.cn
Rong-Xing Qi
ntdocqirongxing@sina.com

[†] These authors have contributed equally to this work

Specialty section:
This article was submitted to General Cardiovascular Medicine, a section of the journal Frontiers in Cardiovascular Medicine

Received: *15 May 2022*
Accepted: *15 June 2022*
Published: *05 July 2022*

Citation:
Wang J, Xie L, Lyu P, Zhou F, Cai H-L, Qi R-X and Zhang Q (2022) Short-Term Prognostic Efficacy of mGPS and LCS in Patients With Acute Heart Failure. Front. Cardiovasc. Med. 9:944424. doi: 10.3389/fcvm.2022.944424

INTRODUCTION

The incidence of acute heart failure (AHF) has been increasing year by year, and has become the most common reason for unplanned admission of patients over 65 years old (1). Patients with acute heart failure have high hospital costs and long-term mortality. Prognostic assessment has played an increasingly important role in the treatment of these patients. The inseparable association of inflammation and heart failure has long been recognized in many studies (2, 3). Recently,

albumin (4, 5), C-reactive protein (6, 7) and lymphocytes (8, 9) have also been reported to predict the prognoses of patients with ADHF, sometimes even better than brain natriuretic peptide in predicting in-hospital death (10).

The modified Glasgow prognostic score (mGPS) and lymphocyte C-reactive protein score (LCS), these two new and readily available markers of inflammation, were initially shown to have independent prognostic value in cancer patients (11–13). Many studies have focused on the correlation between mGPS and prognosis of cardiovascular diseases (14–16), and it has been proved to be an effective and reliable prognostic indicator for patients with acute and chronic heart failure. Recently, Okugawa et al. developed a new inflammatory scoring system based on lymphocyte count and serum CRP level, known as the LCS (12), which has not been demonstrated the effect on prognosis in patients with AHF.

The aim of this study was to evaluate the clinically prognostic efficacy of mGPS and LCS for mortality in patients with AHF and to determine the most clinical practical scoring system for predicting outcomes of patients with AHF.

METHODS

Study Population

A total of 250 patients with AHF who were hospitalized in the Department of Cardiology, The Second Affiliated Hospital of Nantong University from October 2019 to October 2020 were eventually included in this study (156 males and 94 females). All patients met the diagnostic criteria for acute heart failure (17).

Patients with rheumatic disease; patients with hematological disease; patients with malignant tumors; patients with chronic or infectious disease; patients with incomplete data and lost to follow-up and pregnant patients were excluded from the study. Patients were also excluded due to chronic or infectious disease or due to taking immunosuppressive drugs for disease control that may influence the status of mGPS and LCS.

Two hundred and fifty-eight patients were initially enrolled in this study, but 250 patients were eventually included according to the exclusion criteria. Of those, 5 patients were excluded because they lacked one of the lymphocyte, CRP and albumin data. For these 5 patients, follow-up was still carried out, and no death occurred in 5 patients. In addition, only 3 patients were lost to follow-up in this study, and these patients were also excluded.

The investigation conformed to the principles outlined in the Declaration of Helsinki. The study was approved by the Ethics Committee of The Affiliated Hospital 2 of Nantong University, Nantong (IRB number: 2019KN104), and informed consent was obtained from all patients.

Abbreviations: AHF, acute heart failure; mGPS, modified Glasgow prognostic score; LCS, lymphocyte C-reactive protein score; BMI, body mass index; CRP, C-reactive protein; NT-proBNP, N-terminal brain natriuretic peptide; AST, aspartate transaminase; LVEF, left ventricular ejection fraction; LAD, left atrial diameter; LVEDD, left ventricular end diastolic diameter; LVESD, left ventricular end systolic diameter; CKD-EPI, chronic kidney disease epidemiology collaboration; TNF-α, tumor necrosis factor-α.

TABLE 1 | Two types of systemic inflammation-based prognostic scores.

LCS	Points allocated
Lym $\geq 1 \times 10^9$/L and CRP $\leq$ 3 mg/L	0
Lym $< 1 \times 10^9$/L and CRP $<$ 3 mg/L	1
Lym $> 1 \times 10^9$/L and CRP $>$ 3 mg/L	1
Lym $< 1 \times 10^9$/L and CRP $>$ 3 mg/L	2
mGPS	
CRP $\leq$ 10 mg/L and albumin $\geq$ 35 g/L	0
CRP $>$ 10 mg/L and albumin $\geq$ 35 g/L	1
CRP $\leq$ 10 mg/L and albumin $<$ 35 g/L	1
CRP $>$ 10 mg/L and albumin $<$ 35 g/L	2

CRP, C-Reactive protein; LCS, lymphocyte C-reactive protein score; Lym, Lymphocyte count; mGPS, modified Glasgow prognostic score.

Data Collection

Demographic data (age, gender, body mass index (BMI), blood pressure, heart rate and treatment) was obtained from medical records. Diagnoses of hypertension and diabetes mellitus, and dyslipidemia were obtained from the patients' medical records or records of patient histories of previous medical therapy. The levels of lymphocyte count, leucocytes, C-reactive protein (CRP) and N-terminal brain natriuretic peptide (NT-proBNP) were measured immediately after admission. All the other measurements such as aspartate transaminase (AST), albumin, total bilirubin, direct bilirubin, total cholesterol, serum creatinine and urea nitrogen were performed on the second day of hospitalization, after fasting. Echocardiographic parameters include left ventricular ejection fraction (LVEF), left atrial diameter (LAD), left ventricular end diastolic diameter (LVEDD), and left ventricular end systolic diameter (LVESD). The glomerular filtration rate was estimated using the chronic kidney disease epidemiology collaboration (CKD-EPI) equation (18). Body mass index (BMI) was calculated as kg/ m².

Follow-Up

All patients were prospectively followed up for 3 months or until death. All-cause mortality was defined as the study end point, and data was obtained from the telephone interview and outpatient visits.

The Definition of Two Scores

The mGPS, defined based on the combination of serum CRP and albumin, was described as **Table 1**. Patients with both CRP $\leq$10 mg/L and albumin $\geq$35 g/L were classified to a score of 0; patients with either CRP $>$10 mg/L or albumin $\geq$35 g/L were classified to a score of 1 and patients with both CRP $>$10 mg/L and albumin $<$35 g/L were classified to a score of 2 (12).

The LCS, was established using the circulating lymphocyte count and CRP level as mentioned earlier. Patients with both the lymphocyte count $\geq 1 \times 10^9$/L and CRP $\leq$ 3 mg/L were scored as 0. If only one parameter changes, that is, lymphocyte count $<1 \times 10^9$/L or CRP $>$3 mg/L, 1 point was allocated. If both parameters were altered, that is, CRP$>$3 mg/L and lymphocyte count $<1 \times 10^9$/L, patients received 2 points (**Table 1**) (11).

TABLE 2 | Characteristics of patients who reached and did not reach the primary outcome.

Variables	Totality ($n = 250$)	Survivors ($n = 235$)	Non-survivors ($n = 15$)	*p*-value
Gender, male%	156 (62.4)	144 (61.3)	12 (80)	0.147
Age, years	75 (65, 80)	74 (65, 80)	79 (57, 81)	0.479
BMI, kg/ m²	23.56 (20.81, 26)	23.50 (20.81, 25.92)	22.89 (20.22, 27.16)	0.927
Systolic pressure, mmHg	125 (109, 138.25)	126 (110, 139)	103 (91, 125)	**0.023**
Diastolic pressure, mmHg	76 (65, 87)	76 (67, 87)	62 (56, 80)	**0.018**
Heart rate	85 (71, 100.25)	85 (71, 100)	84 (66, 110)	0.825
Smoking	53 (21.20)	49 (20.85)	4 (26.67)	0.593
NYHA IV	119 (47.6)	107 (45.5)	12 (80.0)	**0.010**
Comorbidities				
Hypertension	134 (53.60)	127 (54.04)	7 (46.67)	0.579
Diabetes	65 (26.00)	61 (25.96)	4 (26.67)	0.952
Atrial fibrillation	117 (46.80)	111 (47.23)	6 (40)	0.585
Prior MI	39 (15.60)	33 (14.04)	6 (40)	**0.007**
Laboratory data				
Leucocytes, 10^9/L	9.0 (6.9, 11.2)	6.9 (5.1, 9.1)	7.0 (3.8, 8.1)	0.601
Lymphocyte count, 10^9/L	1.1 (0.8, 1.5)	1.1 (0.8, 1.6)	0.9 (0.7, 1.3)	0.106
Hemoglobin, g/L	124 (113, 135.25)	124 (113, 135)	122 (112, 137)	0.760
CRP, mg/L	7.70 (2.55, 20.89)	6.76 (2.17, 20.06)	40.08 (10.89, 92.91)	**0.001**
Albumin, g/l	36.10 ± 4.09	36.21 ± 4.08	34.34 ± 3.96	0.087
AST, U/L	29 (21, 54.75)	28 (20, 53)	49 (26, 90)	**0.030**
Total bilirubin, μmol/L	15.75 (10.9, 24.08)	15.6 (10.85, 23.7)	18.7 (10.9, 49.7)	0.200
Direct bilirubin, μmol/L	5.4 (3.5, 9.0)	5.3 (3.5, 8.9)	8.4 (4.8, 22.5)	0.086
Total cholesterol, mmol/L	3.72 (2.97, 4.41)	3.75 (2.98, 4.42)	3.46 (2.32, 4.00)	0.099
Creatinine, μmol/L	85.25 (70, 108.38)	85 (69.80, 105.95)	114 (82, 144)	**0.018**
Urea nitrogen, mmol/L	7.31 (5.30, 9.84)	7.22 (5.26, 9.71)	9.07 (7.07, 21.20)	**0.020**
eGFR, ml/min	70.64 (50.08, 90.08)	71.6 (50.23, 90.89)	56.22 (39.23, 80.9)	0.063
NT-proBNP, pg/ml	5,575 (2824.5, 11,062)	5,255 (2753.25, 10,855)	8,365 (5,762, 20,115)	**0.014**
Echocardiographic data				
LVEF, %	46 (35, 59)	46 (36.3, 60)	30.5 (24.5, 46)	**0.003**
LVESD, mm	43 (34, 52.5)	42.5 (34, 52)	50 (43.5, 65.5)	**0.021**
LVEDD, mm	57 (50, 65)	57 (49.25, 65)	61 (55.5, 73.5)	0.052
Treatment				
ACEI/ARB	158 (63.2)	151 (64.3)	7 (46.7)	0.179
βblocker	179 (71.6)	170 (72.3)	9 (60.0)	0.375
Diuretics	231 (92.4)	219 (93.2)	12 (80.0)	0.094
LCS				
0	40 (16)	40 (17.02)	0	
1	141 (56.4)	136 (57.87)	5 (33.3)	**0.001**
2	69 (27.6)	59 (25.11)	10 (66.67)	
mGPS				
0	107 (42.8)	105 (44.7)	2 (13.3)	
1	87 (34.8)	81 (34.5)	6 (40)	**0.006**
2	56 (22.4)	49 (20.9)	7 (46.7)	

AST, aspartate transaminase; BMI, body mass index; eGFR, estimated glomerular filtration rate; LVEF, left ventricular ejection fraction; LVEDD, left ventricular end diastolic diameter; LVESD, left ventricular end systolic diameter; MI, myocardial infarction; NYHA, New York Heart Association; NT-proBNP, N-terminal pro B-type natriuretic peptide.
Values with $P < 0.05$ in the table are shown in bold.

TABLE 3 | Univariate and multivariate analysis of variables associated with prognosis in patients with acute heart failure.

Variable	Unadjusted OR (95% CI)	*P*-value	Adjusted OR (95% CI)	*p*-value
NYHA	4.785 (0.057–0.760)	0.017		
Systolic pressure	0.979 (0.958–1.000)	0.049		
Diastolic pressure	0.956 (0.918–0.994)	0.024		
Albumin	0.900 (0.796–1.016)	0.088		
Total cholesterol	0.607 (0.341–1.082)	0.091		
Total bilirubin	1.032 (1.006–1.058)	0.016		
Direct bilirubin	1.057 (1.013, 1.104)	0.012	1.096 (1.019–1.178)	0.014
Urea nitrogen	1.093 (1.028–1.162)	0.004		
eGFR	0.983 (0.963–1.003)	0.087		
CRP	1.016 (1.007–1.026)	0.001	1.036 (1.008–1.065)	0.011
LVEF	0.942 (0.902–0.983)	0.006	0.845 (0.750–0.952)	0.006
LVESD	1.052 (1.008–1.098)	0.021		
LVEDD	1.048 (0.998–1.101)	0.058		
LCS	5.286 (1.876–14.896)	0.002	11.694 (1.433–95.409)	0.022
mGPS	2.541 (1.256–5.141)	0.009		

Statistical Analysis

Baseline continuous variables were presented as mean ± standard deviations (SD) or median with the first and fourth quartile (Q1–Q4); depending on the distribution of the data. Categorical data is presented as counts and percentages. For comparisons between the patient groups with different endpoints, the independent samples *t*-test, the Mann–Whitney *U* test, and the χ^2 test were used. Multivariate analysis using stepwise logistic regression model tested variables that were significant ($P < 0.1$) in the univariate analysis to determine independent predictors of all-cause mortality. Receiver operating characteristic curve (ROC) was used to evaluate the predictive value of various independent predictors for mortality in patients with acute heart failure. For all tests, a p-value < 0.05 was considered statistically significant. Analyses were performed with the statistical package SPSS 25.0 (SPSS Inc., Chicago, IL).

RESULTS

Patient Characteristics

Two hundred and fifteen patients were included in the study. Demographic, clinical, and laboratory characteristics of patients on admission who reached the endpoint are shown in **Table 2**. The all-cause mortality rate was 6% in 3 months. The levels of LCS and mGPS in the death group were significantly higher than those in the survival group ($P < 0.05$). Besides this, the death group had lower LVEF, systolic and diastolic blood pressure, but higher CRP, AST, creatinine, urea nitrogen, NT-proBNP levels, LVESD and incidence of previous myocardial infarction events than the survival group ($P < 0.05$). No significant differences were observed with respect to gender, age, BMI, white blood cell count, lymphocyte count, hemoglobin, total bilirubin, direct bilirubin, total cholesterol, eGFR and treatment.

Predicting Clinical Outcome

On univariate analyses, higher New York Heart Association class, CRP, total bilirubin, direct bilirubin, urea nitrogen, LVESD, LCS and mGPS but lower LVEF, systolic and diastolic blood pressure at admission were significantly associated with outcome ($P < 0.05$; **Table 2**). Variables that had a p-value <0.1 in the univariate analyses were used in a multivariate logistic regression analysis model. After adjusting for other potential confounding factors, multivariate analyses showed that only direct bilirubin (OR: 1.096, 95%CI: 1.019∼1.178, $p = 0.014$), CRP (OR: 1.036, 95%CI: 1.008∼1.065, $p = 0.011$), LVEF (OR: 0.845, 95%CI: 0.750∼0.952, $p < 0.01$) and LCS (OR: 11.694, 95%CI: 1.433∼95.409, $p = 0.022$) at admission were independently associated with the mortality outcomes (**Table 3**).

ROC Curve Analysis

The area under the ROC curve of the mGPS for predicting death was 0.695, with a cut-off level of 0.5 (95%CI: 0.567∼0.823), sensitivity of 86.7%, and specificity of 44.7% ($p < 0.01$; **Figure 1**). The area under the ROC curve of the LCS for predicting death was 0.736, with a cut-off level of 1.5 (95%CI: 0.616∼0.856), sensitivity of 66.7%, and specificity of 74.9% ($p < 0.01$; **Figure 1**). Although the AUC of LCS was slightly larger, there was no statistical difference between these two methods ($P > 0.05$; **Figure 1**). However, the results of multivariate analyses showed that only LCS was independently associated with the prognosis of patients with acute heart failure.

DISCUSSION

In recent years, more and more studies have elucidated the key role of inflammatory biomarkers in the development of acute heart failure (7, 19–21). Although the role of inflammation in heart failure has been recognized, inflammation scores have not been included in the risk assessment of acute heart failure, and this gap needs to be filled. As mGPS, an inflammatory-based prognostic risk score, has been gradually explored in predicting the prognosis of patients with different types of cancer, cardiovascular physicians are discovering its value in predicting the poor prognosis of patients with acute and chronic heart failure (14–16). In 2019, LCS developed by Okugawa et al. was also proved to be a reliable marker of inflammatory response in patients with

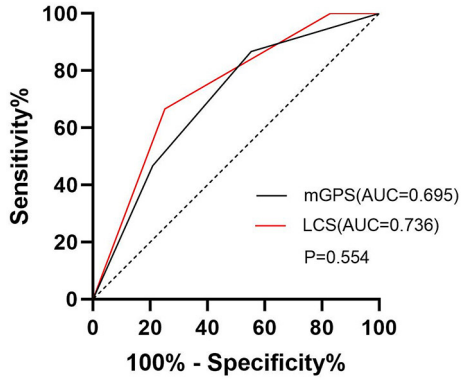

FIGURE 1 | Receiver operating characteristic curves for LCS, and mGPS in the prediction of mortality in patients with acute heart failure. The area under the receiver operating characteristic curve (AUC) for LCS was 0.736, AUC for mGPS was 0.695.

gastric cancer (12). To our knowledge, this is the first study to evaluate the predictive value of LCS in patients with acute heart failure and the first study to compare the correlation between mGPS, LCS and prognosis in patients with acute heart failure.

The study showed that the levels of LCS and mGPS in the death group were significantly higher than those in the survival group. Although both mGPS and LCS were associated with 3-month mortality in the univariate analyses ($p < 0.05$), and there was no significant statistical difference of the AUC between these two scoring systems, only LCS is found to be independently associated with prognosis after adjustment for relevant factors, while mGPS was excluded. In conclusion, LCS has a more promising application in predicting the prognosis of acute heart failure.

The increased level of tumor necrosis factor-α (TNF-α) in the circulation of patients with chronic heart failure since Levine (22) first advocated it in 1990, has been widely explored for decades, and accumulating studies have elucidated the pivotal role of the inflammatory biomarkers in acute and chronic heart failure (7, 19–21). The inflammation-based prognostic score LCS combining CRP and lymphocyte count was originally used to measure systemic inflammatory status and predict prognosis in cancer patients. Similar to heart failure, cancer is also a systemic disease with activated inflammatory response. Previous studies have shown that low lymphocyte counts can help identify patients at higher risk of death in heart transplant patients and in patients with various types of acute or chronic heart failure (9, 23). In addition, high CRP levels on admission and discharge are considered to be closely associated with poor prognosis in patients with acute decompensated heart failure (7, 24). In the LCS scoring system, a lower lymphocyte count and a higher CRP level are assigned a higher score. In fact, several previous studies have hinted in part at the predictive power of LCS in patients with acute heart failure. The elevation of these inflammatory biomarkers in ADHF indicates that ADHF patients are in a significant systemic inflammatory state. In the LCS scoring system, a lower lymphocyte count and a higher CRP level are assigned a higher score, quantifying the inflammatory status and providing a more comprehensive measure of systemic inflammation. This study confirmed the relationship between a more activated inflammatory state and worse prognosis in acute heart failure and reported the successful implementation of the cancer-cohort-derived LCS risk score to a cohort with AHF patients.

CONCLUSIONS

In conclusion, this study has shown the clinical utility of the simple and objective inflammation-based score in acute heart failure patients. An activated inflammatory state appears to be characteristic for a more advanced disease. Compared with mGPS, LCS is independently associated with short-term outcomes in patients with acute heart failure. The LCS may help clinicians to identify AHF patients with worse prognosis, for whom more intensive and aggressive treatment may be needed and thus improve their prognosis.

LIMITATIONS

This study was retrospective and all patients enrolled were from the same institution. In the next step, we will include a larger sample size to validate the conclusions of this study and determine whether controlling inflammatory levels in patients with acute heart failure improves patient outcomes. Besides, the follow-up time of this study was only 3 months, so the follow-up time could be extended for further verification.

DATA AVAILABILITY STATEMENT

The original contributions presented in the study are included in the article/supplementary material, further inquiries can be directed to the corresponding authors.

ETHICS STATEMENT

The studies involving human participants were reviewed and approved by the Ethics Committee of The Affiliated Hospital 2 of Nantong University, Nantong (IRB number: 2019KN104). The patients/participants provided their written informed consent to participate in this study.

AUTHOR CONTRIBUTIONS

JW: conceptualization, methodology, investigation, data curation, formal analysis, writing—original draft, and writing—review and editing. LX: conceptualization, methodology, investigation, data curation, and writing—original draft. PL, FZ, and H-LC: investigation and

data curation. R-XQ: resources, writing—review and editing, visualization, project administration, and supervision. QZ: resources, formal analysis, writing—original draft, writing—review and editing, visualization, project administration, and supervision. All authors contributed to the article and approved the submitted version.

FUNDING

This work was supported by the Scientific Research Project of Nantong Municipal Health Commission (MA2020004, MB2021010), Project of Nantong Science and Technology Bureau (JCZ21099), and Kangda College of Nanjing Medical University (KD2021KYJJZD012).

REFERENCES

1. Arrigo M, Jessup M, Mullens W, Reza N, Shah AM, Sliwa K, et al. Acute heart failure. *Nat Rev Dis Primers.* (2020) 6:16. doi: 10.1038/s41572-020-0151-7
2. Van Linthout S, Tschöpe C. inflammation - cause or consequence of heart failure or both? *Curr Heart Fail Rep.* (2017) 14:251–65. doi: 10.1007/s11897-017-0337-9
3. Murphy SP, Kakkar R, McCarthy CP, Januzzi JL Jr. Inflammation in heart failure: JACC state-of-the-art review. *J Am Coll Cardiol.* (2020) 75:1324–40. doi: 10.1016/j.jacc.2020.01.014
4. Mene-Afejuku TO, Moisa EA, Akinlonu A, Dumancas C, Veranyan S, Perez JA, et al. The relevance of serum albumin among elderly patients with acute decompensated heart failure. *J Geriatr Cardiol.* (2019) 16:522–8. doi: 10.11909/j.issn.1671-5411.2019.07.005
5. Ancion A, Allepaerts S, Robinet S, Oury C, Pierard L, Lancellotti P. Serum albumin level and long-term outcome in acute heart failure. *Acta Cardiol.* (2019) 74:465–71. doi: 10.1080/00015385.2018.1521557
6. Kalogeropoulos AP, Tang WH, Hsu A, Felker GM, Hernandez AF, Troughton RW, et al. High-sensitivity C-reactive protein in acute heart failure: insights from the ASCEND-HF trial. *J Card Fail.* (2014) 20:319–26. doi: 10.1016/j.cardfail.2014.02.002
7. Matsumoto H, Kasai T, Sato A, Ishiwata S, Tatsu S, Shitara J, et al. Association between C-reactive protein levels at hospital admission and long-term mortality in patients with acute decompensated heart failure. *Heart Vessels.* (2019) 34:1961–8. doi: 10.1007/s00380-019-01435-9
8. Milo-Cotter O, Teerlink JR, Metra M, Felker GM, Ponikowski P, Voors AA, et al. Low lymphocyte ratio as a novel prognostic factor in acute heart failure: results from the Pre-RELAX-AHF study. *Cardiology.* (2010) 117:190–6. doi: 10.1159/000321416
9. Marçula M, de Souza Buto MF, Madaloso BA, Nunes RA, Cuoco MA, de Paula RS, et al. Lymphocyte count and prognosis in patients with heart failure. *Int J Cardiol.* (2015) 188:60–2. doi: 10.1016/j.ijcard.2015.04.043
10. Arques S, Roux E, Stolidi P, Gelisse R, Ambrosi P. Usefulness of serum albumin and serum total cholesterol in the prediction of hospital death in older patients with severe, acute heart failure. *Arch Cardiovasc Dis.* (2011) 104:502–8. doi: 10.1016/j.acvd.2011.06.003
11. McMillan D. The systemic inflammation-based Glasgow Prognostic Score: a decade of experience in patients with cancer. *Cancer Treat Rev.* (2013) 39:534–40. doi: 10.1016/j.ctrv.2012.08.003
12. Okugawa Y, Toiyama Y, Yamamoto A, Shigemori T, Ichikawa T, Yin C, et al. Lymphocyte-to-C-reactive protein ratio and score are clinically feasible nutrition-inflammation markers of outcome in patients with gastric cancer. *Clin Nutr.* (2020) 39:1209–17. doi: 10.1016/j.clnu.2019.05.009
13. Chen YR, Chen YL, Ouyang SS, Xu HW, Li P, He LJ, et al. Prognostic efficacy of preoperative mGPS, SIS and LCS in patients with gastric cancer. *Clin Chim Acta.* (2020) 511:81–9. doi: 10.1016/j.cca.2020.09.027
14. Bolat I, Biteker M. Modified Glasgow Prognostic Score is a novel predictor of clinical outcome in heart failure with preserved ejection fraction. *Scand Cardiovasc J.* (2020) 54:174–8. doi: 10.1080/14017431.2019.1709656
15. Cho A, Arfsten H, Goliasch G, Bartko PE, Wurm R, Strunk G, et al. The inflammation-based modified Glasgow prognostic score is associated with survival in stable heart failure patients. *ESC Heart Fail.* (2020) 7:654–62. doi: 10.1002/ehf2.12625
16. Namiuchi S, Sugie T, Saji K, Takii T, Suda A, Kato A. The systemic inflammation-based Glasgow Prognostic Score as a prognostic factor in patients with acute heart failure. *J Cardiovasc Med.* (2015) 16:409–15. doi: 10.2459/JCM.0000000000000184
17. Ponikowski P, Voors AA, Anker SD, Bueno H, Cleland JGF, Coats AJS, et al. 2016 ESC Guidelines for the diagnosis and treatment of acute and chronic heart failure: the Task Force for the diagnosis and treatment of acute and chronic heart failure of the European Society of Cardiology (ESC) Developed with the special contribution of the Heart Failure Association (HFA) of the ESC. *Eur Heart J.* (2016) 37:2129–200. doi: 10.1093/eurheartj/ehw128
18. Levey AS, Stevens LA, Schmid CH, Zhang YL, Castro AF III, Feldman HI, et al. A new equation to estimate glomerular filtration rate. *Ann Internal Med.* (2009) 150:604–12. doi: 10.7326/0003-4819-150-9-200905050-00006
19. Tromp J, Khan MAF, Mentz RJ, O'Connor CM, Metra M, Dittrich HC, et al. Biomarker profiles of acute heart failure patients with a mid-range ejection fraction. *JACC Heart Fail.* (2017) 5:507–17. doi: 10.1016/j.jchf.2017.04.007
20. Goonewardena S, Stein A, Tsuchida R, Rattan R, Shah D, Hummel S. Monocyte subsets and inflammatory cytokines in acute decompensated heart failure. *J Card Fail.* (2016) 22:358–65. doi: 10.1016/j.cardfail.2015.12.014
21. Mann D. Incident heart failure in chronic inflammatory diseases: is it time to rethink stage A heart failure? *JACC Heart Fail.* (2020) 8:499–500. doi: 10.1016/j.jchf.2020.02.006
22. Levine B, Kalman J, Mayer L, Fillit H, Packer M. Elevated circulating levels of tumor necrosis factor in severe chronic heart failure. *N Engl J Med.* (1990) 323:236–41. doi: 10.1056/NEJM199007263230405
23. Acanfora D, Gheorghiade M, Trojano L, Furgi G, Pasini E, Picone C, et al. Relative lymphocyte count: a prognostic indicator of mortality in elderly patients with congestive heart failure. *Am Heart J.* (2001) 142:167–73. doi: 10.1067/mhj.2001.115792
24. Nishimoto Y, Kato T, Morimoto T, Yaku H, Inuzuka Y, Tamaki Y, et al. C-reactive protein at discharge and 1-year mortality in hospitalised patients with acute decompensated heart failure: an observational study. *BMJ Open.* (2020) 10:e041068. doi: 10.1136/bmjopen-2020-041068

Conflict of Interest: The authors declare that the research was conducted in the absence of any commercial or financial relationships that could be construed as a potential conflict of interest.

Publisher's Note: All claims expressed in this article are solely those of the authors and do not necessarily represent those of their affiliated organizations, or those of the publisher, the editors and the reviewers. Any product that may be evaluated in this article, or claim that may be made by its manufacturer, is not guaranteed or endorsed by the publisher.

frontiers | Frontiers in Cardiovascular Medicine

TYPE Original Research
PUBLISHED 11 August 2022
DOI 10.3389/fcvm.2022.936212

OPEN ACCESS

EDITED BY
Jia Qi,
Shanghai Jiao Tong University, China

REVIEWED BY
Lan Ma,
Shanghai Jiao Tong University, China
Xuedong Shen,
Shanghai Jiao Tong University, China

*CORRESPONDENCE
Jing Wu
ntsywj@163.com

SPECIALTY SECTION
This article was submitted to General Cardiovascular Medicine, a section of the journal Frontiers in Cardiovascular Medicine

RECEIVED 05 May 2022
ACCEPTED 05 July 2022
PUBLISHED 11 August 2022

CITATION
Zhu J, Xie S, Ji H, Gu X and Wu J (2022) Evaluation of anthracycline-induced subclinical LV dysfunction by using myocardial composite index and two-dimension speckle tracking echocardiography technique. *Front. Cardiovasc. Med.* 9:936212. doi: 10.3389/fcvm.2022.936212

Evaluation of anthracycline-induced subclinical LV dysfunction by using myocardial composite index and two-dimension speckle tracking echocardiography technique

Jiabao Zhu[1], Shuhui Xie[1], Hanzhen Ji[2], Xingxing Gu[1] and Jing Wu[1]*

[1]Department of Ultrasound, Nantong Third People's Hospital, Nantong University, Nantong, China, [2]Department of Library and Information Science, Nantong Third People's Hospital, Nantong University, Nantong, China

Objective: To obtain various myocardial strain parameters by using two-dimension speckle tracking echocardiography (2D-STE) technique, calculate the myocardial composite index (MCI) which combines the global longitudinal strain (GLS) of left ventricle and the left ventricular twist (LVtw), and evaluate their diagnostic efficacies for subclinical left ventricular (LV) dysfunction in patients undergoing anthracycline chemotherapy.

Methods: A total of 35 female breast cancer patients, who underwent postoperative chemotherapy in the Department of Thyroid and Breast Surgery of Nantong Third People's Hospital from September 2018 to December 2019 and had successful follow-up, were included into the chemotherapy group, and the patients were evaluated respectively at baseline and in early, interim and later chemotherapy stages according to the course of chemotherapy; in addition, 30 healthy women undergoing physical examination during the same period were included into the control group. In different chemotherapy stages, the data such as left ventricular end diastolic diameter (LVEDD), left ventricular end systolic diameter (LVESD), interventricular septal thickness (IVST), left ventricular posterior wall thickness (LVPWT) and left ventricular ejection fraction (LVEF) were collected by using conventional echocardiography, and various myocardial strain parameters such as GLS, global radial strain (GRS), global circumferential strain(GCS) and LVtw were measured using 2D-STE, and then MCI was calculated. Receiver operating characteristic (ROC) curve analysis was performed to evaluate the application values of various parameters in the diagnosis of early cardiotoxicity.

Results: There was a difference in MCI between patients at baseline and in the early chemotherapy stage; there were differences in GLS, LVtw and MCI between patients at baseline and in the interim chemotherapy stage; there were differences in four parameters such as MCI, GLS, LVtw and GCS between patients at baseline and in the later chemotherapy stage; The AUC of MCI was 0.915, when the cutoff value was −210.89 (%×°), the sensitivity and specificity were 84.37% and 90.41%, respectively.

Conclusion: MCI combines the longitudinal and torsional motions of myocardium, and thus has a better diagnostic value for early detection of subclinical LV dysfunction caused by anthracycline chemotherapy drugs compared with strain parameters in a single direction.

KEYWORDS

speckle tracking technique, myocardial composite index, anthracycline chemotherapy, subclinical LV dysfunction, left ventricular function

Introduction

The anthracycline chemotherapy drugs are widely used in the treatment of hematological and solid tumors. The anthracycline-based chemotherapy regimen is a classic first-line regimen for the treatment of breast cancers. However, anthracycline drugs have side effects such as bone marrow suppression and cardiotoxicity, and the cardiotoxicity will be gradually aggravated and even irreversible along with the increase of dosage of anthracycline drugs and irreversible at the same time (1). A number of studies have confirmed that the patients may suffer from organic myocardial injury when they firstly use anthracycline drugs (2). Therefore, clinicians should pay great attention to the early detection of cardiotoxicity when using the anthracycline drugs. However, the myocardial injury is often underestimated according to left ventricular ejection fraction (LVEF), and the patients with normal LVEF may also have subclinical LV dysfunction. Therefore, LVEF is not sensitive enough for early detection of early subclinical LV dysfunction (3). The speckle-tracking echocardiography (STE) can be used to quantitatively analyze the movement and changes of myocardium through tracking the movement trajectory of myocardial echo spots on two-dimensional (2D) images, and this is currently a research hotspot in the diagnosis of early cardiac injury. However, two-dimension speckle-tracking echocardiography (2D-STE) technique can only analyze single parameters such as global longitudinal strain (GLS), global circumferential strain (GCS), global radial strain (GRS) and left ventricular twist (LVtw) of the regional myocardium. Myocardial composite index (MCI) can combine left ventricular GLS with LVtw, which can more comprehensively reflect the movement and changes of left ventricular myocardium in the three-dimensional (3D) directions. In this study, the effect of anthracycline drugs on myocardial movement in patients undergoing breast cancer chemotherapy was analyzed by using STE technique, and the application values of various parameters of STE technique in the diagnosis of early cardiotoxicity were evaluated.

Materials and methods

Study subjects

Methods: A total 35 female patients, who underwent chemotherapy after breast cancer surgery in the Department of Thyroid and Breast Surgery, Nantong Third People's Hospital from September 2018 to December 2019 and had successful follow-up, were included into the chemotherapy group, and the patients were evaluated respectively at baseline and in the early (after 2 chemotherapy cycles), interim (after 4 chemotherapy cycles) and later (after 6 chemotherapy cycles) chemotherapy stages according to the course of chemotherapy. In addition, 30 healthy women undergoing physical examination in the hospital during the same period were included into the control group. Inclusion criteria: (1) all patients received anthracycline-based chemotherapy (FAC protocol: fluorouracil 500 mg/m^2 iv d1, d8; adriamycin 50 mg/m^2 iv d1; cyclophosphamide 500 mg/m^2 iv d1; 21 days as a cycle)regimen and completed a total of 6 cycles of chemotherapy; (2) no obvious abnormalities were found in the electrocardiograms of patients before chemotherapy; (3) the patients with basic diseases such as hypertension, diabetes and coronary heart disease were excluded; and (4) the patients

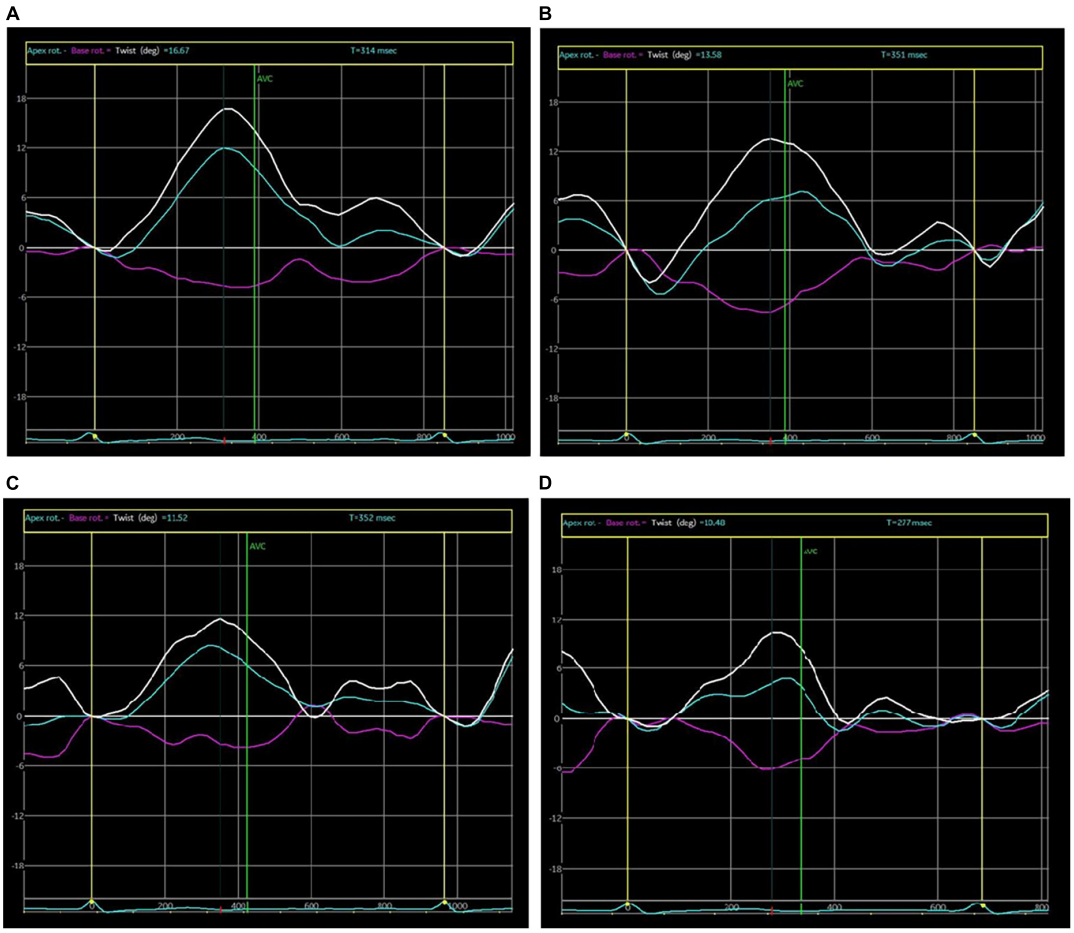

FIGURE 1
Curve of left ventricular twist. **(A)** at baseline; **(B)** after 2 chemotherapy cycles; **(C)** after 4 chemotherapy cycles; **(D)** after 6 chemotherapy cycles.

had no obvious abnormalities in routine blood biochemical indexes. A total of 50 patients were collected, of whom, 35 were followed up successfully and finally included into the chemotherapy group. The patients aged from 30 to 68 years old, with an average age of (51.66 ± 9.32) years old. The patients at baseline underwent routine echocardiography and 2D-STE at one day before chemotherapy, and the patients in other stages underwent routine echocardiography and 2D-STE at 20 days after chemotherapy. Images were collected and relevant parameters were recorded. All subjects signed an informed consent form, and this study was approved by the ethics committee of our hospital.

Instruments and methods

VIVID E9 color Doppler ultrasonic instrument of GE Company was adopted, which was equipped with M5S probe with a frequency of 1.5–4.3 MHz and EchoPAC offline workstation. Under the condition of calm breathing, the subjects were placed in a proper left lateral position and connected to an ECG monitor at the same time. The interventricular septum thickness (IVST) at end-diastole, left ventricular end diastolic dimension (LVEDD), left ventricular posterior wall thickness (LVPWT) at end-diastole and left ventricular end systolic diameter (LVESD) were measured with a probe on the long axial section of the left parasternal ventricle. LVEF was detected by using the biplane modified Simpson's method, the 2D images of three consecutive cardiac cycles were scanned respectively from the short axis views at left ventricular mitral valve annulus, papillary muscle and apical levels, apical four-chamber view, two-chamber view and three-chamber view, which were stored in the DICOM format, then imported into EchoPAC offline workstation and played back frame-by-frame; the myocardial area was manually traced, and the software automatically divided the left ventricular myocardium into 17 segments, and displayed the strain-time curve of each segment and the corresponding bull's eye diagram. GLS, GCS, GRS and LVtw (**Figure 1**) were measured. MCI was calculated according to the following formula: MCI = GLS × LVtw (unit:%×°).

Statistical analysis

SPSS 17.0 software was used for statistical analysis, the measurement data in each group were expressed as mean ± standard deviation and tested for normal distribution and homogeneity of variance. *t*-test or one-way analysis of variance (ANOVA) was used to compare the differences between the groups. A bivariate correlation analysis was performed using Pearson correlation analysis. The receiver operating characteristic (ROC) curves of all global strain parameters were drawn to evaluate their diagnostic values for subclinical LV dysfunction, and the area under the curve (AUC) and the optimal cutoff value were determined.

Results

Comparison of various indexes between the control group and the patients at baseline

Table 1 showed that there were no significant differences in various indexes between the control group and the patients at baseline (all $P > 0.05$).

Comparison of various indexes in the chemotherapy group among different chemotherapy stages

Table 2 indicated that the patients in chemotherapy group showed no significant differences in LVEDD, LVESD, IVST, LVPWT, LVEF and GRS among different chemotherapy stages (all $P > 0.05$). The MCI in the early chemotherapy stage was higher than that at baseline, the GLS and MCI in the interim chemotherapy stage were higher than those at baseline, and LVtw in the interim chemotherapy stage was lower than that at baseline. GCS, GLS and MCI in the later chemotherapy stage were higher than those at baseline, and LVtw in the later chemotherapy stage was lower than that at baseline.

TABLE 1 Comparison of various indexes between the control group and the patients at baseline ($\bar{x} \pm s$).

Indexes	Control group	Patients at baseline	*t*	*P*
Age (years)	47.1 ± 9.36	51.66 ± 9.32	−1.942	0.057
LVEDD (mm)	43.55 ± 3.93	43.71 ± 3.44	−0.176	0.861
LVESD (mm)	28.00 ± 2.70	27.83 ± 2.42	0.268	0.790
IVST (mm)	8.13 ± 0.86	8.33 ± 0.81	−0.976	0.333
LVPWT (mm)	8.30 ± 0.70	8.21 ± 0.81	0.447	0.656
LVEF (%)	65.00 ± 3.87	65.83 ± 3.17	−0.942	0.350
GRS (%)	48.19 ± 3.11	47.47 ± 1.96	1.087	0.283
GCS (%)	−18.94 ± 1.77	−19.04 ± 1.7	0.229	0.820
GLS (%)	−19.41 ± 1.68	−18.73 ± 1.41	−1.764	0.083
LVtw (°)	14.58 ± 1.46	14.94 ± 1.05	−1.160	0.250
MCI (%×°)	−271.72 ± 33.51	−280.24 ± 32.62	1.027	0.308

$P < 0.05$ indicated a statistically significant difference.

Analysis on the correlations of the cumulative dose of adriamycin with global radial strain, global circumferential strain, global longitudinal strain, left ventricular twist and myocardial composite index

The cumulative doses of adriamycin at baseline and in early, interim and later stages were 0, 100, 200, and 300 mg/m^2, respectively. Spearman correlation analysis showed that the cumulative dose of adriamycin was positively correlated with GCS, GLS and MCI, and negatively correlated with GRS and LVtw. With the increase of cumulative dose of adriamycin, all absolute values of GRS, GCS, GLS, LVtw and MCI were decreased (Table 3).

Evaluation of effectiveness of two-dimension speckle tracking echocardiography parameters and myocardial composite index in the prediction of subclinical dysfunction

The results of this study showed that the AUCs of GRS, GCS, GLS, LVtw and MCI for subclinical LV dysfunction prediction were 0.607, 0.601, 0.893, 0.814, and 0.915, respectively, and their corresponding sensitivities were 53.13%, 71.87%, 93.75%, 75.00% and 84.37%, respectively, and their corresponding specificities were 68.49%, 52.05%, 71.23%, 80.82% and 90.41%, respectively (Table 4 and Figure 2).

Discussion

Anthracycline-induced cardiotoxicity and its mechanism

Anthracycline-induced cardiotoxicity mainly causes changes in cardiac electrophysiology and cardiac hemodynamics, which are manifested as abnormal ECG, decreased LVEF and abnormal myocardial activity, and may eventually lead to heart failure.

The pathological manifestations of the damaged myocardium caused by anthracycline toxicity mainly include myocardial edema, disappearance of myocardial

TABLE 2 Comparison of various indexes in the chemotherapy group among different chemotherapy stages ($\bar{x} \pm s$).

Item	Baseline	Early chemotherapy stage	Interim chemotherapy stage	Later chemotherapy stage	*F*	*P*
LVEDD (mm)	43.71 ± 3.44	43.74 ± 3.22	43.77 ± 3.39	43.49 ± 4.09	0.047	0.986
LVESD (mm)	27.83 ± 2.42	27.71 ± 2.8	28.6 ± 2.69	28.26 ± 3.29	0.730	0.536
IVST (mm)	8.33 ± 0.81	8.37 ± 0.77	8.21 ± 0.83	8.45 ± 0.79	0.529	0.663
LVPWT (mm)	8.21 ± 0.81	8.24 ± 0.78	8.25 ± 0.7	8.44 ± 0.63	0.708	0.549
LVEF (%)	65.83 ± 3.17	65.66 ± 3.11	64.43 ± 3.3	63.77 ± 5.79	2.131	0.099
GRS(%)	47.47 ± 1.96	46.72 ± 1.86	46.35 ± 1.90	45.63 ± 1.77	2.504	0.062
GCS(%)	−19.04 ± 1.70	−17.93 ± 2.90	−17.72 ± 2.93	−16.34 ± 2.57*	6.492	<0.001
GLS(%)	−18.73 ± 1.41	−18.04 ± 1.27	−16.46 ± 1.64*	−15.87 ± 1.48*	24.54	<0.001
LVtw(°)	14.94 ± 1.05	14.42 ± 0.95	13.58 ± 0.78*	12.36 ± 0.76*	49.15	<0.001
MCI(%×°)	−280.24 ± 32.62	−250.41 ± 28.15*	−224.13 ± 24.62*	−196.13 ± 21.41*	62.63	<0.001

*Compared with the patients at baseline, $P < 0.05$ indicated a statistically significant difference.

TABLE 3 Analysis on the correlations of the cumulative dose of adriamycin with GRS, GCS, GLS, LVtw, and MCI.

Item	*r*	*P*
GRS	−0.414	0.000
GCS	0.428	0.000
GLS	0.627	0.000
LVtw	−0.741	0.000
MCI	0.760	0.000

cells, interstitial fibrosis and sarcoplasmic reticulum expansion under light microscope, and myocardial fibrinolysis, extensive disappearance of fiber bundles, deformed and broken Z-line, mitochondrial lysis and vacuole formation in myocardial cells under the electron microscope (4).

The cardiotoxicity of anthracycline anticancer drugs can be divided into the following three types according to its onset time and progression speed: (1) acute or subacute cardiotoxicity which usually occurs within 2 weeks after the start of treatment; (2) chronic cardiotoxicity which usually occurs within 1 year after the completion of chemotherapy and is the most common clinical cardiotoxicity; (3) delayed cardiotoxicity which is cardiac injury occurring at 1 year after completion of chemotherapy (5).

The exact mechanism of anthracycline-induced cardiotoxicity remains unclear. At present, the main categories of views are as follows: (1) The most classic oxidative stress theory: Anthracycline drugs can generate oxidative active substances such as superoxide anions through a series of processes in the mitochondria of myocardial cells, which can lead to apoptosis and necrosis of myocardial cells. Meanwhile, anthracycline drugs can lead to a failure of myocardial cells to metabolize harmful substances such as oxygen free radicals in time and further aggravate the myocardial injury (6). Anthracycline drugs can increase the iron content in myocardial cells, leading to the production of hydroxyl radicals, which in turn damage mitochondrial DNA (7). (2) Calcium overload theory: Anthracycline drugs can rapidly increase the intracellular free Ca^{2+} content, which can inhibit the excitation-contraction coupling of myocardial cells and induce arrhythmias (8).

Evaluation of cancer therapeutics-related cardiac dysfunction and subclinical LV dysfunction

Endocardial myocardial biopsy is recognized as the gold standard for evaluating the anthracycline-induced cardiotoxicity, but this method is invasive and rarely used in clinical practice. Therefore, LVEF is generally used to evaluate cardiac dysfunction related to cancer treatment in clinical practice. American Society of Echocardiography (ASE) and European Association of Cardiovascular Imaging (EACVI) defines the cancer therapeutics-related cardiac dysfunction (CTRCD) as: the decrease in LVEF caused by cancer treatment is > 10% of baseline LVEF and reaches less than 53% absolute value (9). In this study, finally it was found that 5 patients finally met the diagnostic criteria for cancer therapeutics-related cardiac dysfunction (CTRCD). However, LVEF has some limitations in monitoring cardiotoxicity. LVEF is a load-dependent index, which is easily affected by preload, afterload and rhythm of the heart. At the same time, the chemotherapy-induced cardiotoxicity is regional, and some myocardial segments may compensate for the loss of function of other myocardial segments, thus maintaining a normal LVEF level at least in the early stage (10). Moreover, this is credible only

TABLE 4 Results of ROC analysis of 2D-STE parameters and MCI.

Indexes	AUC	Standard error	*P*	95%*CI*	Cutoff value	Sensitivity (%)	Specificity (%)
GRS (%)	0.607	0.0595	0.096	0.507–0.701	44.91	53.13	68.49
GCS (%)	0.601	0.0608	0.073	0.501–0.696	−17.73	71.87	52.05
GLS (%)	0.893	0.0339	<0.001	0.818–0.945	−17.06	93.75	71.23
LVtw (°)	0.814	0.0463	<0.001	0.727–0.883	12.97	75.00	80.82
MCI (:%×°)	0.915	0.0328	<0.001	0.845–0.961	−210.89	84.37	90.41

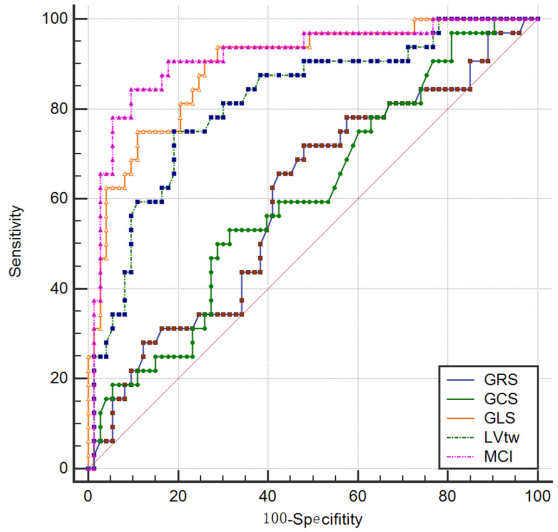

FIGURE 2
ROC curve for 2D-STE parameters and MCI.

if the difference in LVEF measured by 2D echocardiography among paitents in different stages reaches 10%. However, this is the same magnitude of change used to adjudicate CTRCD. Therefore, scholars doubt the sensitivity of LVEF measured by 2D echocardiography in diagnosing CTRCD (9).

In addition, many studies have shown that the myocardium has been injured before the abnormal LVEF occurs (2), and the myocardial injury has been irreversible at that time (1), so that the timing for cardioprotective intervention is delayed. Therefore, LVEF is not sensitive for early detection of subclinical heart disease, and it cannot sensitively reflect the small changes in left ventricular function.

Based on this, clinicians have been trying to diagnose this latent subclinical myocardial injury before LVEF is significantly reduced in clinical practice. At present, the imaging diagnosis methods of subclinical LV dysfunction mainly contain various new ultrasound technologies such as velocity vector imaging, strain rate imaging, tissue Doppler imaging and STE, of which, the STE technique (mainly including 2D-STE and 3D-STE techniques) is not affected by the angle of sound beam and thus can be used to perform quantitative analyses, which can also be visually displayed with the "bull's eye diagram" at the same time, it has the characteristics of sustainable dynamic detection and low cost, shows increasing obvious advantages and has become a research hotspot in recent years. The main observation indexes of STE technique include parameters such as longitudinal strain, radial strain, circumferential strain, area strain, twist and synchronization of left ventricular myocardium. The STE technique is not only used to analyze the basal segment, the middle segment and the apical segment of the standard section separately, but also used to stratifiedly analyze the epimyocardium, mid-myocardium and endomyocardium of the left ventricular wall. It is recommended by the consensus committee consisting of ASE and EACV that a relative reduction of more than 15% in GLS from baseline in patients receiving anticancer therapy can be used as a diagnostic criterion for subclinical LV dysfunction (9). In this study, finally it was found that 22 patients met the diagnostic criteria for subclinical LV dysfunction.

Assessment of anthracycline -induced cardiotoxicity by global longitudinal strain, left ventricular twist and myocardial composite index

Many studies have shown that GLS is considered to be the most sensitive marker of subclinical LV dysfunction in the application of 2D-STE (11–14), and there are mainly the following two views on its pathological basis: (1) According to Torrent-Guasp's myocardial band theory, the cardiac pulsation is composed of a complex towel-wringing-like movement of the myocardium; and (2) the endomyocardium is mainly composed of longitudinal myocardial fibers responsible for longitudinal movement, and the endocardium is more vulnerable to damage due to its direct contact with chemotherapy drugs. In this study, there was a difference in GLS between patients in the interim chemotherapy stage and at baseline, and GLS was decreased gradually with the increase of the cumulative dose of adriamycin, which was similar to previous research results at home and abroad.

This study also showed that LVtw also presented a good diagnostic value, and there was a significant difference in LVtw between patients in the interim chemotherapy stage and at baseline, which was decreased continuously with the

increase of the cumulative dose of adriamycin. An in vitro study has confirmed that there are two main mechanisms for the decrease in twist mechanics in patients treated with anthracycline drugs. First, Anthracycline drugs can cause myofilament degradation by activating calpain, resulting in myofilament disorder. Carnosine is the largest known protein and a component of myofilament system, and its effect on the activation and recovery of cardiomyocytes has been confirmed. Second, it has been reported that twist mechanics is closely related to the transmural gradient of carnosine subtypes in animal models (15).

Systole and diastole of left ventricle are a complex movement process in 3D space, which can be divided into the longitudinal, radial and circumferential movements, and its own torsion movement at the same time. MCI can comprehensively analyze the movements in both directions of left ventricular twist and longitudinal strain at the same time. Previous studies have shown that MCI has a better diagnostic efficacy compared with the index in single direction for early cardiotoxic injury (11–13, 16). In this study, there were no differences in GLS and LVtw between patients in the early chemotherapy stage and at baseline, but MCI combining two parameters such as GLS and LVtw showed a difference between patients in the early chemotherapy stage and at baseline. Meanwhile, MCI showed a trend of continuous worsening with the increase of chemotherapy cycles, indicating that MCI was related to the cumulative dose of adriamycin. Moreover, the area under the curve (AUC) of MCI was largest after ROC analysis, and its diagnostic efficacy was higher than those of other parameters in a single direction.

In a previous study on the latest 3D-STE technique, the global area strain (GAS) has been used as a new index, which simultaneously integrates the longitudinal and circumferential strains of the myocardium (17). Compared with the strain in a single direction, the GAS is superior to the conventional strain parameters in detecting early left ventricular systolic dysfunction (18, 19).

At present, there are few research reports on MCI, and more research data are needed to evaluate the subclinical LV dysfunction. In addition, MCI needs to be calculated manually. Subsequently, if the echocardiography manufacturers can realize the objective of directly calculating this index in the analysis software used for the STE technique, the convenience of operation will can be improved.

Clinical significance

This study shows that STE technique is of great significance in identifying early myocardial injury, and can help clinicians predict the cardiotoxicity of anthracycline in the treatment of breast cancer patients earlier. Because the cardiac pulsation is a complex 3D movement, MCI can comprehensively analyze the movements of the heart in the multi-dimensional space, and can detect the subclinical cardiac injury earlier. This index can help clinicians timely participate in the cardioprotective treatment, control the accumulated dose of chemotherapy drug and reduce the cardiotoxicity of drugs to avoid the irreversible myocardial injury.

Limitations

The limitations of this study were as follows: (1) The sample size of this study was small, and we will conduct a relative study with a larger sample size in the future; (2) the patients in this study were followed up for a short period of time, and the long-term effects of chemotherapy drugs on various cardiac parameters could not be observed; (3) biomarkers such as troponin were not included into this study, and these indexes can be included into subsequent study; and (4) the selected patients were not analyzed using 3D-STE technique, and GAS was not included in the comparative analysis, which will be analyzed in the future studies.

Conclusion

STE technique can detect anthracycline-induced myocardial injury in time; compared with 2D-STE parameters in a single direction (GLS, GCS, GRS, and LVtw), MCI can detect subclinical LV dysfunction earlier and has a better diagnostic efficiency; the patients receiving anthracycline chemotherapy may have subclinical LV dysfunction even if their LVEF is normal, and the subclinical LV dysfunction is manifested as deteriorated GLS, LVtw, and MCI, which are correlated with the cumulative dose of anthracycline drugs.

Data availability statement

The original contributions presented in the study are included in the article/supplementary material, further inquiries can be directed to the corresponding author.

Ethics statement

The study was approved by the ethics committee of Nantong Third People's Hospital. The patients/participants

provided their written informed consent to participate in this study.

Author contributions

JZ and JW designed the study. HJ, JZ, SX, and XG contributed to data collection, analyses and interpretation. JZ contributed to the statistical analysis. HJ, JZ, and JW contributed to the manuscript writing, reviewing and editing. All authors read and approved the final manuscript.

Funding

This study was supported by Nantong Municipal Health Commission (No. MB2021055).

Conflict of interest

The authors declare that the research was conducted in the absence of any commercial or financial relationships that could be construed as a potential conflict of interest.

Publisher's note

References

1. Lipshultz SE, Lipsitz SR, Sallan SE, Dalton VM, Mone SM, Gelber RD, et al. Chronic progressive cardiac dysfunction years after doxorubicin therapy for childhood acute lymphoblastic leukemia. *J Clin Oncol.* (2005) 23:2629–36. doi: 10.1200/JCO.2005.12.121

2. Lipshultz SE, Rifai N, Sallan SE, Lipsitz SR, Dalton V, Sacks DB, et al. Predictive value of cardiac troponin T in pediatric patients at risk for myocardial injury. *Circulation.* (1997) 96:2641–8. doi: 10.1161/01.CIR.96.8.2641

3. Chinese Society of Clinical Oncology, Chinese Anti-cancer Association, Chinese Society of Hematology, Chinese Medical Association. [An interpretation of expert panel consensus statement on prevention and treatment of anthracycline cardiotoxicity]. *Chin. J. Hematol.* (2011) 32:727–8. doi: 10.3760/cma.j.issn.0253-2727.2011.10.25

4. Chinese Society of Hematology. Chinese expert consensus on prevention and treatment of cardiotoxicity of anthracycline antineoplastic drugs (2011 edition). *J Clin Oncol.* (2011) 16:1122–9. doi: 10.3969/j.issn.1009-0460.2011.12.017

5. Barry E, Alvarez JA, Scully RE, Miller TL, Lipshultz SE. Anthracycline-induced cardiotoxicity: course, pathophysiology, prevention and management. *Expert Opin Pharmacother.* (2007) 8:1039–58. doi: 10.1517/14656566.8.8.1039

6. Vejpongsa P, Yeh ET. Prevention of anthracycline-induced cardiotoxicity: challenges and opportunities. *J Am Coll Cardiol.* (2014) 64:938–45. doi: 10.1016/j.jacc.2014.06.1167

7. Simůnek T, Stérba M, Popelová O, Adamcová M, Hrdina R, Gersl V. Anthracycline-induced cardiotoxicity: overview of studies examining the roles of oxidative stress and free cellular iron. *Pharmacol Rep.* (2009) 61:154–71. doi: 10.1016/S1734-1140(09)70018-0

8. Nelson-Veniard M, Thambo JB. [Chemotherapy-induced cardiotoxicity: incidence, diagnosis and prevention]. *Bull Cancer.* (2015) 102:622–6. doi: 10.1016/j.bulcan.2015.03.014

9. Plana JC, Galderisi M, Barac A, Ewer MS, Ky B, Scherrer-Crosbie M, et al. Expert consensus for multimodality imaging evaluation of adult patients during and after cancer therapy: a report from the American society of echocardiography and the European association of cardiovascular imaging. *J Am Soc Echocardiogr.* (2014) 27:911–39. doi: 10.1016/j.echo.2014.07.012

10. Sawaya H, Sebag IA, Plana JC, Januzzi JL, Ky B, Cohen V, et al. Early detection and prediction of cardiotoxicity in chemotherapy-treated patients. *Am J Cardiol.* (2011) 107:1375–80. doi: 10.1016/j.amjcard.2011.01.006

11. Yong H, Ming C, Qu J, Xia L, Yun D, Min X, et al. The role of speckle tracking echocardiography in identifying postoperative chemotherapeutic cardiotoxicity in patients with breast cancer. *Chin J Med Ultrasound.* (2014) 11:397–402. doi: 10.3877/cma.j.issn.1672-6448.2014.05.009

12. Liu B, Zheng H, Zhou W, Xu FF, Zhang JX. Evaluation of occult myocardial toxicity in GP chemotherapy regimen of lung cancer patients by 3D-STI combined with cardiac comprehensive index. *Med Inform.* (2019) 32:100–4.

13. Xu FF, Zheng H, Hu LL, Chen N, Zhou W, Li CM, et al. Evaluation of cardiotoxicity after receiving anthracycline in patients with breast cancer by using myocardial composite index based on 3D-STI. *Acta Univ Med Anhui.* (2018) 53:146–51. doi: 10.19405/j.cnki.issn1000-1492.2018.01.03

14. Potter E, Marwick TH. Assessment of left ventricular function by echocardiography: the case for routinely adding global longitudinal strain to ejection fraction. *JACC Cardiovasc Imaging.* (2018) 11(2 Pt 1):260–74. doi: 10.1016/j.jcmg.2017.11.017

15. Motoki H, Koyama J, Nakazawa H, Aizawa K, Kasai H, Izawa A, et al. Torsion analysis in the early detection of anthracycline-mediated cardiomyopathy. *Eur Heart J Cardiovasc Imaging.* (2012) 13:95–103. doi: 10.1093/ejechocard/jer172

16. Mornoş C, Petrescu L. Early detection of anthracycline-mediated cardiotoxicity: the value of considering both global longitudinal left ventricular strain and twist. *Can J Physiol Pharmacol.* (2013) 91:601–7. doi: 10.1139/cjpp-2012-0398

17. Yao J, Xu D, Dai Y, Zhang YJ, Xie B, Li XQ. Evaluation of left ventricular contraction pattern and function in normal subjects with area strain. *Chin J Ultrasonogr.* (2013) 22:1–5. doi: 10.3760/cma.j.issn.1004-4477.2013.01.001

18. Galderisi M, Esposito R, Schiano-Lomoriello V, Santoro A, Ippolito R, Schiattarella P, et al. Correlates of global area strain in native hypertensive patients: a three-dimensional speckle-tracking echocardiography study. *Eur Heart J Cardiovasc Imaging.* (2012) 13:730–8. doi: 10.1093/ehjci/jes026

19. Wen H, Liang Z, Zhao Y, Yang K. Feasibility of detecting early left ventricular systolic dysfunction using global area strain: a novel index derived from three-dimensional speckle-tracking echocardiography. *Eur J Echocardiogr.* (2011) 12:910–6. doi: 10.1093/ejechocard/jer162

frontiers | Frontiers in Cardiovascular Medicine

TYPE Original Research
PUBLISHED 12 August 2022
DOI 10.3389/fcvm.2022.983803

OPEN ACCESS

EDITED BY
Jia Qi,
Shanghai Jiao Tong University, China

REVIEWED BY
Xuelian Wang,
Shanghai General Hospital, China
Sheng Cai,
Zhejiang University, China

*CORRESPONDENCE
Jianguo He
hejianguofw@163.com

SPECIALTY SECTION
This article was submitted to General Cardiovascular Medicine, a section of the journal Frontiers in Cardiovascular Medicine

RECEIVED 01 July 2022
ACCEPTED 28 July 2022
PUBLISHED 12 August 2022

CITATION
Lin Y, Pang L, Huang S, Shen J, Wu W, Tang F, Su W, Zhu X, Sun J, Quan R, Yang T, Han H and He J (2022) Impact of borderline pulmonary hypertension due to left heart failure on mortality in a multicenter registry study: A 3-year survivorship analysis. *Front. Cardiovasc. Med.* 9:983803. doi: 10.3389/fcvm.2022.983803

Impact of borderline pulmonary hypertension due to left heart failure on mortality in a multicenter registry study: A 3-year survivorship analysis

Yangyi Lin[1], Lingpin Pang[2], Shian Huang[2], Jieyan Shen[3], Weifeng Wu[4], Fangming Tang[5], Weiqing Su[6], Xiulong Zhu[7], Jingzhi Sun[8], Ruilin Quan[1], Tao Yang[1], Huijun Han[9] and Jianguo He[1]*

[1]Department of Pulmonary Vascular Disease, State Key Laboratory of Cardiovascular Disease, Fuwai Hospital, National Center for Cardiovascular Diseases, Chinese Academy of Medical Sciences & Peking Union Medical College, Beijing, China, [2]Cardiovascular Medicine Center, Affiliated Hospital of Guangdong Medical University, Zhanjiang, China, [3]Department of Cardiology, Renji Hospital, Shanghai Jiaotong University School of Medicine, Shanghai, China, [4]Department of Cardiology, The First Affiliated Hospital of Guangxi Medical University, Nanning, China, [5]Department of Cardiology, Nongken Central Hospital of Guangdong Province, Zhanjiang, China, [6]Department of Cardiology, Lianjiang People's Hospital, Lianjiang, China, [7]Department of Cardiology, People's Hospital of Gaozhou, Gaozhou, China, [8]Department of Cardiology, Affiliated Hospital of Jining Medical University, Jining, China, [9]Department of Epidemiology and Biostatistics, Institute of Basic Medical Sciences, Chinese Academy of Medical Sciences and School of Basic Medicine, Peking Union Medical College, Beijing, China

Background: Patients with left heart failure (LHF) are often associated with the development of pulmonary hypertension (PH) which leads to an increased risk of death. Recently, the diagnostic standard for PH has changed from mean pulmonary arterial pressure (mPAP) ≥25 mmHg to >20 mmHg. Nonetheless, the effect of borderline PH (mPAP: 21–24 mmHg) on the prognosis of LHF patients is unclear. This study aimed to investigate the relationship between borderline PH and 3-year clinical outcomes in LHF patients.

Methods: A retrospective analysis of a prospective cohort study was done for LHF patients who underwent right heart catheterization (RHC) between January 2013 and November 2016. The primary outcome was all-cause mortality; the secondary outcome was rehospitalization.

Results: Among 344 patients, 62.5% were identified with a proportion of PH (mPAP ≥ 25), 10.8% with borderline PH (21–24), and 26.7% with non-PH (≤20), respectively. Multivariable Cox analysis revealed that borderline PH patients had a higher adjusted mortality risk (HR = 3.822; 95% CI: 1.043–13.999; $p = 0.043$) than non-PH patients. When mPAP was treated as a continuous variable, the hazard ratio for death increased progressively with increasing mPAP starting at 20 mmHg (HR = 1.006; 95% CI: 1.001–1.012). There was no statistically significant difference in adjusted rehospitalization between borderline PH and non-PH patients (HR = 1.599; 95% CI: 0.833–3.067; $p = 0.158$).

Conclusions: Borderline PH is independently related to increased 3-year mortality in LHF patients. Future research is needed to evaluate whether more

close monitoring, and managing with an intensifier improves clinical outcomes in borderline PH caused by LHF.

Clinical trials registration: www.clinicaltrials.gov NCT02164526.

KEYWORDS

borderline pulmonary hypertension, left heart failure, mean pulmonary artery pressure (mPAP), mortality, right heart catheterization (RHC)

Introduction

Pulmonary hypertension (PH) due to left heart failure (PH-LHF), also known as post-capillary pulmonary hypertension [pulmonary arterial wedge pressure (PAWP) >15 mmHg], is the most prevalent kind of PH, affecting around 5% of people aged 65 and older (1). Elevated mean pulmonary arterial pressure (mPAP) of ≥25 mmHg determined by right heart catheterization (RHC) at rest in supine position is the essential condition for PH diagnosis (2, 3). However, in the 6th World Symposium on Pulmonary Hypertension (WSPH), this threshold value was dropped to 20 mmHg to define PH for all subgroups (mPAP > 20 mmHg) (4). Nonetheless, data on modestly raised mPAP (21–24 mmHg), sometimes known as borderline PH, remain scarce (5). This proposal has sparked extensive debate among academic institutions (6, 7).

Opponents have stated that the diagnosis is "life-threatening," but no approved or evidence-based therapy is available so far, the immediate and profound psychological damage may outweigh the benefits of an early PH diagnosis. Furthermore, physicians may face treatment dilemmas, such as whether borderline PH patients may be administered off-label treatment (6). As no specific PH treatment is currently available, the new criterion has little or no impact on therapy for PH-LHF patients (8). Should the new hemodynamic criterion be worth adopting in LHF patients? Therefore, investigating the outcome of borderline PH-LHF will provide an essential foundation for deciding whether to adopt the new criterion or not.

Although previous researches have suggested that mPAP may be prognostic in patients with left heart disease, it is unknown whether borderline PH worsens mortality in people with LHF. For instance, one study revealed that mPAP is the strongest hemodynamic predictor of mortality in patients with LHF. However, this study did not analyze whether there is a survival difference between patients without PH (mPAP ≤ 20 mmHg) and those with borderline PH (9). Additionally, two large cohort studies demonstrated that the borderline PH is associated with an increased risk of death (10, 11). Nevertheless, they defined borderline PH as mPAP between 19 and 24 mmHg, and LHF proportion was 8.8 and 48.2%, respectively, in their recruited patients. As a result, their outcomes may be insufficient in LHF patients. Thus, our study sought to determine whether borderline PH is related to higher mortality in LHF patients.

Materials and methods

Study design and participants

The study design and patient selection flowchart is shown in Figure 1, which was a retrospective analysis of a prospective, multicenter registry study of LHF patients who received RHC between January 2013 and November 2016. The study protocol was approved by Fuwai Hospital's Institutional Review Board (Approval No. 2012-401) and was carried out adopting the Helsinki Declaration, and was registered on ClinicalTrials.gov (Identifier: NCT02164526). All patients enrolled were provided written informed consent.

Patients were enrolled in the study according to the following criteria: (1) patients with a verified diagnosis of LHF following the current heart failure guideline (12). (2) patients who underwent RHC between January 2013 and November 2016. Patients were excluded if they met any of the following criteria: (1) hypertrophic obstructive cardiomyopathy; (2) right ventricular outflow tract stenosis; (3) pericardial disease; (4) patients with chronic lung disease; (5) HF due to valvular heart disease; (6) pre-capillary PH (mPAP > 20 mmHg, PAWP ≤ 15 mmHg).

Measurements and data collection

PH-LHF patients were extensively clinically assessed by PH experts to exclude PH due to other etiologies. Biochemical blood tests were performed within 24-h of admission. The initial measurement on admission was used to acquire the blood pressure, heart rate, echocardiographic, and biochemical parameters. RHC and left heart catheterization were used to achieve hemodynamic parameters. RHC was conducted to confirm a physician's diagnosis of suspected PH-LHF, performed in stable and non-acute clinical settings. PAWP was measured at end-diastole at rest; when PAWP measurement is unreliable, left cardiac catheterization was used to determine left ventricular end-diastolic pressure (LVEDP). Traditionally defined PH is an increase in mPAP ≥ 25 mmHg at rest; borderline PH is defined as an mPAP value of 21–24 mmHg. Coronary artery disease (CAD) is defined as 50% or more stenosis of at least one coronary artery by quantitative coronary angiography

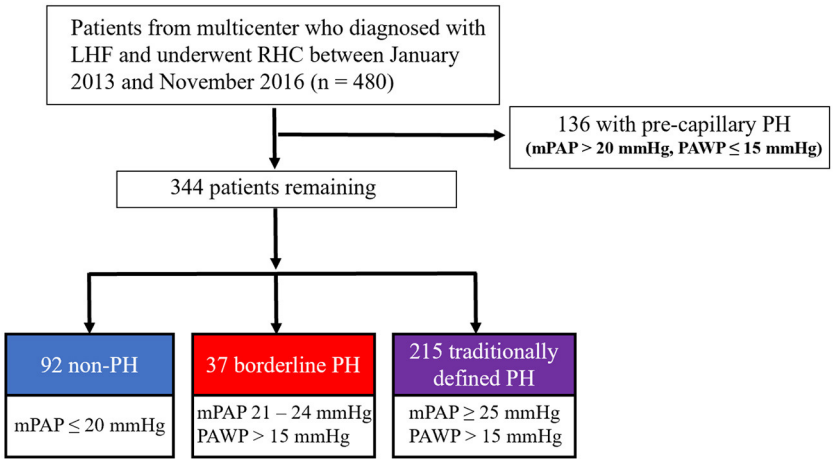

FIGURE 1
The study design and flowchart for the selection of patients. LHF, left heart failure; RHC, right heart catheterization; PH, pulmonary hypertension.

or having a prior physician-documented history of CAD. HFpEF, HFmrEF, and HFrEF are defined as left ventricular ejection fraction (LVEF) ≥ 50%, LVEF 41–49%, and LVEF ≤ 40%, respectively. All enrolled patients had data from two-dimensional echocardiography and RHC. Medical histories, demographics, baseline clinical and radiograph data, laboratory results, and treatments were reviewed from our registry study's database records.

Exposure

The exposure was mPAP as reported in our dataset. To determine if borderline PH affects mortality in patients with LHF, patients were divided into three groups i.e., non-PH (mPAP ≤ 20 mmHg), borderline PH (mPAP: 21–24 mmHg), and the traditionally defined PH (mPAP ≥ 25 mmHg) (2).

Outcomes and follow-up

Our primary outcome measure was the time interval between enrolment and all-cause mortality. The secondary outcome measure was the time interval between enrollment and rehospitalization for any reason. Every 6 months ± 2 weeks, patients were followed up by phone calls, messages, or outpatient visits, and it was confirmed whether they died or were re-hospitalized at each follow-up. Patients who could not be reached by phone, message, hospital system, or other available means more than three times and lasted for more than 6 months were defined as lost to follow-up.

Missing and extreme data

Linear interpolation was used to handle the missing variables, which were then fed into the multivariable model for analysis. Missing data was defined as the absence of both values concurrently for variables with the same clinical significance, such as BNP and NT-proBNP. Biomarker levels below the detection limit were set to half that level, while those over the detection limit were set to the upper limit level. Hemodynamic parameters were examined for physiologically incredible values, which were classified as mPAP <5 or >80 mmHg, and PAWP <0 or >60 mmHg. As a result, none of the patients possessed extraordinary values.

Statistical analysis

The statistical analysis was performed using R (version 4.0.2) and SPSS (version 24.0). Continuous variables were presented as mean ± standard deviation for normally distributed data, or, in case of skewed distributions, median with interquartile range (IQR, 25th−75th percentiles), categorical variables were reported as counts and percentages (%). Whenever appropriate, continuous variables were transformed into categorical variables using a median or mean in regression analysis. The baseline demographic, clinical, and hemodynamic characteristics of non-PH, borderline PH, and traditionally defined PH groups were compared using one-way analysis of variance (ANOVA) with least significant difference (LSD) *post hoc* test or Games-Howell *post hoc* test for normally distributed variables, Kruskal-Wallis with Bonferroni correction *post hoc* test for skew distributed variables and the Chi-square test for categorical variables. We

TABLE 1 Baseline demographic, clinical and hemodynamic characteristics by non-PH, borderline PH, and traditionally defined PH status.

	mPAP (mmHg)				
	≤20 (*n* = 92)	21–24 (*n* = 37)	≥25 (*n* = 215)	P value	*P* for trend
Age (years)	62.7 ± 11.1	61.8 ± 11.8	63.8 ± 12.4	0.557	0.401
Female, *n* (%)	19 (20.7%)	9 (24.3%)	63 (29.3%)	0.317	0.498
BMI (kg/m^2)	22.3 ± 2.6	21.8 ± 2.0	23.2 ± 3.0*#	0.005	0.006
NYHA FC, *n* (%)					
II	72 (78.3%)	30 (81.1%)	126 (58.6%)*#	0.001	<0.001
III/IV	20 (21.7%)	7 (18.9%)	89 (41.4%)*#	0.001	<0.001
Types of HF					
HFpEF, *n* (%)	76 (82.6%)	31 (83.8%)	148 (68.8%)*#	0.015	0.007
HFmrEF, *n* (%) ∫∫	3 (3.3%)	3 (8.1%)	40 (18.6%)		
HFrEF, *n* (%) ∫∫	13 (14.1%)	3 (8.1%)	27 (12.6%)		
Heart rate (bpm)	74.1 ± 14.6	75.7 ± 12.9	76.8 ± 15.2	0.327	0.136
Respiratory rate (bpm)	19.3 ± 1.8	18.9 ± 2.2	19.4 ± 1.9	0.268	0.425
SBP (mmHg)	138.1 ± 23.2	135.7 ± 20.0	132.7 ± 22.8	0.152	0.052
DBP (mmHg)	79.5 ± 14.5	75.4 ± 12.1	76.3 ± 12.1	0.100	0.064
CAD, *n* (%)	77 (83.7%)	30 (81.1%)	156 (72.6%)	0.085	0.029
Hypertension, *n* (%)	41 (44.6%)	18 (48.6%)	100 (46.5%)	0.906	0.791
Hyperlipidemia, *n* (%)	20 (21.7%)	7 (18.9%)	60 (27.9%)	0.335	0.208
Diabetes, *n* (%)	25 (27.2%)	8 (21.6%)	59 (27.4%)	0.757	0.878
Ischemic stroke, *n* (%) ∫∫	7 (7.6%)	2 (5.4%)	16 (7.5%)		
Biochemistry					
Hemoglobin (g/L)	134.0 ± 15.4	133.6 ± 20.5	132.5 ± 20.4	0.820	0.537
Platelet (×10^9/L)	220.5 ± 60.5	225.8 ± 77.5	220.6 ± 70.3	0.909	0.963
ALT (IU/L)	21.5 (14.6/35.2)	22.4 (15.2/36.2)	22.2 (15.5/37.0)	0.695	0.512
AST (IU/L)	21.0 (16.0/35.9)	21.0 (17.2/31.0)	23.2 (17.0/37.1)	0.775	0.983
TBil (umol/L)	11.8 (8.0/16.7)	12.0 (9.0/15.9)	12.0 (8.0/17.7)	0.968	0.357
Albumin (g/L)	39.7 ± 4.8	40.3 ± 5.5	39.1 ± 5.3	0.361	0.300
FBG (mmol/L)	5.1 (4.7/5.9)	5.1 (4.8/6.1)	5.4 (4.7/6.3)	0.100	0.040
eGFR (ml/min)	74.9 ± 27.9	70.2 ± 21.3	72.6 ± 30.8	0.675	0.590
BUN (mmol/L)	5.3 (4.0/7.3)	5.2 (4.1/6.8)	5.4 (4.3/7.0)	0.683	0.857
Uric acid (umol/L)	343.1 ± 111.4	404.3 ± 126.7*	383.6 ± 125.1*	0.009	0.016
Natriuretic peptides					
BNP (pg/mL)	168.5 (120.0/378.4)	164.0 (111.5/466.5)	337 (185.7/649.5)	0.054	0.608
NT-proBNP (pg/mL)	353.5 (100.8/1459.3)	250.0 (110.0/994.2)	1039.0 (235.0/2528.5)*#	0.003	0.014
Triglyceride (mmol/L)	1.5 (1.0/2.2)	1.5 (1.0/2.2)	1.4 (1.0/2.0)	0.923	0.827
Cholesterol (mmol/L)	4.6 (3.7/5.5)	4.8 (4.0/5.8)	4.5 (3.6/5.6)	0.409	0.639
LDL (mmol/L)	2.5 (1.7/3.5)	2.9 (1.9/3.3)	2.7 (2.1/3.6)	0.608	0.744
HDL (mmol/L)	1.2 ± 0.4	1.2 ± 0.4	1.1 ± 0.3	0.160	0.092
RHC					
mRAP (mmHg)	9.6 ± 3.9	12.7 ± 3.4*	14.6 ± 4.2*#	<0.001	<0.001
RVSP (mmHg)	28.7 ± 6.2	33.2 ± 7.1*	47.8 ± 13.1*#	<0.001	<0.001
RVEDP (mmHg)	9.0 (6.8/12.0)	11.0 (9.5/13.0)*	15.0 (10.8/16.0)*#	<0.001	<0.001
sPAP (mmHg)	28.6 ± 6.9	33.4 ± 4.1*	48.2 ± 12.2*#	<0.001	<0.001
dPAP (mmHg)	12.9 ± 3.1	18.3 ± 3.1*	24.0 ± 7.0*#	<0.001	<0.001
mPAP (mmHg)	18.0 (17.0/20.0)	22.0 (21.0/23.0)*	30.0 (27.0/36.0)*#	<0.001	<0.001
PAWP (mmHg)	17.0 (16.0/20.0)	19.5 (17.0/24.0)	19.0 (17.0/24.5)	0.353	0.581
LVEDP (mmHg)	14.0 (12.0/15.0)	18.0 (16.0/21.0)*	17.0 (16.0/20.0)*	<0.001	<0.001

(Continued)

TABLE 1 Continued

	mPAP (mmHg)				
	≤20 ($n = 92$)	21–24 ($n = 37$)	≥25 ($n = 215$)	P value	*P* for trend
Echocardiography					
LAAPD (mm)	33.4 ± 5.1	32.8 ± 4.7	36.6 ± 7.2*#	<0.001	<0.001
LVEDD (mm)	45.5 ± 6.5	46.1 ± 7.8	50.8 ± 8.5*#	<0.001	<0.001
RVAPD (mm)	18.4 ± 3.3	18.4 ± 1.9	20.8 ± 6.1*#	<0.001	0.001
LVEF (%)	55.4 ± 10.2	56.6 ± 9.1	53.3 ± 11.0	0.104	0.081
PE, *n* (%)∫∫	3 (3.3%)	1 (2.7%)	11 (5.1%)		
Medications, *n* (%)					
Aldactone	25 (27.2%)	11 (29.7%)	125 (58.1%)*#	<0.001	<0.001
ACEI	37 (40.2%)	14 (37.8%)	98 (45.6%)	0.532	0.337
ARB	19 (20.7%)	12 (32.4%)	50 (23.3%)	0.321	0.644
Beta blocker	65 (70.7%)	24 (64.9%)	149 (69.3%)	0.811	0.884
Diuretic	27 (29.3%)	9 (24.3%)	108 (50.2%)*#	<0.001	<0.001
CCB	16 (17.4%)	6 (16.2%)	44 (20.5%)	0.730	0.491
Statin	83 (90.2%)	31 (83.8%)	185 (86.0%)	0.511	0.370
Antiplatelet	72 (78.3%)	28 (75.7%)	186 (86.5%)	0.092	0.054

Among the 326 patients, the number of missing values for the covariates were: 1 (0.3%) for Platelet; 2 (0.6%) for ALT and Albumin; 3 (0.9%) for AST, Tbil, Uric acid, and RVEDP; 4 (1.2%) for Triglyceride, Cholesterol, HDL, and RVSP; 5 (1.5%) for LDL and mRAP; 6 (1.7%) for FBG; 18 (5.2%) for RVAPD; 42 (12.2%) for Natriuretic peptides.

PH, pulmonary hypertension; mPAP, mean pulmonary artery pressure; BMI, body mass index; NYHA FC, New York Heart Association Functional Class; HF, heart failure; HFrEF, heart failure with reduced ejection fraction; HFmrEF, heart failure with mildly reduced ejection fraction; HFpEF, left ventricular diastolic dysfunction heart failure with preserved ejection fraction; SBP, systolic blood pressure; DBP, diastolic blood pressure; CAD, coronary artery disease; ALT, alanine aminotransferase; AST, aspartate aminotransferase; TBil, total bilirubin; FBG, fasting blood glucose; eGFR, estimated glomerular filtration rate; BUN, blood urea nitrogen; BNP, b-type natriuretic peptide; NT-pro BNP, N-terminal pro b-type natriuretic peptide; LDL, low-density lipoprotein cholesterol; HDL, high-density lipoprotein cholesterol; RHC, right heart catheterization; mRAP; mean right atrial pressure; RVSP, right ventricular systolic pressure; RVEDP, right ventricular end diastolic pressure; sPAP, systolic pulmonary artery pressure; dPAP, diastolic pulmonary artery pressure; mPAP, mean pulmonary artery pressure; PAWP, pulmonary artery wedge pressure; LVEDP, left ventricular end-diastolic pressure; LAAPD, left atrial anteroposterior diameter; LVEDD, left ventricular end diastolic diameter; RVAPD, right ventricular anteroposterior diameter; LVEF, left ventricular ejection fraction; PE, Pericardial effusion; ACEI, angiotensin-converting enzyme inhibitors; ARB, angiotensin receptor blocker; CCB, calcium channel blocker.

*$p < 0.05$ vs. without PH (mPAP ≤ 20 mmHg).

#$p < 0.05$ vs. borderline PH (21 ≤ mPAP ≤ 24 mmHg).

∫∫ A Chi-square test was not performed in these variables of very low counts.

employed one-way ANOVA with trend analysis or Linear-by-Linear Associated trend analysis to determine whether variables tended in one direction across groups. To identify factors linked with PH, univariate and multivariate logistic regression were used. Kaplan-Meier survival curves were produced using either death or rehospitalization as events, and log-rank tests were used to make unadjusted group comparisons for time to event outcomes. Patients with more than 3 years of follow-up were censored after 36 months. Univariate Cox proportional hazard regression analyses were followed by multivariate Cox proportional hazard regression to identify predictors of death or rehospitalization. The proportionality of hazards for each variable was determined by examining the statistical significance of interactions between follow-up time and variables. A cubic spline model was built to describe the association between mPAP and all-cause mortality hazard ratio (HR); the number of knots was chosen to produce the best fit as measured by the Akaike information criteria. To determine the predictive accuracy of mPAP for mortality, the Youden's index and area under the curve of the time-dependent receiver operating characteristic (ROC) curve were determined. The statistical significance level was established at 0.05 on a two-sided scale.

Results

Characteristics of study population

After applying the inclusion and exclusion criteria, 92 (26.7%) patients were found to be without PH, 37 (10.8%) with borderline PH, and 215 (62.5%) with traditionally defined PH and were regarded as appropriate for this study (Figure 1). This cohort study patients were primarily male subjects ($n = 253$, 73.5%) and had been diagnosed with LHF within 30 days ($n = 298$, 86.6%) with a mean age of 63.3 years (standard deviation [*SD*], 12.0 years) for all included patients. The median mPAP was 27 mmHg (interquartile range [IQR], 20–32 mmHg; minimum, 7 mmHg; maximum, 70 mmHg), and the distribution of mPAP is depicted in the histogram (Supplementary figure S1).

The median PAWP was found to be 19 mmHg (IQR, 17–24 mmHg; minimum, 16 mmHg; maximum, 45 mmHg), and mean ejection fraction (EF) was 54.2% (*SD*, 10.6%; minimum, 16%; maximum, 80.0%). CAD was the most prevalent co-morbidity (n = 263, 76.5%); among which, 208 (79.1%) had HFpEF, 32 (12.2%) had HFmrEF, and 23 (8.7%) had HFrEF. Table 1 summarizes the cohort's baseline demographic, clinical, and hemodynamic parameters. Except for the uric acid and hemodynamic variables determined by RHC, there were no significant differences between the non-PH and borderline PH groups (Table 1). Covariate variables had missing values ranging from 0.3% for platelets to 12.2% for natriuretic peptides (Table 1).

Impact of borderline PH on outcomes

Within 3 years, 18 (5.2%) patients were lost to follow-up, one with borderline PH, four with non-PH, and 13 with traditionally defined PH. The Kaplan-Meier survival analysis revealed that the unadjusted mortality was intermediated for borderline PH relative to traditionally defined PH and the non-PH group (Figure 2A), with a 3-year mortality rate of 4.5% for the non-PH group, 16.7% for the borderline PH group, and 23.1% for traditionally defined PH group, respectively. The non-PH, borderline PH and traditionally defined PH groups had 1-year death rates of 1.1, 2.8, and 5.2%, respectively, while it was 2.2, 8.3, and 13.3% in 2 years. After controlling for clinical factors that were individually significant in univariate Cox regression analysis, the traditionally defined PH group had the maximum mortality hazard ratio (HR = 4.023; 95% CI: 1.411–11.465; p = 0.009). Additionally, a 3.8-fold increase in the risk of adjusted hazard for mortality in the borderline PH group (HR = 3.822; 95% CI: 1.043–13.999; p = 0.043) compared to the non-PH group (Table 2) was observed. By employing either forward or backward stepwise regression, borderline and traditionally defined PH were retained in the model and demonstrated the most significant predictive performance. Furthermore, we also observed that the rehospitalization was intermediated for borderline PH relative to traditionally defined PH and the non-PH group (Figure 2B), with 3-year rehospitalization rates of 27.3% for the non-PH group, 40.5% for borderline PH group, and 53.7% for traditionally defined PH group, respectively. The 1-year rehospitalization rates were 14.1% for non-PH, 21.6% for borderline PH, and 24.0% for traditionally defined PH, respectively, while they were 22.9, 32.4, and 43.5%, respectively, after 2 years. The adjusted HR for rehospitalization was highest in patients with traditional defined PH (HR = 2.010; 95% CI: 1.263–3.197; p = 0.003), but there was no statistically significant difference in the increased HR in borderline PH patients compared to the non-PH group (HR = 1.599; 95% CI: 0.833–3.067; p = 0.158) (Supplement Table S1). The small sample size may explain this result.

Impact of mPAP on mortality

When mPAP was treated as a continuous variable, the adjusted HR for all-cause mortality increased promptly and incrementally across a wide range of mPAP values, beginning at 20 mmHg (HR = 1.006; 95% CI: 1.001–1.012) and continuing to 70 mmHg (Figure 3A). Additionally, it was discovered that a one mmHg incremental increase in mPAP has the most significant effect on death risk between 21 and 24 mmHg, the effect

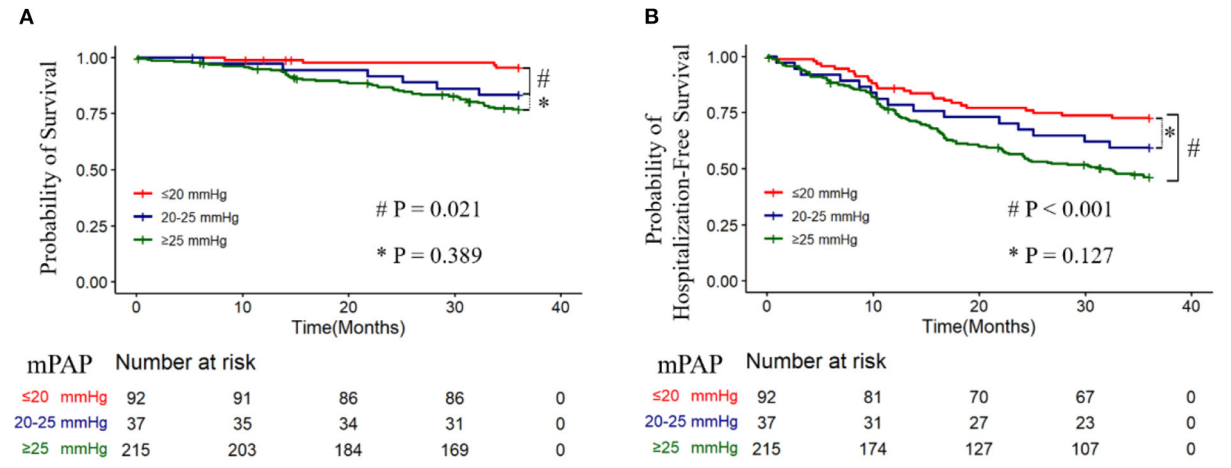

FIGURE 2
3-year survival and hospitalization-free survival for without pulmonary hypertension (PH) (mPAP ≤ 20 mmHg), borderline PH (21–24 mmHg), and traditionally defined PH (≥25 mmHg) patients, and Kaplan-Meier analysis of the probability of all-cause mortality **(A)** (Log-rank, $p < 0.001$) and rehospitalization **(B)** (Log-rank, $p < 0.001$) was performed.

TABLE 2 Hazard ratio for mortality among patients assigned to the borderline PH and traditionally defined PH groups compared with the non-PH group.

Variables	Crude HR (95%CI)	Crude *P* value	Adj. HR (95%CI)	Adj. *P* value
mPAP				
Without PH	1.0 (reference)		1.0 (reference)	
Borderline PH	3.970 (1.120–14.069)	0.033	3.822 (1.043–13.999)	0.043
PH	5.760 (2.077–15.975)	0.001	4.023 (1.411–11.465)	0.009
NYHA FC				
II	1.0 (reference)		1.0 (reference)	
III/IV	3.658 (2.151–6.220)	< 0.001	2.559 (1.392–4.706)	0.002
Hypertension				
No	1.0 (reference)		1.0 (reference)	
Yes	2.393 (1.392–4.113)	0.002	2.896 (1.618–5.183)	< 0.001
Age (years)	1.044 (1.019–1.070)	< 0.001	1.039 (1.005–1.073)	0.024
BUN (mmol/L)	1.140 (1.070–1.214)	< 0.001	1.151 (1.059–1.251)	0.001
Uric acid (umol/L)	1.005 (1.003–1.007)	< 0.001	1.003 (1.001–1.005)	0.008
NP (BNP ≥288 or NT-pro BNP ≥635)				
No	1.0 (reference)			
Yes	1.818 (1.064–3.106)	0.029		
Hemoglobin (g/L)	0.985 (0.974–0.995)	0.003		
FBG (mmol/L)	1.063 (1.002–1.128)	0.042		
eGFR (ml/min)	0.983 (0.973–0.994)	0.002		
HDL (mmol/L)	0.420 (0.188–0.942)	0.035		
LAAPD (mm)	1.044 (1.010–1.079)	0.010		
LVEDD (mm)	1.039 (1.012–1.067)	0.004		

PH, pulmonary hypertension; Adj. HR, adjusted hazard ratio; CI, confidence interval; mPAP, mean pulmonary artery pressure; NYHA FC, New York Heart Association Functional Class; BUN, blood urea nitrogen; NP, Natriuretic peptides; BNP, b-type natriuretic peptide; NT-pro BNP, N-terminal pro b-type natriuretic peptide; FBG, fasting blood glucose; eGFR, estimated glomerular filtration rate; HDL, high-density lipoprotein cholesterol; LAAPD, left atrial anteroposterior diameter; LVEDD, left ventricular end diastolic diameter.

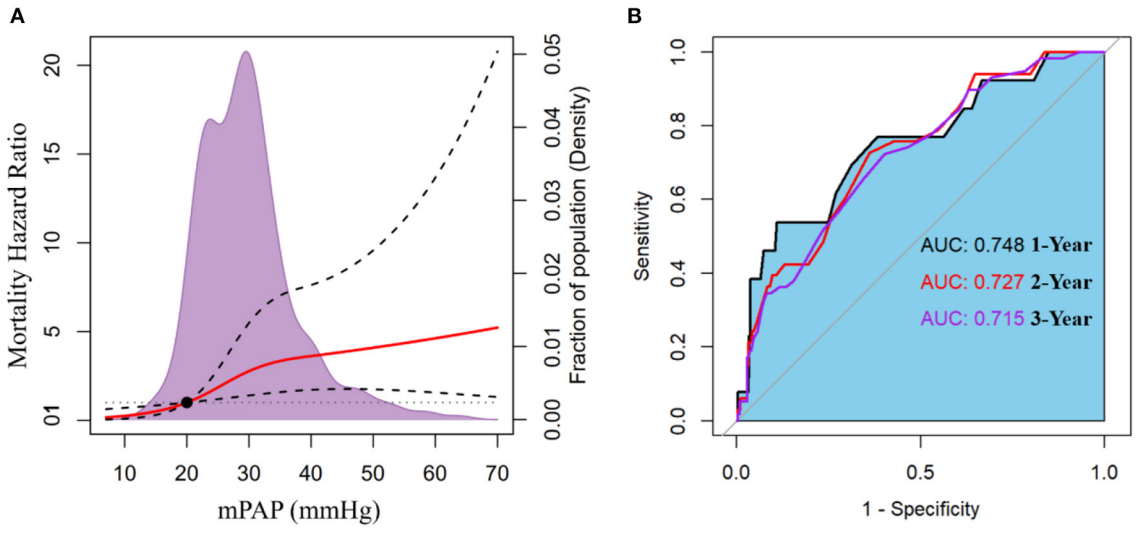

FIGURE 3
(A) The adjusted hazard ratio for mortality according to mean pulmonary artery pressure (mPAP). **(B)** Receiver operator characteristic (ROC) curves with associated area under the curve (AUC) of mPAP to predict mortality at 1-, 2-, and 3-year.

gradually weakened beyond this range (Supplement Figure S2). This finding implies that patients with borderline PH are susceptible when exposed to the progressively increased mPAP. ROC curves indicated that the discriminating power of mPAP to predict death was greatest at 1 year (Figure 3B). ROC analysis identified a cut-off value of 37.5 (mmHg) for mPAP as a predictor of 1-year mortality, with a sensitivity of 53.8%, specificity of 89.1%, positive predictive value (PPV) of 16.3%, and negative predictive value (NPV) of 98.0%.

Factors associated with new and traditionally defined PH

A logistic regression analysis was used to investigate the association of factors (excluding RHC variables) with new defined PH (mPAP > 20 mmHg) and traditional defined PH (mPAP ≥ 25 mmHg). Multivariate logistic regression analysis showed that left ventricular end diastolic diameter (LVEDD) and right ventricular anteroposterior diameter (RVAPD) were independent predictive factors of both prediction models (for predicting new defined PH, and traditionally defined PH, respectively) (Supplementary Tables S2, S3). LVEDD contributed more predictors to both prediction models than RVAPD, as measured by the partial chi-square statistic minus the predictor degrees of freedom (7.4 vs. 4.3, 10.0 vs. 4.7, respectively).

Discussion

The current study analysis of LHF patients who underwent RHC from a multicenter registry cohort revealed not just traditionally defined PH but borderline PH is also independently linked with increased 3-year all-cause mortality. Additionally, as the mPAP value was above 20 mmHg, the adjusted mortality hazard ratio increased directly and progressively, with the most remarkable interval change observed in patients with an mPAP between 21 and 24 mmHg. These findings demonstrate that borderline PH has the same clinical significance as traditionally defined PH and supports the new PH hemodynamic criteria (mPAP > 20 mmHg) adopted in LHF patients.

At the first WSPH in 1973, an mPAP > 25 mmHg was used as the hemodynamic threshold for diagnosing PH (13). However, because the conference was focused on primary PH, the threshold of 25 mmHg was intended to differentiate primary PH from other causes of PH, such as left heart disease or chronic lung disease, which typically present with significantly lower mPAP. Therefore, the cut-off value of 25 mmHg was arrived at empirically and pragmatically rather than scientifically. In 2008, the fourth WSPH suggested that an mPAP of <20 mmHg be deemed normal (14). Based on a systematic evaluation of 1,187 individuals from 47 studies, the normal mPAP was reported to be 14.0 mmHg with an SD of 3.3 mmHg. The upper limit of normal (20 mmHg) was determined by adding two SDs (6.6 mmHg) to the mean (14.0 mmHg) (15). As a result, the name "borderline PH" was considered for mPAP values between 21 and 24 mmHg but was rejected due to a lack of management strategies, epidemiology, and prognosis data for this group. Finally, they slightly modified the mPAP value for diagnosing PH (>25 to ≥25 mmHg) (14). Recently, multiple studies indicated an association between modestly raised mPAP and mortality (10, 11, 16, 17). As a result, the 6th WSPH hold in 2018, decided to lower the mPAP threshold to >20 mmHg for all forms of PH (4). However, because none of these studies included subgroup analyses by type of PH, the data on whether borderline PH was related to unfavorable clinical outcomes remained ambiguous across all PH types.

The Veterans Affairs Clinical Assessment, Reporting, and Tracking Program (VA CART) is the most extensive study investigating the relationship between borderline PH and mortality (11). They enrolled 21,727 individuals (23% of borderline PH patients, $n = 5{,}030$) in the VA CART trial and discovered that the mortality HR rose to start at 19 mmHg (HR = 1.183; 95% CI: 1.004–1.393), and borderline PH is related with increased all-cause mortality and rehospitalization. Our study reveals that the effect of borderline PH on all-cause mortality persists in LHF patients; consequently, we believe that the new definition of PH for LHF patients (mPAP > 20 mmHg) is appropriate. Furthermore, investigations have revealed that borderline PH also has a negative effect on patients' exercise ability, with the 6 min walk distance and peak oxygen uptake significantly lower in borderline PH patients than in the non-PH group (16–18). The repeated RHC data provides the evidence for progression of borderline PH to traditionally defined PH (mPAP ≥25 mmHg), 43 of 70 (61%) patients with borderline PH developed PH that mainly of post-capillary PH, most of whom were undergoing repeated RHC within 1 year (median interval between RHC, 35 weeks; IQR, 12–124 weeks), and the median increase in mPAP was 10 mmHg (10). In this present study, we noticed the proportion of borderline PH was relatively lower, 11% with borderline PH, and 62.0% with traditionally defined PH. Our findings and the repeated RHC data indicate that borderline PH in LHF patients may be a transient stage and relatively rapid transition to PH. The unresolved issue of the two large cohort studies is the causality between borderline PH and mortality. Individuals with borderline PH involved in both studies had a higher prevalence of coronary artery disease, systemic hypertension, diabetes, and heart failure than the non-PH group (10, 11). Although the authors control for cardiac and metabolic disorders, they acknowledge that residual confounding may affect the mortality differences. As a result, it is unknown whether the increased death is due to borderline PH itself or a higher incidence of these illnesses. On the contrary, our study showed no significant differences in these illnesses between the borderline PH and non-PH groups.

While this could be because all patients recruited had LHF, our data imply that borderline PH is more likely to cause increased mortality. Experimental and human studies have indicated that borderline PH contributes to right ventricular dysfunction (19, 20). Similarly, our investigation discovered that borderline PH patients had greater right ventricular end-diastolic pressure (RVEDP) than non-PH patients (Table 1). Furthermore, earlier research has established a strong link between right ventricular dysfunction and higher mortality in individuals with LHF (21–23). Consequently, we hypothesize that right ventricular dysfunction may contribute to mortality in borderline PH patients.

In LHF patients, the primary driving force of PH is an increase in left ventricular (LV) filling pressure, which as a result increases left atrial (LA) pressure. Over time, LA loses its ability to act as a buffer zone shielding the pulmonary system from the passive backward transmission of increased LV filling pressure, eventually resulting in PH (24). Therefore, if the underlying LHF continues to deteriorate, the borderline PH will probably develop to the traditionally defined PH. The new definition of PH will enable these individuals (mPAP: 21–24 mmHg) to receive closer monitoring, and intensification of management, perhaps mitigating the longitudinal disease burden.

Current PH guidelines make a weak recommendation for RHC in individuals suspected of having PH due to left heart disease (IIb) (2). For patients with suspected PH-LHF, with no specific PH treatment, early RHC has significant implications for identifying at-risk individuals, as mPAP > 20 mmHg is associated with unfavorable outcomes. Taken together, this observational study established that borderline PH is related to an elevated risk of death from any cause in LHF patients. We hypothesize that patients with PH-LHF may benefit from early diagnosed by RHC, that the future phase of PH-LHF may focus on early diagnosis, and that the role of RHC in patients with suspected PH-LHF justifies further exploration.

Study limitations

Numerous limitations existed in this study, which should be considered when interpreting our findings. To begin, this was a retrospective analysis of a prospective cohort study, which entails inherent limitations such as selection and referral bias. Second, because the fluid challenge was not included in the protocol for our RHC trial, we may have underestimated the prevalence of PH-LHF by removing patients with PAWP beyond the upper range of normal (13–15 mmHg). Lastly, the two subtypes of PH-LHF (isolated post-capillary PH and combined post-capillary and pre-capillary PH) cannot be separated because the pulmonary vascular resistance parameter is unavailable.

Conclusions

Borderline PH was an independent predictor of 3-year all-cause mortality in patients with LHF, indicating that borderline PH is clinically significant and supports the revised hemodynamic PH criterion applied in LHF patients. Overall, our findings suggest that the risk of mortality increases immediately and incrementally when the mPAP value exceeds 20 mmHg, and support future prospective studies examining the efficacy of closer interval monitoring or management intensification in patients with borderline PH, as well as the importance of performing RHC early in patients with suspected PH-LHF.

Data availability statement

The raw data supporting the conclusions of this article will be made available by the authors, without undue reservation.

Ethics statement

The studies involving human participants were reviewed and approved by the Institutional Review Board of Fuwai Hospital. The patients/participants provided their written informed consent to participate in this study.

Author contributions

YL and JH contributing to the conception and design. YL drafting the article. LP, SH, JSh, WW, FT, XZ, WS, JSu, and TY data collection, analysis, and interpretation. RQ and HH revising the article. All authors contributed to the article and approved the submitted version.

Funding

This study was supported by the National Key Technology R&D Program of China (Project No: 2011BAI11B15) and the National Key Research and Development Program of China (Project No: 2016YFC1304400).

Acknowledgments

The authors thank the staff of the participating research centers for contributing to this study.

Conflict of interest

The authors declare that the research was conducted in the absence of any commercial or financial relationships that could be construed as a potential conflict of interest.

The handling editor JQ declared a shared affiliation with the author(s) JSh at the time of review.

Publisher's note

All claims expressed in this article are solely those of the authors and do not necessarily represent those of their affiliated organizations, or those of the publisher, the editors and the reviewers. Any product that may be evaluated in this article, or claim that may be made by its manufacturer, is not guaranteed or endorsed by the publisher.

Supplementary material

The Supplementary Material for this article can be found online at: https://www.frontiersin.org/articles/10.3389/fcvm.2022.983803/full#supplementary-material

References

1. Hoeper MM, Humbert M, Souza R, Idrees M, Kawut SM, Sliwa-Hahnle K, et al. A global view of pulmonary hypertension. *Lancet Respir Med.* (2016) 4:306–22. doi: 10.1016/S2213-2600(15)00543-3

2. Galie N, Humbert M, Vachiery JL, Gibbs S, Lang I, Torbicki A, et al. 2015 ESC/ERS Guidelines for the diagnosis and treatment of pulmonary hypertension: The Joint Task Force for the Diagnosis and Treatment of Pulmonary Hypertension of the European Society of Cardiology (ESC) and the European Respiratory Society (ERS): Endorsed by: Association for European Paediatric and Congenital Cardiology (AEPC), International Society for Heart and Lung Transplantation (ISHLT). *Eur Heart J.* (2016) 37:67–119. doi: 10.1093/eurheartj/ehv317

3. Hoeper MM, Bogaard HJ, Condliffe R, Frantz R, Khanna D, Kurzyna M, et al. Definitions and diagnosis of pulmonary hypertension. *J Am Coll Cardiol.* (2013) 62:D42–50. doi: 10.1016/j.jacc.2013.10.032

4. Simonneau G, Montani D, Celermajer DS, Denton CP, Gatzoulis MA, Krowka M, et al. Haemodynamic definitions and updated clinical classification of pulmonary hypertension. *Eur Respir J.* (2019) 53:1801913. doi: 10.1183/13993003.01913-2018

5. Brusca SB, Zou Y Elinoff JM. How low should we go? Potential benefits and ramifications of the pulmonary hypertension hemodynamic definitions proposed by the 6th World Symposium. *Curr Opin Pulm Med.* (2020) 26:384–90. doi: 10.1097/MCP.0000000000000699

6. Gibbs JSR Torbicki A. Proposed new pulmonary hypertension definition: is 4 mm(Hg) worth re-writing medical textbooks? *Eur Respir J.* (2019) 53:1900197. doi: 10.1183/13993003.00197-2019

7. Hoeper MM Humbert M. The new haemodynamic definition of pulmonary hypertension: evidence prevails, finally! *Eur Respir J.* (2019) 53:1900038. doi: 10.1183/13993003.00038-2019

8. Vachiery JL, Tedford RJ, Rosenkranz S, Palazzini M, Lang I, Guazzi M, et al. Pulmonary hypertension due to left heart disease. *Eur Respir J.* (2019) 53:1801897. doi: 10.1183/13993003.01897-2018

9. Cappola TP, Felker GM, Kao WH, Hare JM, Baughman KL, Kasper EK. Pulmonary hypertension and risk of death in cardiomyopathy: patients with myocarditis are at higher risk. *Circulation.* (2002) 105:1663–8. doi: 10.1161/01.CIR.0000013771.30198.82

10. Assad TR, Maron BA, Robbins IM, Xu M, Huang S, Harrell FE, et al. Prognostic effect and longitudinal hemodynamic assessment of borderline pulmonary hypertension. *JAMA Cardiol.* (2017) 2:1361–8. doi: 10.1001/jamacardio.2017.3882

11. Maron BA, Hess E, Maddox TM, Opotowsky AR, Tedford RJ, Lahm T, et al. Association of borderline pulmonary hypertension with mortality and hospitalization in a large patient cohort: insights from the veterans affairs clinical assessment, reporting, and tracking program. *Circulation.* (2016) 133:1240–8. doi: 10.1161/CIRCULATIONAHA.115.020207

12. McMurray JJ, Adamopoulos S, Anker SD, Auricchio A, Bohm M, Dickstein K, et al. ESC Guidelines for the diagnosis and treatment of acute and chronic heart failure 2012: the task force for the diagnosis and treatment of acute and chronic heart failure 2012 of the European society of cardiology. Developed in collaboration with the Heart Failure Association (HFA) of the ESC. *Eur Heart J.* (2012) 33:1787–847. doi: 10.1093/eurheartj/ehs104

13. Hatano S Strasser T. *Primary Pulmonary Hypertension: Report on a WHO Meeting*, Geneva, 15–17 (1975).

14. Badesch DB, Champion HC, Gomez Sanchez MA, Hoeper MM, Loyd JE, Manes A, et al. Diagnosis and assessment of pulmonary arterial hypertension. *J Am Coll Cardiol.* (2009) 54:S55–66. doi: 10.1016/j.jacc.2009.04.011

15. Kovacs G, Berghold A, Scheidl S, Olschewski H. Pulmonary arterial pressure during rest and exercise in healthy subjects: a systematic review. *Eur Respir J.* (2009) 34:888–94. doi: 10.1183/09031936.00145608

16. Kovacs G, Avian A, Tscherner M, Foris V, Bachmaier G, Olschewski A, et al. Characterization of patients with borderline pulmonary arterial pressure. *Chest.* (2014) 146:1486–93. doi: 10.1378/chest.14-0194

17. Douschan P, Kovacs G, Avian A, Foris V, Gruber F, Olschewski A, et al. Mild elevation of pulmonary arterial pressure as a predictor of mortality. *Am J Respir Crit Care Med.* (2018) 197:509–16. doi: 10.1164/rccm.201706-1215OC

18. Nemoto K, Oh-Ishi S, Akiyama T, Yabuuchi Y, Goto H, Nonaka M, et al. Borderline pulmonary hypertension is associated with exercise intolerance and increased risk for acute exacerbation in patients with interstitial lung disease. *BMC Pulm Med.* (2019) 19:167. doi: 10.1186/s12890-019-0932-5

19. Lamia B, Muir JF, Molano LC, Viacroze C, Benichou J, Bonnet P, et al. Altered synchrony of right ventricular contraction in borderline pulmonary hypertension. *Int J Cardiovasc Imaging.* (2017) 33:1331–9. doi: 10.1007/s10554-017-1110-6

20. Pagnamenta A, Dewachter C, McEntee K, Fesler P, Brimioulle S, Naeije R. Early right ventriculo-arterial uncoupling in borderline pulmonary hypertension on experimental heart failure. *J Appl Physiol.* (1985) 109:1080–5. doi: 10.1152/japplphysiol.00467.2010

21. Aschauer S, Zotter-Tufaro C, Duca F, Kammerlander A, Dalos D, Mascherbauer J, et al. Modes of death in patients with heart failure and preserved ejection fraction. *Int J Cardiol.* (2017) 228:422–6. doi: 10.1016/j.ijcard.2016.11.154

22. Kjaergaard J, Akkan D, Iversen KK, Kober L, Torp-Pedersen C, Hassager C. Right ventricular dysfunction as an independent predictor of short- and long-term mortality in patients with heart failure. *Eur J Heart Fail.* (2007) 9:610–6. doi: 10.1016/j.ejheart.2007.03.001

23. Meluzin J, Spinarova L, Hude P, Krejci J, Dusek L, Vitovec J, et al. Combined right ventricular systolic and diastolic dysfunction represents a strong determinant of poor prognosis in patients with symptomatic heart failure. *Int J Cardiol.* (2005) 105:164–73. doi: 10.1016/j.ijcard.2004.12.031

24. Rosenkranz S, Gibbs JS, Wachter R, De Marco T, Vonk-Noordegraaf A, Vachiery JL. Left ventricular heart failure and pulmonary hypertension. *Eur Heart J.* (2016) 37:942–54. doi: 10.1093/eurheartj/ehv512

frontiers | Frontiers in Cardiovascular Medicine

TYPE Original Research
PUBLISHED 18 August 2022
DOI 10.3389/fcvm.2022.967463

OPEN ACCESS

EDITED BY
Haineng Xu,
University of Pennsylvania,
United States

REVIEWED BY
Yanna Tian,
Augusta University, United States
Mengyuan Ge,
University of Miami, United States
Quanyi Zhao,
Chinese Academy of Medical Sciences,
China

*CORRESPONDENCE
Xufeng Qi
qixufeng@jnu.edu.cn
Dongqing Cai
tdongbme@jnu.edu.cn

†These authors have contributed equally to this work

SPECIALTY SECTION
This article was submitted to General Cardiovascular Medicine, a section of the journal Frontiers in Cardiovascular Medicine

RECEIVED 12 June 2022
ACCEPTED 01 August 2022
PUBLISHED 18 August 2022

CITATION
Li L, Guo H, Lai B, Liang C, Chen H, Chen Y, Guo W, Yuan Z, Huang R, Zeng Z, Liang L, Zhao H, Zheng X, Li Y, Pu Q, Qi X and Cai D (2022) Ablation of cardiomyocyte-derived BDNF during development causes myocardial degeneration and heart failure in the adult mouse heart. *Front. Cardiovasc. Med.* 9:967463. doi: 10.3389/fcvm.2022.967463

Ablation of cardiomyocyte-derived BDNF during development causes myocardial degeneration and heart failure in the adult mouse heart

Lilin Li[1,2,3,4†], Hongyan Guo[1,2,3,4,5†], Binglin Lai[1,2,3,4†], Chunbao Liang[1,2,3,4], Hongyi Chen[1,2,3,4], Yilin Chen[1,2,3,4], Weimin Guo[1,2,3,4], Ziqiang Yuan[6], Ruijin Huang[7,8], Zhaohua Zeng[9], Liying Liang[9], Hui Zhao[10], Xin Zheng[1,2,3,4], Yanmei Li[1,2,3,4], Qin Pu[7], Xufeng Qi[1,2,3,4*] and Dongqing Cai[1,2,3,4*]

[1]Key Laboratory of Regenerative Medicine, Ministry of Education, Jinan University, Guangzhou, China, [2]Joint Laboratory for Regenerative Medicine, Chinese University of Hong Kong-Jinan University, Guangzhou, China, [3]International Base of Collaboration for Science and Technology (JNU), The Ministry of Science and Technology and Guangdong Province, Guangzhou, China, [4]Department of Developmental and Regenerative Biology, Jinan University, Guangzhou, China, [5]Jiangxi Provincial Key Laboratory of Medical Immunology and Immunotherapy, Jiangxi Academy of Medical Sciences, Nanchang, China, [6]Department of Medical Oncology, Robert Wood Johnson of Medical School, Cancer Institute of New Jersey, New Brunswick, NJ, United States, [7]Department of Neuroanatomy, Institute of Anatomy, University of Bonn, Bonn, Germany, [8]Department of Anatomy and Molecular Embryology, Institute of Anatomy and Cell Biology, University of Freiburg, Freiburg, Germany, [9]Division of Cardiology, Department of Internal Medicine, The First Affiliated Hospital of Guangzhou Medical University, Guangzhou, China, [10]Stem Cell and Regeneration TRP, School of Biomedical Sciences, Chinese University of Hong Kong, Shatin, Hong Kong SAR, China

Objective: Brain-derived neurotrophic factor (BDNF) and its receptor TrkB-T1 were recently found to be expressed in cardiomyocytes. However, the functional role of cardiomyocyte-derived BDNF in heart pathophysiology is not yet fully known. Recent studies revealed that BDNF-TrkB pathway plays a critical role to maintain integrity of cardiac structure and function, cardiac pathology and regeneration of myocardial infarction (MI). Therefore, the BDNF-TrkB pathway may be a novel target for myocardial pathophysiology in the adult heart.

Approach and results: In the present study, we established a cardiomyocyte-derived BDNF conditional knockout mouse in which BDNF expression in developing cardiomyocytes is ablated under the control of the Myosin heavy chain 6 (MYH6) promoter. The results of the present study show that ablation of cardiomyocyte-derived BDNF during development does not impair survival, growth or reproduction; however, in the young adult heart, it causes cardiomyocyte death, degeneration of the myocardium, cardiomyocyte

hypertrophy, left atrial appendage thrombosis, decreased cardiac function, increased cardiac inflammation and ROS activity, and metabolic disorders, leading to heart failure (HF) in the adult heart and eventually resulting in a decrease in the one-year survival rate. In addition, ablation of cardiomyocyte-derived BDNF during the developmental stage leads to exacerbation of cardiac dysfunction and poor regeneration after MI in adult hearts.

Conclusion: Cardiomyocyte-derived BDNF is irreplaceable for maintaining the integrity of cardiac structure and function in the adult heart and regeneration after MI. Therefore, the BDNF-TrkB pathway will be a novel target for myocardial pathophysiology in the adult heart.

KEYWORDS

cardiomyocyte, cardiomyocyte-derived BDNF conditional knockout, heart failure, degeneration of the myocardium, myocardial infarction

Introduction

The brain-derived neurotrophic factor (BDNF) pathway is highly active in the nervous system and plays critical roles in promoting growth, survival, synaptic connection, neuronal repair and regeneration of the nervous system as well as the treatment of neurological diseases (1–3). In addition, BDNF also plays important roles in non-neuronal tissues, including vasculature (4), platelets (5), vascular smooth muscle cells and macrophages (6, 7), early hematopoietic cells (8, 9), activated lymphocytes (10) monocytes (11), and skeletal muscle (12).

Among the notable progresses related to BDNF-TrkB signaling, the BDNF-TrkB pathway plays a key role in the pathophysiology and regeneration of the cardiovascular system. BDNF and its receptor TrkB are expressed in the endothelial cells of the coronary arteries (13) and are known to be associated with capillary development and cardiac endothelium formation (14, 15) in heart tissue during the late gestation period (7). BDNF has been reported to play an important role in diminished endothelial cell-cell contact and endothelial cell apoptosis in mouse embryonic intramyocardial arteries, capillaries, and the heart, while BDNF knockout leads to intraventricular wall hemorrhage and perinatal lethality (13, 16–18). Overexpression of BDNF in the midgestational mouse heart results in an increase in capillary density (18). Separately, $TrkB^{-/-}$ mice showed a marked reduction in blood vessel density and an increased number of apoptotic endothelial cells, predominantly in the subepicardial region of the developing heart (17). Recently, we demonstrated that BDNF promoted the migration of young cardiac microvascular endothelial cells (CMECs) *via* activation of the BDNF-TrkB-FL-PI3K/Akt pathway, which may benefit angiogenesis after MI. However, the aging of CMECs led to changes in the expression of isoforms of the receptor TrkB: among the three isoforms of TrkB (TrkB-FL, TrkB-T1, and TrkB-T2), only the truncated TrkB-T1 isoform continued to be expressed, which led to dysfunction of its ligand, decreased CMEC migration, and increased injury in aging hearts. Although the efficacy of promoting migration via the BDNF-TrkB-T1 pathway in aged CMECs was significantly decreased compared with that in young CMECs via the BDNF-TrkB-FL pathway, the BDNF-TrkB-T1 pathway in aged CMECs was still able to promote the migration of aged CMECs (19). More recently, we further demonstrated that aged CMECs utilized BDNF-TrkB-T1 signaling to recruit Willin as a downstream effector to activate the Hippo pathway and then promote migration. This finding suggests that the aging process shifts aged CMECs that express TrkB-T1 receptors by transducing BDNF signals via the BDNF-TrkB-T1-Willin-Hippo pathway and that this change might be an important mechanism and therapeutic target behind the dysfunction of cardiac angiogenesis observed in aged hearts (20). All these findings clearly reveal that the BDNF-TrkB pathway plays an essential role in the development and growth of the vasculature as well as angiogenesis by maintaining the integrity and regenerative capacity of the cardiovascular system.

In addition to endothelial cells, recent progress has demonstrated that cardiomyocytes also express BDNF and its receptor TrkB-T1 (14, 21–23). BDNF-TrkB signaling is required for the heart to fully contract and relax. These actions occur independently from and in addition to β-adrenergic influence. BDNF-induced enhancement of myocardial performance occurs via direct modulation of Ca^{2+} cycling in a calmodulin-dependent protein kinase II-dependent manner (23). It was reported that BDNF regulates the cardiac contraction force independent of nervous system innervation. This function

is mediated by the truncated TrkB-T1 receptor expressed in cardiomyocytes. Loss of TrkB-T1 in these cells impairs calcium signaling and causes cardiomyopathy (14). These findings suggest that cardiomyocyte-derived BDNF plays a critical role in cardiomyocyte contraction. In addition, it has been reported that homozygous systemic BDNF knockout mice die due to Heart failure (HF) in the fetal period (18). In hearts from an adult tamoxifen-induced systemic BDNF deletion myocardial infarction (MI) model, decreased cardiac function and myocardial angiogenesis in the infarct border zone, decreased expression of the prosurvival molecule Bcl-2 and increased infarct size, cardiomyocyte apoptosis and expression of the proapoptotic molecule Bax were found compared with those in wild-type MI hearts. These results suggested that systemic deletion of BDNF leads to exacerbation of cardiac dysfunction after MI. However, heart size and cardiac function were found at basal levels in tamoxifen-induced 2-month-old cardiomyocyte-specific BDNF conditional knockout mice. Ablation of BDNF in cardiomyocytes did not affect cardiac remodeling, cardiac function, myocardial angiogenesis or infarct size after MI. In contrast, in 2-month-old cardiomyocyte-specific inducible TrkB conditional knockout MI mouse model hearts, decreased cardiac function and myocardial angiogenesis in the infarct border zone and increased infarct size and cardiomyocyte apoptosis were found compared with those in wild-type MI hearts (22). The above findings combined with the inconsistent pathological outcomes observed in the adult inducible BDNF and TrkB conditional knockout models suggest that endogenous BDNF from cardiomyocytes plays an important role in regulating and maintaining cardiac pathophysiology. However, to date, whether cardiomyocyte-derived BDNF is irreplaceable for maintaining the integrity of cardiac structure and function in the heart and its exact functional role and molecular mechanism in cardiac pathophysiology are still unclear.

Owing to the limitation of the adult inducible cardiomyocyte-specific BDNF conditional knockout model, which only ablates BDNF from cardiomyocytes for a short amount of time in the adult heart, it is not an appropriate model for elucidating the importance of cardiomyocyte-derived BDNF in maintaining cardiac structure and function in dynamic scenarios from development to the adult stage. Therefore, the present study was designed to investigate the effects of ablating cardiomyocyte-derived BDNF during development on cardiac pathophysiology. Our results demonstrate that ablation of cardiomyocyte-derived BDNF during the development stage does not impair survival, growth or reproduction; however, in the young adult heart, it causes cardiomyocyte death, degeneration of the myocardium, cardiomyocyte hypertrophy, decreased cardiac function, increased cardiac inflammation and ROS activity, and metabolic disorders, leading to HF in the adult heart and eventually resulting in a decrease in the one-year survival rate. In addition, ablation of cardiomyocyte-derived BDNF during the developmental stage leads to exacerbation of cardiac dysfunction and poor regeneration after MI in adult hearts.

Materials and methods

Animals and generation of the cardiomyocyte-specific BDNF conditional knockout mouse

Stock BDNF (tm3Jae)/J mice (*BDNF*$^{flox/flox}$; Stock #004339) and B6.FVB-Tg(Myh6-cre)2182Mds/J mice (Stock #011038) were obtained from the Jackson Laboratory. By expressing bacteriophage P1 Cre recombinase (Cre) in a tissue or cell-type specific manner, genes that are engineered with flanking loxP sites can be deleted or overexpressed in an analogous fashion. In the cardiac myocyte, this is most often achieved using Cre expression driven by the cardiac myocyte-specific alpha myosin heavy chain promoter (24, 25). Cre expression from this promoter has been shown to be both cardiac myocyte specific and to drive highly efficient recombination (24). In present study, in order to avoid the potential cardiotoxicity from Myh6-Cre, the mating strategy to generate Myh6-Cre-BDNF^{flox} mice with mixed background was adopted (26, 27). The stock BDNF (tm3Jae)/J mice (*BDNF*$^{flox/flox}$) were mated with the B6.FVB-Tg(Myh6-cre)2182Mds/J mice to obtain heterozygous cardiomyocyte-specific conditional BDNF knockout mice (Myh6-Cre$^{\pm}$-BDNF$^{flox/\Delta}$) that were backcrossed to the *BDNF*$^{flox/flox}$ mice to obtain homozygous cardiomyocyte-specific conditional BDNF knockout mice (Myh6-Cre$^{\pm}$-BDNF$^{flox/flox}$) with mixed background. *BDNF*$^{flox/flox}$ mice were used as controls (WT). The One Step Mouse Genotyping Kit (PD101-01, Vazyme) was applied to confirm the genotypes of MYH6-Cre-BDNF$^{-/-}$ and wild-type (WT) mice using whole genomic DNA. The following primers were used for genotyping: MYH6-Cre-F: 5′- ATG ACA GAC AGA TCC CTC CTA TCT CC-3′, MYH6-Cre-R: 5′-CTC ATC ACT CGT TGC ATC ATC GAC-3′, MYH6-Cre-F2: 5′-CAA ATG TTG CTT GTC TGG TG-3′, MYH6-Cre-R2: 5′-GTC AGT CGA GTG CAC AGT TT-3′; *BDNF*$^{flox/flox}$-F: 5′-TGTGATTGTGTTTCTGGTGAC-3′; and *BDNF*$^{flox/flox}$-R: 5′- GCCTTCATGCAACCGAAGTATG-3′. The MYH6-Cre-F/R primers identify the B6.FVB-Tg (Myh6-cre) allele (∼300 bp). The MYH6-Cre-BDNF-F/R primers identify the BDNF null allele (487 bp). The *BDNF*$^{flox/flox}$-F/R primers identify the wild-type and flox alleles (∼437 bp). Animal care, surgery and handling procedures in this study were approved by the Jinan University Animal Care Committee (No. 20160413104350).

Cardiomyocyte isolation

The cardiomyocytes of 3-month-old male MYH6-Cre-BDNF$^{-/-}$ and WT (*BDNF*$^{flox/flox}$ mice) mice were isolated by the Langendorff method. The mice were injected with 100 μL heparin (125 U/mouse) via orbital injection. After 15 min, the abdominal cavity of the mouse was injected with 200 μL of 20% ethylurethane (40 mg/mouse), and then the cardiomyocytes were isolated by the Langendorff perfusion method. Briefly, after disinfecting the mice with 70% alcohol, the heart was quickly removed in a sterile hood and put into precooled perfusion buffer (135 mM NaCl; 14.7 mM KCl; 1 mM $MgCl_2$; 10 mM HEPES; 0.33 mM NaH_2PO_4; 30 mM BDM; 10 mM D-glucose; 30 mM taurine; 5 mM creatine; 2 mM sodium pyruvate; 25 mM $NaHCO_3$; 2 mM L-glutamine; 0.6 mM KH_2PO_4; 5 mM adenosine). After removing the non-cardiac tissues, the aorta of the isolated heart was inserted into the Langendorff perfusion system, fixed with fine wire, perfused at a velocity of 3 mL/min, and instilled for 3 min with perfusion buffer. Then, the heart was digested for 5–10 min with digestion buffer (0.01% collagenase II + 0.01% collagenase IV). Digestion was considered sufficient when the myocardial tissue became loose, soft and pink. The isolated heart was put into termination buffer and torn into small pieces, followed by trituration with a pipette to isolate single cardiomyocytes. After isolation, the cardiomyocyte suspension was passed through a 250 μm filter to remove the undigested tissue, and then gradient centrifugation (50 × g, 3 min; 30 × g, 2 min; 20 × g, 2 min) was used to remove the cell fragments, blood cells and endothelial cells. The isolated cardiomyocytes were suspended in termination buffer and prepared for nuclear staining and analysis. Three mice from each group were used in this experiment.

Semiquantitative analysis of the area of cardiomyocytes and the area and number of cardiomyocyte nuclei

The cardiomyocytes of 3-month-old MYH6-Cre-BDNF$^{-/-}$ and WT hearts were isolated by the Langendorff method as described above. Hoechst 33342 (2 μL; 5 mg/mL; Thermo, United States) was added to the cardiomyocyte suspension (1 mL; 2.5 × 10^4 cells) and incubated at room temperature for 15 min. After three washes with termination buffer, the suspension was placed on an inverted fluorescence microscope, and images were captured with excitation at 346 nm. Image-Pro Plus 6 was used to measure the areas of cardiomyocytes and nuclei. A total of 1,007 cardiomyocytes and their respective nuclei collected from 3 male mice were analyzed in this experiment.

Histological analysis

Hematoxylin-eosin (H&E) staining: Whole hearts were collected and fixed overnight in 4% paraformaldehyde then dehydrated, cleared, and embedded in paraffin wax. Sections (5 μm) were prepared for staining. The sections were deparaffinized in xylene (3 × 5 min) and rehydrated with successive 3-min washes in 100, 90, 80, and 70% ethanol with one final wash in tap water. The sections were then stained with hematoxylin for 5 min, rinsed with tap water for 1 min, rinsed with 1% hydrochloric acid in 80% ethanol for 5 s, rinsed with a 1% ammonia solution for 5 s, and rinsed with tap water for 1 min. The sections were then stained with eosin for 5 min and rinsed with tap water for 1 min. After dehydration in an ethanol gradient and clearing with xylene, the slides were mounted with resinene (Shanghai Yiyang Instrument Co., Ltd.). The stained sections were scanned by PANNORAMIC MIDI II (Hungary, 3DHISTECH) for image capture. The size of the ventricular chamber was measured using ImageJ software. Three mice per group were used in this experiment. The semi-quantitative analysis for cardiomyocyte death and cardiac degenerative changes (focal loss of nuclei in cardiomyocytes, muscle fiber atrophy and disorder, unclear transverse striation of myocardial fibers and interstitial loosening) is applied as follows: −: non-detectable cardiomyocyte death and cardiac degenerative change; + : scattered cardiomyocyte death and cardiac degenerative change; + + : cardiomyocyte death and cardiac degenerative change in multiple places; + + + : extensive cardiomyocyte death and cardiac degenerative change.

Masson's trichrome staining

Paraffin sections were dewaxed and rinsed with water using a routine protocol for H&E staining. After iron hematoxylin staining (5 min), the sections were rinsed with distilled water, differentiated with 80% ethanol containing 1% hydrochloric acid (5 s) followed by 1% ammonia solution (5 s) and rinsed with running water (2 min). Then, the sections were stained with ponceau acid fuchsin (10 min) and rinsed with distilled water. After differentiation using a phosphomolybdic acid solution (8 min), the sections were sequentially stained with aniline blue (3 min) and 1% acetic acid (2 min). After staining, the sections were dehydrated, cleared in xylene, and then mounted with resinene (Shanghai Yiyang Instrument Co., Ltd.). The stained sections were scanned by 3DHISTECH (Hungary) for image capture. The infarct size was measured using ImageJ software. Three mice per group were used in this experiment. The semi-quantitative analysis for cardiac fibrosis is used as follows: −: non-detectable fibrosis; + : scattered fibrosis; + + : extensive fibrosis.

Wheat germ agglutinin staining

Paraffin sections were dewaxed and rinsed with water using a routine protocol for H&E staining. WGA working solution (10 μg/mL; Cat. No. W11261; Invitrogen) was prepared with distilled water, and then an appropriate amount of working solution was added to each tissue sample, and the samples were incubated at room temperature for 30 min. After two rinses with distilled water, the sections were sealed with anti-fluorescence quenching sealant. Ten random fields were captured from each slide under fluorescence microscopy (20X; Leica, Germany) at a wavelength of 488 nm. The area of cardiomyocytes was measured using Image-Pro Plus 6.0 software. Three mice per group were used in this experiment.

Isolation of total ribonucleic acid and real-time RT-PCR

Total ribonucleic acid (RNA) was extracted using TRIzol reagent (Cat. No. 15596018; Invitrogen) according to the manufacturer's protocol. Total RNA concentration was determined using a NanoDrop spectrophotometer (NanoDrop, Thermo Scientific). For the analysis of BDNF, ANP, BNP, α-SMA, and β-MHC gene expression, the extracted RNA (1 μg) was reverse-transcribed into first-strand cDNA using ReverTra Ace q-PCR RT Master Mix with gDNA Remover (Cat. No. FSQ-301, Toyobo) according to the manufacturer's instructions, and then the mRNA levels were quantified using SYBR Green-based real-time PCR. The reaction mixture was composed of 10 μL of SYBR Green PCR Master Mix (Cat. No. B21202; Biotool), 0.8 μl of each primer, 6.4 μL of PCR-grade water and 2 μL of the cDNA template. The following primers were used (5′–3′): BDNF forward: TACCTGGATGCCGCAAACAT, reverse: TTTATCTGC CGCTGTGACCC; ANP forward: AGGCAGTC GATTCTGCTTGA, reverse: CGT GATAGATGAAGGCAGG AAG; BNP forward: CAGGCGGTGCTGTCTCTCTAT, reverse: GGCAGGGCATAACCCTCATA; α-SMA forward: TATCGATGACCT GGAGCTGA, reverse: AGTATTGACCTT GTCTTCCTC; β-MHC forward: GCT GTAACGCACTGAAGT TGT, reverse: TCAAAGGTGGTCCCAGAGCT; β-actin forward: CGTAAAGACCTCTATGCCAACAC, reverse: CTT GATCTTCATGGT GCTAGGAG; and GAPDH forward: TG TGTCCGTCGTGGATCTGA, reverse: CCTGCTTCACCACCT TCTTGA. Amplifications were performed with a Mini-Opticon System using the following program: 95°C for 10 min followed by 40 cycles of denaturation at 95°C for 15 s and primer annealing at 62°C for 1 min and then extension at 72°C for 30 s. Relative expression was determined using the $2^{-\Delta\Delta Ct}$ comparative threshold method. All cDNA samples were amplified in triplicate and were normalized to β-actin or GAPDH on the same plate. The results of this experiment were generated from 3 to 4 mice.

Western blotting

The protein expression level of BDNF was measured by western blotting, and protein lysates of isolated cardiomyocytes were prepared in RIPA buffer (Beyotime, China) with 1 mM PMSF and a protease inhibitor cocktail (Halt Inhibitor Cocktail, Thermo, United States; Halt Phosphatase Inhibitor Cocktail, Thermo, United States). The total protein concentration was determined using a NanoDrop spectrophotometer (NanoDrop, Thermo Scientific). The protein (50 μg) was denatured in loading buffer (5 × SDS-PAGE loading buffer containing 0.5 M Tris-HCl, pH 6.8; 0.05% β-mercaptoethanol; 1% SDS; 0.005% bromophenol blue; and 50% glycerol) for 8 min at 95°C and loaded into a 15% SDS-PAGE gel. After electrophoresis, the isolated proteins were transferred onto a PVDF membrane (Bio-Rad, United States). The membrane was incubated overnight at 4°C with rabbit anti-BDNF (1:2,000, Abcam, United States) and mouse anti-GAPDH antibodies (1:4,000, Proteintech, United States) and then with donkey anti-rabbit IgG (1:5,000, Thermo, United States) and donkey anti-mouse IgG (1:5,000, Thermo, United States) secondary antibodies conjugated to horseradish peroxidase. The immunoreactive bands were detected using an ECL kit (Millipore, United States) and were analyzed using GeneSnap (Sygene). Three mice per group were used in this experiment.

Myocardial infarction studies

MI was generated via ligation of the left anterior descending coronary artery (LAD) in 5-month-old male MYH6-Cre-BDNF$^{-/-}$ mice and WT mice as previously described (19, 28, 29). Briefly, the mice were anesthetized with ketamine (100 mg/kg, i.p.) and underwent a left intercostal thoracotomy. The LAD was identified and then ligated directly below the left atrial appendage with 8-0-gauge nylon sutures. The presence of pallor and abnormal movement of the left ventricle (LV) confirmed LAD occlusion. The chest wall was then closed, the lungs were inflated, the mouse was extubated, and the thoracotomy was closed. After recovery, the mice were returned to the animal facility. After the cardiac function of ligated mice was analyzed 2 weeks after MI, the mice were euthanized, and their hearts were harvested. The collected hearts were fixed with 4% paraformaldehyde, embedded in paraffin wax and sectioned for further experiments. Six to eight mice were included in each group.

Echocardiography

Transthoracic echocardiogram was performed to analyze cardiac function. In this study, 3-month-old MYH6-Cre-BDNF$^{-/-}$ mice (male and female), 3-month-old WT mice (male and female), 8-month-old MYH6-Cre-BDNF$^{-/-}$ mice (female), 8-month-old WT mice (female), 5-month-old MYH6-Cre-BDNF$^{-/-}$ MI mice (male) and 5-month-old WT mice (male) were analyzed. Briefly, the mice from the above groups were anesthetized with ketamine (100 mg/kg, i.p.). The echocardiographic parameters were collected using an Acuson Sequoia 256c ultrasound system equipped with a 13-MHz linear transducer from a Vevo 770 echocardiogram (VisualSonics, Canada). The anterior chest wall was shaved, and the mouse was placed in a left lateral decubitus position. A rectal temperature probe was inserted, and the body temperature was carefully maintained between 37°C° and 37.5°C on a heating pad throughout the study. Parasternal long-axis, parasternal short-axis and 2 apical four-chamber views were collected in 2D-M-mode. The systolic and diastolic anatomic parameters were obtained from M-mode tracings at the mid-papillary level. The ejection fraction (EF) was calculated using the area-length method (28, 29). Three mice per group were used in this analysis.

Transmission electron microscopy analysis

Cross-sections of samples from 8-month-old female MYH6-Cre-BDNF$^{-/-}$ and WT hearts were fixed in a solution of 1% osmium tetroxide and 1.25% potassium ferrocyanide for 30 min at room temperature. After washing in PBS (pH 7.2) for 5 min at room temperature, the specimens were immersed overnight in 0.1% osmium tetroxide in PBS at room temperature and then processed for TEM observation. Three mice per group were used in this analysis.

Enzyme-linked immunosorbent assay

Enzyme-linked immunosorbent assay (ELISA) kits (CUSABIO, Wuhan) were applied to analyze plasma levels of NT-proBNP, BNP, Galectin-3, BDNF, Insulin and Leptin. The detailed protocols are described in the manufacturer's recommendations. All the parameters were analyzed in duplicate. Four to eleven mice per group were used in these assays.

Transcriptome sequencing

Total RNA was isolated using RNeasy mini kit (Qiagen, Germany). Paired-end libraries were synthesized by using the TruSeq RNA Sample Preparation Kit (Illumina, United States) following TruSeq RNA Sample Preparation Guide. Briefly, the poly-A containing mRNA molecules were purified using poly-T oligo-attached magnetic beads. Following purification, the mRNA was fragmented into small pieces using divalent cations under 94°C for 8 min. The cleaved RNA fragments were copied into first strand cDNA using reverse transcriptase and random primers. This was followed by second strand cDNA synthesis using DNA Polymerase I and RNase H. These cDNA fragments then went through an end repair process which was added a single "A" base, and then was ligated of the adapters. The products were then purified and enriched with PCR to create the final cDNA library. Purified libraries were quantified by Qubit 2.0 Fluorometer (Life Technologies, United States) and validated by Agilent 2100 bioanalyzer (Agilent Technologies, United States) to confirm the insert size and calculate the mole concentration. Cluster was generated by cBot with the library diluted to 10 pM and then were sequenced on the Illumina HiSeq 2500 (Illumina, United States). The library construction and sequencing was performed at Shanghai Biotechnology Corporation, China.

Ingenuity pathway analysis

The selected genes with the fold change greater than 1.5 and $Q < 0.5$ were applied to a further analysis to identify the regulatory networks and disease-function analysis using an ingenuity pathway analysis (IPA).[1] The analysis results were applied to core-analysis in the IPA system. In the present study, only the analyzed data that were to predicted "decrease" or "increase," which was indicated by the Z-score larger than 2 or less than −2, were selected as positive predictors.

Statistics

All measured data are presented as the means ± standard errors. Two-tailed Student's t-test was used to calculate the statistical significance between two groups. $P < 0.05$ was considered statistically significant.

Results

The one-year survival rate of MYH6-Cre-BDNF$^{-/-}$ mice is significantly reduced

The gene and protein expression levels of BDNF in MYH6-Cre-BDNF$^{-/-}$ cardiomyocytes were significantly lower than those in cardiomyocytes from WT littermates (hereafter referred to as "WT"; comparisons are made between same-sex

1 http://www.ingenuity.com

littermates) (Figures 1Ia,b; $p < 0.01$). In addition, the expression of the BDNF receptors TrkB-FL and TrkB-T1 in MYH6-Cre-BDNF$^{-/-}$ cardiomyocytes was not significantly different from that in WT cardiomyocytes (Figures 1Ic,d; $p > 0.05$). The embryonic development and reproduction of MYH6-Cre-BDNF$^{-/-}$ mice did not show abnormal effects, as MYH6-Cre-BDNF$^{-/-}$ mice were able to grow and reproduce successfully. However, the one-year survival rate of MYH6-Cre-BDNF$^{-/-}$ mice (13.6%) was significantly lower than that of WT mice (78.8%) (Figure 1II; $p < 0.01$). In addition, the body weights of MYH6-Cre-BDNF$^{-/-}$ mice observed from 2 to 7 months of age were significantly higher than those of WT mice (Figure 1III; $p < 0.01$).

Cardiac dysfunction and somatic edema are found in adult MYH6-Cre-BDNF$^{-/-}$ mice

Echocardiography documented that in 3-month-old males, the left ventricular ejection fraction (LVEF) and left ventricular fractional shortening (LVFS) of MYH6-Cre-BDNF$^{-/-}$ hearts were significantly lower than those of WT hearts (Figures 2Ia,b,d,e; $p < 0.05$), while the left ventricular end-systolic internal diameter (LVIDs), left ventricular end-diastolic internal diameter (LVIDd), left ventricular end-systolic volume (LVESV) and left ventricular end-diastolic volume (LVEDV) of MYH6-Cre-BDNF$^{-/-}$ hearts were significantly higher than those of WT hearts (Figure 2Ia,b,f–i; $p < 0.05$). From 3 months of age onwards, some MYH6-Cre-BDNF$^{-/-}$ mice had osmotic edema, which had been never occurred in WT mice (21 osmotic edema cases [male: 9; female: 12] out of 55 MYH6-Cre-BDNF$^{-/-}$ mice; approximately 38.2%; edema ratio: 40% for male, 36% for female), and 3-month-old male MYH6-Cre-BDNF$^{-/-}$ mice with osmotic edema had worse cardiac function parameters (LVEF, LVFS, LVIDs, LVIDd, LVESV and LVEDV) than 3-month-old WT mice (Figure 2Ia–i; $P < 0.05$). All MYH6-Cre-BDNF$^{-/-}$ mice died approximately 1 week after somatic edema occurred (Figure 2IIa–e).

In addition, all the observed parameters tended to be worse in 3-month-old MYH6-Cre-BDNF$^{-/-}$ female mice than in 3-month-old female WT mice of the same litter; however, the differences were not statistically significant (Figure 2Ia–i; $P > 0.05$). To investigate whether cardiac dysfunction also occurs in middle-aged female MYH6-Cre-BDNF$^{-/-}$ mice, 8-month-old MYH6-Cre-BDNF$^{-/-}$ female mice were observed. The LVEF and LVFS of 8-month-old MYH6-Cre-BDNF$^{-/-}$ female hearts were significantly smaller than those of 8-month-old WT female hearts, and the same result was observed at 3 months of age (Figures 2IIIa–d; $P < 0.01$), while the LVIDs, LVIDd, LVESV, and LVEDV of 8-month-old MYH6-Cre-BDNF$^{-/-}$ hearts were significantly higher than those of 8- and 3-month-old WT hearts as well as 3-month-old MYH6-Cre-BDNF$^{-/-}$ hearts (Figures 2IIIa,b,e–h; $P < 0.05$). These results suggested that the pathological phenotypes that occurred in MYH6-Cre-BDNF$^{-/-}$ mice were not sex dependent; however, the time window of cardiac dysfunction in female MYH6-Cre-BDNF$^{-/-}$ hearts was later than that in male MYH6-Cre-BDNF$^{-/-}$ hearts. Therefore, the subsequent investigation of other parameters focused on male mice.

Cardiomyocyte hypertrophy, increased areas of cardiomyocyte cells and nuclei, and an increased percentage of single-nucleus cardiomyocytes are found in young adult MYH6-Cre-BDNF$^{-/-}$ mice

The left ventricular area of 3-month-old MYH6-Cre-BDNF$^{-/-}$ hearts was significantly larger than that of WT hearts (Figure 3I; $p < 0.05$). In contrast, the differences of heart weight and the ratio of heart weight/body weight were not statistics significance between 3-month-old MYH6-Cre-BDNF$^{-/-}$ mice and 3-month-old WT mice (Figures 3IIg,h; $p > 0.05$). However, all three parameters of 3-month-old MYH6-Cre-BDNF$^{-/-}$ osmotic edema mice were significantly higher than those of 3-month-old MYH6-Cre-BDNF$^{-/-}$ and WT mice ($p < 0.0001$) (Figures 3I,II). Echocardiography documented that the interventricular septum end-systolic thickness (IVSTs) and left ventricular posterior wall end-systolic thickness (LVPWTs) of 3-month-old MYH6-Cre-BDNF$^{-/-}$ hearts and MYH6-Cre-BDNF$^{-/-}$ osmotic edema hearts were smaller than those of WT hearts (Figures 3IIIa,c; $P < 0.05$). Furthermore, the interventricular septum end-diastolic thickness (IVSTd) of 3-month-old MYH6-Cre-BDNF$^{-/-}$ hearts was smaller than that of WT hearts (Figure 3IIIb; $P < 0.05$). The difference in left ventricular posterior wall end-diastolic thickness (LVPWTd) among WT, 3-month-old MYH6-Cre-BDNF$^{-/-}$ hearts and 3-month-old MYH6-Cre-BDNF$^{-/-}$ osmotic edema hearts was not statistically significant (Figure 3IIId; $P > 0.05$). In parallel, semiquantification of WGA immunofluorescence staining revealed that the mean area of cardiomyocytes in 3-month-old MYH6-Cre-BDNF$^{-/-}$ hearts was significantly higher than that in WT hearts (Figure 3IV; $P < 0.05$). Furthermore, the quantitative analysis of isolated single cardiomyocytes demonstrated that the mean area of cardiomyocytes from 3-month-old MYH6-Cre-BDNF$^{-/-}$ hearts was significantly higher than that of WT hearts (Figure 3V; $P < 0.05$). The findings revealed cardiomyocyte hypertrophy in 3-month-old MYH6-Cre-BDNF$^{-/-}$ hearts, while this pathological change was more serious in 3-month-old MYH6-Cre-BDNF$^{-/-}$ osmotic edema hearts. In addition, the mean area of cardiomyocyte nuclei in 3-month-old MYH6-Cre-BDNF$^{-/-}$ hearts was significantly higher than that in WT hearts (Figure 3VI; $P < 0.05$). The percentage of single-nucleus cardiomyocytes in 3-month-old MYH6-Cre-BDNF$^{-/-}$ hearts was significantly higher than that in WT hearts (Figure 3VII; $P < 0.05$).

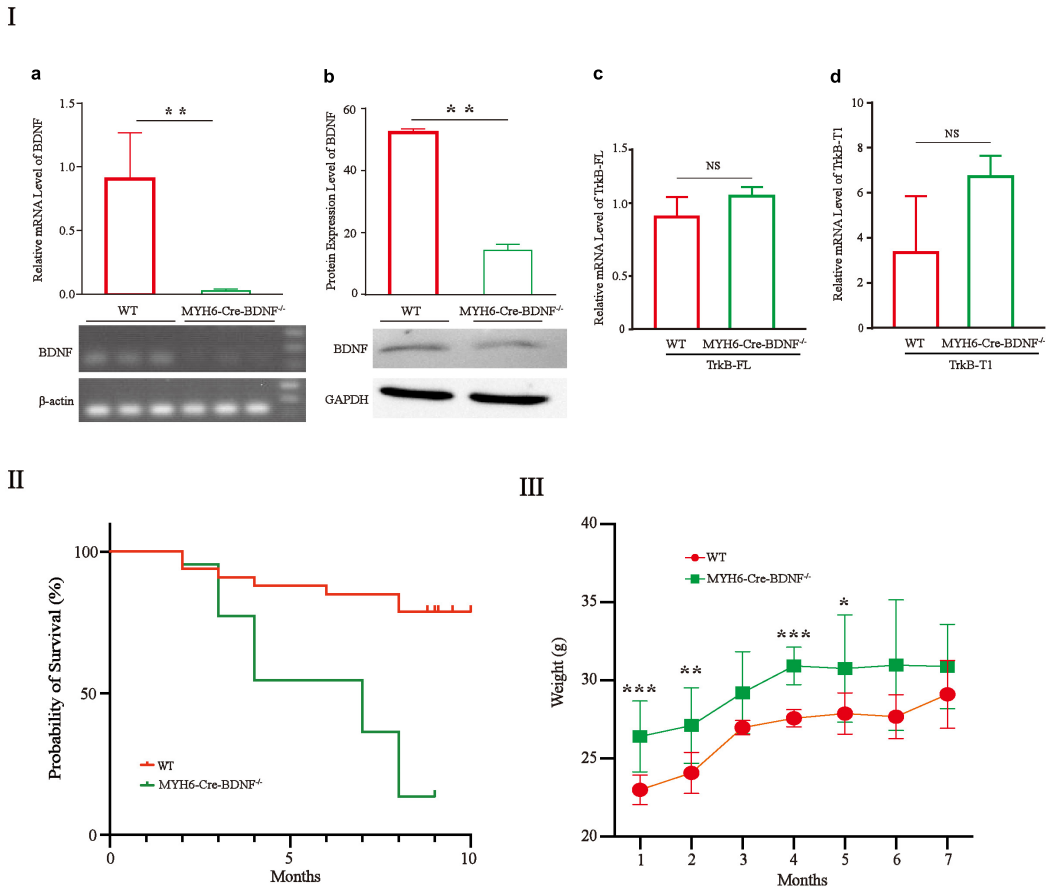

FIGURE 1
The one-year survival rate of MYH6-Cre-BDNF$^{-/-}$ mice is significantly reduced: **(I)** The expression of BDNF at the gene **(a)** and protein levels **(b)** in MYH6-Cre-BDNF$^{-/-}$ cardiomyocytes was significantly lower than that in WT cardiomyocytes from littermates. $^{**}p < 0.01$, $n = 3$. In addition, the expression of the BDNF receptors TrkB-FL and TrkB-T1 in MYH6-Cre-BDNF$^{-/-}$ cardiomyocytes was not significantly different from that in WT cardiomyocytes **(c,d)**. **(II)** The one-year survival rate of MYH6-Cre-BDNF$^{-/-}$ mice was significantly lower than that of WT mice, $p < 0.01$. **(III)** The body weights of MYH6-Cre-BDNF$^{-/-}$ mice in 1-, 2-, 4-, and 5-month-old of age were significantly higher than those of WT mice. $^{*}p < 0.05$, $^{**}p < 0.01$, $^{***}p < 0.001$, $n = 12$ for the 1-month-old WT and MYH6-Cre-BDNF$^{-/-}$ groups respectively. $n = 10$ for the 2-month-old WT and MYH6-Cre-BDNF$^{-/-}$ groups respectively. $n = 5$ and 7 for the 3-month-old group WT and MYH6-Cre-BDNF$^{-/-}$ groups. $n = 10$ and 3 for the 4-month-old WT and MYH6-Cre-BDNF$^{-/-}$ groups. $n = 8$ for the 5-month-old WT and MYH6-Cre-BDNF$^{-/-}$ groups. $n = 3$ and 6 for the 6-month-old WT and MYH6-Cre-BDNF$^{-/-}$ groups. $n = 3$ for the 7-month-old WT and MYH6-Cre-BDNF$^{-/-}$ groups respectively.

Cardiomyocyte death, degenerative changes in the myocardium (degeneration of cardiomyocytes, increased interstitial fibrosis, serious mitophagy and swelling of mitochondria) and left atrial appendage thrombus are found in young adult MYH6-Cre-BDNF$^{-/-}$ hearts

In addition to cardiomyocyte hypertrophy, H&E histological staining revealed that, focal cardiomyocyte death, focal degenerative changes in cardiomyocytes, focal loss of nuclei in cardiomyocytes and focal inflammation in the myocardium were found in 3-month-old MYH6-Cre-BDNF$^{-/-}$ hearts but not in WT hearts (**Figures 4Ia–c,II**). In 3-month-old MYH6-Cre-BDNF$^{-/-}$ hearts with osmotic edema, in addition to the above pathological changes, severe muscle fiber atrophy and disorder, unclear transverse striation of myocardial fibers and interstitial loosening were also found in the myocardium (**Figures 4Id–f,II**). Moreover, left atrial appendage thrombosis was found in most osmotic edema MYH6-Cre-BDNF$^{-/-}$ hearts (**Supplementary Figures 1A,E,H**). In addition to left atrial appendage thrombosis, some MYH6-Cre-BDNF$^{-/-}$ osmotic edema hearts also showed right atrial appendage thrombosis, left and right atrial thrombosis and left ventricular thrombosis (**Supplementary Figures 1E–K**). In addition, H&E staining revealed that the thrombosis had a mixed pathological

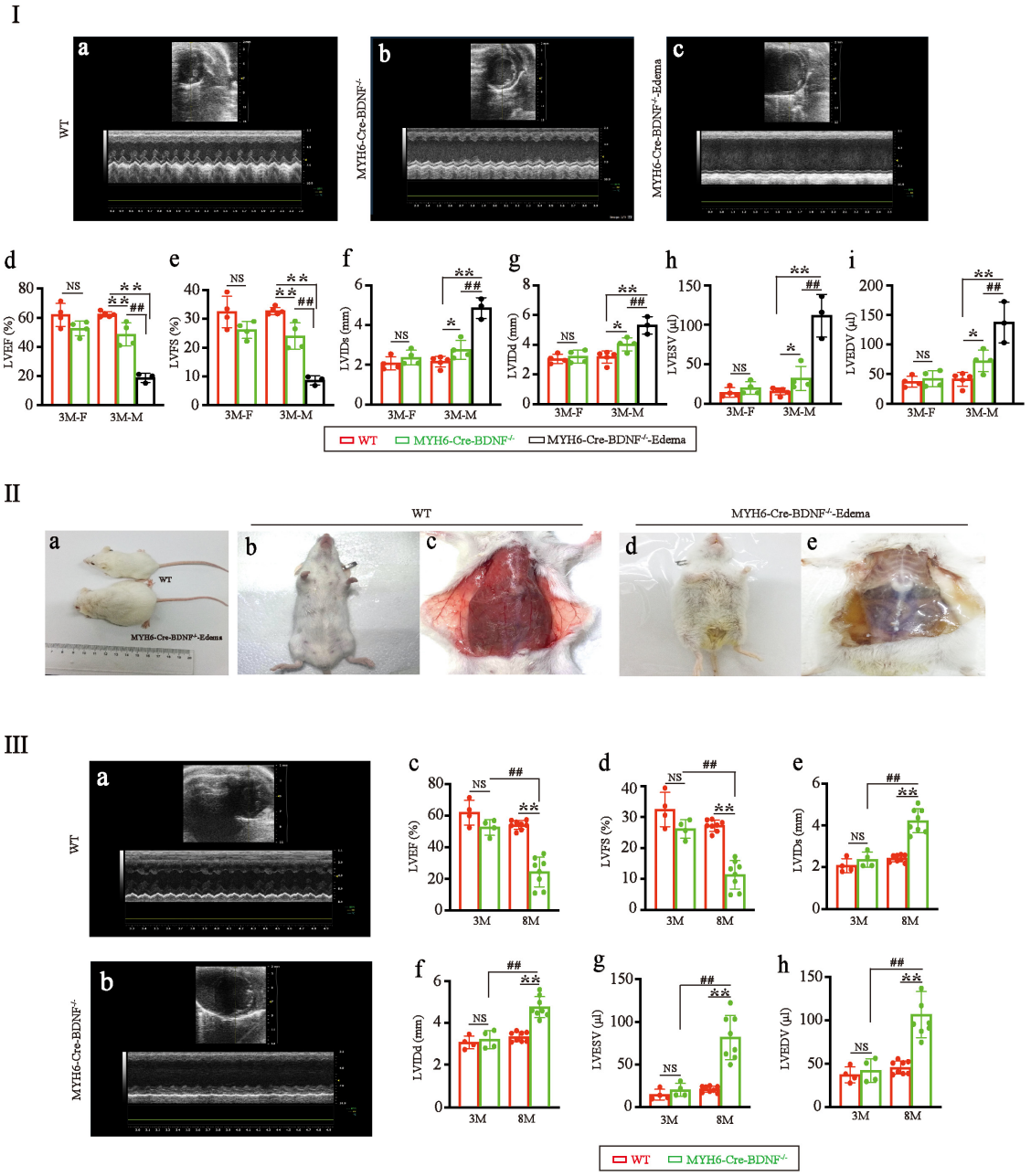

FIGURE 2
Cardiac dysfunction and osmotic edema are found in adult MYH6-Cre-BDNF$^{-/-}$ mice: **(I)** Representative echocardiography of WT hearts **(a)**, MYH6-Cre-BDNF$^{-/-}$ hearts **(b)** and MYH6-Cre-BDNF$^{-/-}$-edema hearts **(c)**. Echocardiography showed that in 3-month-old males, the left ventricular ejection fraction (LVEF) **(d)** and left ventricular fractional shortening (LVFS) **(e)** of MYH6-Cre-BDNF$^{-/-}$ hearts were significantly lower than those of WT hearts, while the left ventricular end-systolic internal diameter (LVIDs) **(f)**, left ventricular end-diastolic internal diameter (LVIDd) **(g)**, left ventricular end-systolic volume (LVESV) **(h)** and left ventricular end-diastolic volume (LVEDV) **(i)** of MYH6-Cre-BDNF$^{-/-}$ hearts were significantly higher than those of WT hearts. Three-month-old osmotic edema MYH6-Cre-BDNF$^{-/-}$ male mice had worse cardiac function parameters (LVEF, LVFS, LVIDs, LVIDd, LVESV and LVEDV) than 3-month-old WT mice **(a–i)**. *$p < 0.05$, **, $^{\#\#}p < 0.01$. $n = 4$ for the 3-month-old female WT and MYH6-Cre-BDNF$^{-/-}$ groups respectively; $n = 5$ and 4 for the 3-month-old male WT and MYH6-Cre-BDNF$^{-/-}$ groups. $n = 3$ for the 3-month-old male MYH6-Cre-BDNF$^{-/-}$ edema group. **(II)** Starting at 3 months of age, some MYH6-Cre-BDNF$^{-/-}$ mice exhibited osmotic edema **(a,d,e)** compared to WT mice **(a–c)**. **(III)** Representative echocardiography of 8-month-old WT hearts **(a)** and 8-month-old MYH6-Cre-BDNF$^{-/-}$ hearts **(b)**. The LVEF **(c)** and LVFS **(d)** of 8-month-old MYH6-Cre-BDNF$^{-/-}$ female hearts were significantly smaller than those of 8-month-old WT female hearts, 3-month-old MYH6-Cre-BDNF$^{-/-}$ female hearts and 3-month-old WT female hearts, while LVIDs **(e)**, LVIDd **(f)**, LVESV **(g)**, and LVEDV **(h)** of 8-month-old MYH6-Cre-BDNF$^{-/-}$ female hearts were significantly higher than those of 8-month-old WT female hearts, 3-month-old MYH6-Cre-BDNF$^{-/-}$ female hearts and 3-month-old WT female hearts. **, $^{\#\#}p < 0.01$. $n = 4$ for the 3-month-old female WT and MYH6-Cre-BDNF$^{-/-}$ groups respectively; $n = 8$ for the 8-month-old female WT and MYH6-Cre-BDNF$^{-/-}$ groups respectively.

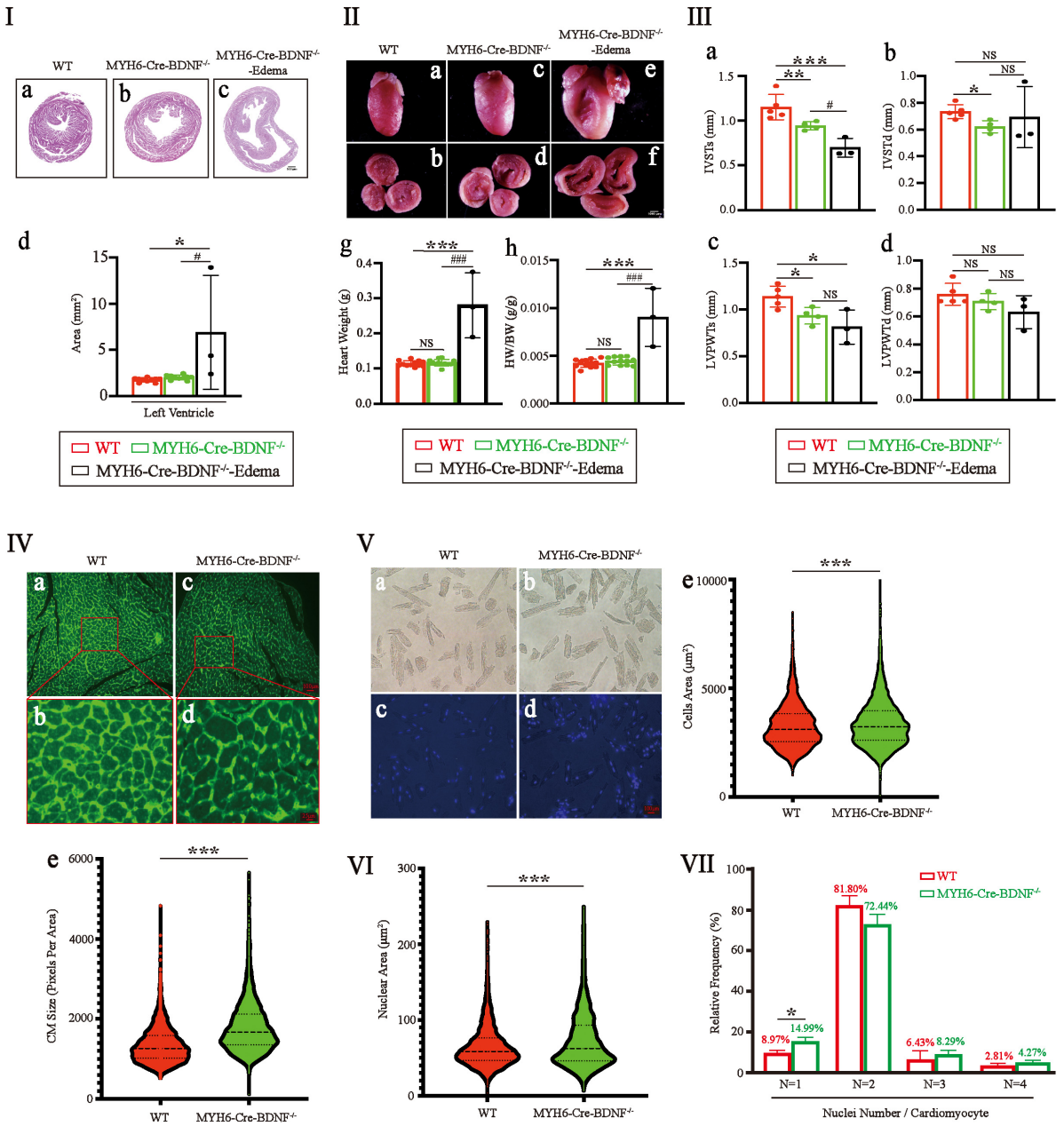

FIGURE 3
Eccentric myocardial hypertrophy accompanied by an increase in the area of the cardiomyocyte nucleus and an increase in the percentage of single-nucleus cardiomyocytes were found in young adult MYH6-Cre-BDNF$^{-/-}$ mice: **(I,II)** The left ventricular area of 3-month-old MYH6-Cre-BDNF$^{-/-}$ male hearts was significantly larger than that of WT hearts **(I)**. In addition, the ventricular area, heart weight and ratio of heart weight/body weight of 3-month-old MYH6-Cre-BDNF$^{-/-}$ osmotic edema mice were significantly higher than those of 3-month-old MYH6-Cre-BDNF$^{-/-}$ and WT mice **(I,II)**. n = 10 for the 3-month-old male WT and MYH6-Cre-BDNF$^{-/-}$ groups respectively; n = 3 for the 3-month-old male MYH6-Cre-BDNF$^{-/-}$ edema group. **(III)** Echocardiography showed that the interventricular septum end-systolic thickness (IVSTs) and left ventricular posterior wall end-systolic thickness (LVPWTs) of 3-month-old MYH6-Cre-BDNF$^{-/-}$ hearts were significantly smaller than those of WT hearts **(a,c)**. In addition, the IVSTs of 3-month-old MYH6-Cre-BDNF$^{-/-}$ osmotic edema hearts was significantly smaller than those of 3-month-old MYH6-Cre-BDNF$^{-/-}$ hearts and WT hearts **(c)**. Furthermore, the interventricular septum end-diastolic thickness (IVSTd) of 3-month-old MYH6-Cre-BDNF$^{-/-}$ hearts was significantly smaller than that of WT hearts **(b)**. n = 5 and 4 for the 3-month-old male WT and MYH6-Cre-BDNF$^{-/-}$ groups respectively; n = 3 for the 3-month-old male MYH6-Cre-BDNF$^{-/-}$ edema group. **(IV)** Semiquantification of WGA immunofluorescence staining revealed that the mean area of cardiomyocytes in 3-month-old MYH6-Cre-BDNF$^{-/-}$ hearts was significantly higher than that in WT hearts. n = 6. **(V)** Quantification analysis of isolated single cardiomyocytes demonstrated that the mean area of cardiomyocytes in 3-month-old MYH6-Cre-BDNF$^{-/-}$ hearts was significantly higher than that in WT hearts. n = 3. **(VI)** The mean area of cardiomyocyte nuclei of 3-month-old MYH6-Cre-BDNF$^{-/-}$ hearts was significantly higher than that of WT hearts. n = 3. **(VII)** The percentage of single-nucleus cardiomyocytes in 3-month-old MYH6-Cre-BDNF$^{-/-}$ hearts (N: Number of nuclei per cell) was significantly higher than that in WT hearts, n = 3. *, $^{\#}p < 0.05$, **$p < 0.01$, ***, $^{\#\#\#}p < 0.001$.

morphology that was infiltrated with red blood cells, macrophages, lymphocytes and nodular eosinophilic material (**Supplementary Figures 1F,H–K**). Degenerative changes in the myocardium occurred in MYH6-Cre-BDNF$^{-/-}$ hearts, leading us to further observe cardiac fibrosis. Masson's trichrome staining revealed that compared to WT myocardium, MYH6-Cre-BDNF$^{-/-}$ myocardium had more extensive perivascular fibrosis and scattered focal interstitial fibrosis, mainly in the inner myocardium (**Supplementary Figure 2**). Furthermore, in MYH6-Cre-BDNF$^{-/-}$ osmotic edema hearts, more extensive interstitial fibrosis was found in the myocardium and thromboses, which were located in the atrial appendage and atrial and ventricular cavity, than in MYH6-Cre-BDNF$^{-/-}$ hearts and WT hearts (**Supplementary Figure 3**). Moreover, more extensive cardiomyocyte death and interstitial fibrosis were observed in 8-month-old MYH6-Cre-BDNF$^{-/-}$ osmotic edema myocardium than in 8-month-old MYH6-Cre-BDNF$^{-/-}$, 8-month-old WT, 3-month-old MYH6-Cre-BDNF$^{-/-}$ osmotic edema and 3-month-old MYH6-Cre-BDNF$^{-/-}$ myocardium (**Supplementary Figure 4** vs. **Figure 4** and **Supplementary Figure 2**). In addition, the above pathological phenotypes were more severe in 8-month-old WT myocardium than in 3-month-old WT myocardium (**Supplementary Figure 4** vs. **Figure 4** and **Supplementary Figure 2**). In addition, in 8-month-old MYH6-Cre-BDNF$^{-/-}$ myocardium, focal interstitial fibrosis was found between the inner and external myocardium (**Supplementary Figure 4**); in contrast, the focal interstitial fibrosis found in 3-month-old MYH6-Cre-BDNF$^{-/-}$ myocardium was mainly located in the inner myocardium (**Supplementary Figures 2E,F**). Furthermore, transmission electron microscopy (TEM) revealed significantly disrupted mitochondrial distribution, swollen mitochondria, decreased mitochondrial density and serious mitophagy as well as blurred myofilament structures in cardiomyocytes, unclear sarcomere structures and Z lines, and unclear boundaries between the dark zone and the bright zone in 8-month-old MYH6-Cre-BDNF$^{-/-}$ hearts (**Supplementary Figure 5**).

Significant increases in heart failure indices, cardiomyocyte hypertrophy, and increased serum brain-derived neurotrophic factor and insulin levels are found in young adult MYH6-Cre-BDNF$^{-/-}$ mice

The HF phenotypes (such as osmotic edema, cardiomyocyte hypertrophy, increased cardiomyocyte death, degeneration of the myocardium and cardiac dysfunction) that occurred in MYH6-Cre-BDNF$^{-/-}$ mice led us to investigate HF parameters in the myocardium and peripheral serum. The qPCR results showed that, 3-month-old MYH6-Cre-BDNF$^{-/-}$ hearts showed significantly higher expression of the HF markers atrial natriuretic peptide (ANP) and brain natriuretic peptide (BNP) in the left ventricle than WT hearts (**Figures 5Ia,b**; $p < 0.05$). Analysis of the HF indices N-terminal pro-brain natriuretic peptide (NT-proBNP), BNP and Galectin-3 also confirmed that serum levels of NT-proBNP, BNP and Galectin-3 in 3-month-old MYH6-Cre-BDNF$^{-/-}$ mice were significantly higher than those in WT mice (**Figures 5IIa–c**; $p < 0.05$). In addition, qPCR showed that 3-month-old MYH6-Cre-BDNF$^{-/-}$ mice showed significantly higher expression of the cardiomyocyte hypertrophy markers alpha smooth muscle actin (αSMA) and beta myosin heavy chain (β-MHC) in the left ventricle than WT mice (**Figures 5Ic,d**; $p < 0.05$). These results confirm that HF and dilated cardiomyopathy occurred in 3-month-old MYH6-Cre-BDNF$^{-/-}$ hearts. Metabolism-related parameters (glucose, insulin, leptin and BDNF) were also measured. Compared to those in WT mice, the serum levels of BDNF and insulin in 3-month-old MYH6-Cre-BDNF$^{-/-}$ mice were significantly increased (**Figures 5IIIa,b**; $p < 0.01$). While the differences in glucose and leptin levels were not statistically significant between 3-month-old MYH6-Cre-BDNF$^{-/-}$ mice and 3-month-old WT mice (**Figures 5IIIc,d**; $p > 0.05$). Metabolic disruption of BDNF, increased expression of non-cardiomyocyte-derived BDNF and activation of insulin metabolism were observed in 3-month-old MYH6-Cre-BDNF$^{-/-}$ mice.

Poor cardiac function and regeneration are found in young adult MYH6-Cre-BDNF$^{-/-}$ hearts during myocardial infarction

The possible damaging effect on myocardial regeneration in MYH6-Cre-BDNF$^{-/-}$ hearts during MI was also investigated. The one-year survival rate of MYH6-Cre-BDNF$^{-/-}$ mice showed that the survival rate of 4–6-month-old mice decreased to approximately 58% from approximately 80% in 3-month-old mice; therefore, 5-month-old male MYH6-Cre-BDNF$^{-/-}$ mice were used in this experiment. After MI, the LVEF and LVFS of MYH6-Cre-BDNF$^{-/-}$ mice were apparently smaller (**Figures 5IVa,b**; $p< 0.05$), while the LVIDd, LVIDs, LVEDV and LVESV were not statistically significant compared to those in WT mice (**Figures 5IVc–f**; $p> 0.05$). Furthermore, the infarct size of MYH6-Cre-BDNF$^{-/-}$ MI hearts was significantly larger than that of WT hearts (**Figure 5V**; $p < 0.05$). In addition, the smallest ventricular wall thickness of the infarct zone and the thickness of the infarct border zone of MYH6-Cre-BDNF$^{-/-}$ MI hearts were significantly smaller than those of wild-type MI hearts (**Figure 5VI**; $p < 0.05$).

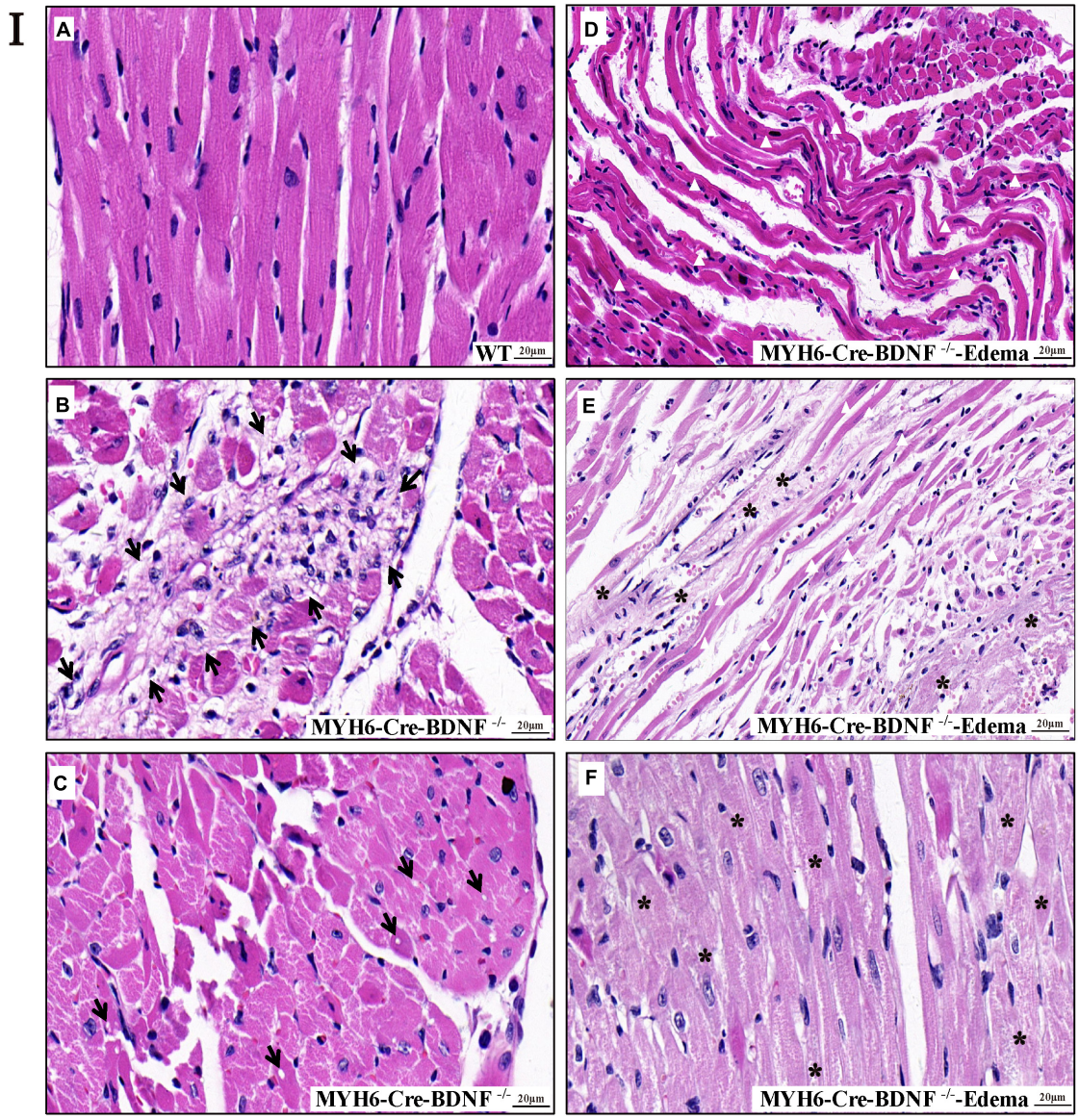

FIGURE 4

Cardiomyocyte death and degenerative changes in the myocardium are found in young adult MYH6-Cre-BDNF$^{-/-}$ hearts **(I)** H&E histological staining revealed that in 3-month-old MYH6-Cre-BDNF$^{-/-}$ hearts but not in WT hearts **(a)**, focal cardiomyocyte death, focal degenerative changes in cardiomyocytes, focal inflammation in the myocardium (**b**; arrow) and focal loss of nuclei in cardiomyocytes (**c**; arrow) were found, while in 3-month-old osmotic edema MYH6-Cre-BDNF$^{-/-}$ hearts, in addition to the above pathological changes, severe muscle fiber atrophy and disorder (**d,e**; white triangle), unclear transverse striation of myocardial fibers (**e,f**; asterisk) and interstitial loosening **(d,e)** were also found in the myocardium. *n* = 5 and 4 for the 3-month-old male WT and MYH6-Cre-BDNF$^{-/-}$ groups respectively; *n* = 3 for the 3-month-old male MYH6-Cre-BDNF$^{-/-}$ edema group. **(II)** Semi-quatitation of I. *n* = 3. Bar size as shown in the figure.

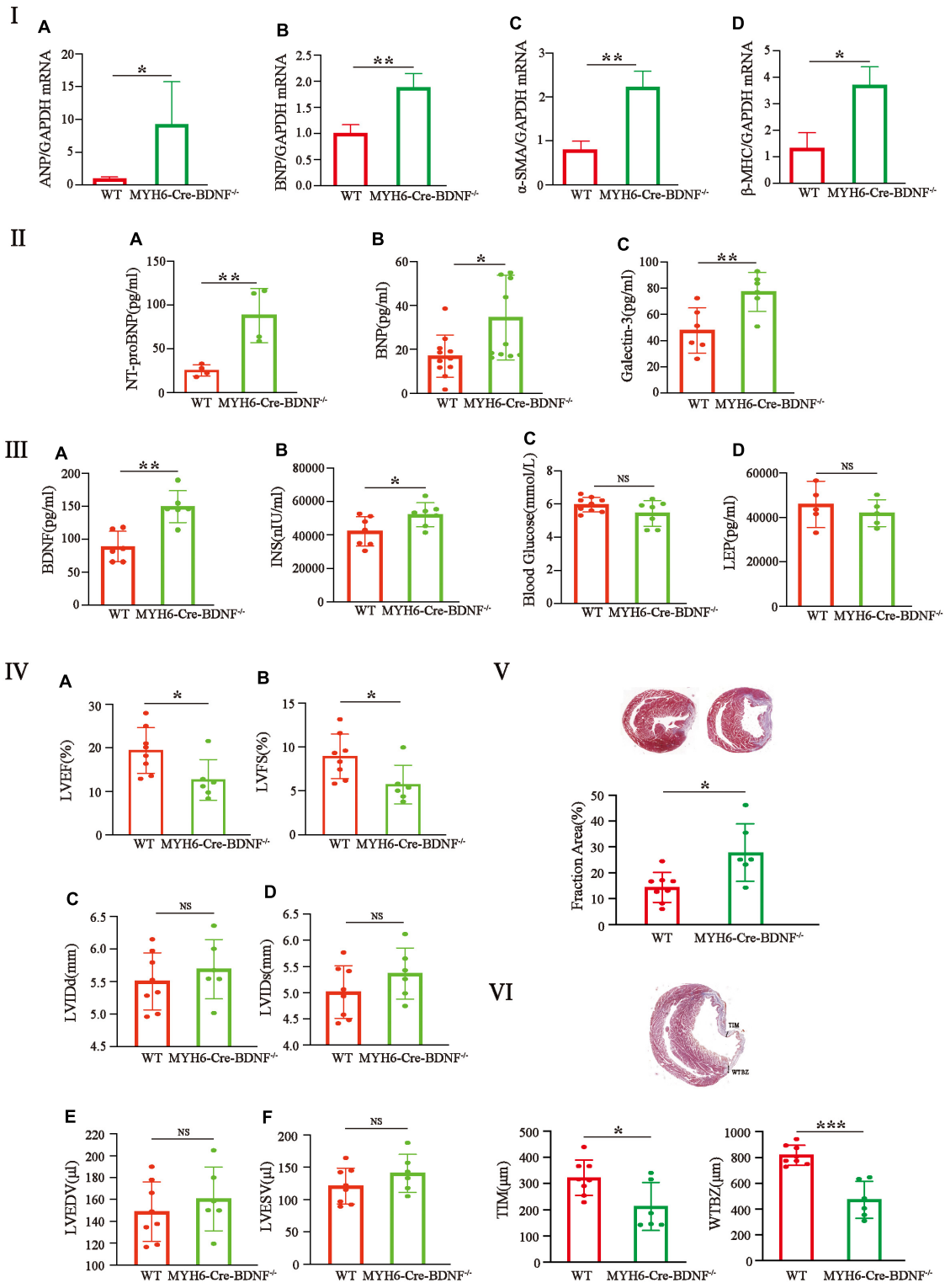

FIGURE 5

Significant increases in heart failure indices, pathological hypertrophy in the left ventricle, serum BDNF and insulin levels and poor cardiac function and regeneration are found in young adult MYH6-Cre-BDNF$^{-/-}$ mice: **(I–III)** The qPCR results showed that the expression of the heart failure markers atrial natriuretic peptide (ANP) **(Ia)** and brain natriuretic peptide (BNP) **(Ib)** was significantly higher in the left ventricle of 3-month-old MYH6-Cre-BDNF$^{-/-}$ hearts than in that of WT hearts. The analysis of the heart failure indices, N-terminal pro-brain natriuretic peptide (NT-proBNP), BNP and Galectin-3, also confirmed that serum levels of NT-proBNP **(IIa)**, BNP **(IIb)** and Galectin-3 **(IIc)** in 3-month-old MYH6-Cre-BDNF$^{-/-}$ mice were significantly higher than those in WT mice. In addition, qPCR showed that compared to WT, the expression of

(Continued)

FIGURE 5
the myocardial hypertrophy markers alpha smooth muscle actin (αSMA) **(Ic)** and beta myosin heavy chain (β-MHC) **(Id)** was significantly higher in the left ventricle of 3-month-old MYH6-Cre-BDNF$^{-/-}$ mice. Moreover, compared to those in WT mice, the metabolism-related parameters, serum levels of BDNF and insulin in 3-month-old MYH6-Cre-BDNF$^{-/-}$ mice were significantly increased **(IIIa,b)**. n = 3 for the WT and MYH6-Cre-BDNF$^{-/-}$ groups respectively in **(Ia,b)**; n = 4 for the WT and MYH6-Cre-BDNF$^{-/-}$ groups respectively in **(IIa)**; n = 11 for the WT and MYH6-Cre-BDNF$^{-/-}$ groups respectively in **(IIb)**; n = 6 for the WT and MYH6-Cre-BDNF$^{-/-}$ groups respectively in **(IIc)**; n = 6 for the WT and MYH6-Cre-BDNF$^{-/-}$ groups respectively in **(IIIa)**; n = 7 for the WT and MYH6-Cre-BDNF$^{-/-}$ groups respectively in **(IIIb)**; n = 9 and 7 for the WT and MYH6-Cre-BDNF$^{-/-}$ groups respectively in **(IIIc)**; n = 5 for the WT and MYH6-Cre-BDNF$^{-/-}$ groups respectively in **(IIId)**. **(IV–VI)** After MI, the LVEF and LVFS of 5-month-old MYH6-Cre-BDNF$^{-/-}$ mice were significantly smaller than those of WT mice **(IVa,b)**. While the LVIDd, LVIDs, LVEDV, and LVESV were not statistically significant compared to those in WT mice **(IVc–f)**. In parallel, the infarct size of MYH6-Cre-BDNF$^{-/-}$ MI hearts were significantly larger than that of WT hearts **(V)**. In addition, the smallest ventricular wall thickness of the infarct zone and the thickness of the infarct border zone of MYH6-Cre-BDNF$^{-/-}$ MI hearts were significantly smaller than those of wild-type MI hearts **(VI)**. n = 8 and 6 for the WT and MYH6-Cre-BDNF$^{-/-}$ groups respectively in **(IV–VI)**. LVEF, Left ventricular ejection fraction; LVFS, Left ventricular fractional shortening; LVIDs, Left ventricular end-systolic internal diameter; LVIDd, Left ventricular end-diastolic internal diameter; LVESV, Left ventricular end-systolic volume; LVEDV, Left ventricular end-diastolic volume; MYH6-Cre-BDNF$^{-/-}$, Cardiomyocyte-derived BDNF conditional knockout. *$p < 0.05$, **$p < 0.01$, ***$p < 0.001$.

Transcriptome sequencing combined with ingenuity pathway analysis reveals the pathways and gene interaction networks involved in cardiomyocyte death, myocardial degeneration, cardiac inflammation, ROS production, body weight increase and metabolic disruption seen in MYH6-Cre-BDNF$^{-/-}$ mice

Comparison of whole-transcriptome sequencing between 3-month-old male MYH6-Cre-BDNF$^{-/-}$ hearts and WT hearts combined with IPA was applied to identify underlying gene interaction networks and pathways affected by the deletion of cardiomyocyte-derived BDNF. A total of 501 differentially expressed genes (fold change $\geq$ 1.5; $q < 0.5$) were selected for IPA to identify the genes related to canonical pathways, biofunctions and diseases, and interaction networks. Indeed, IPA revealed that the differential expression of 9 genes (6 upregulated genes and 3 downregulated genes; MYH6-Cre-BDNF$^{-/-}$ vs. WT; all comparisons hereafter are the same) was related to increased apoptotic activity in the heart (**Table 1**). The interaction network of these 9 genes to regulate the activation of heart apoptosis was revealed by IPA, as shown in **Figure 6**, which provided a possible molecular mechanism for the cardiomyocyte death seen in MYH6-Cre-BDNF$^{-/-}$ hearts. In addition, the synthesis of reactive oxygen species (ROS) was increased in MYH6-Cre-BDNF$^{-/-}$ hearts compared to WT hearts, which was related to 19 genes (upregulated: 16 genes; downregulated: 3 genes; **Table 2**) via their interaction network to regulate the increase in ROS, as shown in **Figure 7**. In addition, the IPA for canonical pathways revealed that the pathway for the production of nitric oxide and reactive oxygen species in macrophages was activated in MYH6-Cre-BDNF$^{-/-}$ hearts compared to WT hearts and was related to 7 genes (upregulated: 6 genes; downregulated: 1 gene; **Table 3**) via their interaction network, which regulated this effect, as shown in **Supplementary Figure 6**. The findings provide a molecular mechanism and the relevant genes for the cardiomyocyte death, cardiac dysfunction, cardiomyocyte degeneration and hypotrophy, HF and increased ROS activity seen in MYH6-Cre-BDNF$^{-/-}$ hearts.

In addition, IPA identified that the regulation of weight gain was increased in differentially expressed genes between MYH6-Cre-BDNF$^{-/-}$ mice and WT mice; (9 upregulated genes; **Supplementary Table 1**) and their interaction network (**Supplementary Figure 7**) were related to this function. Moreover, the activity of lipid metabolism was discovered to be increased in MYH6-Cre-BDNF$^{-/-}$ mice compared to WT mice. The activated functions included synthesis of fatty acids (11 genes upregulated and 1 gene downregulated, as shown in **Supplementary Table 2** and in the interaction network in **Supplementary Figure 8**), synthesis of lipids (15 genes upregulated and 2 genes downregulated, as shown in **Supplementary Table 3** and in the interaction network in **Supplementary Figure 9**), biosynthesis of polyunsaturated fatty acids (8 upregulated genes and 1 downregulated gene, as shown in **Supplementary Table 4** and in the interaction network in **Supplementary Figure 10**), synthesis of eicosanoids (8 upregulated genes and 1 downregulated gene, as shown in **Supplementary Table 5** and in the interaction network in **Supplementary Figure 11**), the concentration of colfosceril palmitate (4 upregulated genes, as shown in **Supplementary Table 6** and in the interaction network in **Supplementary Figure 12**) and concentration of triacylglycerol (11 genes upregulated and 2 genes downregulated, as shown in **Supplementary Table 7** and in the interaction network in **Supplementary Figure 13**) as well as fatty acid metabolism (17 upregulated genes and 1 downregulated gene, as shown in **Supplementary Table 8** and in the interaction network in **Supplementary Figure 14**). Furthermore, IPA of canonical pathways identified that the STAT3, melatonin degradation I and acetone degradation I (to methylglyoxal) pathways were activated in MYH6-Cre-BDNF$^{-/-}$ hearts. The increase in the expression of 6 genes with the interaction network for STAT3

TABLE 1 IPA analysis identifies increase of apoptosis of heart in MYH6-Cre-BDNF$^{-/-}$ heart (activation *z*-score = 2.028; p = 2.06E-02).

Genes	ID	Expr log ratio	Phospho false discovery	Location
ADIPOQ	ENSMUSG00000022878	↑1.964	1.08E-05	Extracellular space
ANGPT1	ENSMUSG00000022309	↓-0.815	3.18E-01	Extracellular space
CXADR	ENSMUSG00000022865	↓-0.598	1.08E-01	Plasma membrane
FASN	ENSMUSG00000025153	↑1.524	4.21E-03	Cytoplasm
GAPDH	ENSMUSG00000057666	↑2.240	1.23E-01	Cytoplasm
LCN2	ENSMUSG00000026822	↑1.344	4.48E-01	Extracellular space
PPP1R10	ENSMUSG00000039220	↓-0.633	1.48E-01	Nucleus
RAC1	ENSMUSG00000001847	↑1.404	6.32E-02	Plasma membrane
SCD	ENSMUSG00000037071	↑2.001	7.42E-03	Cytoplasm

pathway activation is shown in **Supplementary Table 9** and **Supplementary Figure 15**. The increase in the expression of 4 genes in the interaction network for the activation of melatonin degradation I and acetone degradation I is shown in **Supplementary Table 10** and **Supplementary Figures 16**, **17**. The findings uncovered a molecular mechanism by which the syntheses of fatty acids, lipids, polyunsaturated fatty acids and eicosanoids, the concentration of colfosceril palmitate and triacylglycerol and the metabolism of fatty acids are increased that is related to the loss of cardiomyocyte-derived BDNF, and the molecular mechanism was involved in the increased body weight seen in MYH6-Cre-BDNF$^{-/-}$ mice.

Furthermore, IPA revealed that 41 inflammation regulatory genes (upregulated: 38 genes; downregulated: 3 genes; **Supplementary Tables 11–20**) were involved in regulating the increase in inflammatory activity in MYH6-Cre-BDNF$^{-/-}$ hearts compared to WT hearts. The increased biofunctions related to these 41 genes were as follows: inflammatory response (upregulated: 25 genes; downregulated: 1 gene; **Supplementary Table 11**), recruitment of phagocytes (upregulated: 13 genes; downregulated: 1 gene; **Supplementary Table 12**), chemotaxis of neutrophils (upregulated: 11 genes; **Supplementary Table 13**), granulocytes (upregulated: 12 genes; **Supplementary Table 14**) and leukocytes (upregulated: 16 genes; **Supplementary Table 15**) as well as activation of leukocytes (upregulated: 19 genes; downregulated: 1 gene; **Supplementary Table 16**), macrophages (upregulated: 9 genes; downregulated: 1 gene; **Supplementary Table 17**), mononuclear leukocytes (upregulated: 12 genes; **Supplementary Table 18**), phagocytes (upregulated: 12 genes; downregulated: 1 gene; **Supplementary Table 19**) and lymphocytes (upregulated: 11 genes; **Supplementary Table 20**). The interaction networks of the included genes for individual increased biofunctions are shown in **Supplementary Figures 18–27**. The findings suggested that loss of cardiomyocyte-derived BDNF increased the inflammatory response and activity in the myocardium by increasing chemotaxis of neutrophils, granulocytes, phagocytes, and leukocytes and by activating leukocytes, macrophages, mononuclear leukocytes, phagocytes and lymphocytes. The molecular mechanisms involved in these processes are controlled by the identified genes and their interaction networks, as shown in **Supplementary Table 14** and **Supplementary Figures 18–27**. These results provide one of the possible mechanisms underlying the cardiomyocyte death and degeneration, interstitial fibrosis, and thrombi in the atrial appendages, atria and ventricles as well as the increased inflammation seen in MYH6-Cre-BDNF$^{-/-}$ hearts.

Discussion

Currently, the physiopathological role of cardiomyocyte-derived BDNF in the heart is still not precisely known. In the present study, as **Figure 8** shown, we established cardiomyocyte-specific BDNF conditional knockout mice (MYH6-Cre-BDNF$^{-/-}$) in which BDNF is ablated specifically in cardiomyocytes upon activation of the myosin heavy chain 6 (MYH6) promoter during development. The MYH6-Cre-BDNF$^{-/-}$ mouse line is able to normally develop, grow and produce offspring. This suggests that ablation of cardiomyocyte-derived BDNF during the development of cardiomyocytes in the embryonic stage can be compensated to maintain whole-body development, growth and reproduction. However, in young adult, 3-month-old MYH6-Cre-BDNF$^{-/-}$ mice, cardiac function was significantly decreased, as we found that the LVEF and LVFS of MYH6-Cre-BDNF$^{-/-}$ hearts declined significantly compared to those of WT hearts. In addition, pathological dilation of the left ventricle was found in 3-month-old MYH6-Cre-BDNF$^{-/-}$ mouse hearts, which was confirmed by their significantly increased LVIDs, LVIDd, LVESV and LVEDV compared to those of WT hearts. Moreover, from 3 months of age onwards, some MYH6-Cre-BDNF$^{-/-}$ mice had somatic edema, and these mice died approximately 1 week after osmotic edema occurred. Echocardiography demonstrated that 3-month-old osmotic edema MYH6-Cre-BDNF$^{-/-}$ hearts have worse cardiac function than non-osmotic edema MYH6-Cre-BDNF$^{-/-}$ and WT hearts, which was supported by their significantly worse LVEF, LVFS, LVIDs, LVIDd,

FIGURE 6
Activated regulation of heart apoptosis played a role in heart failure induced by loss of cardiomyocyte-derived BDNF: Integrated IPA identified that apoptosis in cardiomyocyte-derived BDNF conditional knockout hearts was higher than that in wild-type hearts (p-value = 2.06E-02; activation z-score = 2.028). The interaction network demonstrated that 9 genes (6 upregulated genes and 3 downregulated genes) were included that were involved in the activation of apoptosis in cardiomyocyte-derived BDNF conditional knockout hearts. The shown interaction network only showed the predicted interaction by IPA analysis. Other interaction networks shown in this study are presented as the same format.

LVESV, and LVEDV. Furthermore, the time window of cardiac dysfunction in female MYH6-Cre-BDNF$^{-/-}$ hearts was later than that in male MYH6-Cre-BDNF$^{-/-}$ hearts. The findings suggest that when endogenous BDNF in cardiomyocytes is ablated during the development of cardiomyocytes, the outside source of BDNF is only able to compensate for the physiological requirements of the heart in the embryonic and young adult stages (approximately 1–2 months old); however, the later lack of compensation causes cardiac structural and functional impairment with increasing age, beginning at approximately 3 months old in males and slightly later in females. Additionally, cardiomyocyte-derived BDNF plays an important role in maintaining the integrity of the heart structurally and functionally, and the tolerance for ablation of cardiomyocyte-derived BDNF is better in females than in males. With increasing age, the lack of compensation of ablated cardiomyocyte-derived BDNF is fatal. Indeed, we found that MYH6-Cre-BDNF$^{-/-}$ mice at 3 months of age and older exhibited a HF phenotype with impaired cardiac function, pathological remodeling and osmotic edema and then died, which led to most MYH6-Cre-BDNF$^{-/-}$ mice dying within 1 year after birth.

Cardiac functional analyses combined with histological and cellular analyses showed that ablation of cardiomyocyte-derived BDNF also causes dilated cardiac cardiomyopathy in young adult hearts. This was confirmed by *in vivo* morphological

TABLE 2 IPA analysis identifies increase of synthesis of reactive oxygen species in MYH6-Cre-BDNF$^{-/-}$ heart (activation *z*-score = 2.418; *p* = 6.05E-06).

Genes	ID	Expr log ratio	Phospho false discovery	Location
CYP2A6	ENSMUSG00000000547	↑∞	2.00E-01	Cytoplasm
APOC2	ENSMUSG00000002992	↑∞	1.52E-01	Extracellular space
SERPINA1	ENSMUSG00000072849	↑∞	4.78E-01	Extracellular space
SERPINA3	ENSMUSG00000021091	↑1.304	4.75E-03	Extracellular space
RPL26	ENSMUSG00000060938	↑6.286	5.03E-95	Cytoplasm
LTF	ENSMUSG00000032496	↑3.135	2.34E-01	Extracellular space
CCL5	ENSMUSG00000035042	↑2.969	4.72E-01	Extracellular space
S100A8	ENSMUSG00000056054	↑2.748	1.82E-01	Cytoplasm
CYP2E1	ENSMUSG00000025479	↑1.893	1.70E-08	Cytoplasm
RAC1	ENSMUSG00000001847	↑1.404	6.32E-02	Plasma membrane
ITGAM	ENSMUSG00000030786	↑1.227	4.75E-03	Plasma membrane
CFB	ENSMUSG00000090231	↑1.044	1.31E-03	Extracellular space
EGF	ENSMUSG00000028017	↑0.834	9.48E-02	Extracellular space
CXCL14	ENSMUSG00000021508	↑0.718	3.33E-01	Extracellular space
NCF1	ENSMUSG00000015950	↑0.688	2.77E-01	Cytoplasm
MRC1	ENSMUSG00000026712	↑0.610	1.59E-03	Plasma membrane
HBB	ENSMUSG00000052305	↓-0.740	2.93E-01	Cytoplasm
CAV1	ENSMUSG00000007655	↓-0.872	1.81E-02	Plasma membrane
HBA1/HBA2	ENSMUSG00000069917	↓-0.944	4.36E-04	Extracellular space

analysis of the heart by echocardiography, which showed that the IVSTs, IVSTd and LVPWTs of 3-month-old MYH6-Cre-BDNF$^{-/-}$ hearts and osmotic edema MYH6-Cre-BDNF$^{-/-}$ hearts were significantly lower than those of WT hearts. Thus, the results indicated that dilated cardiomyopathy occurred. Indeed, the anatomical and histological analyses of isolated hearts both confirmed that the cross-sectional areas of 3-month-old MYH6-Cre-BDNF$^{-/-}$ and somatic edema MYH6-Cre-BDNF$^{-/-}$ hearts were significantly larger than those of WT hearts. Importantly, both WGA immunofluorescence staining for cardiomyocyte area in tissue and analysis of isolated cardiomyocytes at the cellular level showed that the area of cardiomyocytes in 3-month-old MYH6-Cre-BDNF$^{-/-}$ hearts was significantly larger than that in WT hearts. All facts clearly showed that dilated cardiomyopathy associated with cardiomyocyte hypertrophy was one of the pathological phenotypes caused by deletion of cardiomyocyte-derived BDNF in young adult hearts. Intriguingly, our isolated cardiomyocyte analysis also revealed cardiomyocyte hypertrophy in cardiomyocytes, and an increase in the area of cardiomyocyte nuclei was found in 3-month-old MYH6-Cre-BDNF$^{-/-}$ hearts. The exact mechanism regarding this phenotype is still unknown. One explanation might be that this was a parallel change to adapt to the changes associated with dilated cardiomyopathy and other pathological phenotypes seen in MYH6-Cre-BDNF$^{-/-}$ hearts, which require more gene activation to compensate for the ablation of BDNF in cardiomyocytes. In support of this hypothesis, comparison of whole-transcriptome sequencing results between 3-month-old male MYH6-Cre-BDNF$^{-/-}$ hearts and WT hearts identified the activation of many genes, pathways and biofunctions in the myocardium. In addition, an approximately 6% increase in single-nucleus cardiomyocytes was found in adult MYH6-Cre-BDNF$^{-/-}$ hearts. Most adult mammalian cardiomyocytes have two nuclei, and in the adult stage, only single-nucleus cardiomyocytes still maintain the potential for cell division (30–33). The increase in single-nucleus cardiomyocytes in young adult MYH6-Cre-BDNF$^{-/-}$ hearts might suggest that ablation of BDNF in cardiomyocytes might be able to decrease the production of double-nuclei cardiomyocytes from single-nucleus cardiomyocytes *via* an unknown mechanism that is probably related to maintaining proliferation potential to compensate for pathological remodeling and cardiomyocyte death. The exact cellular and molecular mechanisms need to be further studied in the future.

Cardiomyocyte death, degenerative changes in the myocardium and left atrial appendage thrombus are other notable pathological phenotypes seen in young adult MYH6-Cre-BDNF$^{-/-}$ hearts. Our histological analysis clearly demonstrated focal cardiomyocyte death, focal degenerative changes in cardiomyocytes, focal loss of nuclei in cardiomyocytes, focal inflammation, perivascular fibrosis and focal interstitial fibrosis in young adult MYH6-Cre-BDNF$^{-/-}$ hearts but not in WT hearts, while these pathological phenotypes were found to be more severe in same-age osmotic edema MYH6-Cre-BDNF$^{-/-}$ hearts and older MYH6-Cre-BDNF$^{-/-}$ hearts. Importantly, TEM ultrastructural analysis identified serious damage

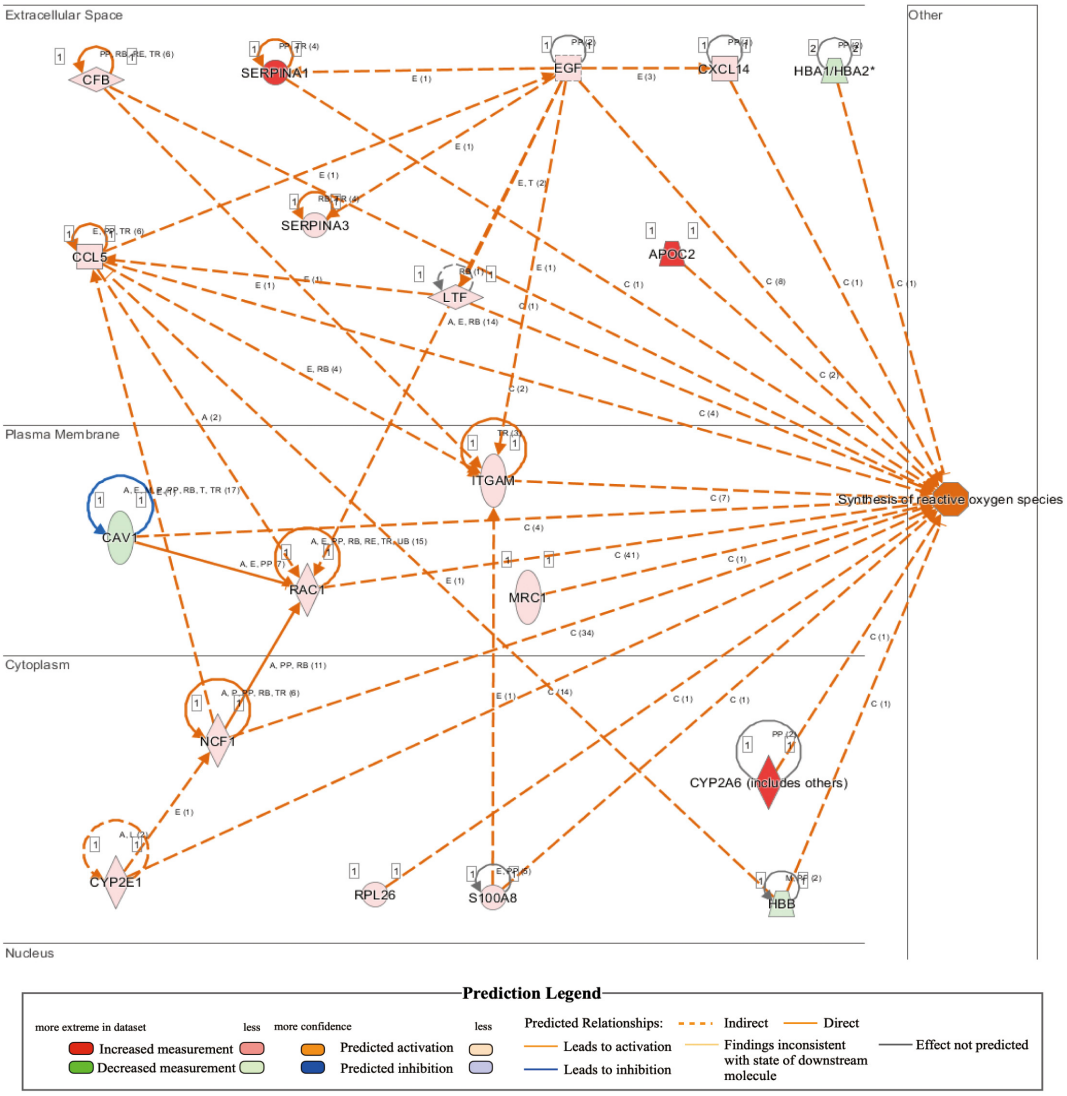

FIGURE 7
Activated regulation of reactive oxygen species synthesis played a role in heart failure induced by the loss of cardiomyocyte-derived BDNF: IPA revealed that the synthesis of reactive oxygen species in cardiomyocyte-derived BDNF conditional knockout hearts was higher than that in wild-type hearts (p-value = 6.05E-06; activation z-score = 2.418). The interaction network demonstrated that 19 genes (16 upregulated genes and 3 downregulated genes) were included, as shown in the interaction network for the activation of reactive oxygen species synthesis in cardiomyocyte-derived BDNF conditional knockout hearts.

TABLE 3 IPA analysis identifies activation of pathway for production of nitric oxide and reactive oxygen species in macrophages in MYH6-Cre-BDNF$^{-/-}$ heart (activation z-score = 2.65; p = 3.51E-02).

Genes	ID	Expr log ratio	Phospho false discovery	Location
APOC2	ENSMUSG00000002992	↑∞	1.52E-01	Extracellular space
LYZ	ENSMUSG00000069515	↑1.139	4.23E-01	Extracellular space
NCP1	ENSMUSG00000015950	↑0.688	2.77E-01	Cytoplasm
PPP1R10	ENSMUSG00000039220	↓-0.633	1.48E-01	Nucleus
RAC1	ENSMUSG00000001847	↑1.404	6.32E-02	Plasma membrane
S100A8	ENSMUSG00000056054	↑2.748	1.82E-01	Cytoplasm
SERPINA1	ENSMUSG00000072849	↑∞	4.78E-01	Extracellular space

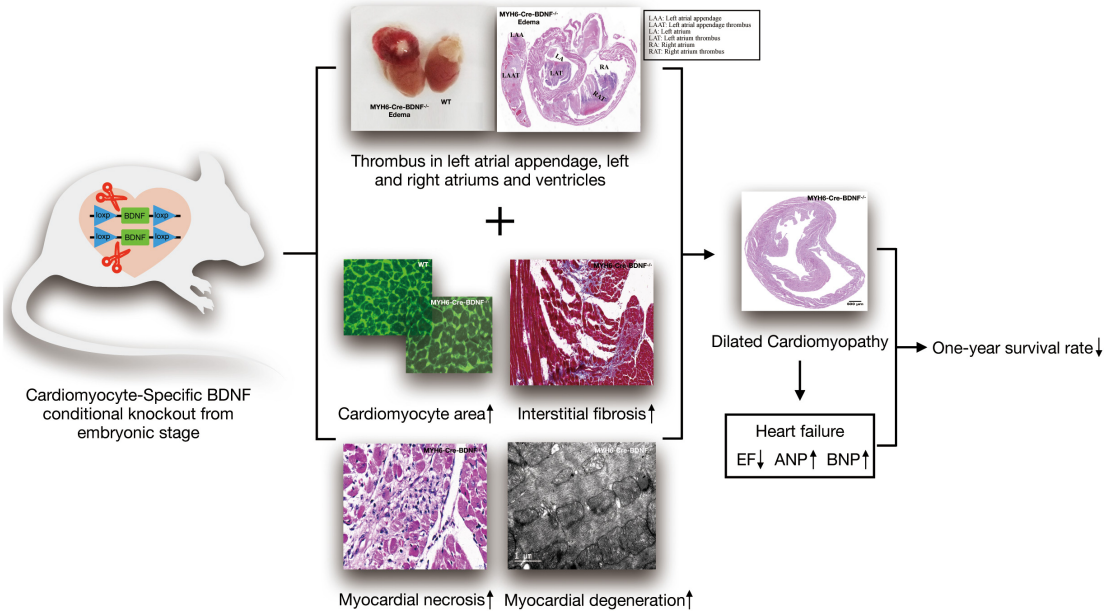

FIGURE 8
Schematic diagram of the ablation of cardiomyocyte-derived BDNF during development resulting in cardiac degeneration pathology, heart failure and low one-year survival rate.

to cardiomyocyte structure and mitochondrial pathology (disordered distribution, swelling mitochondria, loss of density of mitochondria and serious mitophagy) in young adult MYH6-Cre-BDNF$^{-/-}$ hearts. The above identified pathological changes are related to the cardiomyocyte death, cardiac dysfunction and cardiomyocyte hypertrophy caused by the ablation of cardiomyocyte-derived BDNF. Therefore, this ablation leads to HF and death in adult MYH6-Cre-BDNF$^{-/-}$ mice. In support of this hypothesis, in addition to cardiomyocyte death, degenerative and damage-related changes in the myocardium, cardiomyocyte hypertrophy and osmotic edema, the levels of HF markers (ANP and BNP) were found to be significantly higher in young adult MYH6-Cre-BDNF$^{-/-}$ myocardium, while HF indices (NT-proBNP, BNP and Galectin-3) were also found to be significantly higher in young adult MYH6-Cre-BDNF$^{-/-}$ mouse serum than in WT mouse serum. Thus, ablation of cardiomyocyte-derived BDNF mediated pathological changes in cardiac structure and function, leading to HF, which was a major reason for MYH6-Cre-BDNF$^{-/-}$ mouse death.

Left atrial appendage thrombosis is a unique pathology found in most osmotic edema MYH6-Cre-BDNF$^{-/-}$ hearts. Some osmotic edema MYH6-Cre-BDNF$^{-/-}$ hearts also exhibited right atrial appendage thrombosis, left and right atrial thrombosis and/or left ventricular thrombosis. The thrombi were consistent with mixed thrombus pathological morphology, which includes infiltration with red blood cells, macrophages, lymphocytes and nodular eosinophilic material. In this study, we still cannot explain the exact reason and mechanism underlying this pathological phenotype. A possible explanation might be attributed to hemodynamic changes incurred by dilated cardiomyopathy and the progression of HF combined with the activation of inflammation and ROS as well as metabolic disorders in the myocardium after BDNF ablation, which were identified via transcriptome sequencing combined with IPA. The underlying molecular mechanism needs to be further studied.

The results of a MI study using MYH6-Cre-BDNF$^{-/-}$ mice clearly demonstrated that ablation of cardiomyocyte-derived BDNF in adult hearts was deleterious regardless of cardiac function and regeneration when young adult hearts experience MI. This suggests that endogenous BDNF in cardiomyocytes is indispensable in maintaining the physiological integrity of cardiac structure and function as well as in healing and regeneration of ischemic myocardial pathology. In support of this hypothesis, we found that the serum level of BDNF in MYH6-Cre-BDNF$^{-/-}$ mice was significantly higher than that in WT mice. This result means that BDNF from other cell and tissue sources might fail to compensate for the loss of cardiomyocyte-derived BDNF.

In the present study, the underlying molecular mechanism of cardiac pathology initiated by ablation of cardiomyocyte-derived BDNF was also investigated by whole-transcriptome

sequencing of young adult MYH6-Cre-BDNF$^{-/-}$ hearts and parallel WT hearts. IPA is based on an experimentally confirmed reported knowledge database, and the effectors for biofunction, canonical pathways and interaction networks identified by IPA have high reliability; therefore, in the present study, the IPA system was applied to analyze the regulated biofunctions, canonical pathways and interaction networks of genes that were differentially expressed due to BDNF ablation in cardiomyocytes. Indeed, IPA identified pathways and gene interaction networks involved in increased heart apoptosis, activation of cardiac inflammation and ROS, and increased body weight and metabolic disorders in MYH6-Cre-BDNF$^{-/-}$ hearts. Among them, nine genes (upregulated: ADIPOQ, FASH, GAPDH, LCN2, RAC1, and SCD; downregulated: ANGPT1, CXADR, and PPP1R10) and their interaction network were revealed to be related to the increased apoptosis in MYH6-Cre-BDNF$^{-/-}$ hearts. As shown in the interaction network predicted by IPA, these nine genes are able to regulate the activation of heart apoptosis. In addition, IPA revealed that biofunctions involved in the synthesis of reactive oxygen species (ROS) (19 related genes in **Table 2**) and pathways for the production of nitric oxide and reactive oxygen species in macrophages (upregulated: APOC2, LYZ, NCF1, RAC1, S100A8, and SERPINA1; downregulated: PPP1R10) were activated in MYH6-Cre-BDNF$^{-/-}$ hearts. Furthermore, 41 inflammation regulatory genes were identified to regulate the increase in the inflammatory response in MYH6-Cre-BDNF$^{-/-}$ hearts compared to WT hearts via activation of the following functions (**Supplementary Tables 11–20** and **Supplementary Figures 18–27**): inflammatory response; recruitment of phagocytes; chemotaxis of neutrophils, granulocytes and leukocytes; and activation of leukocytes, macrophages, mononuclear leukocytes, phagocytes and lymphocytes. In addition, the STAT3 pathway (6 genes in **Supplementary Figure 15**) was activated in MYH6-Cre-BDNF$^{-/-}$ hearts. Hence, increased heart apoptosis, inflammation, ROS production and STAT3 pathway activation regulated by the identified genes and their interaction networks and pathways in MYH6-Cre-BDNF$^{-/-}$ hearts are proposed as possible molecular mechanisms mediating the cardiomyocyte death, cardiac dysfunction and degeneration and HF caused by the ablation of cardiomyocyte-derived BDNF.

Nine genes (**Supplementary Table 1**) were revealed to be related to an increase in weight gain. Increased lipid metabolism was also found in MYH6-Cre-BDNF$^{-/-}$ hearts compared to WT hearts via activation of the following functions (**Supplementary Tables 2–8** and **Supplementary Figures 8–14**): synthesis of fatty acids, synthesis of lipids, biosynthesis of polyunsaturated fatty acids, synthesis of eicosanoids, concentration of colfosceril palmitate and concentration of triacylglycerol as well as fatty acid metabolism. Furthermore, melatonin degradation I and acetone degradation I (to methylglyoxal) (4 genes in **Supplementary Figures 16**, **17**) were revealed to be activated in MYH6-Cre-BDNF$^{-/-}$ hearts. Hence, increases in weight gain and disordered metabolism of lipids and fatty acids as well as melatonin and acetone degradation regulated by the identified genes and their interaction networks as well as pathways in MYH6-Cre-BDNF$^{-/-}$ hearts are proposed as possible molecular mechanisms to mediate the increases in body weight, inflammation and ROS seen in MYH6-Cre-BDNF$^{-/-}$ mice.

The findings of the present study demonstrate that cardiomyocyte-derived BDNF is irreplaceable for maintaining the integrity of cardiac structure and function in the adult heart and regeneration after MI. It appears that the compensatory effect of non-cardiomyocyte-derived BDNF is merely able to meet the demands of embryonic and young adult (approximately 1–2-month-old) cardiac physiology when endogenous BDNF in cardiomyocytes is ablated. According to the findings from the present study, the pathological phenotypes caused by the lack of compensation for the ablated cardiomyocyte-derived BDNF during the developmental stage will occur in young adult hearts. In a previous report, ablation of cardiomyocyte-derived BDNF using an inducible 2-month-old cardiomyocyte-specific BDNF conditional knockout model did not show effects on cardiac remodeling, cardiac function, or myocardial angiogenesis or infarct size after MI; this can be explained by the increased plasma BDNF levels in non-cardiomyocytes compared to those in WT non-cardiomyocytes. Non-cardiomyocyte-derived BDNF successfully compensates and meets the demand for BDNF to maintain cardiac structure and function during short-term ablation of cardiomyocyte-derived BDNF, in which the heart is still under compensatory conditions (22). However, ablating cardiomyocyte-derived BDNF during development results in a different outcome and is harmful to young adult hearts. In support of this hypothesis, the pathological phenotypes seen in this study and the report using an inducible 2-month-old cardiomyocyte-specific TrkB conditional knockout MI mouse model (blockade of cardiomyocyte and non-cardiomyocyte-derived BDNF signaling), which included decreased cardiac function and myocardial angiogenesis in the infarct border zone and increased infarct size and cardiomyocyte apoptosis (22), clearly suggest that in the adult heart, cardiomyocyte-derived BDNF is irreplaceable for maintaining the integrity of cardiac pathophysiology and regenerating injured myocardium.

In fact, BDNF has been demonstrated to have protective effects against myocardial ischemia through survival-related signaling pathways, including the vascular endothelial growth factor (VEGF) and transient receptor potential canonical (TRPC)3/6 channel pathways (34, 35). Exogenous BDNF was found to promote the migration of Sca-1 cardiac progenitor cells

derived from the failing heart and repress cell cycle progression, suggesting its potency to ameliorate HF (36). Exercise training increased BDNF protein in skeletal muscles and the non-infarcted area of the left ventricle after MI, which may contribute to the improvement of muscle dysfunction and cardiac function after MI (12). All these findings are consistent with the results of the present study, which shows that the BDNF-TrkB pathway effectively plays a protective role in adult hearts after MI.

In addition, recent studies have revealed that BDNF plays important roles in cardiac pathology and HF. BDNF attenuates doxorubicin-induced cardiac dysfunction by activating Akt signaling (37), and BDNF protects the heart against septic cardiac dysfunction by reducing oxidative stress and apoptosis via TrkB and activating the eNOS/NO pathway (38). Low serum BDNF levels were found to be associated with future coronary events and mortality in patients with angina pectoris (39) and in patients with chronic HF (40) as well as higher cardiac death or rehospitalization due to worsening HF in discharged HF patients (41) and was positively correlated with HF severity (42). These findings support the deduction of the present study that cardiomyocyte-derived BDNF plays a critical role in protection against HF.

Taking into consideration of contrary reports, which the mice with Myh6-Cre or Myh6-MerCreMer (Tamoxifen inducible Cre recombinase) might display potential cardiotoxicity (43–48), or no Myh6-Cre induced cardiactoxicity found in many other researches (49–54). And it was reported that the Myh6-Cre mice with similar but mixed genetic background displayed no cardiotoxicity (26, 27). In present study, in order to avoid the potential cardiotoxicity from Myh6-Cre, the mating strategy to generate Myh6-Cre-BDNF^{flox} mice with mixed background was adopted as shown in methodology. Thus, pathological phenotypes and dysfunction of cardiac function found in present study from our established Myh6-Cre$^{\pm}$-BDNF$^{flox/flox}$ mice were attributed to the ablation of BDNF but not the potential cardiotoxicity of Myh6-Cre (**Supplementary Figures 28–31**).

Due to the limitations of time, model and technique, the function studies of IPA predicted pathways (such as for degeneration pathology and cardiac inflammation, etc.), and the rescue analysis of BDNF for neonatal myocardium were not performed in present study. In addition, due to the reason which it was found the pathological phenotypes that occurred in MYH6-Cre-BDNF$^{-/-}$ mice were not sex dependent; however, the time window of cardiac dysfunction in female MYH6-Cre-BDNF$^{-/-}$ hearts was later than that in male MYH6-Cre-BDNF$^{-/-}$ hearts. In the period of this study, we fail to collect the 3-month-old female MYH6-Cre-BDNF$^{-/-}$ edema mice. Therefore, 3-month-old female MYH6-Cre-BDNF$^{-/-}$ edema mice was not observed. All these issues will be set as our future study.

In summary, the present study demonstrated that ablation of cardiomyocyte-derived BDNF during the developmental stage did not impair embryonic survival, growth or reproduction; however, in young adult hearts, it caused cardiomyocyte death, myocardial degeneration, cardiomyocyte hypertrophy, left atrial appendage thrombosis, decreased cardiac function, increased cardiac inflammation and ROS activity, and metabolic disorders, leading to HF in adult hearts and eventually resulting in a decrease in the one-year survival rate. In addition, ablation of cardiomyocyte-derived BDNF during the developmental stage led to the exacerbation of cardiac dysfunction and poor regeneration after MI in adult hearts. Thus, cardiomyocyte-derived BDNF is irreplaceable for maintaining the integrity of cardiac structure and function in the adult heart and regeneration after MI. Therefore, the BDNF-TrkB pathway will be a novel target for myocardial pathophysiology in the adult heart.

Data availability statement

The datasets presented in this study can be found in online repositories. The names of the repository/repositories and accession number(s) can be found below: https://www.ncbi.nlm.nih.gov/, PRJNA857912.

Ethics statement

This animal study was reviewed and approved by the Jinan University Animal Care Committee.

Author contributions

LL, HG, and BL performed most of the experiments and analyzed the data. CL, WG, YC, HC, XZ, and YL contributed to knockout animal breeding and part of the data collection. ZY, RH, ZZ, LYL, HZ, QP, and XQ contributed to the discussion. DC conceived and designed this work and wrote the manuscript. All authors contributed to the article and approved the submitted version.

Funding

This work was supported by the National Natural Science Foundation of China (grant nos. 81971303, 81670236, 81470433, and 81170324), the National Natural Science Foundation of China-Key Program (grant no. 91649203), the National Key R&D Program of China (grant nos. 2016YFE0204700 and 2017YFA0103302), the Science and Technology Planning Project of Guangdong Province (grant no. 2015B020211010), and the Research grant of the Department of Education of Guangdong (grant no. 2012gjhz0003).

Conflict of interest

The authors declare that the research was conducted in the absence of any commercial or financial relationships that could be construed as a potential conflict of interest.

Publisher's note

All claims expressed in this article are solely those of the authors and do not necessarily represent those of their affiliated organizations, or those of the publisher, the editors and the reviewers. Any product that may be evaluated in this article, or claim that may be made by its manufacturer, is not guaranteed or endorsed by the publisher.

Supplementary material

The Supplementary Material for this article can be found online at: https://www.frontiersin.org/articles/10.3389/fcvm.2022.967463/full#supplementary-material

References

1. Mirowska-Guzel, D. The role of neurotrophic factors in the pathology and treatment of multiple sclerosis. *Immunopharmacol Immunotoxicol.* (2009) 31:32–8. doi: 10.1080/08923970802379819

2. Cohen-Cory S, Kidane AH, Shirkey NJ, Marshak S. Brain-derived neurotrophic factor and the development of structural neuronal connectivity. *Dev Neurobiol.* (2010) 70:271–88. doi: 10.1002/dneu.20774

3. Gezen-Ak D, Dursun E, Hanagasi H, Bilgiç B, Lohman E, Araz ÖS, et al. BDNF, TNFalpha, HSP90, CFH, and IL-10 serum levels in patients with early or late onset Alzheimer's disease or mild cognitive impairment. *J Alzheimers Dis.* (2013) 37:185–95. doi: 10.3233/JAD-130497

4. Kim H, Li Q, Hempstead BL, Madri JA. Paracrine and autocrine functions of brain-derived neurotrophic factor (BDNF) and nerve growth factor (NGF) in brain-derived endothelial cells. *J Biol Chem.* (2004) 279:33538–46. doi: 10.1074/jbc.M404115200

5. Fujimura H, Altar CA, Chen RY, Nakamura T, Nakahashi T, Kambayashi J, et al. Brain-derived neurotrophic factor is stored in human platelets and released by agonist stimulation. *Thromb Haemostasis.* (2002) 87:728–34.

6. Ejiri J, Inoue N, Kobayashi S, Shiraki R, Otsui K, Honjo T, et al. Possible role of brain-derived neurotrophic factor in the pathogenesis of coronary artery disease. *Circulation.* (2005) 112:2114–20. doi: 10.1161/Circulationaha.104.476903

7. Hong JH, Park HM, Byun KH, Lee BH, Kang WC, Jeong GB. BDNF expression of macrophages and angiogenesis after myocardial infarction. *Int J Cardiol.* (2014) 176:1405–8. doi: 10.1016/j.ijcard.2014.08.019

8. Paczkowska E, Kaczynska K, Pius-Sadowska E, Rogińska D, Kawa M, Ustianowski P, et al. Humoral activity of cord blood-derived stem/progenitor cells: Implications for stem cell-based adjuvant therapy of neurodegenerative disorders. *PLoS One.* (2013) 8:e83833. doi: 10.1371/journal.pone.0083833

9. Paczkowska E, Piecyk K, Luczkowska K, Kotowski M, Roginska D, Pius-Sadowska E, et al. Expression of neurotrophins and their receptors in human Cd34(+) bone marrow cells. *J Physiol Pharmacol.* (2016) 67:151–9.

10. Kerschensteiner M, Gallmeier E, Behrens L, Leal VV, Misgeld T, Klinkert WE, et al. Activated human T cells, B cells, and monocytes produce brain-derived neurotrophic factor in vitro and in inflammatory brain lesions: A neuroprotective role of inflammation? *J Exp Med.* (1999) 189:865–70. doi: 10.1084/jem.189.5.865

11. Schulte-Herbruggen O, Nassenstein C, Lommatzsch M, Quarcoo D, Renz H, Braun A. Tumor necrosis factor-alpha and interleukin-6 regulate secretion of brain-derived neurotrophic factor in human monocytes. *J Neuroimmunol.* (2005) 160:204–9. doi: 10.1016/j.jneuroim.2004.10.026

12. Lee HW, Ahmad M, Wang HW, Leenen FH. Effects of exercise training on brain-derived neurotrophic factor in skeletal muscle and heart of rats post myocardial infarction. *Exp Physiol.* (2017) 102:314–28. doi: 10.1113/EP086049

13. Kermani P, Hempstead B. Brain-derived neurotrophic factor: A newly described mediator of angiogenesis. *Trends Cardiovasc Med.* (2007) 17:140–3. doi: 10.1016/j.tcm.2007.03.002

14. Fulgenzi G, Tomassoni-Ardori F, Babini L, Becker J, Barrick C, Puverel S, et al. BDNF modulates heart contraction force and long-term homeostasis through truncated TrkB.T1 receptor activation. *J Cell Biol.* (2015) 210:1003–12. doi: 10.1083/jcb.201502100

15. Anastasia A, Deinhardt K, Wang S, Martin L, Nichol D, Irmady K, et al. Trkb signaling in pericytes is required for cardiac microvessel stabilization. *PLoS One.* (2014) 9:e87406. doi: 10.1371/journal.pone.0087406

16. Kermani P, Rafii D, Jin DK, Whitlock P, Schaffer W, Chiang A, et al. Neurotrophins promote revascularization by local recruitment of TrkB+ endothelial cells and systemic mobilization of hematopoietic progenitors. *J Clin Invest.* (2005) 115:653–63. doi: 10.1172/JCI22655

17. Caporali A, Emanueli C. Cardiovascular actions of neurotrophins. *Physiol Rev.* (2009) 89:279–308. doi: 10.1152/physrev.00007.2008

18. Donovan MJ, Lin MI, Wiegn P, Ringstedt T, Kraemer R, Hahn R, et al. Brain derived neurotrophic factor is an endothelial cell survival factor required for intramyocardial vessel stabilization. *Development.* (2000) 127:4531–40.

19. Cao L, Zhang L, Chen S, Yuan Z, Liu S, Shen X, et al. BDNF-mediated migration of cardiac microvascular endothelial cells is impaired during ageing. *J Cell Mol Med.* (2012) 16:3105–15. doi: 10.1111/j.1582-4934.2012.01621.x

20. Wang Z, Chen Y, Chen X, Zheng X, Xu G, Yuan Z, et al. The TrkB-T1 receptor mediates BDNF-induced migration of aged cardiac microvascular endothelial cells by recruiting Willin. *Aging Cell.* (2019) 18:e12881. doi: 10.1111/acel.12881

21. Stoilov P, Castren E, Stamm S. Analysis of the human TrkB gene genomic organization reveals novel TrkB isoforms, unusual gene length, and splicing mechanism. *Biochem Biophys Res Commun.* (2002) 290:1054–65. doi: 10.1006/bbrc.2001.6301

22. Okada S, Yokoyama M, Toko H, Tateno K, Moriya J, Shimizu I, et al. Brain-derived neurotrophic factor protects against cardiac dysfunction after myocardial infarction via a central nervous system-mediated pathway. *Arterioscler Thromb Vasc Biol.* (2012) 32:1902–9. doi: 10.1161/ATVBAHA.112.248930

23. Feng N, Huke S, Zhu G, Tocchetti CG, Shi S, Aiba T, et al. Constitutive BDNF/TrkB signaling is required for normal cardiac contraction and relaxation. *Proc Natl Acad Sci U.S.A.* (2015) 112:1880–5. doi: 10.1073/pnas.1417949112

24. Agah R, Frenkel PA, French BA, Michael LH, Overbeek PA, Schneider MD. Gene recombination in postmitotic cells. Targeted expression of Cre recombinase provokes cardiac-restricted, site-specific rearrangement in adult ventricular muscle in vivo. *J Clin Invest.* (1997) 100:169–79. doi: 10.1172/JCI119509

25. Subramaniam A, Jones WK, Gulick J, Wert S, Neumann J, Robbins J. Tissue-specific regulation of the alpha-myosin heavy chain gene promoter in transgenic mice. *J Biol Chem.* (1991) 266:24613–20.

26. Pugach EK, Richmond PA, Azofeifa JG, Dowell RD, Leinwand LA. Prolonged Cre expression driven by the alpha-myosin heavy chain promoter can be cardiotoxic. *J Mol Cell Cardiol.* (2015) 86:54–61. doi: 10.1016/j.yjmcc.2015.06.019

27. Bergo MO, Lieu HD, Gavino BJ, Ambroziak P, Otto JC, Casey PJ, et al. On the physiological importance of endoproteolysis of CAAX proteins: Heart-specific RCE1 knockout mice develop a lethal cardiomyopathy. *J Biol Chem.* (2004) 279:4729–36. doi: 10.1074/jbc.M310081200

28. Zhao B, Chen S, Liu J, Yuan Z, Qi X, Qin J, et al. Cardiac telocytes were decreased during myocardial infarction and their therapeutic effects for ischaemic heart in rat. *J Cell Mol Med.* (2013) 17:123–33. doi: 10.1111/j.1582-4934.2012.01655.x

29. Zhao B, Liao Z, Chen S, Yuan Z, Yilin C, Lee KK, et al. Intramyocardial transplantation of cardiac telocytes decreases myocardial infarction and improves

post-infarcted cardiac function in rats. *J Cell Mol Med.* (2014) 18:780–9. doi: 10.1111/jcmm.12259

30. Li F, Wang X, Capasso JM, Gerdes AM. Rapid transition of cardiac myocytes from hyperplasia to hypertrophy during postnatal development. *J Mol Cell Cardiol.* (1996) 28:1737–46. doi: 10.1006/jmcc.1996.0163

31. Botting KJ, Wang KC, Padhee M, McMillen IC, Summers-Pearce B, Rattanatray L, et al. Early origins of heart disease: Low birth weight and determinants of cardiomyocyte endowment. *Clin Exp Pharmacol Physiol.* (2012) 39:814–23. doi: 10.1111/j.1440-1681.2011.05649.x

32. Paradis AN, Gay MS, Zhang L. Binucleation of cardiomyocytes: The transition from a proliferative to a terminally differentiated state. *Drug Discov Today.* (2014) 19:602–9. doi: 10.1016/j.drudis.2013.10.019

33. Yuan X, Braun T. Multimodal regulation of cardiac myocyte proliferation. *Circ Res.* (2017) 121:293–309. doi: 10.1161/CIRCRESAHA.117.308428

34. Katare RG, Kakinuma Y, Arikawa M, Yamasaki F, Sato T. Chronic intermittent fasting improves the survival following large myocardial ischemia by activation of BDNF/VEGF/PI3K signaling pathway. *J Mol Cell Cardiol.* (2009) 46:405–12. doi: 10.1016/j.yjmcc.2008.10.027

35. Hang P, Zhao J, Cai B, Tian S, Huang W, Guo J, et al. Brain-derived neurotrophic factor regulates TRPC3/6 channels and protects against myocardial infarction in rodents. *Int J Biol Sci.* (2015) 11:536–45. doi: 10.7150/ijbs.10754

36. Samal R, Ameling S, Dhople V, Sappa PK, Wenzel K, Völker U, et al. Brain derived neurotrophic factor contributes to the cardiogenic potential of adult resident progenitor cells in failing murine heart. *PLoS One.* (2015) 10:e0120360. doi: 10.1371/journal.pone.0120360

37. Hang P, Zhao J, Sun L, Li M, Han Y, Du Z, et al. Brain-derived neurotrophic factor attenuates doxorubicin-induced cardiac dysfunction through activating Akt signalling in rats. *J Cell Mol Med.* (2017) 21:685–96. doi: 10.1111/jcmm.13012

38. Zeng N, Xu J, Yao W, Li S, Ruan W, Xiao F. Brain-Derived Neurotrophic Factor Attenuates Septic Myocardial Dysfunction via eNOS/NO Pathway in Rats. *Oxid Med Cell Longev.* (2017) 2017:1721434. doi: 10.1155/2017/1721434

39. Jiang H, Liu Y, Zhang Y, Chen ZY. Association of plasma brain-derived neurotrophic factor and cardiovascular risk factors and prognosis in angina pectoris. *Biochem Biophys Res Commun.* (2011) 415:99–103. doi: 10.1016/j.bbrc.2011.10.020

40. Kadowaki S, Shishido T, Honda Y, Narumi T, Otaki Y, Kinoshita D, et al. Additive clinical value of serum brain-derived neurotrophic factor for prediction of chronic heart failure outcome. *Heart Vessels.* (2016) 31:535–44. doi: 10.1007/s00380-015-0628-6

41. Shibata A, Hanatani A, Izumi Y, Kitada R, Iwata S, Yoshiyama M. Serum brain-derived neurotrophic factor level and exercise tolerance complement each other in predicting the prognosis of patients with heart failure. *Heart and Vessels.* (2018) 33:1325–33. doi: 10.1007/s00380-018-1174-9

42. Takashio S, Sugiyama S, Yamamuro M, Takahama H, Hayashi T, Sugano Y, et al. Significance of low plasma levels of brain-derived neurotrophic factor in patients with heart failure. *Am J Cardiol.* (2015) 116:243–9. doi: 10.1016/j.amjcard.2015.04.018

43. Buerger A, Rozhitskaya O, Sherwood MC, Dorfman AL, Bisping E, Abel ED, et al. Dilated cardiomyopathy resulting from high-level myocardial expression of Cre-recombinase. *J Card Fail.* (2006) 12:392–8. doi: 10.1016/j.cardfail.2006.03.002

44. Hall ME, Smith G, Hall JE, Stec DE. Systolic dysfunction in cardiac-specific ligand-inducible MerCreMer transgenic mice. *Am J Physiol Heart Circ Physiol.* (2011) 301:H253–60. doi: 10.1152/ajpheart.00786.2010

45. Koitabashi N, Bedja D, Zaiman AL, Pinto YM, Zhang M, Gabrielson KL, et al. Avoidance of transient cardiomyopathy in cardiomyocyte-targeted tamoxifen-induced MerCreMer gene deletion models. *Circ Res.* (2009) 105:12–5. doi: 10.1161/CIRCRESAHA.109.198416

46. Molkentin JD, Robbins J. With great power comes great responsibility: Using mouse genetics to study cardiac hypertrophy and failure. *J Mol Cell Cardiol.* (2009) 46:130–6. doi: 10.1016/j.yjmcc.2008.09.002

47. Lexow J, Poggioli T, Sarathchandra P, Santini MP, Rosenthal N. Cardiac fibrosis in mice expressing an inducible myocardial-specific Cre driver. *Dis Model Mech.* (2013) 6:1470–6. doi: 10.1242/dmm.010470

48. Bersell K, Choudhury S, Mollova M, Polizzotti BD, Ganapathy B, Walsh S, et al. Moderate and high amounts of tamoxifen in alphaMHC-MerCreMer mice induce a DNA damage response, leading to heart failure and death. *Dis Model Mech.* (2013) 6:1459–69. doi: 10.1242/dmm.010447

49. Papizan JB, Vidal AH, Bezprozvannaya S, Bassel-Duby R, Olson EN. Cullin-3-RING ubiquitin ligase activity is required for striated muscle function in mice. *J Biol Chem.* (2018) 293:8802–11. doi: 10.1074/jbc.RA118.002104

50. Chen Q, Thompson J, Hu Y, Das A, Lesnefsky EJ. Cardiac specific knockout of p53 decreases er stress-induced mitochondrial damage. *Front Cardiovasc Med.* (2019) 6:10. doi: 10.3389/fcvm.2019.00010

51. Song M, Franco A, Fleischer JA, Zhang L, Dorn GW II. Abrogating mitochondrial dynamics in mouse hearts accelerates mitochondrial senescence. *Cell Metab.* (2017) 26:872–883e5. doi: 10.1016/j.cmet.2017.09.023

52. Vikram A, Lewarchik CM, Yoon JY, Naqvi A, Kumar S, Morgan GM, et al. Sirtuin 1 regulates cardiac electrical activity by deacetylating the cardiac sodium channel. *Nat Med.* (2017) 23:361–7. doi: 10.1038/nm.4284

53. Lehmann LH, Jebessa ZH, Kreusser MM, Horsch A, He T, Kronlage M, et al. A proteolytic fragment of histone deacetylase 4 protects the heart from failure by regulating the hexosamine biosynthetic pathway. *Nat Med.* (2018) 24:62–72. doi: 10.1038/nm.4452

54. Lakhal-Littleton S, Wolna M, Chung YJ, Christian HC, Heather LC, Brescia M, et al. An essential cell-autonomous role for hepcidin in cardiac iron homeostasis. *Elife.* (2016) 5:e19804. doi: 10.7554/eLife.19804

frontiers | Frontiers in Cardiovascular Medicine

TYPE Original Research
PUBLISHED 22 August 2022
DOI 10.3389/fcvm.2022.969553

OPEN ACCESS

EDITED BY
Jia Qi,
Shanghai Jiao Tong University, China

REVIEWED BY
Chunhua Liu,
Nankai University, China
Yan Wang,
Peking University Third Hospital, China
Rong Shi,
Shanghai University of Traditional Chinese Medicine, China

*CORRESPONDENCE
Qing Zhu
zhuqing@ntu.edu.cn
Yizhun Zhu
yzzhu@must.edu.mo

†These authors have contributed equally to this work

SPECIALTY SECTION
This article was submitted to General Cardiovascular Medicine, a section of the journal Frontiers in Cardiovascular Medicine

RECEIVED 15 June 2022
ACCEPTED 28 July 2022
PUBLISHED 22 August 2022

CITATION
Rong W, Li J, Wang L, Luo S, Liang T, Qian X, Zhang X, Zhou Q, Zhu Y and Zhu Q (2022) Investigation of the protective mechanism of leonurine against acute myocardial ischemia by an integrated metabolomics and network pharmacology strategy. *Front. Cardiovasc. Med.* 9:969553. doi: 10.3389/fcvm.2022.969553

Investigation of the protective mechanism of leonurine against acute myocardial ischemia by an integrated metabolomics and network pharmacology strategy

Weiwei Rong[1,2†], Jiejia Li[3†], Lifeng Wang[1], Shanshan Luo[4], Tulu Liang[5], Xunjia Qian[1], Xiaodan Zhang[1,2], Qinbei Zhou[1], Yizhun Zhu[3,4*] and Qing Zhu[1,2*]

[1]School of Pharmacy, Nantong University, Nantong, China, [2]Provincial Key Laboratory of Inflammation and Molecular Drug Target, Nantong, China, [3]School of Pharmacy and State Key Laboratory for the Quality Research of Chinese Medicine, Macau University of Science and Technology, Macau, Macau SAR, China, [4]Shanghai Key Laboratory of Bioactive Small Molecules, Department of Pharmacology, School of Pharmacy, Fudan University, Shanghai, China, [5]Research Center for Intelligent Information Technology, Nantong University, Nantong, China

Background: Leonurus japonicus Houtt has an obvious efficacy on cardiovascular diseases. As the most representative component in the herb, leonurine has attracted increasing attention for its potential in myocardial ischemia. However, its protective mechanism against myocardial ischemia remains incompletely elucidated.

Objectives: The present study aimed to reveal the potential mechanism of leonurine in acute myocardial ischemia using a strategy combining metabolomics and network pharmacology.

Methods: First, a metabolomics method was proposed to identify the differential metabolites of plasma in rats. Then, network pharmacology was performed to screen candidate targets of leonurine against acute myocardial ischemia. A compound-reaction-enzyme-gene network was thus constructed with the differential metabolites and targets. Finally, molecular docking was carried out to predict the binding capability of leonurine with key targets.

Results: A total of 32 differential metabolites were identified in rat plasma, and 16 hub genes were detected through network pharmacology. According to the results of compound-reaction-enzyme-gene network and molecular docking, what was screened included six key targets (GSR, CYP2C9, BCHE, GSTP1, TGM2, and PLA2G2A) and seven differential metabolites (glycerylphosphorylcholine, lysophosphatidylcholine, choline phosphate, linoleic acid, 13-HpODE, tryptophan and glutamate) with four important metabolic pathways involved: glycerophospholopid metabolism, linoleic acid metabolism, tryptophan metabolism and glutamate metabolism. Among them, glycerophospholipid and tryptophan metabolism were shown to be important, since the regulation of leonurine on these two pathways was also observed in our previous metabolomics study conducted on clinical hyperlipidemia patients.

Conclusion: This is the first study of its kind to reveal the underlying mechanism of leonurine against acute myocardial ischemia through a strategy combining metabolomics and network pharmacology, which provides a valuable reference for the research on its future application.

KEYWORDS

leonurine, network pharmacology, metabolomics, acute myocardial ischemia, molecular docking

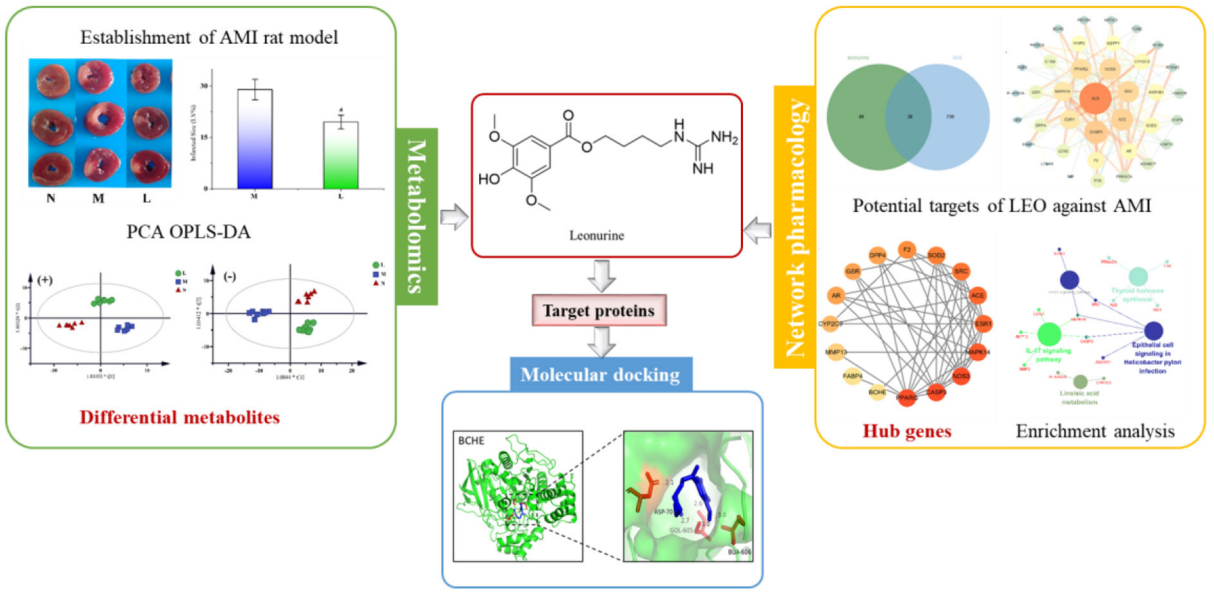

GRAPHICAL ABSTRACT
The strategy to reveal the potential mechanism of leonurine against AMI by combining with metabolomics and network pharmacology.

Highlights

- A compound-reaction-enzyme-gene network was constructed.
- Not only differential metabolites affected by leonurine were found, the upstream targets and pathways were also predicted.
- Some metabolic pathways of this experiment can be verified with previous clinical metabolomics study of leonurine.

Introduction

Coronary atherosclerotic heart disease (CHD), commonly known as ischemic heart disease, is the myocardial damage caused by the change in cardiac coronary circulation, which can result in an imbalance between coronary blood flow and myocardial demand. Ischemic heart disease, especially acute myocardial infarction (AMI), is a serious disease threatening human health due to its severe harmfulness to cardiac tissues and high mortality (1). As a commonly seen disease, CHD has a high morbidity and mortality worldwide. To compound it, stress, unhealthy diet and lifestyle cause CHD to occur in a growing number of young people in many countries, which poses a serve threat to human health (2, 3). Therefore, it is imperative to increase effort on the research and development of anti-myocardial ischemic drugs worldwide.

During ischemia myocardial, reactive oxygen species (ROS) with high reactivity and toxicity are produced, which can exacerbate the degree of myocardial damage when myocardial ischemia occurs (4–6). Leonurus japonicus Houtt. (also known as Herba Leonuri or motherwort) has been used for thousands of years in China. As a classic herbal medicine,

motherwort has a positive effect in the treatment of a variety of diseases, including cardiovascular diseases. A modern medical study found that the excellent antioxidant activity of motherwort extract can reduce the damage caused by ROS and exert cardioprotection during myocardial ischemia (5). In motherwort, alkaloids are considered the most crucial bioactive components, especially leonurine (also known as SCM-198 in our group), which is the main contributor to the antioxidant activity of motherwort extract (7–11). Due to its importance, leonurine was even recorded in the Chinese pharmacopeia as an official index for measuring the quality of motherwort (12). Apart from its significant antioxidant activity, leonurine also exerts cardioprotective effects via other mechanisms. For example, leonurine attenuated apoptosis in cardiac muscle cells induced by hypoxia (13, 14), doxorubicin (15) or hydrogen peroxide (16). The anti-apoptotic effects of leonurine were probably mediated by activating the PI3K/Akt signaling pathway (17). In addition, leonurine prevented cardiac fibrosis in postmyocardial infarction rats through modulation of a Nox4-ROS pathway (10). What is even more encouraging is our discovery that the long-term use of leonurine could help improve the lipid profiles of multiple animal models including mouse, rabbit and rhesus monkeys (18), for which it is widely regarded as an indicator of coronary atherosclerotic heart disease risk, particularly low-density lipoprotein and cholesterol levels (19). As a promising novel drug, leonurine has now been applied in clinical trials in China for treating hyperlipidemia. Despite some achievements made in existing studies on leonurine in ischemic heart diseases, the protective mechanism and targets of leonurine against AMI remain incompletely understood.

It is well-known that cardiac metabolic alterations are the first consequences of AMI (20). For example, Bonanad et al. (21) identified up to 32 serum differential metabolites from swine ($n = 9$) and patients ($n = 20$) during AMI. Among them, creatine increased 2 h after ischemia. Untargeted metabolomics serves as an effective tool for the overall, systematic study of changes in metabolites *in vivo*. According to the statistical analysis of differential metabolites, metabolomics can reveal changes to endogenous metabolites in different physiological states or different physiological states before and after administration, which is essential for inferring the possible etiology or treatment mechanism. However, it is inadequate to infer the protective mechanism of leonurine against AMI based only on differential metabolites. Therefore, it is also necessary to reveal the upstream proteins causing the changes in metabolites and the possible targets of leonurine. Network pharmacology is applicable to systematically predict the possible targets of drugs with the support of statistics, complex networks and other mathematical methods. Although network pharmacology can be efficiently accounted for the mechanism of drugs on diseases from the perspective of systems biology, an independent network pharmacology experiment is limited to predicting the targets and pathways in mathematical dimensions, and there is a lack of statistical support from practical experiments.

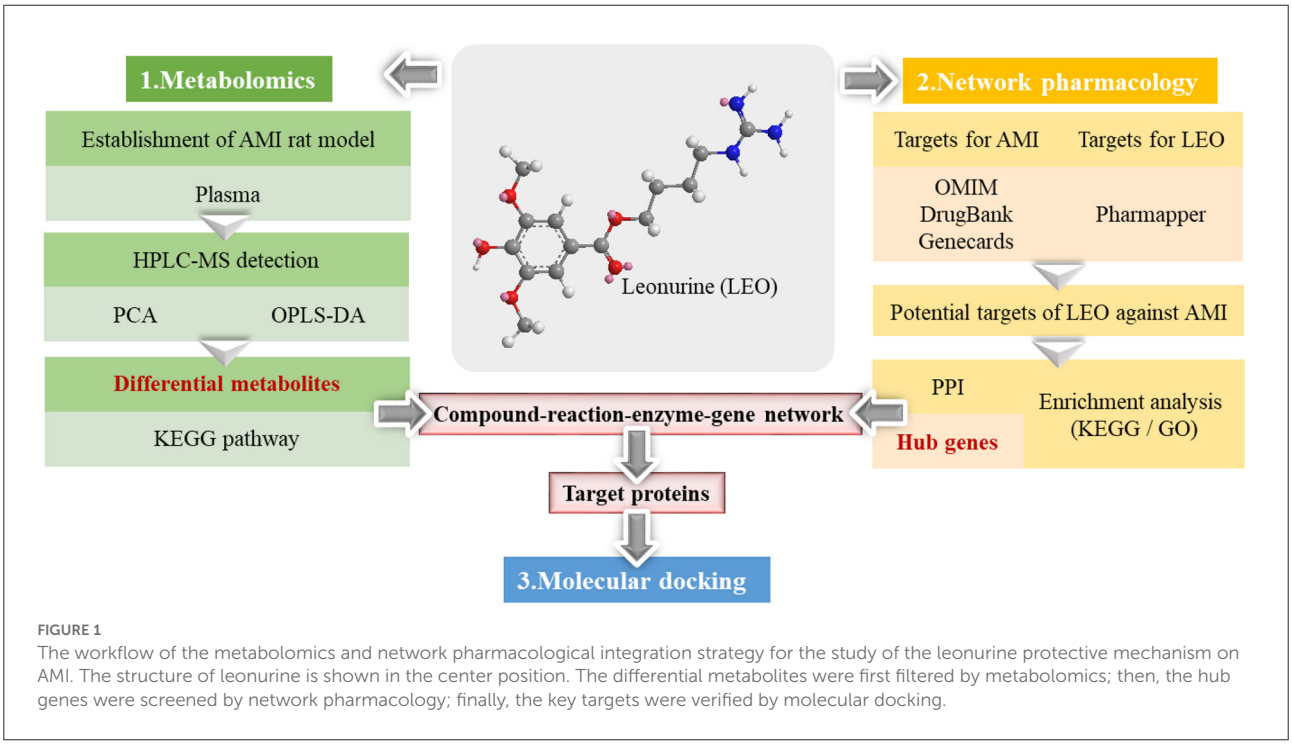

FIGURE 1
The workflow of the metabolomics and network pharmacological integration strategy for the study of the leonurine protective mechanism on AMI. The structure of leonurine is shown in the center position. The differential metabolites were first filtered by metabolomics; then, the hub genes were screened by network pharmacology; finally, the key targets were verified by molecular docking.

For this reason, a strategy combining metabolomics and network pharmacology was applied in this study to integrate the differential metabolites with the key targets effectively, thus establishing a compound-reaction-enzyme-gene network. This strategy was adopted not only to investigate the metabolite changes occurring after leonurine intervention, but also to predict the upstream potential targets that might make a difference to the metabolite levels. Additionally, the potential of key targets to bind with leonurine was also predicted using molecular docking technology. Finally, success was achieved in revealing the protective mechanism of leonurine on AMI. The workflow of the strategy is shown in Figure 1.

Materials and methods

Materials and reagents

Leonurine was synthesized by Professor Zhu Yizhun's research group of Fudan University School of Pharmacy, and its purity was verified as 98% by HPLC. The powder was prepared with normal saline at a concentration of 1.5 mg/mL and administered intraperitoneally at a dose of 15 mg/kg. The structure of leonurine is shown in Figure 1.

HPLC-grade acetonitrile, methanol and formic acid were provided by Merck, USA. Analytical grade chemical reagents were purchased from Shanghai Sinopharm Group Chemical Reagent Co., Ltd. Distilled water was supplied by Wahaha Co. Ltd. Creatine kinase-muscle/brain (CK-MB) and troponin I (Tn-I) kits were purchased from Nanjing Jiancheng Biotechnology Co., LTD.

Animals and modeling

Twenty-four male Sprague–Dawley rats (200 ± 10 g) were supplied by the Experimental Animal Center of Nantong University. They were raised with food and water available *ad libitum* in an air-conditioned room with a temperature of 22 ± 2°C, a humidity of 55 ± 10% and a 12 h light-dark cycle for at least 7 days to adapt to the environment. Then the rats were randomly divided into three groups with eight rats in each group: the sham-operated group (N), the AMI model group (M) and the leonurine-treated group (L, *i.p.*, 15 mg/kg/day). The results of our previous study showed leonurine with a dosage of 15 mg/kg/d could show significant antioxidant activity and exert cardioprotection during AMI (9, 10, 14). The drug solution was administered to rats in the L group preoperatively for 7 days before coronary ligation and immediately after coronary ligation on the same day. The rats in the N and M groups were given an intraperitoneal injection at the same volume of normal saline.

The rats were anesthetized by isoflurane and fixed in the supine position, and electrocardiogram (ECG) monitoring was performed during the surgery. After endotracheal intubation, artificial ventilation was performed. The intercostal muscle of the rats was separated, and a third intercostal thoracotomy was performed along the left margin of the sternum at 0.5 cm. The intercostal incision was opened with a chest dilator, and the pericardium was cut to expose the heart. The pleura was kept intact to preserve autonomous breathing. The left anterior coronary artery was permanently tied between the left atrial ear and the pulmonary artery cone at approximately 2.3 mm from the root of the aorta with a filament needle. If both myocardial whitening in the blood supply area and ST elevation of the standard limb guide ECG were observed, the model was successfully established (22). The chest was then quickly closed and autonomous breathing was resumed. The N group underwent the same operation except the coronary artery was not ligated. All studies on animals were in accordance with the Guidelines of the Committee on the Care and Use of Laboratory Animals in China.

Sample collection and preparation

Heart and blood samples were collected 48 h after coronary ligation surgery. The blood samples were immediately centrifuged at 1,000×g for 15 min to obtain the supernatant, which was separated and stored at −80°C until analysis.

Plasma samples were thawed at room temperature before analysis. An aliquot of 300 μL of methanol was added to 100 μL of plasma and vortexed for ∼3 min for protein precipitation. The mixture was centrifuged at 10,000×g for 15 min at 4°C. The supernatant was separated for LC–MS analysis. Quality control (QC) samples were prepared by mixing equal aliquots of each sample. One QC sample was injected every six samples.

Other plasma samples were taken and measured according to the instructions provided by CK-MB and Tn-I kits. The activity of CK-MB and the content of Tn-I were obtained with a microplate reader.

Histological analysis

The ventricles of rats were cut into multiple horizontal slices with 2 mm thickness and heated in a water bath at 37°C in 1% 2,3,5-triphenyltetrazole chloride (TTC) solution for 10 min. The reaction was terminated with normal saline and then fixed in 4% paraformaldehyde solution for 30 min. Areas stained red indicated normal myocardium, while areas not stained red and that were pale were infarcted. The infarct and ventricular areas were calculated automatically by ImageJ software (Version 3.0) according to the different colors. All data are expressed as the mean ± SD. The results were analyzed by Student's *t*-test, and a p-value < 0.05 was considered to indicate statistical significance.

Infarcted Size (LV%) = Infarct Area/Ventricular Area × 100

Instruments, parameters, and conditions of metabolomics

An LC-Q/TOF-MS (Agilent, 1290 Infinity LC, 6530 UHD and Accurate-Mass Q-TOF/MS) system was used for sample detection. The separation was performed on a C18 chromatographic column (2.1 × 100 mm, 1.8 μm; Agilent, USA) at 40°C. The flow rate was set as 0.4 mL min^{-1}, and the sample injection volume was 5 μL. The mobile phase system was composed of an A phase (0.1% formic acid) and a B phase (0.1% formic acid in acetonitrile). The gradient elution program started with 5% B for 2 min, increased from 5% B to 95% B for 12 min, and remained at 95% B for 2 min.

The raw data were collected in positive and negative electrospray ionization modes (ESI+/–). The source temperature in both modes was 100°C. In positive mode, the capillary voltage was set as 4,000 V, and the sampling cone was set as 3,500 V. The desolvation temperature was 350°C, and the extraction cone was 4 V. The cone and desolvation gas flow were 50 L/h and 600 L/h, respectively. In negative mode, the capillary voltage was set as 3,500 V, and the sampling cone was set as 5,000 V. The desolvation temperature was 300°C, and the desolvation gas flow was 700 L/h. The cone gas flow and extraction cone values were the same as those in positive mode. The scan time was 0.03 s, and interscan time was 0.02 s. The MS scans were ranged from 100 to 1,000 Da. To ensure the accuracy and repeatability of the mass, leucine-enkephalin was used as the lock mass. The $[M+H]^+$ ion 556.2771 Da was produced in positive ion mode, and the $[M–H]^-$ ion 554.2615 Da was produced in negative ion mode.

Statistical analysis of metabolomics

The raw data were processed by MassHunter software. Filtration and peak identification, peak match across samples, and retention time correction were processed by XCMS code. The zero values were reduced based on the "80% rule" (23). Unsupervised principal component analysis (PCA) and supervised orthogonal partial least squares discrimination analysis (OPLS-DA) were used to screen the potential biomarkers by SIMCA software. Hierarchical cluster analysis (HCA) and metabolic pathway analysis were conducted by MetaboAnalyst 5.0 software and KEGG (http://www.genome.jp/kegg/), respectively. Student's *t*-test was used to perform statistical analysis, and the metabolites with variable influence on project (VIP) values >1 were considered to be differential metabolites. The HMDB database (http://www.hmdb.ca/) was applied to annotate the potential biomarkers via their mass information.

Network pharmacology research

The experimental network pharmacology procedure is shown in Figure 1. In detail, the potential target search for leonurine was achieved by the PharmMapper Server (http://www.lilab-ecust.cn/pharmmapper/) (24). The related targets and candidate genes of AMI were obtained from the Drug Bank (https://go.drugbank.com) (25), OMIM (https://omim.org/) (26) and Genecards (https://www.genecards.org/) (27) websites using the keywords "myocardial ischemia" or "acute myocardial ischemia." The intersection of candidate targets for AMI and leonurine was obtained, which was further inputted into the STRING website (https://string-db.org/) (28) to construct a protein–protein interaction (PPI) network (medium confidence > 0.4). Cytoscape software was also used for PPI network visualization. Hub genes were obtained using the CytoHubba plugin in Cytoscape software. Gene ontology (GO) enrichment and KEGG pathway (p-value < 0.05) analysis of potential targets were achieved by the ClueGO plugin. The compound-reaction-enzyme-gene network was established by Metscape plugin to visualize the interactions between metabolites, pathways, enzymes and genes, thereby identifying key metabolites and targets.

Molecular docking

The 3D structure of leonurine was drawn with Chem3D software. The crystal structures of key protein targets were acquired from the RCSB Protein Data Bank website (https://www.rcsb.org/). A total of six protein targets were studied: cholinesterase (BCHE), protein-glutamine gamma-glutamyltransferase 2 (TGM2), glutathione S-transferase P (GSTP1), cytochrome P450 2C9 (CYP2C9), phospholipase A2 (PLA2G2A) and glutathione reductase (GSR). The operation to delete water and add hydrogen atoms was accomplished by AutoDockTools software. Then, the molecular docking study was performed using the AutoDock Vina program. The coordinates of the target active pocket were listed in Supplementary Table S1. The docking results with the highest scores were visualized by PyMOL software.

Results

Pathological changes

The cross sections of the typical infarct myocardial sections of rats in the three groups are shown in Figure 2A. Areas stained red indicated normal myocardium, while areas not stained red and that were pale were infarcted. The myocardial tissue of the N group rats was all stained red without infarction areas, while the myocardial infarction areas of the M group rats were obvious.

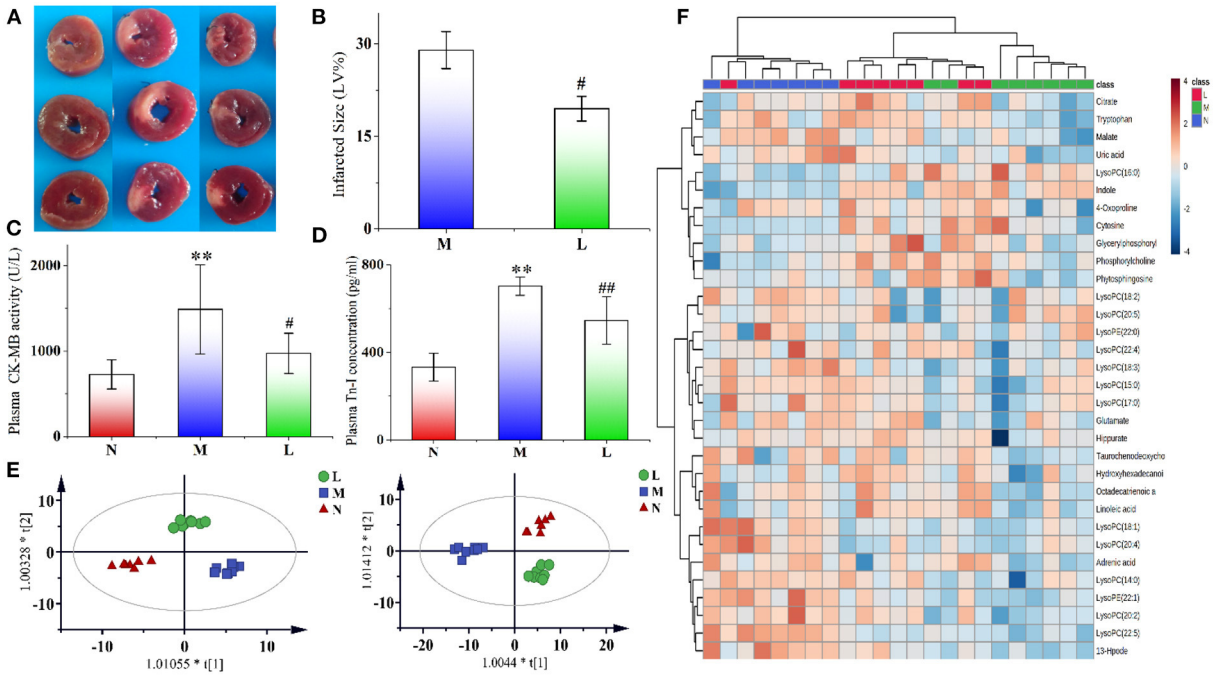

FIGURE 2
(A) Typical cross sections of rat myocardium in the N, M, and L groups. We selected three typical myocardial tissue samples from each group for presentation. Areas stained red indicated normal myocardium, while areas not stained red and that were pale were infarcted. **(B)** Effect of leonurine on myocardial infarction size in rats with AMI. **(C,D)** Effects of leonurine on plasma CK-MB and Tn-I levels in AMI rats. **(E)** OPLS-DA score plots of the N, M, and L groups ($n = 8$) from metabolomics in positive ($R^2 = 0.915$, $Q^2 = 0.772$) and negative ($R^2 = 0.938$, $Q^2 = 0.755$) modes. Red triangles, blue diamonds and green circles indicate the N, M, and L groups, respectively. **(F)** Hierarchical clustering heatmap showing the changes in potential biomarker content in the plasma of rats in the N, M, and L groups. The three groups achieved basic separation based on 32 potential biomarkers. The N and M groups were completely separated, and the L group approached N group. N, the sham-operated group; M, the acute myocardial ischemia model group; L, the leonurine administration group. ** $p < 0.01$ *vs.* the N group; #$p < 0.05$ and ##$p < 0.01$ *vs.* the M group.

After leonurine intervention, the area of myocardial infarction was significantly reduced. ImageJ software was used to analyze the size of myocardial infarction. The results showed that the administration of leonurine effectively improved MI in rats and reduced the size of myocardial infarction (p-value < 0.05). The results are shown in Figure 2B.

Effects of leonurine on CK-MB and Tn-I

It has been widely accepted that CK-MB and TN-I are important indicators of myocardial ischemia (29–31). The effects of leonurine on plasma CK-MB activity and Tn-I concentration in the rats were shown in Figures 2C,D. Compared with the N group, the CK-MB activity and Tn-I concentration in the M group significantly increased (p-value < 0.01), indicating the successful establishment of the AMI model. However, the CK-MB activity and Tn-I concentration decreased significantly after leonurine intervention, indicating that leonurine could significantly improve the AMI in rats.

Metabolomics analysis

After Pareto scaling and log transformation, unsupervised clustering PCA was used to evaluate the performance of different groups. In the score plots of PCA (Supplementary Figure S1A), the QC samples were distributed in the near center in both positive and negative modes. The samples of the M group were significantly separated from those of the N group, indicating that AMI caused significant changes in metabolite levels in rats. Compared with the M group, the L group approached the N group, indicating that the levels of some metabolites in AMI rats were reversed after intraperitoneal injection of leonurine. The R^2 values in positive and negative modes were 0.470 and 0.561, respectively.

To explore the differential metabolites between groups, an OPLS-DA model was also established for analysis. In the score plots of OPLS-DA in Figure 2E and Supplementary Figures S2B,C, complete separation was achieved between the N and M groups, as well as between the L and M groups. The values of R^2 and Q^2 in the OPLS-DA model in both positive and negative modes

were all >0.755. Permutation testing for the OPLS-DA model was also performed, and the results are shown in Supplementary Figure S2. All the candidate metabolites with a VIP value >1 were considered differential metabolites, and then they were identified by comparing their MS information with standard substances and available online biochemical databases. Eighteen metabolites were detected in positive ion mode, and 14 were detected in negative ion mode. Detailed information on the 32 potential biomarkers is listed in Supplementary Table S2. The HCA of 32 potential biomarkers is shown in Figure 2F, and related pathways with influence coefficient are shown in Supplementary Figure S3A. Pathways with an impact value >0.1 were considered to be closely related to AMI, and leonurine exhibited a protective effect on the disorder via the regulation of these pathways, including linoleic acid metabolism, glycerophospholipid metabolism, glutamate metabolism, tryptophan metabolism, and the TCA cycle. Among them, glycerophospholipid metabolism and tryptophan metabolism should receive attention, since they were detected in the plasma of both rat samples with AMI and clinical samples of patients with hyperlipidemia, as shown in Supplementary Figure S3B.

Network pharmacology analysis

Network pharmacology was used to predict the potential targets of leonurine against AMI. A total of 87 targets of leonurine and 768 targets of AMI were obtained from the databases mentioned in Section 2.7 Network pharmacology research. Their shared targets were considered potential targets of leonurine against AMI (Figure 3A). Then, a PPI network was built by the SRING database to further analyze the complex mechanisms of leonurine against AMI. The obtained PPI data was visualized by Cytoscape software (Figure 3B). The CytoHubba plugin in Cytoscape software was used to calculate the hub genes. The top 20 genes were obtained in each algorithm in the CytoHubba plugin (Supplementary Figure S4). The overlapping genes in these algorithms were considered the hub genes (Figure 3C). A total of 16 hub genes (PPARG, CASP3, NOS3, MAPK14, ESR1, ACE, SRC, SOD2, F2, DPP4, GSR, AR, CYP2C9, MMP13, FABP4, BCHE) were thus obtained. The GO and KEGG pathway enrichment analyses were completed by the ClueGO plugin in Cytoscape software, and top terms such as positive regulation of reactive oxygen species metabolic process (GO:2000379), ligand-activated transcription factor activity (GO:0098531), long-chain fatty acid biosynthetic process (GO:0042759), nuclear receptor activity (GO:0042759), regulation of systemic arterial blood pressure (GO:0003073) and regulation of morphogenesis of an epithelium (GO:1905330) are shown in Figure 3D. According to the KEGG enrichment analysis, the pathways significantly affected were linoleic acid, IL-17 signaling pathway, thyroid hormone synthesis, and epithelial cell signaling in Helicobacter pylori infection.

Integrated analysis of metabolomics and network pharmacology

A compound-reaction-enzyme-gene network (Figure 4) was constructed by performing an integrative analysis of the metabolomics-acquired differential metabolites and the hub genes obtained from network pharmacology using the Metscape plugin in Cytoscape software. The network intuitively showed the relationships between differential metabolites and their upstream hub genes. A total of six key targets (GSR, CYP2C9, BCHE, GSTP1, TGM2, and PLA2G2A) were identified in the network map, corresponding to seven differential metabolites (glycerylphosphorylcholine, lysophosphatidylcholine, choline phosphate, linoleic acid, 13-HpODE, tryptophan and glutamate), involved in four important metabolic pathways (glycerophospholopid metabolism, linoleic acid metabolism, tryptophan metabolism and glutamate metabolism). Among these genes, GSR, CYP2C9, and BCHE were hub genes screened by network pharmacology.

Molecular docking

In this work, molecular docking technology was also used to predict the binding ability between leonurine and key targets (GSR, CYP2C9, and BCHE). The results of the docking experiments are shown in Figure 5. In detail, leonurine and the key targets were interacted with hydrogen-bonds, and the binding energies were −4.7 (GSR), −6.5 (BCHE) and −7.2 (CYP2C9) kcal/–mol. As shown in Figure 5A, leonurine made hydrogen-bonding interactions with GLN-10 of GSR at the active sites. To BCHE, leonurine made hydrogen-bonding interactions with ASP-70, GOL-605 and BUA-606 at the active sites. CYP2C9 interacted with leonurine by hydrogen bonding via the active site of four amino acid residues (PHE-419, LYS-423, GLU-400 and PHE-419). The docking results indicated a good affinity between leonurine and the targets.

Discussion

In this study, an integrated network pharmacology and metabolomics strategy was used to explore potential targets and metabolic pathways of leonurine against AMI, and a molecular docking technique was used to validate the key targets. Leonurine is a promising chemical component with multiple effects. Our team's study on leonurine treatment for hyperlipidemia has now entered clinical phase III. According to our metabolomics study on patients with clinical hyperlipidemia

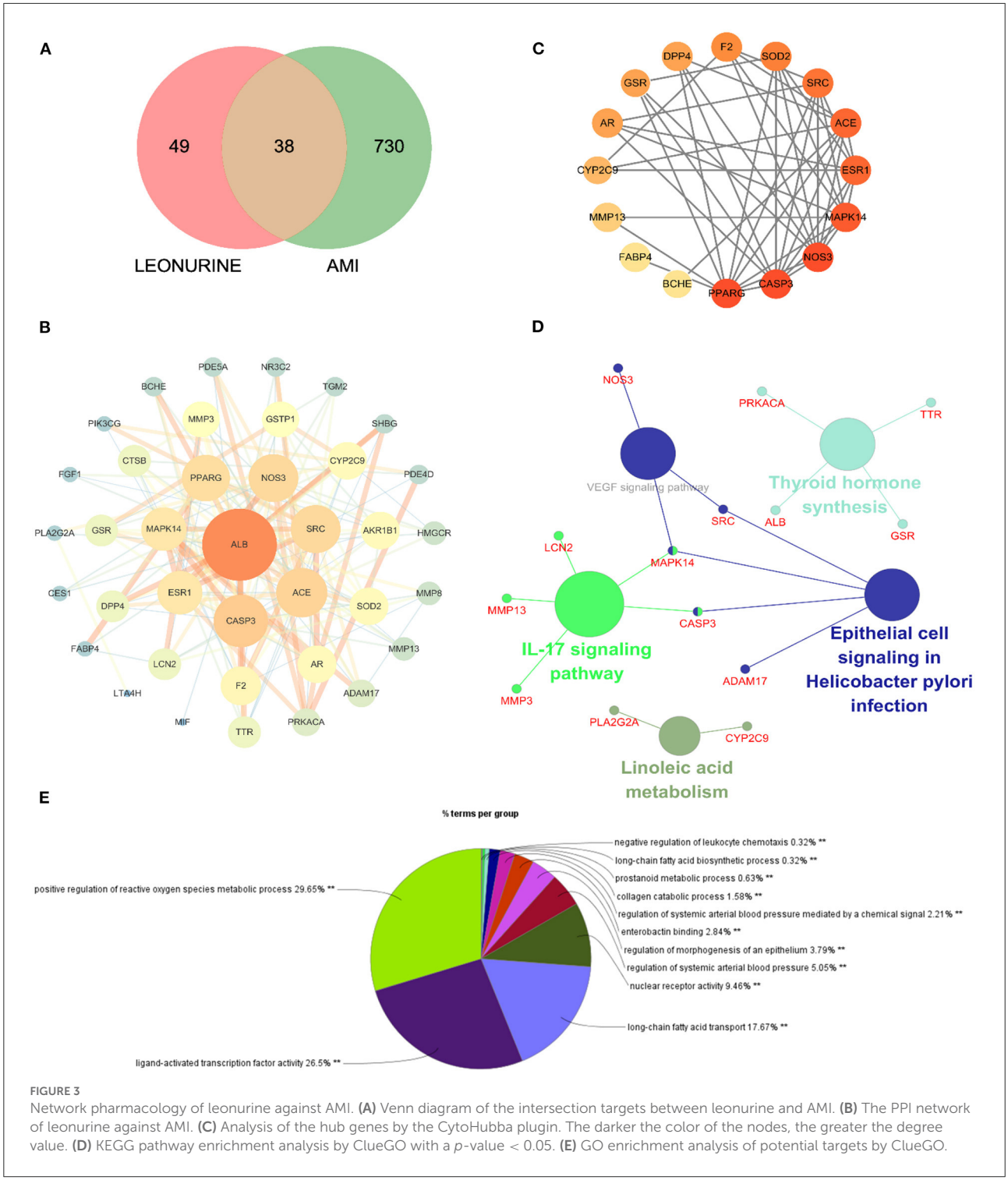

FIGURE 3
Network pharmacology of leonurine against AMI. **(A)** Venn diagram of the intersection targets between leonurine and AMI. **(B)** The PPI network of leonurine against AMI. **(C)** Analysis of the hub genes by the CytoHubba plugin. The darker the color of the nodes, the greater the degree value. **(D)** KEGG pathway enrichment analysis by ClueGO with a p-value < 0.05. **(E)** GO enrichment analysis of potential targets by ClueGO.

(one of the important risk factors for CHD), leonurine showed a great influence on glycerophospholipid metabolism and tryptophan metabolism (Supplementary Figure S3). The regulation of leonurine on these two metabolic pathways was also observed in this study, which greatly aroused our interest. In the metabolomics experiment, a reduced level of glycerylphosphorylcholine (GPC) was observed. GPC is a small molecule that is normally water-soluble *in vivo* that decomposes into choline and glycerol phospholipids under the action of related enzymes, in which choline participates in

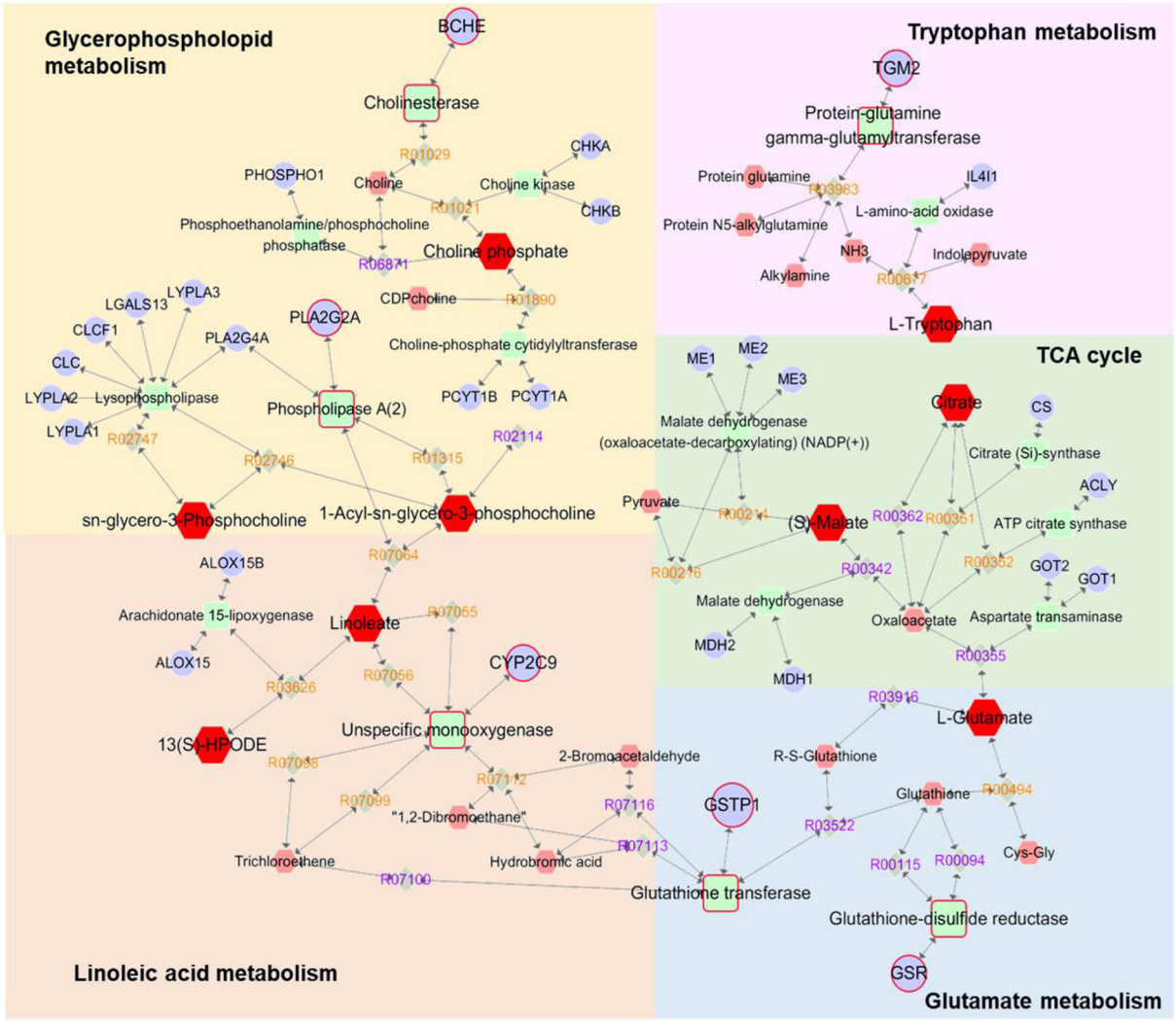

FIGURE 4
Compound-reaction-enzyme-gene networks of the key metabolites and targets. The red hexagons are differential metabolites, gray diamonds are reactions, green round rectangles are proteins and purple circles are genes. The key metabolites, proteins and genes were magnified.

the biosynthesis of acetylcholine, and glycerol phospholipids are involved in phosphatidylcholine (PC) synthesis. PCs can be catalyzed by phospholipase A2 (PLA2G2A) and partially hydrolyzed into lysophosphatidycholines (LysoPCs) (32, 33). In the metabolomics study, a significant decrease in multiple LysoPC species was observed in the AMI group of rats, which was consistent with a previous report (34). However, the LPC levels significantly increased after leonurine intervention. Interestingly, PLA2G2A was predicted to a potential target for leonurine through networked pharmacology studies, whose activity is closely related to LPC levels. Therefore, a molecular docking technique was used to analyze the binding ability between leonurine and PLA2G2A. The results in Figure 5 show that leonurine interacted with PLA2G2A by hydrogen bonds at the active site, with binding energies of −7.4 kcal/–mol, indicating the potential of PLA2G2A to be a target of leonurine. Taken together, we speculated that leonurine may promote the hydrolysis of PCs into LPCs by acting on PLA2G2A to increase the levels of LPCs. Choline phosphate, another differential metabolite found in metabolomics study, was also involved in glycerophospholipid metabolism. A decrease in choline phosphate levels at AMI also interfered with the levels of LPCs. A network pharmacology study predicted that cholinesterase (BCHE) was one of the hub genes against AMI. Leonurine might regulate the levels of choline phosphate by acting on BCHE and thus affect the levels of LPCs. Therefore, leonurine may regulate the levels of LPCs by multiple targets.

Fatty acids (FAs) are the largest energy reservoir within the body. They can be oxidized in mitochondria by β-oxidation, producing acetyl-CoA, and are involved in the Krebs cycle

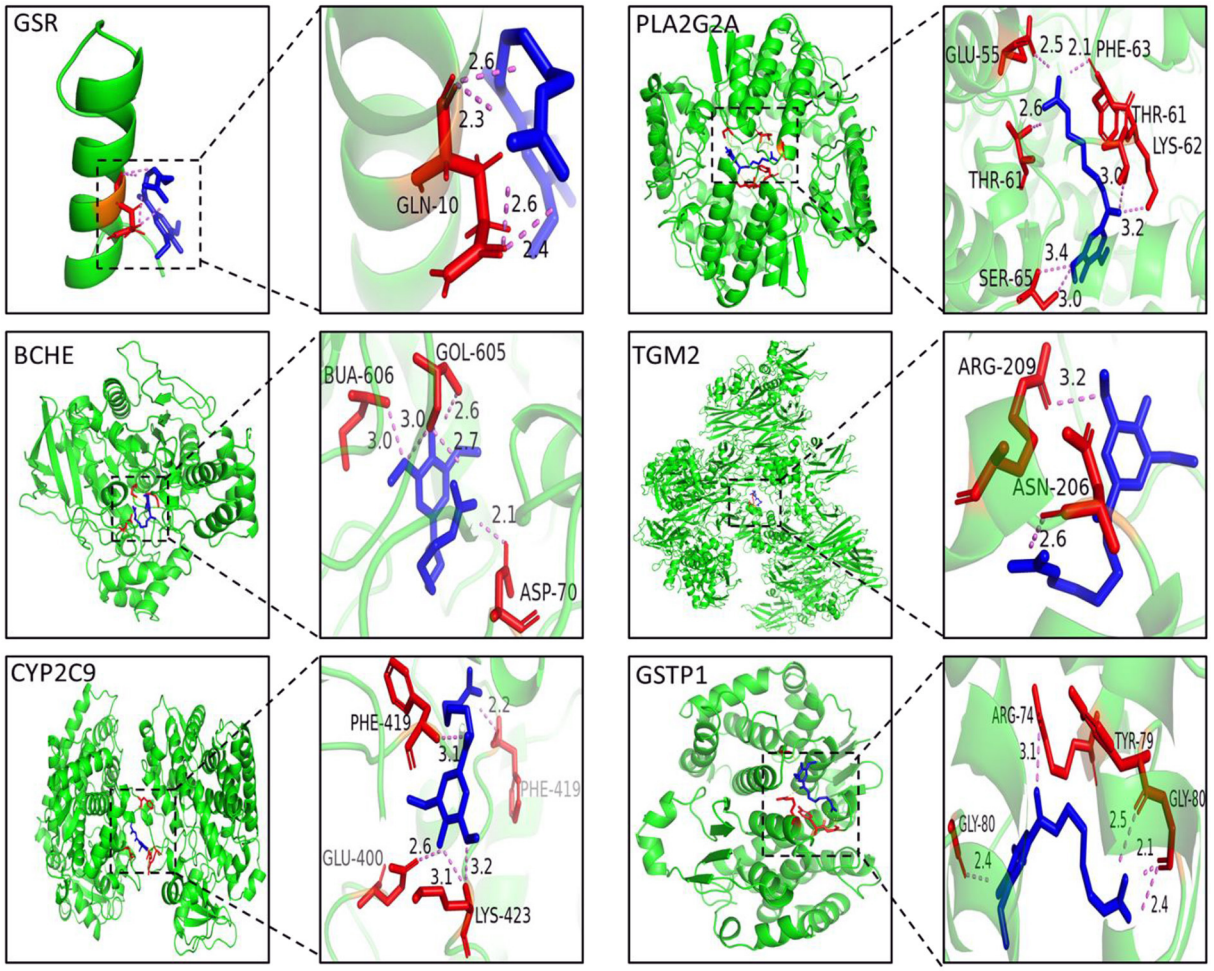

FIGURE 5
The 3D interaction diagrams of leonurine and GSR, BCHE, CYP2C9, PLA2G2A, TGM2 and GSTP1.

(TCA) to provide energy. In AMI, aerobic respiration was limited, which suppressed the TCA cycle and interfered with the β-oxidation process of FAs, leading to the metabolic disorder of FAs and decreased levels of multiple FAs (35, 36). Decrease in unsaturated fatty acids such as linoleic acid, octadecatrienoic acid, hydroxyhexadecanoic acid, adrenic acid and 13-HpODE were observed in the metabolomics experiment. Among them, linoleic acid participates in the synthesis of LPCs, and the change in its level is correlated with the level of LPCs. Cytochrome P450 2C9 (CYP2C9) is a monooxidase that is involved in the metabolism of linoleic acid and generates epoxyoctadecanoic acids (EpOMEs). EpOMEs are further catalyzed by soluble hydroxyhydrolase (sEH) to produce dihydroxyoctadelactic acid (DiHOMEs). EpOMEs and DiHOMEs are closely related to the recovery of cardiac function after AMI (37). The network pharmacology results revealed that CYP2C9 (hub gene) was a possible target for leonurine. Therefore, it was possible that leonurine reduced the degradation of linoleic acid by inhibiting CYP2C9 activity, and thus reduced the harm to myocardial tissue during AMI.

Abnormal decreases in citrate and malate levels in rats with AMI were also observed in this work. As important metabolic intermediates in the TCA cycle, the reduced levels of citrate and malate indicated the inhibition of the TCA cycle. This might be related to the limitation of aerobic respiration during AMI in rats. Hypoxia in mitochondria and the reduction in substrate supply could cause disorders of the myocardial energy metabolism pathway, and the TCA cycle, as the core of energy metabolism, was obviously disturbed (38).

In fact, metabolic drugs improving the function of ischemic myocardium play an important role in the therapy for CHD. One of the representative metabolic drugs is trimetazidine, which could partial blockade of lipid β-oxidation and stimulate glucose oxidation (39). However, the antihypoxic effects of

trimetazidine can be realized only in moderate hypoxia due to regulatory limitation of lipid utilization. Unlike trimetazidine, leonurine show obvious regulation on both TCA cycle and FAs metabolism. Khazanov et al. (40) found that the optimization of energy formation processes in mitochondria using natural mitochondrial metabolites, such as succinate and malate showed more effectively than antihypoxant trimetazidine prevented functional and metabolic disorders in rat myocardium during AMI. This encourages us that leonurine has a good future on the clinical application of AMI therapy.

Glutamate participates in the malate-aspartate shuttle and converts pyruvate to alanine rather than lactic acid; thus, glutamate might be the preferred myocardial fuel for AMI (41, 42). Furthermore, the reduced 4-oxoproline level in this experiment was also associated with an abnormal metabolism of glutamate. The results of a network pharmacology study showed that GSTP1 and GSR have the potential to be targets of leonurine in glutamate metabolism. The glutathione (GSH) redox system is an important antioxidant defense system in cardiomyocytes (43). The absence of GSH aggravated the injury of myocardial tissue, and the reduction in GSH concentration was associated with the decreased activity of glutathione reductase (GSR) (44). Leonurine may repair the myocardial damage caused by AMI by upregulating the concentration of GSH through the activation of GSR. Glutathione S-transferase Ps (GSTPs) protect cardiomyocytes by removing cytotoxic dehydes such as acrolein from the heart (49). Unlike other GSTPs, GSTP1 has the greatest cardio-selectivity and plays a protective role during AMI. Molecular docking results showed that the binding energy between leonurine and GSTP1 was −6.5 kcal/–mol (Figure 5), indicating that GTPS1 was a potential target for leonurine to prevent AMI.

The effect of leonurine on metabolic disorders of the tryptophan pathway was also observed in both a previous metabolomics study of patients with clinical hyperlipidemia and this work. As an antioxidant, tryptophan was reported to alleviate hypoxic myocardial damage (45). Clinical studies have shown that the tryptophan metabolism pathway is closely related to the onset and development of AMI. For example, Petras et al. (46) and Chacko et al. (47) observed a significant reduction in tryptophan levels in patients with AMI 5 min before onset and within 12 h after onset through a metabolomics study. A decrease in tryptophan levels was also observed in this metabolomics study. The network pharmacology study predicted protein-glutamine gamma-glutamyl transferase 2 (TGM2) as a possible target for leonurine in tryptophan metabolism. TGM2 is a member of the transglutaminase (TG) family that contributes to the stabilization or repair of the vasculature. Griffin et al. (48) observed more myocardial fibrosis in TGM2 knockout mice (ApoEe/TGM2/F13a1 knockout and Tgm2/F13a1 knockout mice) than in ApoEe/F13a1 double-knockout and F13a1 single-knockout mice. TGM2 could also promote ATP synthesis and thus limit damage after AMI (49). Thus, the binding ability between leonurine and TGM2 was analyzed by molecular docking. The docking result in Figure 5 shows that the interaction between TGM2 and leonurine was achieved by hydrogen bonding with a binding energy of −6.2 kcal/–mol. In conclusion, we predicted that the tryptophan pathway was greatly affected in rats with AMI, and leonurine probably repaired the myocardial injury caused by AMI by acting on TGM2.

Decreases in other differential metabolites, such as hippurate, taurochenodeoxycholic acid, phytosphingosine, uric acid and cytosine were also observed in metabolomics experiments. Hippurate is the metabolite of phenylalanine, and its decreased level indicates abnormalities in the phenylalanine metabolic pathway (38). Taurine was reported to have protective effects on cardiomyocytes by maintaining calcium (Ca^{2+}) homeostasis, regulating osmotic homeostasis, and mediating antioxidant and anti-apoptotic activities (41, 42). In this study, a decrease in the level of taurochenodeoxycholic acid was observed, which, as a precursor to taurine production, might be one of the causes of abnormal taurine metabolism. Sphingolipid-mediated signaling pathways were also reported to have an important role in cardiovascular pathological physiology and were considered a potential target for MI injury (43). In this study, a decreased level of phytosphingosine was found in AMI rats, which was consistent with the experimental results of Qi et al. (44). After leonurine administration, the level of phytosphingosine recovered, indicating that leonurine also had a regulatory effect on sphingolipid metabolism. Myocardial energy disorders inevitably affect DNA and protein synthesis, resulting in purine and pyrimidine metabolism disorders. It was reported that the level of xanthosine decreased in AMI. As the final product of purine metabolism, uric acid is metabolized by xanthosine and xanthine. Thus, decreases in xanthosine and xanthine resulted in a decrease in the levels of uric acid (35). In addition, cytosine, an intermediate product of pyrimidine metabolism, decreased, indicating that pyrimidine metabolism was also affected by myocardial ischemia. Figure 6 illustrates the underlying mechanism of leonurine against AMI by integrating network pharmacological and metabolomic results.

We preliminarily predicted the potential signaling pathway of leonurine against AMI in this study. Although the experimental results of plasma metabolomics is a powerful support of our prediction of the potential targets, further validation of the predicted targets should be further verified to clarify the mechanism of leonurine against AMI. Especially, tryptophan and glycerophospholipid metabolism, and related targets such as TGM2, BCHE and PLA2G2A should be paid more attention, since the regulation of leonurine on these two pathways was also observed in our previous metabolomics study of clinical hyperlipidemia patients. These two pathways

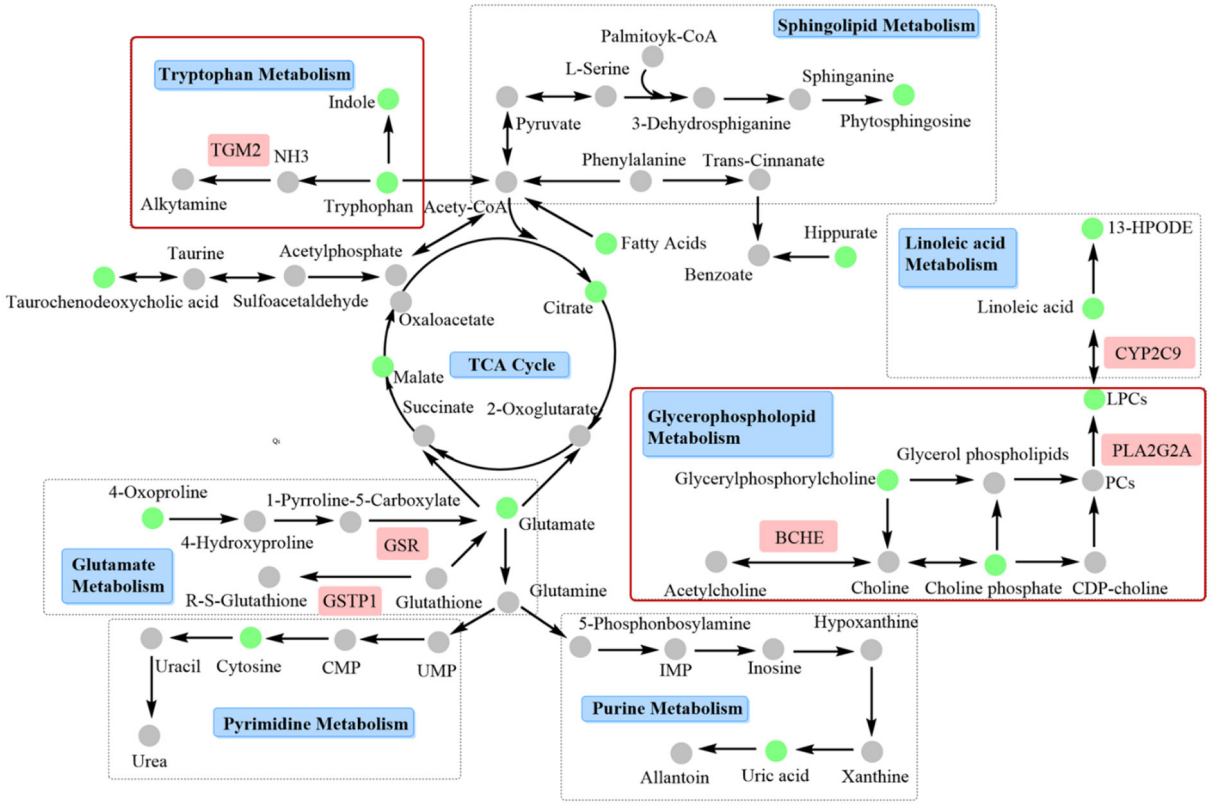

FIGURE 6
Interaction network based on metabolomics and network pharmacology. Tryptophan and glycerophospholipid metabolism, and related targets such as TGM2, BCHE, and PLA2G2A should be paid more attention, since these two pathways may be closely related to the clinical efficacy of leonurine against AMI.

may be closely related to the clinical efficacy of leonurine against AMI.

Conclusion

In this study, we used an integrated metabolomics and network pharmacology strategy to explore the targets and related pathways of leonurine against AMI. A total of four major metabolic pathways were found, namely, glycerophospholipid metabolism, linoleic acid metabolism, tryptophan metabolism and glutamate metabolism, and six possible targets were filtered, three of which were hub genes in network pharmacology. Among them, tryptophan and glycerophospholipid metabolism should be given more attention, because disturbances of these two metabolic pathways were also found in clinical patients with hyperlipidemia. Hyperlipidemia is one of the main risk factors for CHD, and leonurine showed significant regulatory effects on tryptophan and glycerophospholipid metabolism disorders in both AMI rats and clinical hyperlipidemia patients. This work provides a valuable basis for the research and development of leonurine as an anti-AMI drug.

Data availability statement

The original contributions presented in the study are included in the article/Supplementary material, further inquiries can be directed to the corresponding author/s.

Ethics statement

The animal study was reviewed and approved by the Institutional Animal Care and Use Committee of Nantong University.

Author contributions

QingZ conceived and designed the project. YZ provided leonurine sample and consultation. WR and QinbZ performed network pharmacology experiment. WR and JL did the main work. WR integrated the data and wrote the manuscript. JL, XQ, and XZ performed metabolomics experiment. LW performed

animal experiments. SL analyzed histological samples. TL guided data processing. All authors had approved the manuscript.

Funding

This research was funded by grants from National Natural Science Foundation of China (82071238, 81971243, and 81973320), Natural Science Foundation of Jiangsu Province (BK20181459), and the Macau Science and Technology Development Fund (0067/2018/A2, 033/2017/AMJ, 0007/2019/AKP, 0052/2020/A, and 0011/2020/A1). Large Instrument and Equipment Fund of Nantong University (KFJN2267).

Conflict of interest

The authors declare that the research was conducted in the absence of any commercial or financial relationships that could be construed as a potential conflict of interest.

Publisher's note

Supplementary material

The Supplementary Material for this article can be found online at: https://www.frontiersin.org/articles/10.3389/fcvm.2022.969553/full#supplementary-material

References

1. Heusch G. The coronary circulation as a target of cardioprotection. *Circ Res.* (2016) 118:1643–58. doi: 10.1093/cvr/cvr271

2. Knuuti J, Wijns W, Saraste A, Capodanno D, Barbato E, Funck-Brentano C, et al. 2019 esc guidelines for the diagnosis and management of chronic coronary syndromes the task force for the diagnosis and management of chronic coronary syndromes of the european society of cardiology (esc). *Eur Heart J.* (2020) 41:407–77. doi: 10.1093/eurheartj/ehz425

3. Steptoe A, Kivimaeki M. Stress and cardiovascular disease. *Nat Rev Cardiol.* (2012) 9:360–70. doi: 10.1038/nrcardio.2012.45

4. Shang X, Pan H, Wang X, He H, Li M. Leonurus japonicus houtt: Ethnopharmacology, phytochemistry and pharmacology of an important traditional. *Chinese Med J Ethnopharmacol.* (2014) 152:14–32. doi: 10.1016/j.jep.2013.12.052

5. Sun J, Huang SH, Zhu YC, Whiteman M, Wang MJ, Tan BKH, et al. Anti-oxidative stress effects of herba leonuri on ischemic rat hearts. *Life Sci.* (2005) 76:3043–56. doi: 10.1016/j.lfs.2004.11.024

6. Zhu YZ, Huang SH, Tan BKH, Sun J, Whiteman M, Zhu YC. Antioxidants in chinese herbal medicines: a biochemical perspective. *Nat Prod Rep.* (2004) 21:478–89. doi: 10.1039/b304821g

7. Huang L, Xu DQ, Chen YY, Yue SJ, Tang YP. Leonurine, a potential drug for the treatment of cardiovascular system and central nervous system diseases. *Brain Behav.* (2021) 11:1995. doi: 10.1002/brb3.1995

8. Li Y, Lin Y, Liu X, Wang L, Yu M, Li D, et al. Leonurine: from gynecologic medicine to pleiotropic agent. *Chin J Integr Med.* (2020) 26:152–60. doi: 10.1007/s11655-019-3453-0

9. Liu XH, Pan LL, Chen PF, Zhu YZ. Leonurine improves ischemia-induced myocardial injury through antioxidative activity. *Phytomedicine.* (2010) 17:753–9. doi: 10.1016/j.phymed.2010.01.018

10. Liu XH, Pan LL, Deng HY, Xiong QH, Wu D, Huang GY, et al. Leonurine (scm-198) attenuates myocardial fibrotic response via inhibition of nadph oxidase 4. *Free Radical Bio Med.* (2013) 54:93–104. doi: 10.1016/j.freeradbiomed.2012.10.555

11. Liu L, Wang C, Luo X, Wang Y, Li F. Leonurine alleviates hypoxia-induced myocardial damage by regulating mirnas. *Nat. Prod. Commun.* (2021) 16: 1934578X211007274. doi: 10.1177/1934578X211007274

12. The National Pharmacopeia Commission. *Chinese Pharmacopoeia I.* China Medical Science and Technology Press. (2020) 302–303.

13. Liu X, Chen P, Pan L, De Silva R, Zhu Y. 4-guanidino-n-butyl syringate (leonurine, scm 198) protects h9c2 rat ventricular cells from hypoxia-induced apoptosis. *J Cardiovasc Pharm.* (2009) 54:437–44. doi: 10.1097/FJC.0b013e3181bae160

14. Liu XH, Xin H, Hou AJ, Zhu YZ. Protective effects of leonurine in neonatal rat hypoxic cardiomyocytes and rat infarcted heart. *Clin Exp Pharmacol P.* (2009) 36:696–703. doi: 10.1111/j.1440-1681.2008.05135.x

15. Xin H, Liu XH, Zhu YZ. Herba leonurine attenuates doxorubicin-induced apoptosis in h9c2 cardiac muscle cells. *Eur J Pharmacol.* (2009) 612:75–9. doi: 10.1016/j.ejphar.2009.03.067

16. Liu XH, Pan LL, Gong QH, Zhu YZ. Antiapoptotic effect of novel compound from herba leonuri- leonurine (scm-198): a mechanism through inhibition of mitochondria dysfunction in h9c2 cells. *Curr Pharm Biotechno.* (2010) 11:895–905. doi: 10.2174/138920110793262015

17. Liu X, Pan L, Gong Q, Zhu Y. Leonurine (scm-198) improves cardiac recovery in rat during chronic infarction. *Eur J Pharmacol.* (2010) 649:236–41. doi: 10.1016/j.ejphar.2010.08.056

18. Suguro R, Chen S, Yang D, Yang Z, Miao L, Wu W, et al. Anti-hypercholesterolemic effects and a good safety profile of scm-198 in animals: from apoe knockout mice to rhesus monkeys. *Front Pharmacol.* (2018) 9:1468. doi: 10.3389/fphar.2018.01468

19. McQueen MJ, Hawken S, Wang X, Ounpuu S, Sniderman A, Probstfield J, et al. Lipids, lipoproteins, and apolipoproteins as risk markers of myocardial infarction in 52 countries (the interheart study): a case-control study. *Lancet.* (2008) 372:224–33. doi: 10.1016/S0140-6736(08)61076-4

20. Stanley WC, Recchia FA, Lopaschuk GD. Myocardial substrate metabolism in the normal and failing heart. *Physiol Rev.* (2005) 85:1093–129. doi: 10.1152/physrev.00006.2004

21. Bonanad C, Bodi V, Sanchis J, Morales JM, Marrachelli VG, Nunez J, et al. Metabolomic profile of human myocardial ischemia assessed by nuclear magnetic resonance spectroscopy of peripheral blood serum. A translational study based on transient coronary occlusion models. *J Am Coll of Cardiol.* (2012) 59:E558–E558. doi: 10.1016/S0735-1097(12)60559-2

22. Lindsey ML, Bolli R, Canty JM. Jr., Du X-J, Frangogiannis NG, Frantz S, et al. Guidelines for experimental models of myocardial ischemia and infarction. *Am J Physiol-Heart C.* (2018) 314:H812–38. doi: 10.1152/ajpheart.00335.2017

23. Smilde AK, Werf MTJ. Van Der, Sabina B, Jellema RH. Fusion of mass spectrometry-based metabolomics data. *Anal Chem.* (2005) 77:6729. doi: 10.1021/ac051080y

24. Wang X, Shen Y, Wang S, Li S, Zhang W, Liu X, et al. Pharmmapper 2017 update: a web server for potential drug target identification with a comprehensive target pharmacophore database. *Nucleic Acids Res.* (2017) 45:W356–60. doi: 10.1093/nar/gkx374

25. Wishart DS, Feunang YD, Guo AC, Lo EJ, Marcu A, Grant JR, et al. Drugbank 5.0: a major update to the drugbank database for 2018. *Nucleic Acids Res.* (2018) 46:D1074–82. doi: 10.1093/nar/gkx1037

26. Amberger JS, Bocchini CA, Schiettecatte F, Scott AF, Hamosh A. OmimOrg: oOnline mendelian inheritance in man (omim (r)), an online catalog of human genes and genetic disorders. *Nucleic Acids Res.* (2015) 43:D789–98. doi: 10.1093/nar/gku1205

27. Stelzer G, Rosen N, Plaschkes I, Zimmerman S, Twik M, Fishilevich S, et al. The genecards suite: from gene data mining to disease genome sequence analyses. *Curr Protoc Bioinform.* (2016) 54:1.30.31-31.30.33. doi: 10.1002/cpbi.5

28. Szklarczyk D, Morris JH, Cook H, Kuhn M, Wyder S, Simonovic M, et al. The string database in 2017: quality-controlled protein-protein association networks, made broadly accessible. *Nucleic Acids Res.* (2017) 45:D362–8. doi: 10.1093/nar/gkw937

29. Zhang N, Lei J, Liu Q, Huang W, Xiao H, Lei H. The effectiveness of preoperative trimetazidine on myocardial preservation in coronary artery bypass graft patients: a systematic review and meta-analysis. *Cardiology.* (2015) 131:86–96. doi: 10.1159/000375289

30. Mair J, Lindahl B, Hammarsten O, Mueller C, Giannitsis E, Huber K, et al. How is cardiac troponin released from injured myocardium? *Eur Heart J-Acute CA.* (2018) 7:553–60. doi: 10.1177/2048872617748553

31. Mushtaque RS, Hameed S, Mushtaque R, Idrees M, Siraj F. Role of cardio-specific micro-ribonucleicacids and correlation with cardiac biomarkers in acute coronary syndrome: a comprehensive systematic review. *Cureus.* (2019) 11:e5878–e5878. doi: 10.7759/cureus.5878

32. Schmitz G, Ruebsaamen K. Metabolism and atherogenic disease association of lysophosphatidylcholine. *Atherosclerosis.* (2010) 208:10–8. doi: 10.1016/j.atherosclerosis.2009.05.029

33. Paapstel K, Kals J, Eha J, Tootsi K, Ottas A, Piir A, et al. Inverse relations of serum phosphatidylcholines and lysophosphatidylcholines with vascular damage and heart rate in patients with atherosclerosis. *Nutr Metab Cardiovas.* (2018) 28:44–52. doi: 10.1016/j.numecd.2017.07.011

34. Wu J, Zhang Y, Wu Q, Xie D, Dai W, Zhang X, et al. Integrative analyses of myocardial lipidome and proteome implicate mitochondrial dysfunction in lethal ventricular tachyarrhythmia (lvta) induced by acute myocardial ischemia (AMI). *J Proteomics.* (2019) 197:14–22. doi: 10.1016/j.jprot.2019.01.021

35. Wang X, Wang Q, Zhang A, Zhang F, Zhang H, Sun H, et al. Metabolomics study of intervention effects of wen-xin-formula using ultra high-performance liquid chromatography/mass spectrometry coupled with pattern recognition approach. *J Pharmaceut Biomed.* (2013) 74:22–30. doi: 10.1016/j.jpba.2012.10.009

36. Zhang H, Chen X, Hu P, Liang Q, Liang X, Wang Y, et al. Metabolomic profiling of rat serum associated with isoproterenol-induced myocardial infarction using ultra-performance liquid chromatography/time-of-flight mass spectrometry and multivariate analysis. *Talanta.* (2009) 79:254–9. doi: 10.1016/j.talanta.2009.03.045

37. Bannehr M, Loehr L, Gelep J, Haverkamp W, Schunck WH, Gollasch M, et al. Linoleic acid metabolite dihome decreases post-ischemic cardiac recovery in murine hearts. *Cardiovasc Toxicol.* (2019) 19:365–71. doi: 10.1007/s12012-019-09508-x

38. Tan G, Liao W, Dong X, Yang G, Zhu Z, Li W, et al. Metabonomic profiles delineate the effect of traditional chinese medicine sini decoction on myocardial infarction in rats. *PLoS ONE.* (2012) 7:e34157. doi: 10.1371/journal.pone.0034157

39. Kantor PF, Lucien A, Kozak R, Lopaschuk GD. The antianginal drug trimetazidine shifts cardiac energy metabolism from fatty acid oxidation to glucose oxidation by inhibiting mitochondrial long-chain 3-ketoacyl coenzyme a thiolase. *Circ Res.* (2000) 86:580–8. doi: 10.1161/01.RES.86.5.580

40. Khazanov VA, Kiseliova AA, Vasiliev KY, Chernyschova GA. Cardioprotective effects of trimetazidine and a combination of succinic and malic acids in acute myocardial ischemia. *B Exp Biol Med.* (2008) 146:218–22. doi: 10.1007/s10517-008-0259-3

41. Zhang Y, Yang L, Yang YJ, Liu XY, Jia JG, Qian JY, et al. Low-dose taurine upregulates taurine transporter expression in acute myocardial ischemia. *Int J Mol Med.* (2013) 31:817–24. doi: 10.3892/ijmm.2013.1264

42. Wang D, Wang X, Wu J, Su R, Kong J, Yu X. Metabolic risk factors associated with sudden cardiac death (scd) during acute myocardial ischemia. *Forensic Sci Res.* (2017) 2:126–31. doi: 10.1080/20961790.2017.1343269

43. Gundewar S, Lefer DJ. Sphingolipid therapy in myocardial ischemia-reperfusion injury. *BBA-Gen Subjects.* (2008) 1780:571–6. doi: 10.1016/j.bbagen.2007.08.014

44. Qi Y, Gu H, Song Y, Dong X, Liu A, Lou Z, et al. Metabolomics study of resina draconis on myocardial ischemia rats using ultraperformance liquid chromatography/quadrupole time-of-flight mass spectrometry combined with pattern recognition methods and metabolic pathway analysis. *Evid-Based Compl Alt.* (2013) 2013:438680. doi: 10.1155/2013/438680

45. Tao H, Yang X, Wang W, Yue S, Pu Z, Huang Y, et al. Regulation of serum lipidomics and amino acid profiles of rats with acute myocardial ischemia by salvia miltiorrhiza and panax notoginseng herb pair. *Phytomedicine.* (2020) 67:153162. doi: 10.1016/j.phymed.2019.153162

46. Petras M, Kalenska D, Samos M, Bolek T, Sarlinova M, Racay P, et al. NMR plasma metabolomics study of patients overcoming acute myocardial infarction: In the first 12 h after onset of chest pain with statistical discrimination towards metabolomic biomarkers. *Physiol Res.* (2020) 69:823–34. doi: 10.33549/physiolres.934417

47. Chacko S, Mamas MA, El-Omar M, Simon D, Haseeb S. Fath-ordoubadi F, et al. Perturbations in cardiac metabolism in a human model of acute myocardial ischaemia. *Metabolomics.* (2021) 17:76. doi: 10.1007/s11306-021-01827-x

48. Griffin KJ, Newell LM, Simpson KR, Beckers CML, Drinkhill MJ, Standeven KF, et al. Transglutaminase 2 limits the extravasation and the resultant myocardial fibrosis associated with factor xiii-a deficiency. *Atherosclerosis.* (2020) 294:1–9. doi: 10.1016/j.atherosclerosis.2019.12.013

49. Szondy Z, Mastroberardino PG, Varadi J, Farrace MG, Nagy N, Bak I, et al. Tissue transglutaminase (tg2) protects cardiomyocytes against ischemia/reperfusion injury by regulating atp synthesis. *Cell Death Differ.* (2006) 13:1827–9. doi: 10.1038/sj.cdd.4401889

frontiers | Frontiers in Cardiovascular Medicine

TYPE Original Research
PUBLISHED 15 September 2022
DOI 10.3389/fcvm.2022.957340

OPEN ACCESS

EDITED BY
Yanggang Yuan,
Nanjing Medical University, China

REVIEWED BY
Zhiyu Dai,
University of Arizona, United States
Ting Wang,
Florida International University, United States

*CORRESPONDENCE
Hua Cai
hcai@mednet.ucla.edu

†These authors have contributed equally to this work

SPECIALTY SECTION
This article was submitted to General Cardiovascular Medicine, a section of the journal Frontiers in Cardiovascular Medicine

RECEIVED 31 May 2022
ACCEPTED 18 July 2022
PUBLISHED 15 September 2022

CITATION
Youn JY, Wang J, Li Q, Huang K and Cai H (2022) Robust therapeutic effects on COVID-19 of novel small molecules: Alleviation of SARS-CoV-2 S protein induction of ACE2/TMPRSS2, NOX2/ROS, and MCP-1.
Front. Cardiovasc. Med. 9:957340.
doi: 10.3389/fcvm.2022.957340

Robust therapeutic effects on COVID-19 of novel small molecules: Alleviation of SARS-CoV-2 S protein induction of ACE2/TMPRSS2, NOX2/ROS, and MCP-1

Ji Youn Youn[1,2†], Jian Wang[3†], Qian Li[1,2†], Kai Huang[1,2] and Hua Cai[1,2*]

[1]Division of Molecular Medicine, Department of Anesthesiology, David Geffen School of Medicine at University of California, Los Angeles, Los Angeles, CA, United State, [2]Division of Cardiology, Department of Medicine, David Geffen School of Medicine at University of California, Los Angeles, Los Angeles, CA, United States, [3]Department of Cardiology, China-Japan Friendship Hospital, Beijing, China

While new variants of severe acute respiratory syndrome coronavirus 2 (SARS-CoV-2) constantly emerge to prolong the pandemic of COVID-19, robust and safe therapeutics are in urgent need. During the previous and ongoing fight against the pandemic in China, Traditional Chinese Medicine (TCM) has proven to be markedly effective in treating COVID-19. Among active ingredients of TCM recipes, small molecules such as quercetin, glabridin, gallic acid, and chrysoeriol have been predicted to target viral receptor angiotensin-converting enzyme 2 (ACE2) *via* system pharmacology/molecular docking/visualization analyses. Of note, endothelial dysfunction induced by oxidative stress and inflammation represents a critical mediator of acute respiratory distress syndrome (ARDS) and multi-organ injuries in patients with COVID-19. Hence, in the present study, we examined whether quercetin, glabridin, gallic acide and chrysoeriol regulate viral receptors of ACE2 and transmembrane serine protease 2 (TMPRSS2), redox modulator NADPH oxidase isoform 2 (NOX2), and inflammatory protein of monocyte chemoattractant protein-1 (MCP-1) in endothelial cells to mediate therapeutic protection against COVID-19. Indeed, quercetin, glabridin, gallic acide and chrysoeriol completely attenuated SARS-CoV-2 spike protein (S protein)-induced upregulation in ACE2 protein expression in endothelial cells. In addition, these small molecules abolished S protein upregulation of cleaved/active form of TMPRSS2, while native TMPRSS2 was not significantly regulated. Moreover, these small molecules completely abrogated S protein-induced upregulation in NOX2 protein expression, which resulted in alleviated superoxide production, confirming their preventive efficacies against S protein-induced oxidative stress in endothelial cells. In addition, treatment with these small molecules abolished S protein

induction of MCP-1 expression. Collectively, our findings for the first time demonstrate that these novel small molecules may be used as novel and robust therapeutic options for the treatment of patients with COVID-19, *via* effective attenuation of S protein induction of endothelial oxidative stress and inflammation.

KEYWORDS

SARS-CoV-2, COVID-19, endothelial dysfunction, acute respiratory distress syndrome (ARDS), NADPH oxidase isoform 2 (NOX2)

Introduction

As on 1 May 2022, the cases of coronavirus disease 2019 (COVID-19) have surpassed 500 million with 6.0 million deaths worldwide (1). Since the outbreak of the COVID-19 pandemic, extensive research efforts have been made to reveal molecular mechanisms of severe acute respiratory syndrome coronavirus 2 (SARS-CoV-2) infection and the pathogenesis of COVID-19 for effective management of the disease, with many breakthroughs in areas such as rapid and specific identification of viral antigen and variants for accurate diagnosis, and development of robust vaccines and antiviral medications (2, 3). Nonetheless, the COVID-19 pandemic remains challenging to manage with the constant emergence of newly mutated SARS-CoV-2 variants (4). Besides previously defined variants of concern (VOC), Alpha (B.1.1.7), Beta (B.1.351), Gamma (P.1), and Delta (B.1.617.2), the newly emerged variant of SARS-CoV-2 Omicron (B.1.1.529), identified for the first time on 11 November 2021 (5) and now divided into three lineages (BA.1, BA.2, and BA.3) (6), have been known to possess a large number of mutations to confer higher transmissibility, and immune evasion against acquired immunity from natural infection, vaccination (breakthrough infections), or immunotherapies (7). It has been designated as a new VOC (8, 9). Therefore, robust therapeutics for COVID-19 remains in urgent need to contain the COVID-19 pandemic.

During the previous and ongoing flight of the pandemic in China, accumulating evidence has shown that a combination of Traditional Chinese Medicine (TCM) and Western medicine is robustly effective in treating patients with COVID-19, including mild, moderate, and severe cases. Of note, early intervention with TCM has been shown especially beneficial in shortening the course of the disease and preventing the progression of the disease (10). Therefore, we have recently reviewed literature to identify active ingredients/small molecules of TCM recipes that had been predicted to target viral infection and consequent pathological events to effectively treat COVID-19 (11). Among them, quercetin, glabridin, gallic acid, and chrysoeriol (structures shown in **Figure 1**), four small molecules examined in the present study, were predicted to target viral receptor angiotensin-converting enzyme 2 (ACE2) *via* system pharmacology/molecular docking/visualization analyses, based on systematic reviews of literatures (11). Nonetheless, experimental and mechanistic data as to their effects on treating COVID-19 have been lacking. Of interest, some other natural compounds have also been tested or proposed for the treatment efficacies on COVID-19 (12–16).

Spike protein (S protein) of SARS-CoV-2 mediates fusion between viral envelope and cellular membranes for host cell entry through a series of events; first, S protein binds to the membrane-bound receptor of angiotensin-converting enzyme 2 (ACE2), the specific receptor for SARS-CoV-2; then, S protein is cleaved by furin into two subunits of S1 and S2; third, cleavage of S2 domain at discrete cleavage site S' within S2 subunit by transmembrane serine protease 2 (TMPRSS2) exposes fusion peptide (FT) to be subsequently inserted into host cell membrane for fusion (17). Therefore, targeting ACE2 and/or TMPRSS2 to block initial viral entry into the cells could serve as an important therapeutic strategy for COVID-19.

Importantly, endothelial dysfunction is one of the key features of COVID-19, which is considered a major mediator of the development and progression of acute respiratory distress syndrome (ARDS) and multi-organ failure (18, 19, 23). Vascular pathologies, including endothelial morphological disruption, thrombosis, and perivascular inflammation, have been observed in the lungs of patients with COVID-19 (19, 20). Recent studies have shown that exposure of lung vascular endothelial cells to S protein or subunit alone triggers similar signaling responses as a live virus does upon binding to ACE2 receptor (21). Recombinant S1 subunit treated K-18 human ACE2 (hACE2) knock-in mice displayed features of acute lung injury and cytokine storm, as reflected by elevated cytokines in serum and increased expression of inflammatory cytokines/chemokines in the lung (22). We have recently shown that exposure to S protein or interleukin-6 (IL-6) (the primary mediator of cytokine storm) induces NADPH oxidase isoform 2 (NOX2)-dependent excessive oxidative stress in endothelial cells (23). S protein triggers upregulation of ACE2 in endothelial cells, and induction of proinflammatory

protein monocyte chemoattractant protein-1 (MCP-1). All of these responses represent critical underlying mechanisms of endothelial dysfunction and vascular inflammation in COVID-19, driving the development of ARDS/multi-organ failure, and mortality.

Therefore, we examined in the present study whether the small molecules of quercetin, glabridin, gallic acid, and chrysoeriol, regulate ACE2, TMPRSS2, NOX2, and MCP-1 to mediate therapeutic protection against COVID-19. We followed previous experimental protocols in which we found estrogen administration is robustly effective in protecting against endothelial dysfunction *via* abrogation of ACE2 upregulation, and ACE2-dependent activation of NOX2 and MCP-1 (23). We found that quercetin, glabridin, gallic acid, or chrysoeriol treatment of endothelial cells attenuated viral S protein-induced upregulation in ACE2, active TMPRSS2, NOX2, MCP-1 and superoxide production, indicating therapeutic potential of these small molecule compounds for COVID-19 *via* preservation of endothelial function.

Materials and methods

Cell treatment

Bovine aortic endothelial cells (BAECs) (Genlantis, San Diego, CA, United States, passage 4 to 6) were cultured in M199 media supplemented with 10% fetal bovine serum (FBS), 1% vitamin, 1% L-glutamine, and penicillin-streptomycin as previously described (23–30). Confluent BAECs were starved in 5% FBS containing M199 media overnight before treatment with recombinant SARS-CoV-2 spike protein (S protein, 500 ng/ml, #10549-CV-100, R&D, Minneapolis, MN, United States) for 30 min. After 30 min of S protein treatment, cells were exposed to 100 nmol/l of quercetin (#Q4951, MilliporeSigma, St. Louis, MO, United States), glabridin (#G9548, MilliporeSigma, St. Louis, MO, United States), gallic acid (#G7384, MilliporeSigma, St. Louis, MO, United States), and chrysoeriol (derivative of Luteolin, #PHL85725, MilliporeSigma, St. Louis, MO, United States) for 24 h. The drugs were dissolved in dimethyl sulfoxide (DMSO) to make a stock solution and diluted for the treatment of cells. DMSO was also added to the control and S protein groups as vehicle control.

Western blotting

After treatment, BAECs were lysed in lysis buffer (20 mmol/l Tris–HCl pH 7.4, 150 mmol/l NaCl, 1 mmol/l EDTA, 1 mmol/l EGTA, 2.5 mmol/l sodium pyrophosphate, 1 mmol/l β-glycerophosphate, 1 mmol/l sodium orthovanadate, and 1% Triton X-100, supplemented with protease inhibitor cocktail) for 20 min on ice and then supernatant separated by centrifugation at 12,000 rpm for 10 min at 4°C. Following protein concentration determination by DC protein assay (#5000112, Bio-Rad, Hercules, CA, United States), 25–40 μg of protein were separated in 10–15% sodium dodecyl sulfate-polyacrylamide gel electrophoresis (SDS-PAGE), followed by standard Western blotting protocol by probing with antibodies for ACE2 (1:1,000, #ab15348, Abcam, Waltham, MA, United States), TMPRSS2 (1:1,000, #ab92323, Abcam, Waltham, MA, United States), NOX2 (1:250, #611414, BD Biosciences, San Jose, CA, United States), MCP-1 (1:500, #ab9669, Abcam, Waltham, MA, United States), and β-actin (1:1,000, #A2066, MilliporeSigma, St. Louis, MO, United States) as we previously published (23). The protein bands were visualized by enhanced chemiluminescent methods, and band densities quantified using National Institutes of Health (NIH) Image J program.

Determination of superoxide production by electron spin resonance

Superoxide production in BAECs was determined by electron spin resonance (ESR) (eScan, Bruker, Billerica, MA, United States) as we previously published (23–37). After treatment, cells were collected in cold modified Krebs/HEPES (KHB) buffer (99 mmol/l of NaCl, 4.69 mmol/l of KCl, 1.03 mmol/l of KH_2PO_4, 2.50 mmol/l of $CaCl_2$, 1.20 mmol/l of $MgSO_4$, 25.0 mmol/l of $NaHCO_3$, 5.6 mmol/l of glucose, and 20.0 mmol/l of Na-HEPES, pH 7.35). The cell suspension was mixed with superoxide-specific spin trap CMH (1 mmol/l, #ALX-430-117-M250, Enzo Life Sciences, Farmingdale, NY, United States) in nitrogen gas bubbled KHB buffer containing diethyldithiocarbamic acid (5 μmol/l, #D3506, MilliporeSigma, St. Louis, MO, United States) and deferoxamine (25 μmol/l, #D9533, MilliporeSigma, St. Louis, MO, United States). Then, the cell mixture was loaded in glass capillaries and analyzed immediately by ESR. Superoxide signal was measured in the presence or absence of polyethylene glycol-superoxide dismutase (PEG-SOD) (20 U/ml, #S9549, MilliporeSigma, St. Louis, MO, United States). The PEG-SOD inhabitable superoxide signal was calculated and normalized to protein concentrations. The ESR settings used were: center field 3,480.00 G; sweep width 9.00 G; microwave frequency 9.79 GHz; microwave power 21.02 mW; modulation amplitude 2.47 G; 512 points of resolution; and receiver gain 1,000.

Statistical analysis

All the data are presented as mean ± SEM. One-way ANOVA was used to compare the means among multiple groups with the Newman–Keuls *post hoc* test. $p < 0.05$ was considered statistically significant.

Results

Attenuation of severe acute respiratory syndrome coronavirus 2 spike protein-induced upregulation of angiotensin-converting enzyme 2/transmembrane serine protease 2 by small molecule compounds

We have recently demonstrated that ACE2 is abundantly expressed in endothelial cells, and that viral spike protein (S protein) potently upregulates protein expression of ACE2 in both human and bovine endothelial cells (23). This response is fully reversible by estrogen treatment (23). Here, we examined the effects on endothelial ACE2 expression of novel small molecules of TCM recipes/ingredients found effective in treating COVID-19. The chemical structures of the small molecules are presented in **Figure 1**. As shown in **Figures 2**, **3A**, quercetin, glabridin, gallic acid, or chrysoeriol (100 nmol/l) completely attenuated S protein-induced upregulation in ACE2 protein abundance in endothelial cells. Of note, these small molecules (100 nmol/l) also near completely alleviated S protein upregulation of cleaved/active form of TMPRSS2, while native TMPRSS2 was not significantly regulated (**Figures 2**, **3B,C**). Following the binding of S protein to ACE2 *via* receptor-binding domain (RBD), TMPRSS2 cleaves the S2 domain to facilitate membrane fusion and viral entry. The cleaved active form of TMPRSS2 has been known to interact with ACE2 receptor (38). Hence, our results demonstrate potential therapeutic efficacies of TCM ingredient small molecules of quercetin, glabridin, gallic acid, and chrysoeriol, which are attributed to attenuation of ACE2 binding of S protein *via* downregulation of ACE2, and blockade of the activity of ACE2 via reduction of its interaction with the activated form of TMPRSS2.

Attenuation of severe acute respiratory syndrome coronavirus 2 spike protein-induced upregulation of NADPH oxidase isoform 2 and excessive superoxide production by small molecule compounds

We have recently shown that ACE2-dependent selective activation of NOX2 and ROS production by viral S protein can be completely reversed by estrogen (23). In the present study, we also examined the effects on NOX2 protein expression and endothelial superoxide production of novel small molecules of TCM recipes/ingredients found effective in treating COVID-19. As shown in **Figures 2**, **4A**, the expression of NOX2 was upregulated by S protein, which is consistent with our previous findings (23). Treatment with quercetin, glabridin, gallic acid,

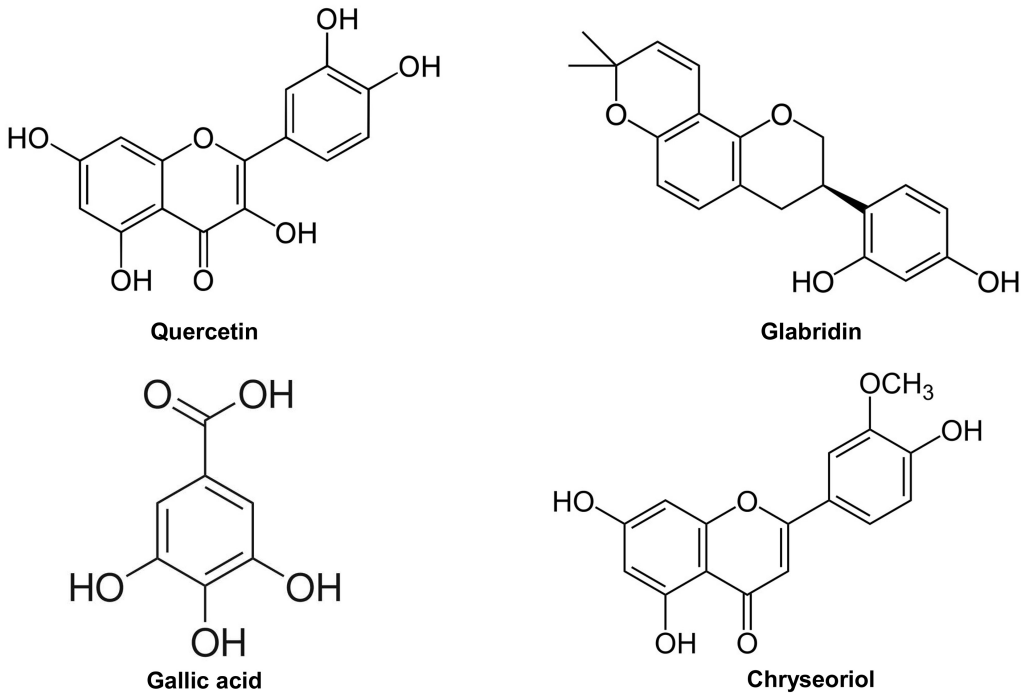

FIGURE 1
Chemical structures of quercetin, glabridin, gallic acid, and chrysoeriol.

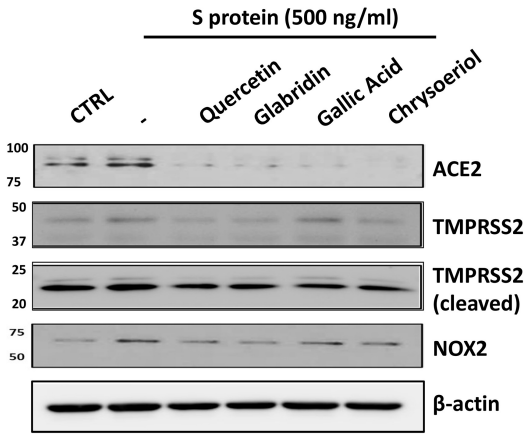

FIGURE 2
Representative Western blots of ACE2/TMPRSS2 and NOX2 in S protein and small molecules treated endothelial cells. Bovine aortic endothelial cells (BAECs) were pretreated with viral spike protein (S protein, 500 ng/ml) for 30 min before exposure to 100 nmol/l of small molecule compounds for 24 h. Shown are representative Western blots of ACE2, native/cleaved TMPRSS2 and NOX2 in S protein, and small molecules treated endothelial cells.

or chrysoeriol following S protein stimulation of endothelial cells near completely attenuated NOX2 protein upregulation at a concentration of 100 nmol/l, indicating robust reversal effects of these small molecules on NOX2 activation. S protein stimulation markedly upregulated superoxide production in endothelial cells, which is consistent with our previous observations (23). Treatment with small molecules (100 nmol/l) following S protein stimulation of endothelial cells near completely alleviated increased superoxide production, indicating robust therapeutic potential of these small molecules on S protein-induced oxidative stress in endothelial cells (Figures 2, 4B).

Attenuation of severe acute respiratory syndrome coronavirus 2 spike protein-induced upregulation of monocyte chemoattractant protein-1 by small molecule compounds

The proinflammatory cytokines such as MCP-1 were found to be elevated along with other inflammatory mediators in patients with COVID-19 (39). In the previous study, we found that S protein exposure induced upregulation of pro-inflammatory protein MCP-1, which was completely alleviated by estrogen (23). Interestingly, treatment with quercetin, glabridin, gallic acid, or chrysoeriol (100 nmol/l) also abolished S protein induction of MCP-1 (Figure 5). The alleviation in MCP-1 can prevent attraction of monocytes/macrophages to endothelial cells to eliminate hyperinflammatory state, as dysregulated levels of MCP-1, –2, and –3 were observed in plasma samples of hospitalized patients with COVID-19 (39). Therefore, quercetin, glabridin, gallic acid, or chrysoeriol (luteolin derivative) can effectively attenuate endothelial dysfunction and inflammation *via* inhibition of ACE2/TMPRSS2, NOX2-dependent superoxide production, and MCP-1, leading to abrogation of ARDS/multi-organ failure and mortality in patients with COVID-19.

Discussion

Spike protein (S protein) of SARS-CoV-2 mediates host cell entry *via* angiotensin-converting enzyme 2 (ACE2) and transmembrane serine protease 2 (TMPRSS2), targeting of

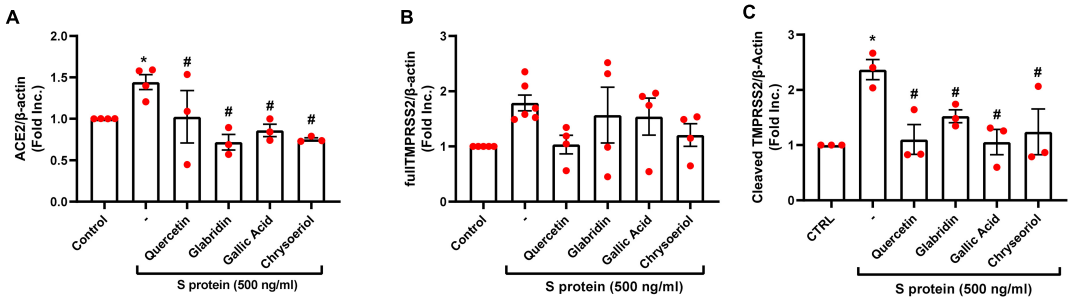

FIGURE 3
Attenuation of SARS-CoV-2 spike protein-induced upregulation of ACE2/TMPRSS2 by quercetin, glabridin, gallic acid, and chrysoeriol. Bovine aortic endothelial cells (BAECs) were pretreated with viral spike protein (S protein, 500 ng/ml) for 30 min before exposure to 100 nmol/l of small molecule compounds for 24 h. **(A)** Grouped data of ACE2 protein expression indicating that S protein-induced upregulation in ACE2 protein abundance was completely attenuated by small molecules. $n = 3–4$. **(B,C)** Grouped data of native and cleaved TMPRSS2 protein expression indicating that S protein activated proteolytic cleavage of TMPRSS2 was near completely attenuated by small molecules. Data are shown as mean ± SEM. $*p < 0.05$, $**p < 0.01$ vs. control group; $\#p < 0.05$, $\#\#p < 0.01$ vs. S protein treated group by one-way ANOVA.

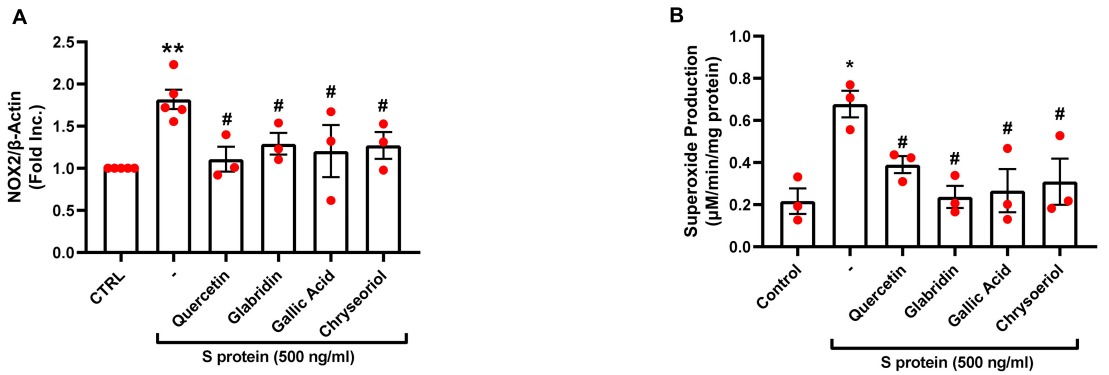

FIGURE 4
Attenuation of SARS-CoV-2 spike protein-induced upregulation of NOX2 and excessive superoxide production by quercetin, glabridin, gallic acid, and chrysoeriol. Bovine aortic endothelial cells (BAECs) were pretreated with viral spike protein (S protein, 500 ng/ml) for 30 min before exposure to 100 nmol/l of small molecule compounds for 24 h. **(A)** Grouped data of NOX2 protein expression indicating upregulation of NOX2 by S protein, which was near completely attenuated by small molecules. n = 3–5. **(B)** Grouped data of superoxide production as determined specifically and quantitatively by electron spin resonance (ESR), indicating S protein induction of excessive superoxide production in endothelial cells, which was near completely alleviated by small molecules. Data are shown as mean ± SEM. n = 3, $^{**}p < 0.01$ vs. control group; $\#p < 0.05$ vs. S protein treated group by one-way ANOVA.

which could serve as an important therapeutic strategy for COVID-19. In the present study, we hypothesized that small molecules quercetin, glabridin, gallic acid, and chrysoeriol, derived from active ingredients of TCM recipes proven effective in treating COVID-19 (11), protect against COVID-19 by inhibiting viral receptors of ACE2 and TMPRSS2 on endothelial cells, thus regulating expression of NOX2 and MCP-1, as well as endothelial cell production of superoxide. We found that expression of ACE2 and cleaved/active form of TMPRSS2 were significantly upregulated by SARS-CoV-2 S protein, both of which were abolished or near completely attenuated by treatment with the small molecules described above. In addition, treatment of endothelial cells with quercetin, glabridin, gallic acid, or chrysoeriol near completely reversed S protein-induced NOX2 activation and NOX2-dependent production of superoxide, as well as upregulation of proinflammatory proteins such as MCP-1.

Among the four molecules, quercetin, glabridin, and chrysoeriol (luteolin derivative) are naturally occurring flavonoids, while gallic acid is a natural polyphenolic compound. Natural flavonoids have been known to reduce oxidative stress and inflammation in endothelial cells, so that it contributes to restoration of endothelial function in diabetes (40), though detailed molecular mechanisms have remained unclear. Gallic acid was demonstrated to have anti-obesity properties by suppressing lipogenesis, improving insulin signaling, and reducing proinflammatory responses and oxidative stress (41). Whether or not these small molecules regulate pathways such as NADPH oxidases has remained unclear. Of note, these small molecules have been predicted to target ACE2 by system pharmacology/molecular docking/visualization analyses. Here, we treated endothelial cells with these small molecules following initial exposure of the cells to S protein, to examine potential reversal effects on pathological consequences of these small molecules. Indeed, four small molecules investigated in this study completely attenuated S protein-induced upregulation in ACE2 protein abundance. Of note, these small molecules near completely attenuated S protein upregulation of cleaved/active form of TMPRSS2, while native TMPRSS2 was not significantly

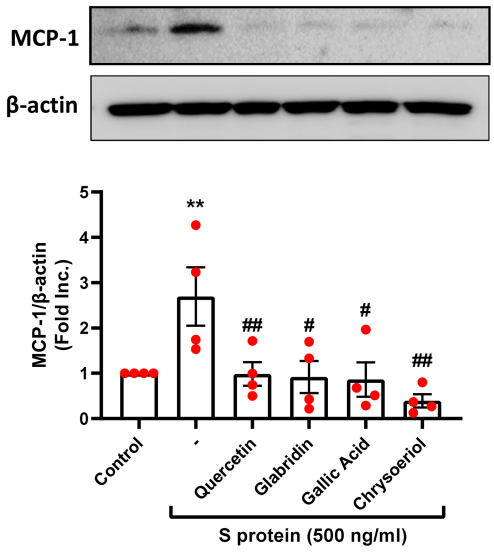

FIGURE 5
Attenuation of SARS-CoV-2 spike protein-induced upregulation of MCP-1 by quercetin, glabridin, gallic acid, and chrysoeriol. Bovine aortic endothelial cells (BAECs) were pretreated with viral spike protein (S protein, 500 ng/ml) for 30 min before exposure to 100 nmol/l of small molecule compounds for 24 h. Shown are representative Western blots and grouped data of MCP-1 protein expression indicating upregulation of proinflammatory protein MCP-1 by S protein, which was completely attenuated by small molecules. Data are shown as mean ± SEM. n = 4. $^{**}p < 0.01$ vs. control group; $\#p < 0.05$, $\#\#p < 0.01$ vs. S protein treated group by one-way ANOVA.

regulated. The detailed molecular mechanisms underlying the inhibition on ACE2 of these small molecules warrant further investigation, while the predicted binding of these small molecules to ACE2 by docking studies might indeed underlie ACE2 inhibition by these compounds (42, 43). Besides the direct targeting of ACE2, network pharmacology analyses predict that these molecules might modulate transcription factors (TFs), including hepatocyte nuclear factor 4 alpha (HNF4A) and peroxisome proliferator-activated receptor gamma (PPARG), or microRNAs (miRNAs), including hsa-miR-2113 and hsa-miR-421, resulting in modulation of these upstream events to target ACE2 (43).

For SARS-CoV-2 entry into host cells, ACE2 and TMPRSS2 are critically required (44). Of note, "viral entry inhibitors," the antiviral class of drugs to block viral entry by inhibiting both TMPRSS2 and ACE2, have been actively investigated for the development of new drugs for COVID-19 (3, 44). The United States Food and Drug Administration (USFDA) has approved approximately 2,800 investigative molecules for further evaluations, which were selected using a virtual docking tool identifying dual-target inhibition of TMPRSS2 and ACE2 (44). In an *in silico* drug repurposing study, lopinavir and valrubicin have been shown superior in terms of dual inhibition (44). Compared to the antivirals targeting the viral life cycle to treat severe, hospitalized patients, such as remdesivir, viral entry inhibitors have the advantages for early intervention of COVID-19 (45). By blocking viral entry, these antivirals possess the potential to prevent disease transition into severe cases and shorten the disease course, which is in line with the observed benefits of TCM therapies during early intervention (10, 11, 45). Hence, as the active components of the proven TCM recipes, these small molecules might represent suitable candidates as viral entry inhibitors.

Oxidative stress and inflammation have been implicated in ARDS and multi-organ injuries in COVID-19 (18). We have recently shown that S protein stimulation of endothelial cells leads to marked elevation in intracellular superoxide production to induce endothelial dysfunction, which is also characterized by activation of inflammatory signaling, including production of cytokines and chemokines such as IL-6 (one of the key cytokines mediating cytokine storm during the pathogenesis of COVID-19) and MCP-1 (23). Our study has demonstrated that exposure to S protein or IL-6 induces excessive oxidative stress in endothelial cells, which is mediated specifically by activation of NADPH oxidase isoform 2 (NOX2), but not NOX1 or NOX4 (23). Here, we confirmed that S protein induced upregulation of ACE2 in endothelial cells, and ACE2-dependent activation of NOX2, superoxide production, and induction of proinflammatory protein MCP-1. All of these responses represent critical underlying mechanisms of endothelial dysfunction and vascular inflammation in COVID-19, driving the development and progression of ARDS/multi-organ failure, and mortality. In this study, four small molecules of quercetin, glabridin, gallic acid and chrysoeriol near completely attenuated S protein-induced upregulation of NOX2 protein expression, which subsequently abolished overproduction of superoxide, indicating their preventive action against S protein-induced oxidative stress in endothelial cells. In addition, S protein exposure resulted in induction of pro-inflammatory protein MCP-1, which was completely alleviated by treatment with these small molecules. Of note, MCP-1 was found upregulated by oxidative stress activation of nuclear factor-kappa B (NF-$_K$B) in endothelial cells (46).

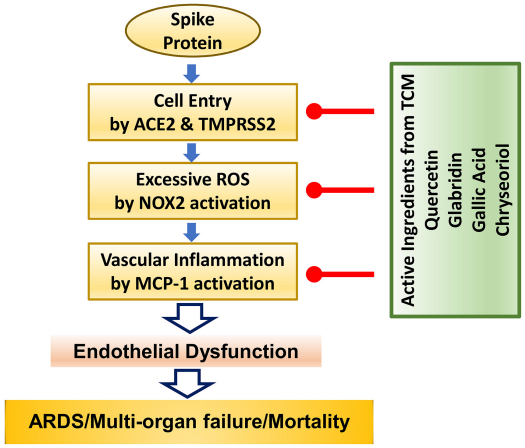

FIGURE 6
The anti-COVID-19 effects of small molecule compounds of quercetin, glabridin, gallic acid, and chrysoeriol. Summary of therapeutic actions of active small molecules in protecting against S protein-induced endothelial dysfunction and inflammation to result in attenuation of ARDS/multi-organ failure and mortality in patients with COVID-19.

In conclusion, we demonstrate for the first time that four small molecules of quercetin, glabridin, gallic acid and chrysoeriol may serve as novel and robust therapeutic options for COVID-19 by: (1) inhibiting viral entry into endothelial cells through downregulation of ACE2/TMPRSS2; (2) preserving endothelial function *via* attenuation of excessive superoxide production elicited by S protein activation of NOX2; and (3) abolishing endothelial inflammation by blocking S protein induction of pro-inflammatory protein MCP-1. These protective effects of the small molecules are anticipated to effectively alleviate ARDS/multi-organ failure/mortality *via* abrogation of endothelial dysfunction. The molecular pathways invovled are shown schematically in **Figure 6**. Therefore, these small molecules can be immediately repurposed as novel therapeutic options for the treatment of patients with COVID-19.

Data availability statement

All data of this study are presented in the article.

Ethics statement

Ethical review and approval was not required for this study in accordance with the local legislation and institutional requirements.

Author contributions

JY: experimentation, data analysis, and drafting of the manuscript. JW, KH, and QL: drafting of the manuscript. HC: project design and administration, data analysis, drafting, and finalizing of the manuscript. All authors contributed to the article and approved the submitted version.

Funding

This study was supported by the National Heart, Lung, and Blood Institute (NHLBI) grants HL077440, HL088975, and HL142951 (HC), HL154754 (HC and AM), and HL162407 (HC and JG).

Conflict of interest

The authors declare that the research was conducted in the absence of any commercial or financial relationships that could be construed as a potential conflict of interest.

Publisher's note

References

1. World Health Organization [WHO]. *Coronavirus Disease 2019 (Covid-19) Weekly Epi Update 90*. (2022). Available online at: https://www.who.int/publications/m/item/weekly-epidemiological-update-on-covid-19---4-may-2022 (accessed May 5, 2022).

2. Zang R, Castro MFG, McCune BT, Zeng Q, Rothlauf PW, Sonnek NM, et al. TMPRSS2 and TMPRSS4 promote SARS-CoV-2 infection of human small intestinal enterocytes. *Sci Immunol.* (2020) 5:eabc3582. doi: 10.1126/sciimmunol.abc3582

3. Hoffmann M, Kleine-Weber H, Schroeder S, Krüger N, Herrler T, Erichsen S, et al. SARS-CoV-2 cell entry depends on ACE2 and TMPRSS2 and is blocked by a clinically proven protease inhibitor. *Cell.* (2020) 181:271–280.e8 doi: 10.1016/j.cell.2020.02.052

4. Wang SY, Juthani PV, Borges KA, Shallow MK, Gupta A, Price C, et al. Severe breakthrough COVID-19 cases in the SARS-CoV-2 delta (B. 1.617. 2) variant era. *Lancet Microbe.* (2022) 3:e4–5. doi: 10.1016/S2666-5247(21)00306-2

5. Jansen L, Tegomoh B, Lange K, Showalter K, Figliomeni J, Abdalhamid B, et al. Investigation of a sars-cov-2 b. 1.1. 529 (omicron) variant cluster—nebraska, november–december 2021. *Morb Mortal Wkly Rep.* (2021) 70:1782. doi: 10.15585/mmwr.mm705152e3

6. World Health Organization [WHO]. *Enhancing Readiness for Omicron (B. 1.1. 529): Technical Brief and Priority Actions for Member States*. Geneva: World Health Organization (2021).

7. Khandia R, Singhal S, Alqahtani T, Kamal MA, Nahed A, Nainu F, et al. Emergence of SARS-CoV-2 Omicron (B. 1.1. 529) variant, salient features, high global health concerns and strategies to counter it amid ongoing COVID-19 pandemic. *Environ Res.* (2022) 2022:112816. doi: 10.1016/j.envres.2022.112816

8. Liu F, Han K, Blair R, Kenst K, Qin Z, Upcin B, et al. CoV-2 infects endothelial cells in vivo and in vitro. *Front Cell Infect Microbiol.* (2021) 11:701278. doi: 10.3389/fcimb.2021.701278

9. World Health Organization [WHO]. *WHO Announces Simple, Easy-To-Say Labels for SARS-CoV-2 Variants of Interest and Concern*. (2021). Available online at: https://www.who.int/news/item/31-05-2021-who-announces-simple-easy-to-say-labels-for-sars-cov-2-variants-of-interest-and-concern (accessed May 31, 2021).

10. Ren J-l, Zhang A-H, Wang X-J. Traditional Chinese medicine for COVID-19 treatment. *Pharmacol Res.* (2020) 155:104743. doi: 10.1016/j.phrs.2020.104743

11. Huang K, Zhang P, Zhang Z, Youn JY, Wang C, Zhang H, et al. Traditional Chinese Medicine (TCM) in the treatment of COVID-19 and other viral infections: Efficacies and mechanisms. *Pharmacol Ther.* (2021) 225:107843. doi: 10.1016/j.pharmthera.2021.107843

12. Rizzuti B, Ceballos-Laita L, Ortega-Alarcon D, Jimenez-Alesanco A, Vega S, Grande F, et al. Sub-micromolar inhibition of SARS-CoV-2 3CLpro by natural compounds. *Pharmaceuticals.* (2021) 14:892. doi: 10.3390/ph14090892

13. Solnier J, Fladerer JP. Flavonoids: A complementary approach to conventional therapy of COVID-19?. *Phytochem Rev.* (2021) 20:773–95. doi: 10.1007/s11101-020-09720-6

14. Wu Y, Crich D, Pegan SD, Lou L, Hansen MC, Booth C, et al. Polyphenols as potential inhibitors of SARS-CoV-2 RNA dependent RNA polymerase (RdRp). *Molecules.* (2021) 26:7438. doi: 10.3390/molecules26247438

15. Shahbazi B, Mafakher L, Teimoori-Toolabi L. Different compounds against angiotensin-converting enzyme 2 (ACE2) receptor potentially containing the infectivity of SARS-CoV-2: An in silico study. *J Mol Model.* (2022) 28:82. doi: 10.1007/s00894-022-05059-1

16. González-Maldonado P, Alvarenga N, Burgos-Edwards A, Flores-Giubi ME, Barúa JE, Romero-Rodríguez MC, et al. Screening of natural products inhibitors of SARS-CoV-2 entry. *Molecules.* (2022) 27:1743. doi: 10.3390/molecules27051743

17. Hoffmann M, Kleine-Weber H, Schroeder S, Kruger N, Herrler T, Erichsen S, et al. SARS-CoV-2 cell entry depends on ACE2 and TMPRSS2 and is blocked by a clinically proven protease inhibitor. *Cell.* (2020) 181:271–280.e8.

18. Nagele MP, Haubner B, Tanner FC, Ruschitzka F, Flammer AJ. Endothelial dysfunction in COVID-19: Current findings and therapeutic implications. *Atherosclerosis.* (2020) 314:58–62. doi: 10.1016/j.atherosclerosis.2020.10.014

19. Varga Z, Flammer AJ, Steiger P, Haberecker M, Andermatt R, Zinkernagel AS, et al. Endothelial cell infection and endotheliitis in COVID-19. *Lancet.* (2020) 395:1417–8. doi: 10.1016/S0140-6736(20)30937-5

20. Ackermann M, Verleden SE, Kuehnel M, Haverich A, Welte T, Laenger F, et al. Pulmonary vascular endothelialitis, thrombosis, and angiogenesis in Covid-19. *N Engl J Med.* (2020) 383:120–8. doi: 10.1056/NEJMoa2015432

21. Suzuki YJ, Nikolaienko SI, Dibrova VA, Dibrova YV, Vasylyk VM, Novikov MY, et al. CoV-2 spike protein-mediated cell signaling in lung vascular cells. *Vascul Pharmacol.* (2021) 137:106823. doi: 10.1016/j.vph.2020.106823

22. Colunga Biancatelli RML, Solopov PA, Sharlow ER, Lazo JS, Marik PE, Catravas JD. The SARS-CoV-2 spike protein subunit S1 induces COVID-19-like acute lung injury in Kappa18-hACE2 transgenic mice and barrier dysfunction in

human endothelial cells. *Am J Physiol Lung Cell Mol Physiol.* (2021) 321:L477–84. doi: 10.1152/ajplung.00223.2021

23. Youn JY, Zhang Y, Wu Y, Cannesson M, Cai H. Therapeutic application of estrogen for COVID-19: Attenuation of SARS-CoV-2 spike protein and IL-6 stimulated, ACE2-dependent NOX2 activation, ROS production and MCP-1 upregulation in endothelial cells. *Redox Biol.* (2021) 46:102099. doi: 10.1016/j.redox.2021.102099

24. Chalupsky K, Cai H. Endothelial dihydrofolate reductase: Critical for nitric oxide bioavailability and role in angiotensin II uncoupling of endothelial nitric oxide synthase. *Proc Natl Acad Sci USA.* (2005) 102:9056–61. doi: 10.1073/pnas.0409594102

25. Nguyen A, Cai H. Netrin-1 induces angiogenesis via a DCC-dependent ERK1/2-eNOS feed-forward mechanism. *Proc Natl Acad Sci USA.* (2006) 103:6530–5. doi: 10.1073/pnas.0511011103

26. Youn JY, Wang T, Cai H. An ezrin/calpain/PI3K/AMPK/eNOSs1179 signaling cascade mediating VEGF-dependent endothelial nitric oxide production. *Circ Res.* (2009) 104:50–9. doi: 10.1161/CIRCRESAHA.108.178467

27. Li H, Li Q, Zhang Y, Liu W, Gu B, Narumi T, et al. Novel treatment of hypertension by specifically targeting E2F for restoration of endothelial dihydrofolate reductase and eNOS function under oxidative stress. *Hypertension.* (2019) 73:179–89. doi: 10.1161/HYPERTENSIONAHA.118.11643

28. Guo Z, Zhang Y, Liu C, Youn JY, Cai H. Toll-like receptor 2 (TLR2) knockout abrogates diabetic and obese phenotypes while restoring endothelial function via inhibition of NOX1. *Diabetes.* (2021) 70:2107–19. doi: 10.2337/db20-0591

29. Huang K, Narumi T, Zhang Y, Li Q, Murugesan P, Wu Y, et al. Targeting MicroRNA-192-5p, a downstream effector of NOXs (NADPH Oxidases), reverses endothelial DHFR (Dihydrofolate Reductase) deficiency to attenuate abdominal aortic aneurysm formation. *Hypertension.* (2021) 78:282–93. doi: 10.1161/HYPERTENSIONAHA.120.15070

30. Huang K, Wang Y, Siu KL, Zhang Y, Cai H. Targeting feed-forward signaling of TGFβ/NOX4/DHFR/eNOS uncoupling/TGFβ axis with anti-TGFβ and folic acid attenuates formation of aortic aneurysms: Novel mechanisms and therapeutics. *Redox Biol.* (2021) 38:101757. doi: 10.1016/j.redox.2020.101757

31. Gao L, Chalupsky K, Stefani E, Cai H. Mechanistic insights into folic acid-dependent vascular protection: Dihydrofolate reductase (DHFR)-mediated reduction in oxidant stress in endothelial cells and angiotensin II-infused mice: A novel HPLC-based fluorescent assay for DHFR activity. *J Mol Cell Cardiol.* (2009) 47:752–60. doi: 10.1016/j.yjmcc.2009.07.025

32. Gao L, Siu KL, Chalupsky K, Nguyen A, Chen P, Weintraub NL, et al. Role of uncoupled endothelial nitric oxide synthase in abdominal aortic aneurysm formation: Treatment with folic acid. *Hypertension.* (2012) 59:158–66. doi: 10.1161/HYPERTENSIONAHA.111.181644

33. Youn JY, Gao L, Cai H. The p47phox- and NADPH oxidase organiser 1 (NOXO1)-dependent activation of NADPH oxidase 1 (NOX1) mediates endothelial nitric oxide synthase (eNOS) uncoupling and endothelial dysfunction in a streptozotocin-induced murine model of diabetes. *Diabetologia.* (2012) 55:2069–79. doi: 10.1007/s00125-012-2557-6

34. Youn JY, Siu KL, Lob HE, Itani H, Harrison DG, Cai H. Role of vascular oxidative stress in obesity and metabolic syndrome. *Diabetes.* (2014) 63:2344–55. doi: 10.2337/db13-0719

35. Siu KL, Miao XN, Cai H. Recoupling of eNOS with folic acid prevents abdominal aortic aneurysm formation in angiotensin II-infused apolipoprotein E null mice. *PLoS One.* (2014) 9:e88899. doi: 10.1371/journal.pone.0088899

36. Siu KL, Lotz C, Ping P, Cai H. Netrin-1 abrogates ischemia/reperfusion-induced cardiac mitochondrial dysfunction via nitric oxide-dependent attenuation of NOX4 activation and recoupling of NOS. *J Mol Cell Cardiol.* (2015) 78:174–85. doi: 10.1016/j.yjmcc.2014.07.005

37. Zhang Y, Murugesan P, Huang K, Cai H. NADPH oxidases and oxidase crosstalk in cardiovascular diseases: Novel therapeutic targets. *Nat Rev Cardiol.* (2020) 17:170–94. doi: 10.1038/s41569-019-0260-8

38. Ko CJ, Huang CC, Lin HY, Juan CP, Lan SW, Shyu HY, et al. Androgen-induced TMPRSS2 activates matriptase and promotes extracellular matrix degradation, prostate cancer cell invasion, tumor growth, and metastasis. *Cancer Res.* (2015) 75:2949–60. doi: 10.1158/0008-5472.CAN-14-3297

39. Sims JT, Krishnan V, Chang CY, Engle SM, Casalini G, Rodgers GH, et al. Characterization of the cytokine storm reflects hyperinflammatory endothelial dysfunction in COVID-19. *J Allergy Clin Immunol.* (2021) 147:107–11. doi: 10.1016/j.jaci.2020.08.031

40. Oteiza PI, Fraga CG, Galleano M. Linking biomarkers of oxidative stress and disease with flavonoid consumption: From experimental models to humans. *Redox Biol.* (2021) 42:101914. doi: 10.1016/j.redox.2021.101914

41. Dludla PV, Nkambule BB, Jack B, Mkandla Z, Mutize T, Silvestri S, et al. Inflammation and oxidative stress in an obese state and the protective effects of gallic acid. *Nutrients.* (2019) 11:23. doi: 10.3390/nu11010023

42. Bhowmik D, Nandi R, Prakash A, Kumar D. Evaluation of flavonoids as 2019-nCoV cell entry inhibitor through molecular docking and pharmacological analysis. *Heliyon.* (2021) 7:e06515. doi: 10.1016/j.heliyon.2021.e06515

43. Niu W, Wu F, Cui H, Cao W, Chao Y, Wu Z, et al. Network pharmacology analysis to identify phytochemicals in traditional Chinese medicines that may regulate ACE2 for the treatment of COVID-19. *Evid Based Complement Alternat Med.* (2020) 2020:1–14. doi: 10.1155/2020/7493281

44. Baby K, Maity S, Mehta CH, Suresh A, Nayak UY, Nayak YSARS-. CoV-2 entry inhibitors by dual targeting TMPRSS2 and ACE2: An in silico drug repurposing study. *Eur J Pharmacol.* (2021) 896:173922. doi: 10.1016/j.ejphar.2021.173922

45. Chitsike L, Duerksen-Hughes P. Keep out! SARS-CoV-2 entry inhibitors: Their role and utility as COVID-19 therapeutics. *Virol J.* (2021) 18:154. doi: 10.1186/s12985-021-01624-x

46. Tumur Z, Shimizu H, Enomoto A, Miyazaki H, Niwa T. Indoxyl sulfate upregulates expression of ICAM-1 and MCP-1 by oxidative stress-induced NF-$_K$B activation. *Am J Nephrol.* (2010) 31:435–41. doi: 10.1159/000299798

frontiers | Frontiers in Cardiovascular Medicine

TYPE Original Research
PUBLISHED 06 October 2022
DOI 10.3389/fcvm.2022.1021112

OPEN ACCESS

EDITED BY
Jia Qi,
Shanghai Jiao Tong University, China

REVIEWED BY
Yibin Pan,
Zhejiang University, China
Xiangwei Gao,
Zhejiang University, China

*CORRESPONDENCE
Tao Zhang
zt801025@sxfby.com
Juan Zhang
zhangjuan_2016@163.com

†These authors have contributed equally to this work

SPECIALTY SECTION
This article was submitted to General Cardiovascular Medicine, a section of the journal Frontiers in Cardiovascular Medicine

RECEIVED 17 August 2022
ACCEPTED 16 September 2022
PUBLISHED 06 October 2022

CITATION
Pan H-T, Xiong Y-M, Zhu H-D, Shi X-L, Yu B, Ding H-G, Xu R-J, Ding J-L, Zhang T and Zhang J (2022) Proteomics and bioinformatics analysis of cardiovascular related proteins in offspring exposed to gestational diabetes mellitus. *Front. Cardiovasc. Med.* 9:1021112. doi: 10.3389/fcvm.2022.1021112

Proteomics and bioinformatics analysis of cardiovascular related proteins in offspring exposed to gestational diabetes mellitus

Hai-Tao Pan[1,2,3†], Yi-Meng Xiong[2†], Hong-Dan Zhu[1,3], Xiao-Liang Shi[1,3], Bin Yu[1,3], Hai-Gang Ding[1,3], Ren-Jie Xu[1,3], Jin-Long Ding[1,3], Tao Zhang[1,3*] and Juan Zhang[1,3*]

[1]Shaoxing Maternity and Child Health Care Hospital, Shaoxing, China, [2]The International Peace Maternity and Child Health Hospital, School of Medicine, Shanghai Jiao Tong University, Shanghai, China, [3]Obstetrics and Gynecology Hospital of Shaoxing University, Shaoxing, China

Introduction: Previous studies have demonstrated that exposed to the initial suboptimal intrauterine environment of gestational diabetes mellitus (GDM) may increase risk of cardiovascular disease in adulthood.

Methods: In order to investigate the underlying mechanisms involved in the increased risk of cardiovascular diseases (CVDs) in the offspring of GDM, we applied a high-throughput proteomics approach to compare the proteomic expression profile of human umbilical vessels of normal and GDM offspring.

Results: A total of significantly different 100 proteins were identified in umbilical vessels from GDM group compared with normal controls, among which 31 proteins were up-regulated, while 69 proteins were down-regulated. Differentially expressed proteins (DEPs) are validated using Western blotting analysis. The analysis of these differently expressed proteins (DEPs) related diseases and functions results, performed by Ingenuity Pathway Analysis (IPA) software. Based on "Diseases and Disorders" analysis, 17 proteins (ACTA2, ADAR, CBFB, DDAH1, FBN1, FGA, FGB, FGG, GLS, GSTM1, HBB, PGM3, PPP1R13L, S100A8, SLC12A4, TPP2, VCAN) were described to be associated with CVD, especially in Anemia, Thrombus and Myocardial infarction. Functional analysis indicated that DEPs involved in many cardiovascular functions, especially in "vasoconstriction of blood vessel" (related DEPs: ACTA2, DDAH1, FBN1, FGA, FGB, and FGG). Upstream regulator analyses of DEPs identifies STAT3 as inhibitor of ACTA2, FGA, FGB, and FGG.

Conclusion: The results of this study indicate that intrauterine hyperglycemia is associated with an elevated risk of cardiovascular risk in the offspring.

KEYWORDS

Gamete and Embryo-Fetal Origins of Adult Diseases, gestational diabetes mellitus (GDM), offspring, umbilical vessel, iTRAQ

Introduction

A growing number of epidemiological and experimental studies suggest that exposure to adverse intrauterine environment during fetal development can be associated with chronic disease in later life, such as CVD, obesity, type 2 diabetes and cognitive disorder (1–6). The theory of Gamete and Embryo-Fetal Origins of Adult Diseases is used preferentially to describe these associations. Gestational diabetes mellitus (GDM) is defined as any degree of glucose intolerance with onset or first diagnosis during gestation. The prevalence of GDM ranged from 9.3 to 25.5% among 15 collaborating centers using the International Association of the Diabetes and Pregnancy Study Group (IADPSG) criteria (7). GDM is a serious health risk for both pregnant women and their offspring.

Emerging evidence suggests that the vasculature of women with a prior case of GDM is permanently altered, predisposing them to CVD. GDM also increases the offspring's risk of developing hypertension and CVD. Elevated systolic blood pressure (SBP) and diastolic blood pressure (DBP) (4, 8–11), increased intima-media thickness (IMT) (12), increased cardiac septal hypertrophy (13), and vascular endothelial dysfunctions were observed in the offspring of GDM mother (14, 15). Consistent with epidemiological results, studies in animal models also showed that diabetes during pregnancy affected the development of fetal cardiovascular system (16, 17). In one of our previous works, we also have indicated that intrauterine hyperglycemia could induce IGT (impaired glucose tolerance) and abnormal blood insulin levels in both F1 and F2 offspring (18). In studies of the mechanisms of cardiovascular dysfunction caused by GDM, numbers of potential pathways have been implicated in endothelial cell, including reduced adenosine transport (14), impaired angiogenesis (15) and redox signaling (19). Although many previous studies have been conducted, its precise mechanism involved in the association between intrauterine hyperglycemia and a higher risk of cardiovascular anomalies has yet to be established.

In the present study, we aimed to investigate the cardiovascular risk proteins in offspring exposed to GDM. A proteomics analysis was conducted in umbilical vessels from newborns of mothers with GDM and normal controls using the isobaric tag for relative and absolute quantitation (iTRAQ)-labeling technique to compare the proteomic expression profile. We analyzed the related diseases and functions using ingenuity pathway analysis (IPA) software. The results of the present study may provide valuable information for further investigation of the mechanisms underlying the cardiovascular dysfunction induced by intrauterine hyperglycemia.

Abbreviations: GDM, Gestational Diabetes Mellitus; DEPs, Differentially Expressed Proteins; FDR, False Discovery Rate; IPA, Ingenuity Pathway Analysis; SCX, Strong Cationic-exchange Chromatography; SBP, Systolic Blood Pressure; IMT, Intima-Media Thickness; FGA, Fibrinogen Alpha Chain; ACTA2, Actin, aortic smooth muscle; IDH3A, Isocitrate dehydrogenase (NAD) subunit alpha, mitochondrial.

Materials and methods

Patients and umbilical cords

Umbilical cords from newborns of 25 mothers with mild GDM and 25 controls were collected by obstetricians in Shaoxing Maternity and Child Health Care Hospital, China. The Ethics Committee of Shaoxing Maternity and Child Health Care Hospital approved the study. All the participants enrolled in this study were with singleton pregnancy and ceased pregnancies with Cesarean section at full term. Tissue samples were stored snap frozen at −80°Cuntil use. The clinical characteristics of the proteomic participants included in this study are outlined in **Table 1**.

GDM were diagnosed between gestational weeks 24 and 28 after overnight fasting (for 8–12 h) by an oral glucose tolerance test (OGTT). According to the IADPSG diagnostic criteria, GDM was defined as fasting venous plasma glucose concentration ≥ 5.1 mM and ≥ 10.0 mM at 1-hand/or ≥ 8.5 mM at 2-h after drinking a solution with 75 g glucose. All women with GDM enrolled in the present study experienced dietary management without insulin treatment. Participants with maternal obesity factor (high pre-pregnancy BMI, excessive weight gain during pregnancy, abnormal lipid level in first-trimester) and macrosomia were excluded. The work described in the present study has been carried out in accordance with The Code of Ethics of the World Medical Association (Declaration of Helsinki). The study protocols were reviewed and approved by the Research and Ethics Committee of the Women's Hospital, School of Medicine, Zhejiang University, China, and informed consents were provided by all participants.

Isobaric tag for relative and absolute quantitation analysis

iTRAQ analysis was performed as previously described (20). Briefly, protein was extracted from umbilical artery and measured by BCA assay (Pierce, Rockford, IL, USA) according to the manufacturer's protocol. Protein digestion was performed according to the FASP procedure, as described by Wisniewski et al. (21). Briefly, 200 μg of total-protein samples were diluted in 30 μL of solution including 4% SDS, 100 mM Tris-HCl pH 8.0 and 100 mM dithiotreitol, and were heated at 95°C for 5 min. After each sample was cooled to room temperature, the sample was loaded onto an ultrafiltration filter (cutoff 10 kDa, Sartorius, Goettingen, Germany). We added 200 μL UT buffer (8 M Urea and 150 mM Tris-HCl, pH 8.0) to the filter and centrifuged it at 14,000 g at 20°C for 30 min. Subsequently,

10.3389/fcvm.2022.1021112

TABLE 1 Clinical characteristic of the participants.

Characteristics	Control	GDM	*P*-value
Cases	25	25	
Gestational age, wk	39.06 ± 0.52	38.85 ± 0.62	0.108
Birth weight, g	3439.57 ± 421.29	3468 ± 456.14	0.241
Maternal age, y	30.21 ± 3.51	31.42 ± 3.11	0.071
BMI of pre-pregnancy, kg/m^2	22.12 ± 2.74	22.79 ± 4.12	0.058
Glycated hemoglobin, %	4.94 ± 0.27	5.10 ± 0.41	0.041*
Pregnancy weight gain, kg	15.65 ± 5.15	14.10 ± 8.59	0.187
OGTT 75 g, 0 h, mmol/L	4.47 ± 0.36	5.02 ± 0.68	< 0.001**
OGTT 75 g, 1 h, mmol/L	8.01 ± 0.93	10.92 ± 1.68	< 0.001**
OGTT 75 g, 2 h, mmol/L	6.56 ± 1.02	9.38 ± 1.60	< 0.001**
Placenta weight,g	598.35 ± 89.92	603.28 ± 116.46	0.097
TC in first-trimester, mmol/L	4.84 ± 0.87	4.78 ± 0.72	0.765
TG in first-trimester, mmol/L	1.23 ± 0.41	1.11 ± 0.14	0.108
HDL in first-trimester, mmol/L	1.67 ± 0.34	1.61 ± 1.48	0.772
LDL in first-trimester, mmol/L	3.12 ± 0.41	3.271 ± 0.37	0.692
Diagnosis	NS	GDM	
Presence of other major cardiovascular risk factor(s) in the mothers	None	None	

Data are showed as means ± *SD*, **P* < 0.05, ***P* < 0.001 compared with control.

100 μL of iodoacetamide solution (50 mM iodoacetamide in UT buffer) was added for blocking reduced cysteines, and, the samples were incubated for 20 min in darkness. Then the filters were centrifuged at 14,000 g at 20°C for 20 min. The filters were washed with 100 μL UT buffer at 14,000 g for 20 min. This step was repeated 2 times. Then, 100 μL dissolution buffer (AB Sciex, Framingham, MA, USA) was added to the filter, and it was centrifuged at 14,000 g at 20°C for 30 min, and, this step was repeated twice. Finally, 40 μL of trypsin (Promega, Madison, WI, USA) buffer (2 μg trypsin in 40 μL dissolution buffer) were added, and, the samples were digested overnight at 37°C. Each filter unit was transferred to a new tube and centrifuged at 14,000 g at 20°C for 30 min. The concentration of resulting peptides was determined by UV light spectral density at OD_{280} (22).

The iTRAQ labeling of digested peptide samples was performed following the manufacturers protocol with 8-plex isobaric tags for relative and absolute quantitation (iTRAQ) labeling kit (AB Sciex, Framingham, MA, USA). Three umbilical arteries from the control group (C) were labeled with mass 114, 115 and 116 isobaric iTRAQ tags, the other three umbilical arteries from the GDM group were labeled with mass 117, 118, and 119 isobaric iTRAQ tags. Identical quantities of peptide mixtures from the 6 peptides mentioned above were labeled with reagent 113 and served as sample IS (internal standard). According to the manufacturers protocol, The labeling reactions were incubated for 2 h at room temperature before further analysis.

After iTRAQ-labeling the peptide samples were combined and subsequently purified using a strong cation exchange (SCX)-cartridge: Polysulfoethyl 4.6 × 100 mm column (5 μm, 200 Å, Poly LC Inc., Columbia, MD, USA). For LC-MS/MS analysis of the resulting peptides, we followed a previously described method (20). Protein identification and quantification for iTRAQ analysis data was carried out using the MASCOT search engine (version 2.2.1; Matrix Science, London, UK) embedded into Proteome Discoverer 1.3 (Thermo Electron, San Jose, CA, USA), searching against the Uniport database of human protein sequences (03-2013, 133549 entries, downloaded from: http://www.uniprot.org/) and the concatenated target-decoy database. The parameters were set as follows: Trypsin as digestion enzyme, cysteine carbamidomethylation as a fixed modification, Oxidation (M), Gln→Pyro-Glu (N-term Q), iTRAQ 8 plex (K), iTRAQ 8 plex (Y), and iTRAQ 8 plex (N-term) as the variable modification.

Western blotting analysis

Human umbilical arteries were lysed in 1 × RIPA buffer with 1μg/mL leupeptin and 1μg/mL phenylmethylsulfonyl fluoride. Aliquots containing 30 μg of protein samples were separated by 12% SDS-PAGE and transferred electrophoretically to a nitrocellulose transfer membrane (Bio-Rad, Hercules, CA, USA). After blocked with 5% BSA in TBS containing 0.01% Tween 20 (TBST) for 1 h at room temperature, the membrane was incubated overnight at 4°C with primary antibodies against FGA (1:1,000, Abcam, Cambridge, MA, USA), ACTA2 (1:1,000, Abcam, Cambridge, MA, USA), IDH3A (1:1,000, Abcam, Cambridge, MA, USA), GAPDH (1:1,000, Abcam, Cambridge,

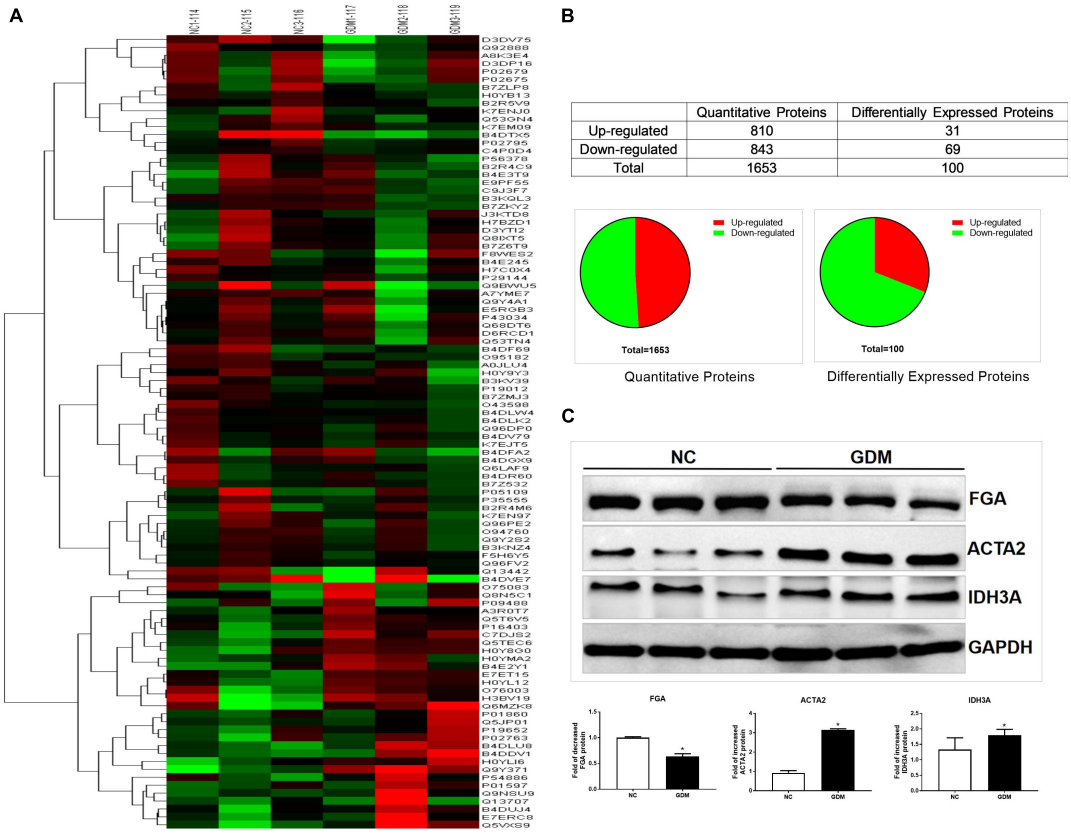

	Quantitative Proteins	Differentially Expressed Proteins
Up-regulated	810	31
Down-regulated	843	69
Total	1653	100

FIGURE 1
iTRAQ analysis results for the GDM umbilical vessels. **(A)** Hierarchical clustering of DEPs. **(B)** The statistic of the proteins identified in umbilical vessels. **(C)** Validation of the differential expression of the selected proteins in umbilical vessels by western blotting: FGA, ACTA2, IDH3A. Data are presented as mean ± SE (n = 3). *p < 0.01.

MA, USA). Subsequently, membranes were washed 10 min for three times with TBST, then each membrane was incubated for 1 h at room temperature with the appropriate secondary antibody (anti-rabbit IgG, anti-mouse IgG; 1:5,000; Abcam). The protein intensities were determined and analyzed using Odyssey® Imager (LI-COR Biosciences, Lincoln, NE, USA).

Bioinformatics analysis of differentially expressed proteins

Proteins exhibiting at least a ± 20% fold change in expression were determined as significantly different. The Cluster 3.0[1] and Java Tree view software[2] were further used to evaluate the capability of the resulting feature proteins in differentiating the two groups of samples. IPA software (QIAGEN, Redwood 185 City, CA) was employed for functional analysis of the identified DEPs between the two groups. In the functional network analysis, the DEPs were represented as nodes, and the biological relationship between two proteins was represented as an edge (line), which was supported by the published articles or the canonical information embedded in the IPA database. Downstream biological processes analysis, which was used to predict the downstream effects of the DEPs based on the observed gene expression changes, was also on the strength of the canonical information embedded in the IPA database. The calculated z-score can be used to infer the activation states ("increased" or "decreased") of implicated biological processes. Fisher's exact test was used to calculate a p-value to determine the probability that the association between proteins in the dataset, and the biological process could be explained by chance alone.

Statistical analysis

All analysis was performed with the software Statistical Analysis Software (SPSS 17.0 software, SPSS Inc., USA). Data are displayed as means ± SEM. Statistical evaluation was conducted

1 http://bonsai.hgc.jp/~mdehoon/software/cluster/software.htm
2 http://jtreeview.sourceforge.net

A

ID	Score	Focus Molecules	Top Diseases and Functions
1	44	20	[Developmental Disorder, Hematological Disease, Hereditary Disorder]
2	44	20	[Cellular Assembly and Organization, Cellular Function and Maintenance, Tissue Development]
3	35	17	[Connective Tissue Disorders, Dermatological Diseases and Conditions, Developmental Disorder]
4	25	13	[Cardiac Arrythmia, Cardiovascular Disease, Cell-To-Cell Signaling and Interaction]
5	16	9	[Cell Death and Survival, Cellular Function and Maintenance, Embryonic Development]

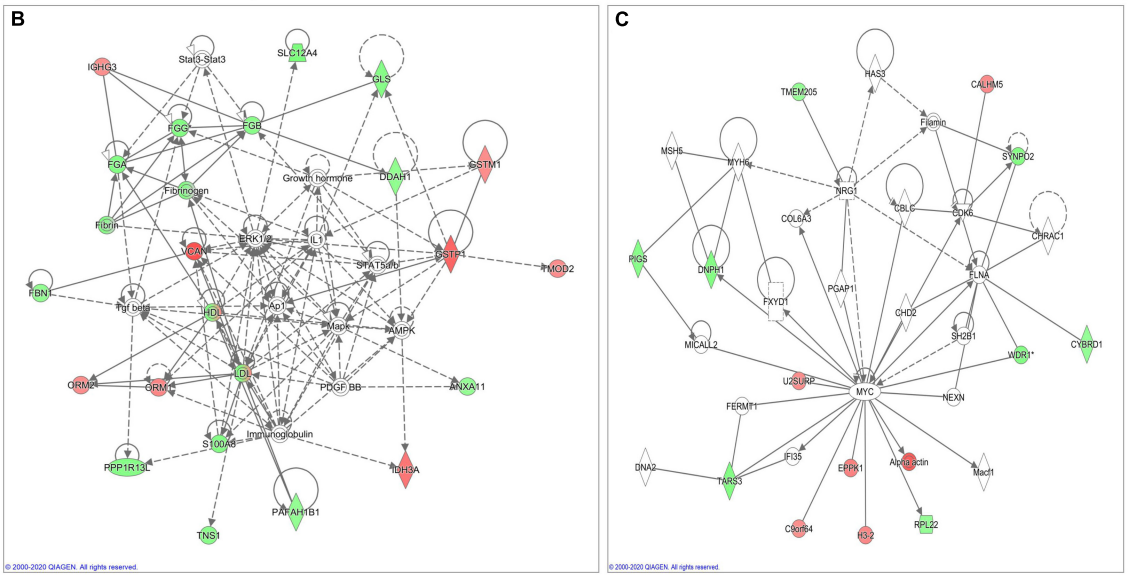

FIGURE 2
Visual representation of the principal network generated by ingenuity pathway analysis (IPA). **(A)** Principal network generated by IPA. **(B)** Developmental Disorder associated network. **(C)** Cardiovascular Disease associated network.

using an unpaired Student's *t*-test, and $P < 0.05$ was considered statistically significant.

Results

The clinical characteristics of the participants

Twenty five pregnancies with GDM and 25 normal controls were enrolled in the present study, and the specific clinical characteristics of the participants and delivery data were shown in **Table 1**. None of them experienced major cardiovascular risk factors, such as cardiovascular system diseases, history of type 2 diabetes, hyperthyroidism, assisted reproductive technology treatment, smoking, congenital defect, and any other pregnancy complications. There was no significant difference between GDM group and the controls about the maternal age, gestational weeks, pre-pregnancy BMI, weight gain during pregnancy, lipid level in first-trimester, birth weight and gender distribution of newborns (all $P > 0.05$). The serum glucose concentration at 0,1, and 2 h of OGTT in the GDM group were significantly higher than that in the normal pregnancies ($p < 0.001$, respectively). Three pairs of the collected umbilical vessels were selected to compare the proteome profiles between GDM and controls by iTRAQ-LC-MS/MS.

Overview of the proteomics analysis

To identify the differentially expressed proteins (DEPs) in the umbilical arteries between GDM and controls in genome-wide level, iTRAQ-LC-MS/MS was performed in 3 GDM samples and 3 control samples. In the present study, a total of 1,653 proteins were quantified in the umbilical arteries from both GDM and the controls (**Supplementary Table 1**). The mass spectrometry proteomics data have been deposited to the ProteomeXchange Consortium (http://proteomecentral.proteomexchange.org) via the iProX partner repository (23) with the dataset identifier PXD024892. Using the screening criteria of fold change over ± 1.2, 100 proteins were regarded as differentially expressed in umbilical arteries from GDM group, of which, 31 proteins were up-regulated and 69 proteins were down-regulated (**Supplementary Table 2** and **Figure 1B**). Hierarchical clustering analysis was further performed with the identified 100 DEPs mentioned above. After unsupervised

Diseases Annotation	p-value	Molecules	Focus Molecules
Anemia	1.99E-02	CBFB,GSTM1,HBB,PGM3,SLC12A4,TPP2	6
Thrombus	1.53E-02	FBN1,FGA,FGB,FGG	4
Myocardial infarction	2.06E-02	ACTA2,FGB,FGG,GSTM1	4
Stasis ulcer	4.23E-06	FGA,FGB,FGG	3
Loeys-Dietz syndrome	1.95E-05	ACTA2,FBN1,VCAN	3
Advanced stage peripheral arterial disease	1.79E-02	ADAR,GLS,HBB	3
Abnormal morphology of artery	1.94E-02	ACTA2,DDAH1,FBN1	3
Intermediate disease stage peripheral arterial disease	2.06E-02	ADAR,GLS,HBB	3
Familial thoracic aortic aneurysm type 2	1.64E-04	ACTA2,FBN1	2
Thoracic aortic aneurysm	1.13E-03	ACTA2,FBN1	2

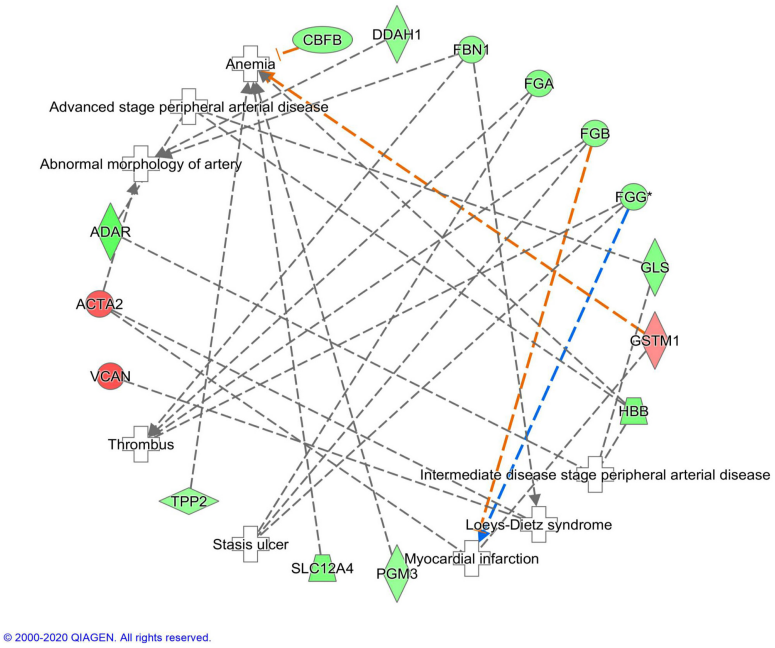

FIGURE 3
Cardiovascular Disease analysis of differentially expressed proteins between normal and GDM umbilical vessels. For this developmental disease network, genes or gene products are represented as *nodes*, and the biological relationship between two nodes is represented as an *edge*. All edges are supported by at least one publication as stored in the Ingenuity Knowledge database. The intensity of the node color indicates the degree of up- (red) or down- (green) regulation.

clustering, the GDM group were significantly distinguished from the controls (**Figure 1A**), indicating the significant effect of intrauterine hyperglycemia on the expression of proteins in umbilical vessels of newborn.

Western blotting validation

To validate the results carried out by iTRAQ-LC-MS/MS, Western blotting was conducted in additional three umbilical vessels from GDM and three normal umbilical vessels. Based on the significant expression difference and the biological function in the cardiovascular system, three proteins, including FGA, ACTA2, and IDH3A, were selected for further investigation. As shown in **Figure 1C**, the change trends of these three proteins within Western blotting analysis were in accordance with iTRAQ analysis results.

Bioinformatics analysis of differentially expressed proteins

To assist functional interpretation of the DEPs, the bioinformatics analysis was performed based on the 100 DEPs. These genes were loaded into IPA database (IPA®, QIAGEN)[3] for pathway, disease and function, and network analysis. Three cardiovascular signaling pathways identified by IPA software (**Supplementary Table 3** and **Supplementary Figure 1**) including "Atherosclerosis Signaling" (related gene: ORM1, ORM2, and S100A8). According to overlapping *p*-values, these 73 subcategories showed in "Disease and Disorder" analysis, including "Developmental Disorder" and "CVD" (**Supplementary Table 4** and **Supplementary Figure 2**). In addition to the gene ontology enrichment, 22 subcategories

3 www.qiagen.com/ingenuity

Functions Annotation	p-value	Molecules	Focus Molecules
Vasoconstriction of blood vessel	4.90E-06	ACTA2,DDAH1,FBN1,FGA,FGB,FGG	6
Abnormal morphology of artery	1.94E-02	ACTA2,DDAH1,FBN1	3
Density of microvessel	6.45E-03	GSTM1,IDH3A	2
Cardiac output	1.36E-02	DDAH1,PPP1R13L	2
Abnormal morphology of aorta	2.00E-02	ACTA2,FBN1	2
Diameter of aortic root	3.34E-03	FBN1	1
Induction of endothelial tube	6.67E-03	ORM1	1
Contraction of vascular tissue	6.67E-03	ACTA2	1
Beat of cardiomyocytes	1.66E-02	NSF	1

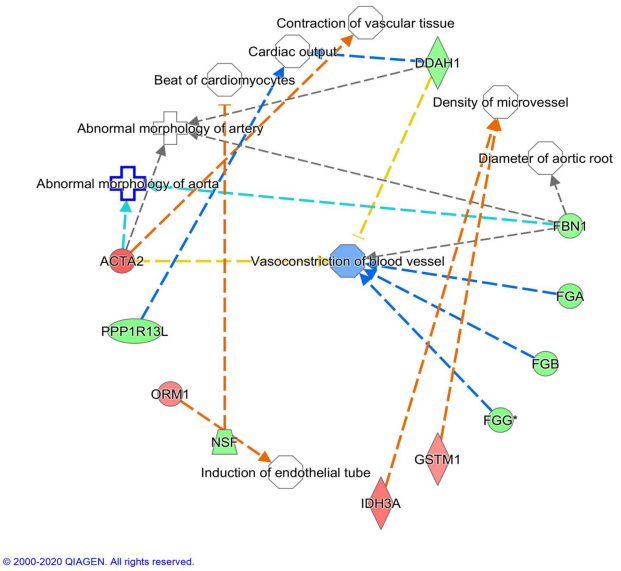

FIGURE 4
Cardiovascular Functional analysis of differentially expressed proteins between normal and GDM umbilical vessels. For this cardiovascular function network, genes or gene products are represented as *nodes*, and the biological relationship between two nodes is represented as an *edge*. All edges are supported by at least one publication as stored in the Ingenuity Knowledge database. The intensity of the node color indicates the degree of up- (red) or down- (green) regulation.

involed in "Physiological System Development and Function," especially in "Cardiovascular System Development and Function" (**Supplementary Table 5** and **Supplementary Figure 3**). Network analysis identified five biological networks (**Figure 2A**), which included developmental network (**Figure 2B**) and cardiovascular network (**Figure 2C**). The most related network emerged comprising 20 of those DEPs. It is associated with the IPA functions "Developmental Disorder" (**Figure 2B**).

Cardiovascular risk proteins analysis

To better understand cardiovascular risk proteins in offspring exposed to GDM, these DEPs were further analyzed in CVDs and functions. Based on "Diseases and Disorders" analysis, 17 proteins (ACTA2, ADAR, CBFB, DDAH1, FBN1, FGA, FGB, FGG, GLS, GSTM1, HBB, PGM3, PPP1R13L, S100A8, SLC12A4, TPP2, VCAN) were described to be associated with CVD, especially in Anemia, Thrombus and Myocardial infarction (**Figure 3**). Based on "Physiological System Development and Functions" analysis, 11 proteins (ACTA2, DDAH1, FBN1, FGA, FGB, FGG, GSTM1, IDH3A, NSF, ORM1, PPP1R13L) were described to be associated with Cardiovascular System Development and Function, especially in the function of "vasoconstriction of blood vessel" (**Figure 4**).

The term "upstream regulator" as used in IPA refers to any molecule that can affect the expression of another molecule. In upstream regulator analysis, STAT3 was predicted in inhibited state (z-score = −2.196) and regulated ACTA2, FBN1, FGA, FGB, and FGG (**Figure 5**).

Discussion

Cardiovascular and metabolic disorders often present in adult life, but may have their origins in changes to the intrauterine environment during fetal development. Previous studies including epidemiological investigations and experimental projects have demonstrated the alteration of

Upstream Regulator	Molecule Type	Predicted Activation State	Activation z-score	p-value of overlap	Target Molecules in Dataset
STAT3	transcription regulator	Inhibited	-2.196	2.02E-04	ACTA2,FGA,FGB, FGG,HBB,IFIT5, STC2,TNS1,VCAN

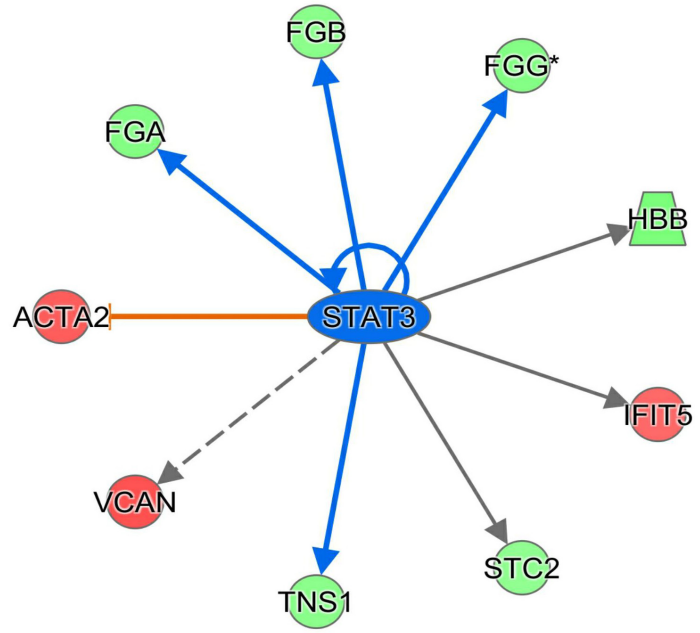

FIGURE 5
Upstream analysis of DEPs. Colorized nodes represented our input proteins. Green, down-regulated proteins. Red, up-regulated proteins.

vascular function and cardiovascular system in the offspring of GDM (8, 24). The current study firstly focus on the proteomics of umbilical vessels from GDM and normal controls, of normal birth weights, which excluded maternal obesity factors (high pre-pregnancy BMI, excessive weight gain during pregnancy, abnormal lipid level in first-trimester). Our results demonstrated that the intrauterine hyperglycemia indeed individually affected the expression patterns of proteins and vessel function.

Several studies implicated that the association between maternal hyperglycemia and childhood metabolic outcomes was attenuated after adjusting for covariates including maternal BMI and weight gain during pregnancy (11), overall, existing evidence suggested gestational diabetes as an independent element. To date, intensified treatment during pregnancy of maternal hyperglycemia reduce maternal weight gain and macrosomia at birth, whether similar associations still exist between maternal hyperglycemia and offspring cardiovascular outcomes is few studied. In the current study, participants with no maternal obesity factors (high pre-pregnancy BMI, excessive weight gain during pregnancy, abnormal lipid level in first-trimester) were recruited, and macrosomia was excluded.

The physiological and pathological regulation of cardiovascular function derives mainly from the collaboration between vascular endothelial cells and VSMCs (Vascular smooth muscle cells). Previous studies stated that characteristics and alterations of umbilical vessels could offer valuable information since umbilical vessel cells experienced the effect of same intrauterine environment (20, 25–27). In consideration of the ethics limited, umbilical vessels is thought to be the best tissue that could be collected in clinical.

Based on the identified DEPs in umbilical arteries between GDM and normal controls, our results suggested that the "Cardiovascular System Development and Function" was impaired exposure to intrauterine hyperglycemia. In this content, the top related function was "Vasoconstriction of blood

vessel," this is consistent with a large number of epidemiological results. These suppressed physiological processes in the umbilical vessels from GDM might lead to impaired vascular repair under stress or diabetic vessel pathological damage.

In this study, we found 20 DEPs (ACTA2, ADAR, CBFB, DDAH1, FBN1, FGA, FGB, FGG, GLS, GSTM1, HBB, PGM3, PPP1R13L, S100A8, SLC12A4, TPP2, VCAN, IDH3A, NSF, ORM1) related with Cardiovascular system. ACTA2 gene mutations in adults associated with thoracic aortic aneurysm and dissection (TAAD) (28). Transgenetic mouse model study proposes that sufficient ADAR2 enzyme activity might play a vital role in preventing cardiovascular defects (29). CBFB may impair the primitive hematopoiesis (30). FBN1 is a gene with a well characterized role in the pathogenesis of thoracic aortic aneurysm (TAA) in the context of Marfan syndrome (31). Inferring that variation in genomic sequences that regulate the fibrinogen genes (FGA, FGB, and FGG) may affect hepatic fibrinogen production and perhaps CVD risk (32). MicroRNA-200c exacerbates the ischemia/reperfusion injury of heart through targeting the glutaminase (GLS)-mediated glutamine metabolism (33). Combined GSTM1*0/GSTA1*A genotypes might be considered as genetic markers for cardiovascular death risk in ESRD patients, which may permit targeting of preventive and early intervention (34). HBB identified to be related to Abdominal aortic aneurysm (AAA) (35). PPP1R13L affecting NFkB activity may be candidate genes in the study of human CVD (36). Levels of S100A8/A9, a proinflammatory and prothrombotic protein complex, are increased in several diseases, and high levels predispose to CVD (37). Total absence of the VCAN gene halts heart development at a stage prior to the heart's pulmonary/aortic outlet segment growth (38).

In summary, in the present study, we discovered that the expression profile of proteins in umbilical vessels of newborns from GDM group was different from that in normal controls. The bio-informatics analysis suggested that some DEPs might play important roles in cardiovascular dysfunction of GDM children. Our findings would contribute to the exploration of the potential mechanism underlying the dysregulated balance of apoptosis and autophagy in vessels, angiogenesis and endothelial cell dysfunction in the offspring of GDM pregnancies. However, deeper analyses will still mostly need to be performed to explore the key factors and potential preventive and therapeutic strategies of cardiovascular dysfunction in GDM offspring.

Data availability statement

The datasets presented in this study can be found in online repositories. The names of the repository/repositories and accession number(s) can be found in the article/**Supplementary material**.

Ethics statement

The studies involving human participants were reviewed and approved by the Ethics Committee of Shaoxing Maternity and Child Health Care Hospital. The patients/participants provided their written informed consent to participate in this study.

Author contributions

H-TP and Y-MX: writing—original draft. H-DZ: methodology. X-LS: formal analysis. BY: visualization. H-GD: validation. R-JX and J-LD: data curation. JZ and TZ: project administration. All authors contributed to the article and approved the submitted version.

Funding

This work was supported by the National Natural Science Foundation of China (82071729), the China Postdoctoral Science Foundation (2020M681336), the Science Technology Department of Zhejiang Province, China (LGD20H040001, LGF21H040003, and LGF21H040004), the Health Commission of Zhejiang Province, China (2022RC277, 2022KY412, 2022KY413, and 2021KY375), and the Science Technology Department of Shaoxing, China (2020A13034 and 2020A13035).

Conflict of interest

The authors declare that the research was conducted in the absence of any commercial or financial relationships that could be construed as a potential conflict of interest.

The handling editor JQ declared a shared parent affiliation with the authors Y-MX and H-TP at the time of review.

Publisher's note

Supplementary material

The Supplementary Material for this article can be found online at: https://www.frontiersin.org/articles/10.3389/fcvm.2022.1021112/full#supplementary-material

SUPPLEMENTARY FIGURE 1
Cardiovascular related pathways.

SUPPLEMENTARY FIGURE 2
Disease and disorder analysis.

SUPPLEMENTARY FIGURE 3
Functional analysis.

SUPPLEMENTARY TABLE 1
A total of 1,653 proteins quantified in the umbilical arteries from both GDM and the controls.

SUPPLEMENTARY TABLE 2
A total of 100 differentially expressed proteins (DEPs) in umbilical vessels.

SUPPLEMENTARY TABLE 3
Ingenuity canonical pathways analysis.

SUPPLEMENTARY TABLE 4
Disease and disorder analysis.

SUPPLEMENTARY TABLE 5
Functional analysis.

References

1. HAPO Study Cooperative Research Group, Metzger BE, Lowe LP, Dyer AR, Trimble ER, Chaovarindr U, et al. Hyperglycemia and adverse pregnancy outcomes. *N Engl J Med.* (2008). 358:1991–2002. doi: 10.1056/NEJMoa0707943

2. Lawlor DA, Lichtenstein P, Langstrom N. Association of maternal diabetes mellitus in pregnancy with offspring adiposity into early adulthood: sibling study in a prospective cohort of 280,866 men from 248,293 families. *Circulation.* (2011) 123:258–65. doi: 10.1161/CIRCULATIONAHA.110.980169

3. Boney CM, Verma A, Tucker R, Vohr BR. Metabolic syndrome in childhood: association with birth weight, maternal obesity, and gestational diabetes mellitus. *Pediatrics.* (2005) 115:e290–6. doi: 10.1542/peds.2004-1808

4. Krishnaveni GV, Veena SR, Jones A, Srinivasan K, Osmond C, Karat SC, et al. Exposure to maternal gestational diabetes is associated with higher cardiovascular responses to stress in adolescent Indians. *J Clin Endocrinol Metab.* (2015) 100:986–93. doi: 10.1210/jc.2014-3239

5. Wu CS, Nohr EA, Bech BH, Vestergaard M, Olsen J. Long-term health outcomes in children born to mothers with diabetes: a population-based cohort study. *PLoS One.* (2012) 7:e36727. doi: 10.1371/journal.pone.0036727

6. Zitser B. Maternal diabetes and autism in offspring. *JAMA.* (2015) 314:407. doi: 10.1001/jama.2015.7250

7. Sacks DA, Hadden DR, Maresh M, Deerochanawong C, Dyer AR, Metzger BE, et al. Frequency of gestational diabetes mellitus at collaborating centers based on IADPSG consensus panel-recommended criteria the hyperglycemia and adverse pregnancy outcome (HAPO) study. *Diabetes Care.* (2012) 35:526–8. doi: 10.2337/dc11-1641

8. Aceti A, Santhakumaran S, Logan KM, Philipps LH, Prior E, Gale C, et al. The diabetic pregnancy and offspring blood pressure in childhood: a systematic review and meta-analysis. *Diabetologia.* (2012) 55:3114–27. doi: 10.1007/s00125-012-2689-8

9. Tam WH, Ma RCW, Yang X, Ko GTC, Tong PCY, Cockram CS, et al. Glucose intolerance and cardiometabolic risk in children exposed to maternal gestational diabetes mellitus in utero. *Pediatrics.* (2008) 122:1229–34. doi: 10.1542/peds.2008-0158

10. Catalano PM, Farrell K, Thomas A, Huston-Presley L, Mencin P, de Mouzon SH, et al. Perinatal risk factors for childhood obesity and metabolic dysregulation. *Am J Clin Nutr.* (2009) 90:1303–13. doi: 10.3945/ajcn.2008.27416

11. Tam WH, Ma RCW, Ozaki R, Li AM, Chan MHM, Yuen LY, et al. In utero exposure to maternal hyperglycemia increases childhood cardiometabolic risk in offspring. *Diabetes Care.* (2017) 40:679–86. doi: 10.2337/dc16-2397

12. Anderwald C, Pfeiler G, Nowotny P, Anderwald-Stadler M, Krebs M, Bischof MG, et al. Glucose turnover and intima media thickness of internal carotid artery in type 2 diabetes offspring. *Eur J Clin Invest.* (2008) 38:227–37. doi: 10.1111/j.1365-2362.2008.01932.x

13. Aman J, Hansson U, Ostlund I, Wall K, Persson B. Increased fat mass and cardiac septal hypertrophy in newborn infants of mothers with well-controlled diabetes during pregnancy. *Neonatology.* (2011) 100:147–54. doi: 10.1159/000323741

14. Westermeier F, Salomón C, González M, Puebla C, Guzmán-Gutiérrez E, Cifuentes F, et al. Insulin restores gestational diabetes mellitus-reduced adenosine transport involving differential expression of insulin receptor isoforms in human umbilical vein endothelium. *Diabetes.* (2011) 60:1677–87. doi: 10.2337/db11-0155

15. Floris I, Descamps B, Vardeu A, Mitiæ T, Posadino AM, Shantikumar S, et al. Gestational diabetes mellitus impairs fetal endothelial cell functions through a mechanism involving MicroRNA-101 and histone methyltransferase enhancer of zester homolog-2. *Arterioscler Thromb Vasc Biol.* (2015) 35:664–74. doi: 10.1161/Atvbaha.114.304730

16. Koukkou E, Ghosh P, Lowy C, Poston L. Offspring of normal and diabetic rats fed saturated fat in pregnancy demonstrate vascular dysfunction. *Circulation.* (1998) 98:2899–904. doi: 10.1161/01.cir.98.25.2899

17. Nehiri T, Van Huyen J-PD, Viltard M, Fassot C, Heudes D, Freund N, et al. Exposure to maternal diabetes induces salt-sensitive hypertension and impairs renal function in adult rat offspring. *Diabetes.* (2008) 57:2167–75. doi: 10.2337/db07-0780

18. Ding GL, Wang F-F, Shu J, Tian S, Jiang Y, Zhang D, et al. Transgenerational glucose intolerance with Igf2/H19 epigenetic alterations in mouse islet induced by intrauterine hyperglycemia. *Diabetes.* (2012) 61:1133–42. doi: 10.2337/db11-1314

19. Cheng X, Chapple SJ, Patel B, Puszyk W, Sugden D, Yin X, et al. Gestational diabetes mellitus impairs Nrf2-mediated adaptive antioxidant defenses and redox signaling in fetal endothelial cells in utero. *Diabetes.* (2013) 62:4088–97. doi: 10.2337/db13-0169

20. Pan HT, Guo M-X, Xiong Y-M, Ren J, Zhang J-Y, Gao Q, et al. Differential proteomic analysis of umbilical artery tissue from preeclampsia patients, using iTRAQ isobaric tags and 2D nano LC-MS/MS. *J Proteomics.* (2015) 112:262–73. doi: 10.1016/j.jprot.2014.09.006

21. Wisniewski JR, Zougman A, Nagaraj N, Mann M. Universal sample preparation method for proteome analysis. *Nat Methods.* (2009) 6:359–62. doi: 10.1038/nmeth.1322

22. Sheng Q, Dai J, Wu Y, Tang H, Zeng R. BuildSummary: using a group-based approach to improve the sensitivity of peptide/protein identification in shotgun proteomics. *J Proteome Res.* (2012) 11:1494–502. doi: 10.1021/pr200194p

23. Ma J, Chen T, Wu S, Yang C, Bai M, Shu K, et al. iProX: an integrated proteome resource. *Nucleic Acids Res.* (2019) 47:D1211–7. doi: 10.1093/nar/gky869

24. West NA, Crume TL, Maligie MA, Dabelea D. Cardiovascular risk factors in children exposed to maternal diabetes in utero. *Diabetologia.* (2011) 54:504–7. doi: 10.1007/s00125-010-2008-1

25. Gao Q, Pan H-T, Lin X-H, Zhang J-Y, Jiang Y, Tian S, et al. Altered protein expression profiles in umbilical veins: insights into vascular dysfunctions of the children born after in vitro fertilization. *Biol Reprod.* (2014) 91:71. doi: 10.1095/biolreprod.114.120659

26. Xu GF, Zhang J-Y, Pan H-T, Tian S, Liu M-E, Yu T-T, et al. Cardiovascular dysfunction in offspring of ovarian-hyperstimulated women and effects of estradiol and progesterone: a retrospective cohort study and proteomics analysis. *J Clin Endocrinol Metab.* (2014) 99:E2494–503. doi: 10.1210/jc.2014-2349

27. Lurbe E, Torro MI. Early vascular phenotypes in the genesis of hypertension. *Pediatr Nephrol.* (2010) 25:763–7. doi: 10.1007/s00467-009-1357-9

28. Meuwissen ME, Lequin MH, Bindels-de Heus K, Bruggenwirth HT, Knapen MFCM, Dalinghaus M, et al. ACTA2 mutation with childhood cardiovascular, autonomic and brain anomalies and severe outcome. *Am J Med Genet A.* (2013) 161:1376–80. doi: 10.1002/ajmg.a.35858

29. Altaf F, Vesely C, Sheikh AM, Munir R, Shah STA, Tariq A, et al. Modulation of ADAR mRNA expression in patients with congenital heart defects. *PLoS One.* (2019) 14:e0200968. doi: 10.1371/journal.pone.0200968

30. Castilla LH, Wijmenga C, Wang Q, Stacy T, Speck NA, Eckhaus M, et al. Failure of embryonic hematopoiesis and lethal hemorrhages in mouse embryos heterozygous for a knocked-in leukemia gene CBFB-MYH11. *Cell.* (1996) 87:687–96. doi: 10.1016/s0092-8674(00)81388-4

31. Newell K, Smith W, Ghoshhajra B, Isselbacher E, Lin A, Lindsay ME, et al. Cervical artery dissection expands the cardiovascular phenotype in FBN1-related Weill-Marchesani syndrome. *Am J Med Genet A.* (2017) 173:2551–6. doi: 10.1002/ajmg.a.38353

32. Fish RJ, Neerman-Arbez M. A novel regulatory element between the human FGA and FGG genes. *Thromb Haemost.* (2012) 108:427–34. doi: 10.1160/TH12-04-0274

33. Liu F, Li Y, Liu G. MicroRNA-200c exacerbates the ischemia/reperfusion injury of heart through targeting the glutaminase (GLS)-mediated glutamine metabolism. *Eur Rev Med Pharmacol Sci.* (2017) 21:3282–9.

34. Suvakov S, Damjanovic T, Pekmezovic T, Jakovljevic J, Savic-Radojevic A, Pljesa-Ercegovac M, et al. Associations of GSTM1*0 and GSTA1*A genotypes with the risk of cardiovascular death among hemodialyses patients. *BMC Nephrol.* (2014) 15:12. doi: 10.1186/1471-2369-15-12

35. Wan L, Huang J, Ni H, Yu G. Screening key genes for abdominal aortic aneurysm based on gene expression omnibus dataset. *BMC Cardiovasc Disord.* (2018) 18:34. doi: 10.1186/s12872-018-0766-8

36. Simpson MA, Cook RW, Solanki P, Patton MA, Dennis JA, Crosby AH, et al. A mutation in NFkappaB interacting protein 1 causes cardiomyopathy and woolly haircoat syndrome of Poll Hereford cattle. *Anim Genet.* (2009) 40:42–6. doi: 10.1111/j.1365-2052.2008.01796.x

37. Lood C, Tydén H, Gullstrand B, Jönsen A, Källberg E, Mörgelin M, et al. Platelet-Derived S100A8/A9 and cardiovascular disease in systemic lupus erythematosus. *Arthritis Rheumatol.* (2016) 68:1970–80. doi: 10.1002/art.39656

38. Burns TA, Dours-Zimmermann MT, Zimmermann DR, Krug EL, Comte-Walters S, Reyes L, et al. Imbalanced expression of Vcan mRNA splice form proteins alters heart morphology and cellular protein profiles. *PLoS One.* (2014) 9:e89133. doi: 10.1371/journal.pone.0089133

frontiers | Frontiers in Cardiovascular Medicine

TYPE Original Research
PUBLISHED 26 October 2022
DOI 10.3389/fcvm.2022.1023982

OPEN ACCESS

EDITED BY
Jia Qi,
Shanghai Jiao Tong University, China

REVIEWED BY
Yongjun Sun,
Hebei University of Science and Technology, China
LouJin Song,
Pfizer, United States

*CORRESPONDENCE
Jian Wu
jianwu12@fudan.edu.cn
Wei Guo
guowei@fudan.edu.cn

†These authors have contributed equally to this work

SPECIALTY SECTION
This article was submitted to General Cardiovascular Medicine, a section of the journal Frontiers in Cardiovascular Medicine

RECEIVED 20 August 2022
ACCEPTED 30 September 2022
PUBLISHED 26 October 2022

CITATION
Wang X, Yu S, Jian Y, Pan H, Guo J, Wu J and Guo W (2022) Hydrogen sulfide against preeclampsia exposure-induced oxidative mitochondrial damage in HTR-8/SVneo cells. *Front. Cardiovasc. Med.* 9:1023982. doi: 10.3389/fcvm.2022.1023982

Hydrogen sulfide against preeclampsia exposure-induced oxidative mitochondrial damage in HTR-8/SVneo cells

Xianli Wang[1†], Shaokun Yu[2†], Yuting Jian[2], Hongmin Pan[3,2], Jiannan Guo[2], Jian Wu[4*] and Wei Guo[2*]

[1]Department of Pharmacy, Obstetrics and Gynecology Hospital of Fudan University, Shanghai, China, [2]Department of Pharmacology, School of Pharmacy, Fudan University, Shanghai, China, [3]Department of Gastrointestinal Surgery, Harbin Medical University Cancer Hospital, Harbin, China, [4]Department of Pharmacy, Huashan Hospital, Fudan University, Shanghai, China

Extravillous trophoblast invasion disorder caused by oxidative stress is involved in the pathogenesis of preeclampsia (PE). In order to identify whether hydrogen sulfide (H_2S) can prevent oxidative stress injury in extravillous trophoblasts. HTR-8/SVneo cells were detected by H_2S inhibiting H_2O_2 induced oxidative mitochondrial damage. Reactive oxygen species (ROS) were detected, as well as malondialdehyde (MDA), catalase (CAT), and superoxide dismutase (SOD). JC-1 detected the potential of the mitochondrial membrane in this experiment. Then to detect the expression level of the apoptosis-inducing protein B-cell lymphoma-2 (Bcl-2) associated X protein (Bax), caspase 3, p53, p-p53, the apoptosis-inhibiting protein Bcl-2, PRAP, and the mitochondria fission protein Drp1, p-Drp1. CCK-8 assay, it was demonstrated that cell proliferation in the NaHS group was significantly higher than that in the Mod group, indicating that H_2S may induce cell proliferation. Transwell assay elucidated that cell invasion in the NaHS group was recovered compared to the Mod group. ROS concentration no matter in cells or mitochondria was decreased by NaHS, which we could get from the comparison between the Mod group, PAG group, and NaHS group. The concentration of MDA was significantly lower in the NaHS group, and the concentration of SOD was extremely high in the NaHS group. Utilized JC-1 to detect mitochondrial membrane potential and found that cells from the NaHS group had a stable potential while cells from the Mod group and PAG group partly lost their potential, which could demonstrate that NaHS could maintain mitochondrial membrane potential. The western blot results revealed that p-Drp1 had a significant decline in the NaHS group, which means mitochondria fission was decreased in the NaHS group. The expression level of Bax and caspase 3 was significantly lower than in the Mod group and PAG group, and the expression level of Bcl-and PRAP was significantly higher in the NaHS group. That could prove that NaHS protect

HTR-8/SVneo cell by inhibiting cell apoptosis. These promising results show that H_2S elicits its effects on cell apoptosis by decreasing ROS concentration, maintaining mitochondrial membrane stability, and promoting apoptosis-inhibiting protein expression in cells.

KEYWORDS

hydrogen sulfide, extravillous trophoblast, preeclampsia, apoptosis, oxidative stress

Introduction

There is no known pathophysiology for preeclampsia (PE), which is a pregnancy-related multisystem disorder. In developing countries, it accounts for 15% of all maternal deaths, neonatal and fetal deaths, and preterm births (1, 2). The condition is characterized by uncontrolled hypertension during pregnancy accompanied by proteinuria, with neurological symptoms such as seizures at the end of pregnancy (3, 4). Despite the fact that the pathophysiology of PE remains unclear, previous studies have indicated that it is closely associated with oxidative stress in trophoblast cells. This led to altered physiologic transformation of spiral arteries, leading to placental hypoperfusion and hypoxia, and ultimately placental insufficiency. During normal placental implantation, extravillous trophoblast migrates into the spiral arteries of the maternal uterus during placental implantation, forming vascular sinuses at the fetal-maternal interface to supply nutrients to the fetus (5). While during PE, trophoblast failed to remodel the spiral artery, leading to placental ischemia and other syndromes of PE.

Oxidative stress may occur as a result of hypoxia and reoxygenation of the placenta caused by a poor spiral artery invasion (6, 7). One of the key features of PE is oxidative stress in the trophoblast, which is partially caused by mitochondrial dysfunction (8). Mitochondrial outer membrane permeabilization (MOMP) is associated with mitochondrial function. When MOMP is destroyed, reactive oxygen species (ROS) increase and cell apoptosis are induced by mitochondrial pathways (9). Pores formed by Bax, a protein from the Bcl-2 family, contribute to the loss of MOMP and then release factors such as cytochrome c to activate caspase, which finally leads to cell apoptosis. Thus, mitochondria could be a trigger for curing PE.

H_2S has been proved by many scientists that it may participate in a lot of pathophysiologic processes, which are quite important in the human body, such as apoptosis, oxidative stress, inflammation, and angiogenesis (10). As a physiologic vascular regulator, H_2S inhibits proliferation and regulates apoptosis and autophagy of vascular cells, thus affecting vascular diseases in various ways (11). In the meantime, it is well known that H_2S regulates long-term potentiation and calcium levels in neuronal cells, so disturbances of H_2S levels in cells have been implicated in neurodegenerative diseases such as Alzheimer's, Parkinson's, strokes, and traumatic brain injuries, which attract a lot of attention (12). H_2S has also been proven to promote cancer cell death, inhibit cancer angiogenesis, and metastasis (13). The mitochondrial enzyme superoxide dismutase (SOD) and ROS are regulated by H_2S, which protects cardiomyocytes and inhibits apoptosis (14, 15). That is to say, H_2S exerts its protective effect on cells through the mitochondria pathway. The L-cysteine/H_2S pathway has been linked to the development of PE in previous studies (16), and H_2S donors may have prevented PE (17–19). As we mentioned above, we postulate that H_2S might be able to protect the placenta in PE. In line with our hypothesis, a study has demonstrated that AP39, a novel mitochondria-targeted hydrogen sulfide donor, could restore mitochondrial health through increasing active mitochondrial content, and decreasing superoxide production (20). We suppose to identify the protection of H_2S on the trophoblast of PE and the mechanism behind that.

Materials and methods

Chemicals

NaHS was used as an H_2S donor When NaHS reacts with water, it provides a solution of H_2S with a concentration of approximately 33% of its original concentration (21). NaHS was purchased from Aladdin (China). Our previous experimental results showed that NaHS within 400 μM promoted the proliferation of HTR-8/Svneo cells. Referring to other kinds of literature and our result (22, 23), we chose the concentration of 200 μM for our experiments. PAG (DL-Propargylglycine), an endogenous hydrogen sulfide generating enzyme inhibitor was purchased from Sigma (USA). Dulbecco's modified Eagle's medium (DMEM), the cell culture medium, was purchased from BasalMedia (China), and fetal bovine serum (FBS), penicillin, and streptomycin were purchased from GIBCO-BRL (USA). CCK-8 (Cell Counting Kit-8) was purchased from Beyotime (China). Rabbit polyclonal antibodies to GAPDH, Bax, Bcl-2,

p53, p-p53, pro-PRAP, and COX IV were purchased from Proteintech (USA). Mice antibodies to p-p53 and Drp1 were purchased from Bioss (USA), and antibodies to pro-caspase 3, and p-Drp1 were purchased from Cell Signaling Technology (USA).

Cell culture

HTR-8/Svneo cell lines (HTR-8) were purchased from Shanghai Zhong Qiao Xin Zhou Biotechnology Co.,Ltd., DMEM supplemented with 10% fetal calf serum, 100 U/mL penicillin, and 100 g/mL streptomycin, at 37°C, 5% CO_2, and saturated humidity were used to culture HTR-8 cells. A 0.25% concentration of trypsin was used to digest logarithmic phase cells for the experiment. A suspension of individual cells was prepared and seeded into an appropriate plate. A suitable condition for dividing cells was achieved by dividing them into four groups: the Control group, the Mod group, the PAG group and the NaHS group. After detection, we chose 0.1 mM as the final concentration of H_2O_2. Serum-free DMEM, H_2O_2 (0.1 mM), H_2O_2 (0.1 mM) and PAG (5 mM), H_2O_2 (0.1 mM), and NaHS (0.2 mM) were added into different groups at the same time for 24 h.

CCK-8 assay

We evaluated cell viability by Cell counting kit 8 assay. Each group got 100 μL of one of the medicine solutions we mentioned above, and the Control group got 100 μL of serum-free DMEM medium. A 100 μL of CCK-8 was added to each culture plate hole after 24 h of cultivation and incubated at 37°C for 3 h. In order to determine the relative survival rate, we selected the wavelength of 450 nm and measured the absorbance of each well on the plate reader (Tecan, Germany, Infinite M Nano).

Transwell assay

A concentration of 1×10^5cells/well was seeded into the filters in 200 μL of FBS-free medium for 24 h, followed by a different treatment. In the lower chambers, 500 μL of medium containing 30% FBS was used. Using a tipped swab, cells on the top side were removed 24 h after treatment Crystal violet (E607309, Sangon Biotech, China) was used to stain cell migration to the lower side. For each group of testing, at least three independent wells were included, and five to six photographs were taken for each group, and the results were analyzed using Image J (Nation Institutes of Health, Bethesda, MD, USA).

Assay of reactive oxygen species generation

A membrane-permeable fluorescent probe, 2′, 7′-dichlorofluorescin diacetate (DCFH-DA), and a fluorescence microscope (ECLIPSE NI, NIKON, Japan) were used to detect intracellular ROS. The fluorescence is detected at 525 nm after excitation at 488 nm. The concentration of mitochondrial ROS was detected utilizing MitoSOX Red Mitochondrial Superoxide Indicator (40778ES50, Yeasen, China) and fluorescence microscope (ECLIPSE NI, NIKON, Japan). The fluorescence is detected at 580 nm after excitation at 510 nm.

Detection of mitochondrial membrane potential

An JC-1 array of fluorescent dyes were used to detect mitochondrial membrane potential ($\Delta\Psi_m$) (10009172, Cayman, Japan). As mitochondrial membrane potential declines, the red fluorescence of the JC-1 assay changes to green. A total of 300 μL of JC-1 staining solution was added to each well after HTR-8 cells were treated with different medicine solutions for 24 h. A 20 min incubation period was performed in the incubator on the plate. Fluorescence microscopy was used to photograph the plate (ECLIPSE Ts2, NIKON, JapanJC-1 monomers were detected at 485 and 535 nm, and JC-1 aggregates were detected at 535 and 595 nm.

Western blot analysis

First, cells were washed with PBS to remove any remaining DMEM on them, and then lysed on ice for 30 min in RIPA buffer (P0013C, Beyotime, China). The protein concentrations of all groups were determined using a BCA protein assay kit (DQ111-01, TransGen Biotech, China). Proteins (30 g) were separated on 10% polyacrylamide SDS gels for nearly 2 h, transferred onto PVDF membranes in running buffer, then blocked in 5% skim milk solution for 2 h following that, the membrane was incubated with polyclonal antibodies against GAPDH (60004-1-ig, Proteintech, America), Bax (50599-2-Ig, Proteintech, America), Bcl-2 (26593-1-AP, Proteintech, America), p53 (10442-1-AP, Proteintech, America), p-p53 (bs-3707R, Bioss, China), pro-PRAP (12926-1-AP, Proteintech, America), COX IV (66110-1-Ig, Proteintech, America), Drp1 (bs-4100R, Bioss, China), pro-caspase 3 (9662, Cell Signaling Technology, America), and p-Drp1 (3455, Cell Signaling Technology, America). As a secondary antibody, HRP-conjugated goat anti-rabbit IgG (A0208, Beyotime, China) and HRP-conjugated goat anti-mice IgG (A0216, Beyotime, China) were used on the second day for cleaning non-specific binding, then incubated for 1 h at room temperature. Chemiluminescence was performed

using ECL ultra-sensitive light-emitting liquid (36208ES76, Yeasen, China) after the membranes had been washed with TBST buffer Chemiluminescence Imaging System (620028-08Q, CLINX, China) and Quantity One software (Bio-Rad, Hercules, CA, USA) were used to measure signal intensity.

Analyses of statistics

The mean and standard deviation are expressed as mean ± SEM. For multiple comparisons, a one-way ANOVA was used followed by a *post hoc* analysis adjusted with a least-significant-difference correction (SPSS Inc., Chicago, IL, USA). The significance level was considered if $^{*}P < 0.05$, $^{**}P < 0.01$, $^{***}P < 0.001$.

Results

H_2O_2 increased oxidative stress in HTR-8/SVneo cells

Previous studies demonstrated that H_2O_2 could be used to increase oxidative stress in HTR-8 cells (24, 25). For experiments with CCK-8 cells, 0.1 mM H_2O_2 for 12 h induced mild apoptosis in HTR-8 cells, moderate apoptosis at 24 h, and severe apoptosis at 48 h (**Figure 1**). We finally chose 0.1 mM H_2O_2 treated for 24 h to continue our following experiments.

H_2O_2-induced cell apoptosis

We utilized DAPI and flow cytometry to confirm cell apoptosis. After attaching to AT regions of DNA, DAPI stains nuclear and chromosomes, which emit blue fluorescence. Thus, it can indicate morphological changes in the nuclear. Nuclear sequestration is a distinctive feature of apoptosis, and DAPI stains the nucleus and shows its morphology. While apoptosis occurs, Phosphatidylserine (PS) transfers from the cell's inner membrane to the outer membrane. Thus, we could use Annexin V to combine PS in the outer membrane of cells to indicate apoptotic cells. PAG is one of the cystathionine γ-lyase (CSE) inhibitors, which can inhibit the endogenous synthesis of H_2S. As shown in **Figure 2C**, after being treated with H_2O_2, we can easily find the change in nuclear morphology from round shapes to irregular shapes. Treated with H_2O_2 and PAG even increased the sequestration, indicating that H_2S might be involved in the HTR-8 cell apoptosis process. Meanwhile, the result of the NaHS (0.2 mM) group showed that NaHS can partly relieve the influence of H_2O_2. Flow cytometry results gave further proof of the above results. **Figures 2A,B** presented that the proportion

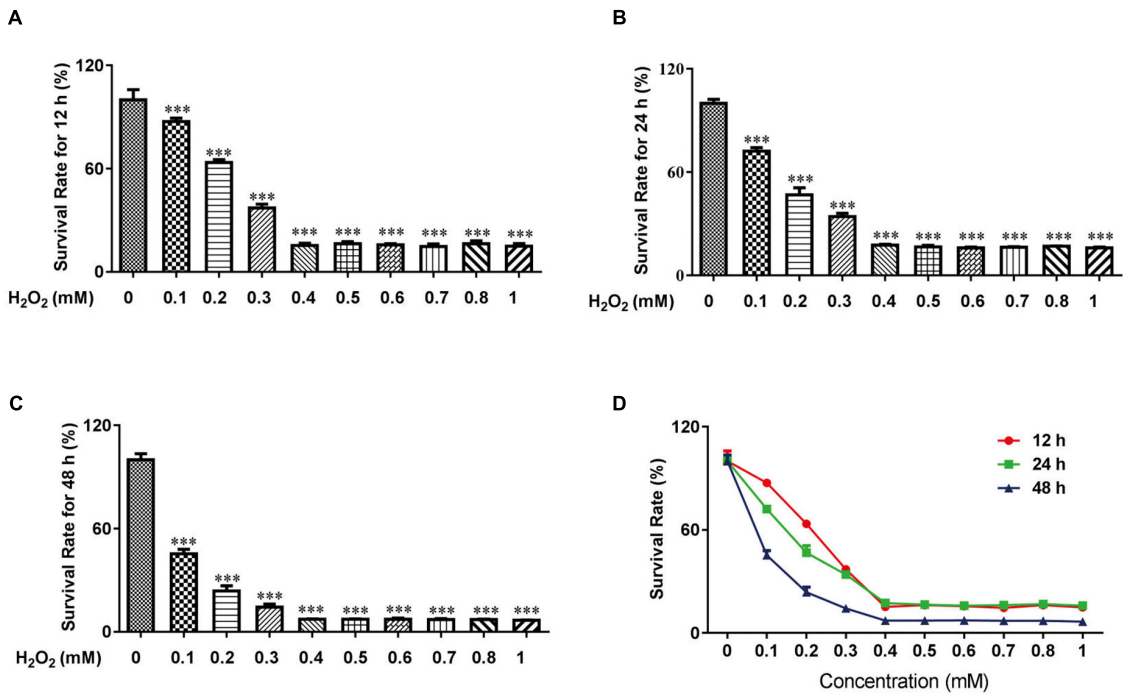

FIGURE 1
H_2O_2 caused oxidative stress damage in HTR-8/SVneo cells. The survival rate of HTR-8/SVneo cells after being treated with different doses of H_2O_2 for 12 h **(A)**, 24 h **(B)** and 48 h **(C)**. Summary of HTR-8/SVneo cells survival rate after 12, 24, and 48 h **(D)**. The data are expressed as mean ± SEM. ****Vs.* Control, $P < 0.001$.

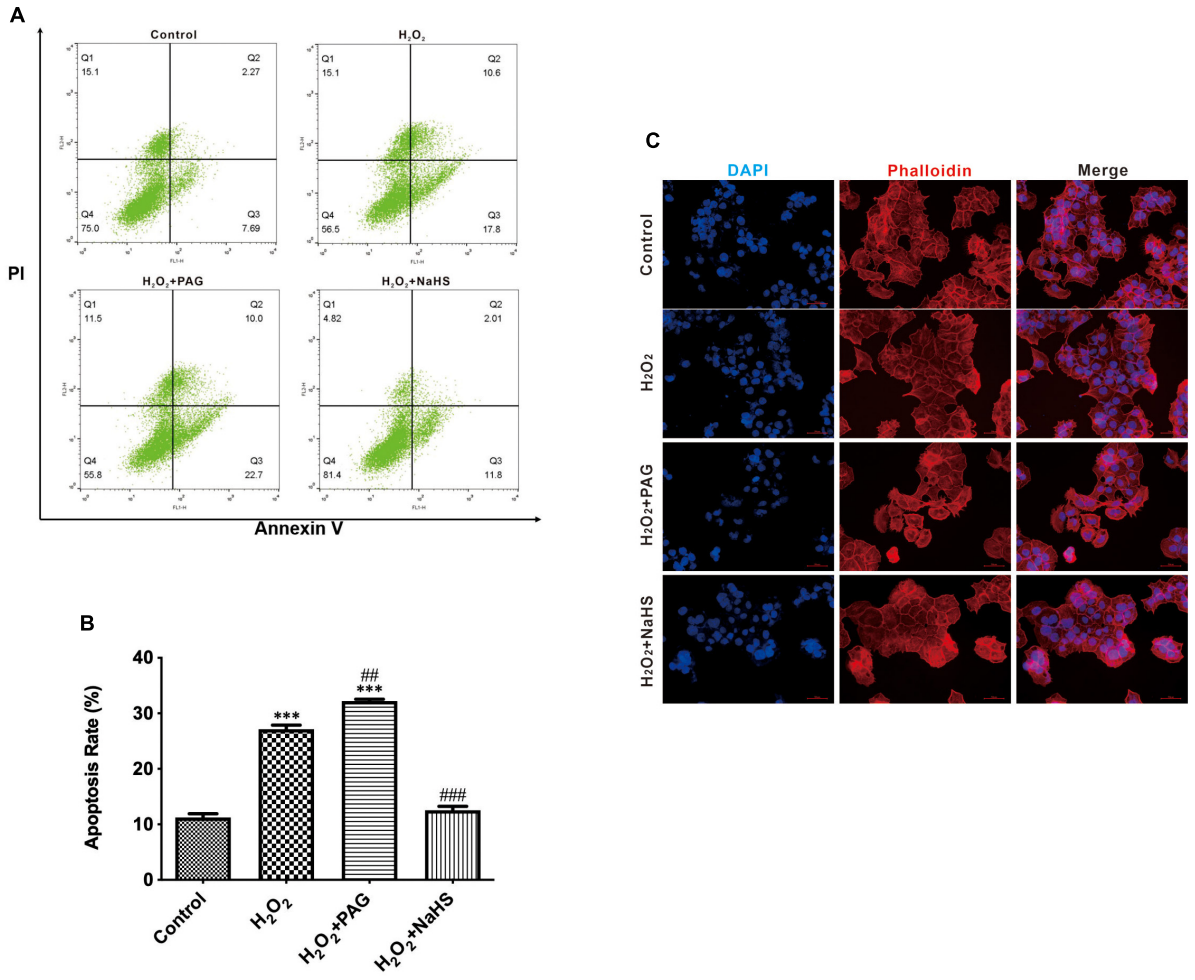

FIGURE 2
H_2O_2 induced HTR-8/SVneo cells apoptosis. The proportion of apoptotic cells was detected by Annexin V. **(A)** Representative pictures of Annexin IV and PI-derived fluorescence in HTR-8/SVneo cells after different treatments. **(B)** Summarize the flow cytometry results. **(C)** Different groups of cells had different morphology changes in the cell nucleus (400×). The data are expressed as mean ± SEM. ****Vs.* Control, $P < 0.001$. $^{\#\#}$*Vs.* H_2O_2, $P < 0.01$. $^{\#\#\#}$*Vs.* H_2O_2, $P < 0.001$. Bar = 50 μm.

of apoptotic cells in the H_2O_2 group and the PAG group were extremely higher than in the control group and the NaHS group ($P < 0.05$). The results demonstrated that H_2O_2 induces HTR-8 cell apoptosis and NaHS could protect HTR-8 cells against H_2O_2-induced injury.

NaHS promoted cell proliferation and invasion after H_2O_2 treatment

In order to demonstrate the effect of NaHS, we analyzed cell proliferation ability by CCK-8 assay and cell invasion ability by invasion assay. CCK-8 assay represented that the survival rate of the NaHS group was significantly higher than the Mod group and the PAG group, indicating that H_2S could induce HTR-8 cells proliferation at 0.2 mM after H_2O_2 treatment, as shown in **Figure 3A**. The invasion assay showed that there were more HTR-8 cells transferring to the lower chambers in the NaHS group (**Figures 3B,C**), by which we could demonstrate that H_2S had the ability to accelerate HTR-8 cell invasion. While in the Mod group, cells were treated with 0.1 mM H_2O_2 for 24 h, thus causing the attenuation of cell invasion. Above all, we could find that H_2S was sufficient to protect HTR-8 cells from oxidative stress, because of its ability to induce cell proliferation and cell invasion.

NaHS reduced the concentration of reactive oxygen species

A ROS is a molecule that contains oxygen and reacts chemically. Excessive ROS can induce apoptosis through both

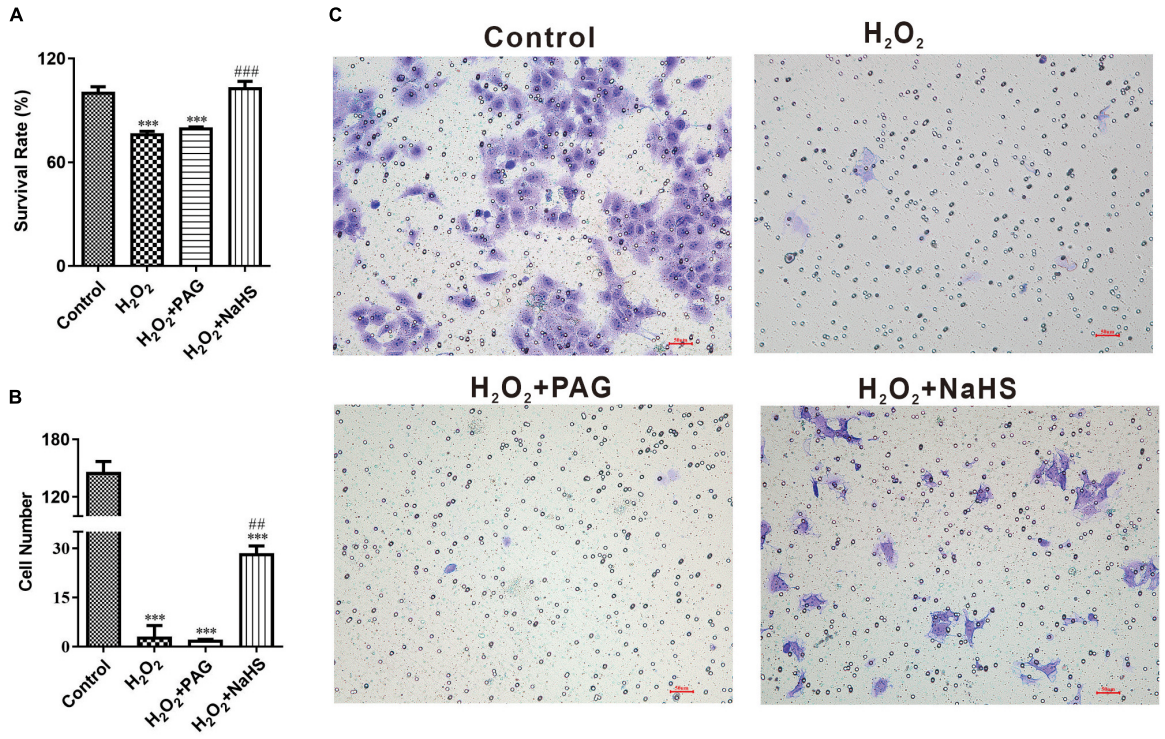

FIGURE 3
NaHS induced HTR-8/SVneo cells invasion and proliferation. **(A)** Summarize of survival rate of HTR-8/SVneo cells after different treatments. **(B)** Summarize cell number detected by invasion assay. **(C)** Representative picture of HTR-8/SVneo cells stained with crystal violet. The data are expressed as mean ± SEM. ***Vs.* Control, $P < 0.001$. ##*Vs.* H_2O_2, $P < 0.01$. ###*Vs.* H_2O_2, $P < 0.001$.

the different pathways and thus do harm to the human body (26). We detected the concentration of intracellular and mitochondrial ROS utilizing DCFH-DA (for cell) and MitoSOX Red (for mitochondria). DCFH-DA is a cell-permeable probe that could be oxidized by ROS and emits green fluorescence, and MitoSOX Red could penetrate into cells and selectively targets mitochondria to visualize the process of ROS production in the mitochondria. In **Figure 4A**, red fluorescence intensity is significantly higher after H_2O_2 treatment, especially in H_2O_2 plus PAG group. And the intensity suppressed in the NaHS group demonstrated that H_2S could inhibit the production of mitochondrial ROS. It is also obvious that NaHS decreased ROS levels in cells. In line with a previous study, H_2S exerts its antioxidant effect by decreasing ROS.

SOD and catalase (CAT) have an important role in scavenging the levels of ROS. Their activity and concentration are highly related to the oxidative condition in cells. Malondialdehyde (MDA) is cytotoxic and commonly used as a lipid peroxidation indicator. After detecting the concentration of SOD, CAT, and MDA (in **Figure 4C**), we could find a higher level of MDA and lower levels of SOD and CAT in the H_2O_2 group and the PAG group, which is consistent with the previous results of ROS. After being treated with NaHS, the concentration of SOD and CAT became significantly higher which indicated that H_2S could protect HTR-8 cells through cleaving ROS.

NaHS restored mitochondrial function

Perturbation of mitochondrial function is associated with loss of the mitochondrial transmembrane potential and the release of apoptogenic factors. Mitochondrial membrane potential ($\Delta\Psi m$) is a sensitive indicator of mitochondrial damage (27). JC-1 is a commonly used fluorescent probe, which is used for the detection of $\Delta\Psi_m$. When $\Delta\Psi_m$ is high, JC-1 emits red fluorescence. Unlike in a high $\Delta\Psi m$ condition, it is not possible for JC-1 to gather together at lower $\Delta\Psi min$ the mitochondrial matrix and produce green fluorescence. As shown in **Figure 4B**, H_2O_2 treatment for 24 h could extremely increase green fluorescence, and H_2O_2 plus PAG undoubtedly made the green fluorescence lighter, which means H_2O_2 has a harmful effect on mitochondrial membrane potential. NaHS reduced the effects of H_2O_2 on $\Delta\Psi_m$ which is proved by the increased red fluorescence in the NaHS group.

Mitochondria are complex organelles, and their cleavage and fusion are precisely regulated by genes, but this balance can be disrupted when apoptosis occurs. In the pro-apoptotic

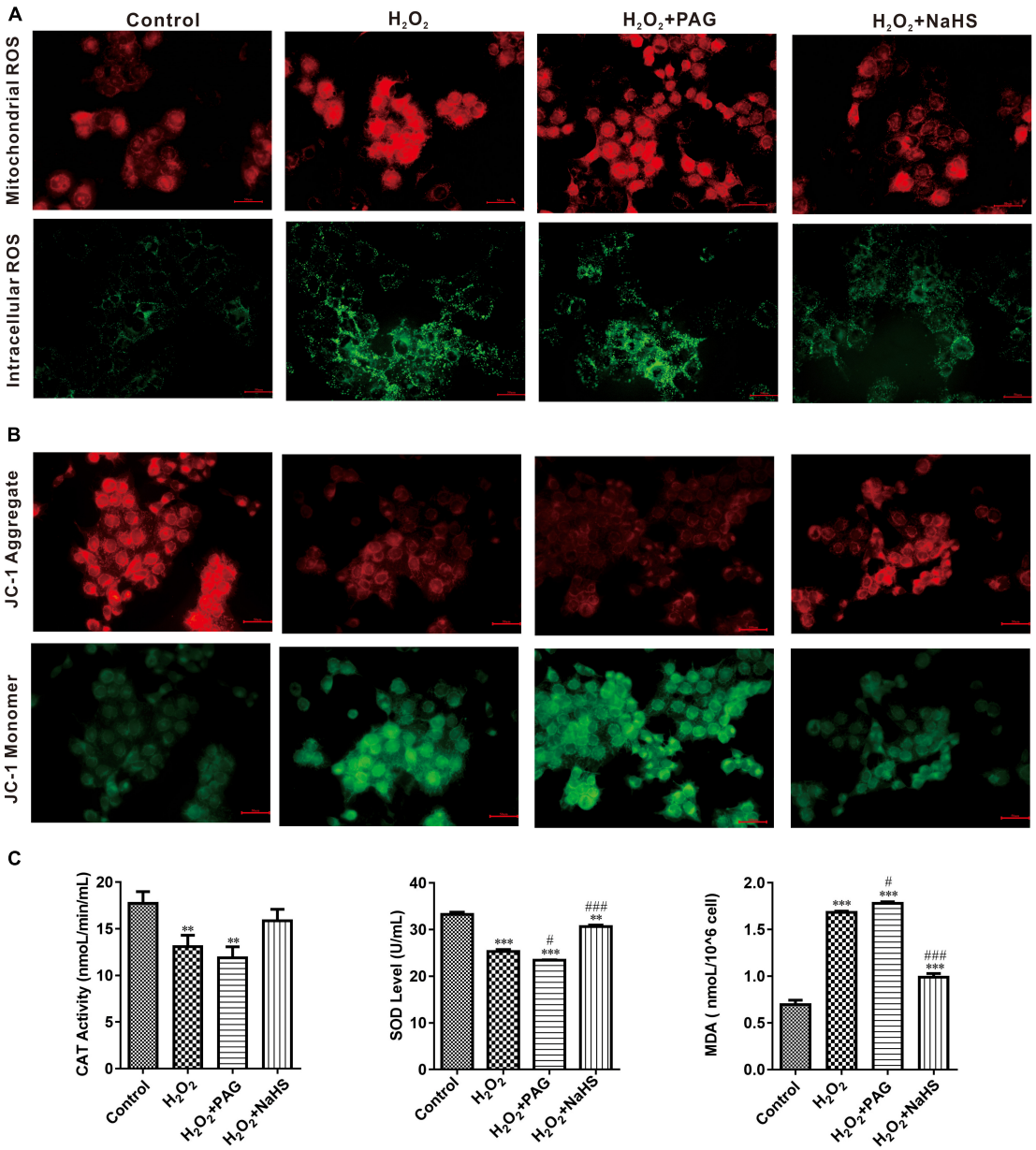

FIGURE 4
NaHS inhibited oxidative stress in HTR-8/SVneo cells. **(A)** The images of different group were obtained with excitation/emission of 525/590 nm for red fluorescence and 490/530 nm for green fluorescence **(B)**. NaHS decreased mitochondrial membrane potential ($\Delta\Psi_m$) in HTR-8/SVneo cells. Red fluorescence and green fluorescence intensity for JC-1 staining of different groups. Bar = 50 μm. **(C)** Effect of NaHS on CAT, SOD and MDA. The data are expressed as mean ± SEM. ***Vs.* Control, $P < 0.01$. ****Vs.* Control, $P < 0.001$. $^{\#}$*Vs.* H_2O_2, $P < 0.05$. $^{\#\#\#}$*Vs.* H_2O_2, $P < 0.001$.

phase, mitochondria undergo cleavage and release a series of pre-apoptotic signals (28). Many factors control mitochondrial cleavage and fusion. One such factor is the family of kinetic-related GTPases (Drp1). Drp1 can promote mitochondrial cleavage when phosphorylated at serine 616 (ser616) (29). Western blot was used to detect the expression of p-Drp1 and Drp1 within and outside the mitochondria. As shown in **Figure 5**, compared with the Control group, the H_2O_2 group and the PAG group showed a significant increase in p-Drp1 inside and outside the mitochondria. The NaHS group showed a significant and extreme decrease in p-Drp1 compared with the H_2O_2 group and the PAG groups. This suggests that H_2O_2 and PAG can promote mitochondrial lysis, implying that this lysis may be related to H_2S concentration. And NaHS have a protective effect on mitochondria by inhibiting its lysis, from which we purposed that it might be related to cell apoptosis.

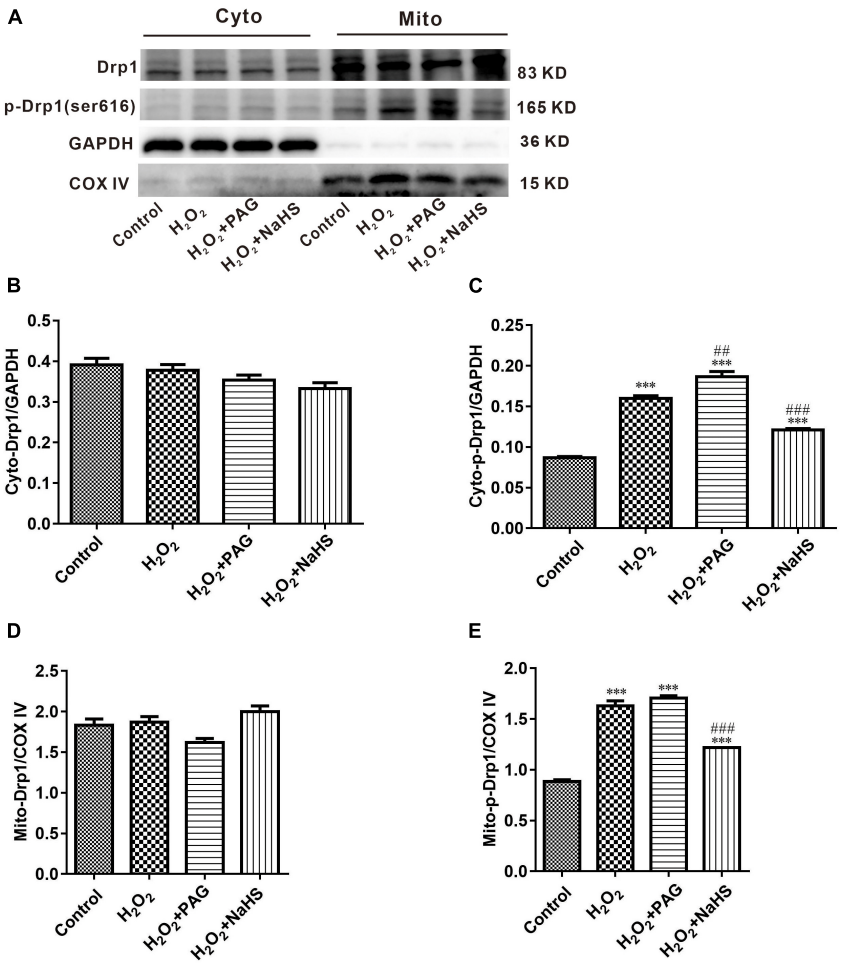

FIGURE 5
Effect of NaHS on mitochondrial cleavage and fusion proteins activity in HTR-8/SVneo cells. **(A)** Representative Western blot showing Drp1, p-Drp1 in cytoplasm and mitochondria in HTR-8/SVneo cells after different treatments. **(B–E)** Bar charts indicating different proteins between different groups. Results in the cytoplasm were normalized against GAPDH, and results in mitochondria were normalized against COX IV. The data are expressed as mean ± SEM. ****Vs.* Control, $P < 0.001$. $^{\#\#}$*Vs.* H_2O_2, $P < 0.01$. $^{\#\#\#}$*Vs.* H_2O_2, $P < 0.001$.

NaHS protected HTR-8/SVneo cells by inhibiting cell apoptosis

Western Blot results indicated the condition of cell apoptosis more clearly. As shown in **Figure 6**, apoptosis-promoting protein Bax, caspase-3 and phosphorylated-p53 demonstrated an increasing trend in the H_2O_2 group and the PAG group, while apoptosis-inhibiting protein Bcl-2 and PRAP demonstrated a reversed trend. The condition is totally different in the NaHS group. The concentration of Bcl-2 and PRAP was significantly higher than in the H_2O_2 group and the PAG group, and caspase 3 was significantly lower in the NaHS group. The results showed the induce-apoptosis effect of H_2O_2 and the protective effect of H_2S on HTR-8 cells at the protein level through the cell apoptosis pathway.

Discussion

There are many complications associated with pregnancy, but one of the most feared is preeclampsia. PE usually begins as hypertension and proteinuria in the third trimester and can quickly progress to more serious conditions, such as death for both mother and child. It is still unclear what causes PE, but clinical and pathological studies suggest the placenta plays a pivotal role in their pathogenesis (5). Also, endogenous H_2S pathway could contribute to the development of PE both in gene level and protein level (30). Based on previous studies, abnormal placental development and angiogenesis are key features of PE, which progresses and eventually leads to ischemia and hypoxia of the placenta. The excessive apoptosis of trophoblast cells is one of the factors that subsequently lead to poor placental development and angiogenesis. In this study, we verified the

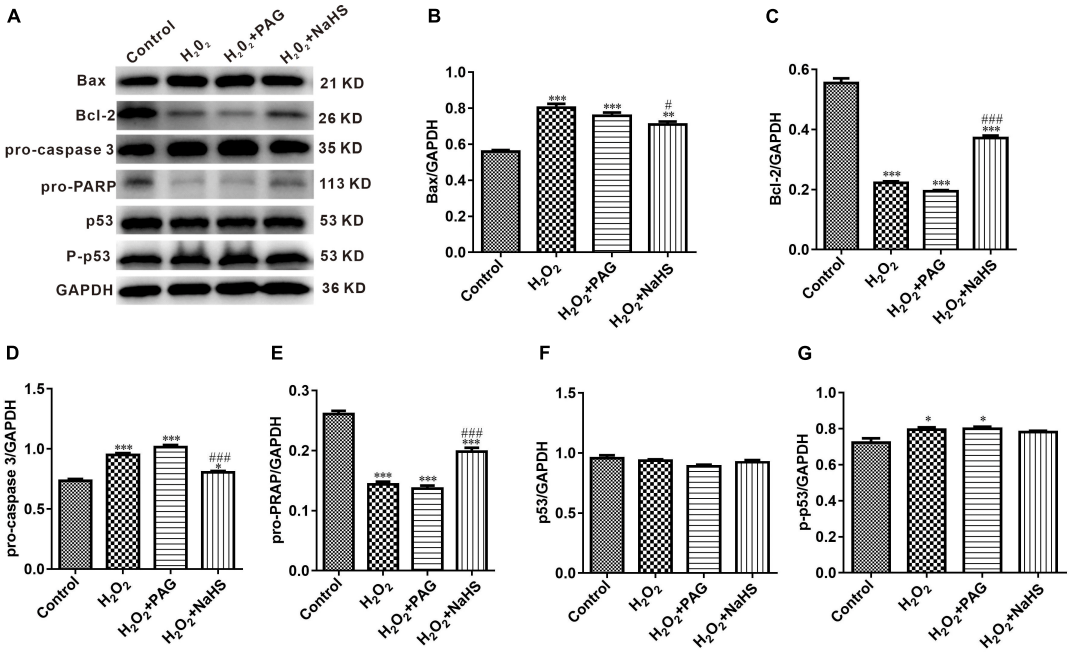

FIGURE 6
Effect of NaHS on cell apoptosis pathway proteins activity in HTR-8/SVneo cells. **(A)** Representative western blot showing Bax, Bcl-2, pro-caspase 3, pro-PRAP, p53, and p-p53 in HTR-8/SVneo cells after different treatments. **(B–G)** Bar charts indicating different apoptosis-related proteins between different groups. Results were normalized against GAPDH. The data are expressed as mean ± SEM. **Vs.* Control, $P < 0.05$. ****Vs.* Control, $P < 0.001$. *#Vs.* H_2O_2, $P < 0.05$. *###Vs.* H_2O_2, $P < 0.001$.

inhibitory effect of H_2S on apoptosis of trophoblast cells and further investigated its mechanism. Finally, we revealed the protective effect of H_2S on the placenta in PE and its mechanism.

HTR-8/Svneo cell line is an immortalized extravillous trophoblast cell line derived from normal human early pregnancy placenta. It is a common cell line used to study the function of early pregnancy trophoblast *in vitro* (31). In this experiment, we confirmed that H_2S could promote the proliferation and invasion of HTR-8 cells after H_2O_2 treatment which is consistent with our previous study (23), and its antioxidant effect reduced the production of ROS, maintained the function of mitochondria, and suppress the synthesis of apoptosis-related proteins. To confirm the role of H_2S in promoting cell proliferation and invasion, CCK-8 assay and invasion assay were utilized to detect both the proliferation and invasion abilities of cells, and the results showed that the survival rate of cells and the migration of cells were significantly increased after the addition of NaHS compared with the Mod group. This verified the protective effect of H_2S on HTR-8 cells under excessive oxidative stress.

H_2S inhibits cell apoptosis at low concentrations. There are three ways in which H_2S inhibits apoptosis: First, it regulates the MAPK pathway through ATP-sensitive potassium channels and thus inhibits apoptosis; Second, H_2S is oxidized in the cytoplasm and can hypersulfide caspase 9 and other proteins, thus disabling them and the subsequent apoptotic process will be inhibited; Third, H_2S hypersulfates NF-κB and directly induced it's combining with anti-apoptosis gene promoter. H_2S exerts its effect on mitochondria through regulating mitochondrial fission and fusion, which is achieved by regulating the Drp1 protein, a major factor controlling mitochondrial fission, which can form helical oligomers and thus contribute to mitochondrial division (32). Our study confirmed that low concentrations of H_2S can reduce the intracellular p-Drp1/Drp1 ratio, thus reducing mitochondrial cleavage and further reducing the accumulation of ROS and thus inhibiting apoptosis. We also demonstrated that H_2S could restore mitochondrial membrane potential, reduce mitochondrial cleavage, and decrease ROS levels in mitochondria, which lead to the inference that the inhibitory effect of H_2S on apoptosis in HTR-8 cells is partly dependent on the mitochondrial pathway.

p53 is an intracellular antitumor factor that is used in the field of tumor therapy because of its ability to inhibit cell growth and promote apoptosis. When cells are stimulated by an internal or external environment (e.g., DNA damage or hypoxia), the p53 expression level will be up-regulated, thus causing apoptosis. p53 expression promotes the up-regulation of the expression of the pro-apoptotic signal Bax (Bcl-2 associated × protein) and the down-regulation of the expression of the anti-apoptotic signal Bcl-2 in the Bcl-2 gene family. The Bax protein forms pores in the mitochondrial membrane, resulting

in destroying mitochondrial permeability and subsequent loss of mitochondrial membrane potential and release of cytochrome c (33). Caspase 9, a protein of the aspartate family (caspase family) that is essential in the mitochondrial apoptotic pathway, is upstream of the entire cascade reaction and can have an effect by activating downstream acting proteins, and is an initiator protein. When activated, the initiator protein can activate downstream caspase 3, thus activating DNA degradation by deoxyribonucleases, triggering apoptosis. Our study confirmed that H_2S can inhibit apoptosis in the mitochondrial pathway by down-regulating the expression of Bax and caspase 3 proteins and up-regulating the expression of Bcl-2, PRAP proteins.

However, many details still need to be added in the future. We verified at the cellular level that H_2S inhibited apoptosis of HTR-8 cells after H_2O_2 treatment *via* the mitochondrial pathway, and confirmed that its antioxidant effect was sufficient to promote the proliferation and invasion of HTR-8 cells after H_2O_2 treatment. PE is a disease which is quite difficult to research, because of its unique characteristics, we here provide a potential way to cure or prevent the happening of PE. And we also replenish the function of H_2S which is a core-compound in our laboratory. Even though, these results need to be confirmed at the animal level in order to have a better clinical meaning.

Data availability statement

The original contributions presented in the study are included in the article/supplementary material, further inquiries can be directed to the corresponding author/s.

Author contributions

WG and XW designed the study. XW, SY, and JW wrote the manuscript, originated the central idea, and supervised the work. XW, SY, YJ, HP, JG, and WG performed experiments and analyzed the data. HP and JW contributed the experiment materials supply. XW, SY, YJ, HP, JG, JW, and WG analyzed the data and read the manuscript. All authors contributed to the article and approved the submitted version.

Funding

This work was supported by the Shanghai Municipal Health Commission (No. 202140065), the National Natural Science Foundation of China (No. 81803516), the Shanghai Municipal Health Commission (No. 20184Y0102), and the Special Funds for People's Livelihood Research Medical and Health Project of Shanghai (No. PKJ2019-Y22).

Acknowledgments

We thank Muye Ma at Fudan University for technical assistance.

Conflict of interest

The authors declare that the research was conducted in the absence of any commercial or financial relationships that could be construed as a potential conflict of interest.

Publisher's note

References

1. Nirupama R, Divyashree S, Janhavi P, Muthukumar SP, Ravindra PV. Preeclampsia: pathophysiology and management. *J Gynecol Obstet Hum Reprod.* (2021) 50:101975. doi: 10.1016/j.jogoh.2020.101975

2. Committee on Practice Bulletins–Obstetrics. Gestational hypertension and preeclampsia: ACOG practice bulletin summary, number 222. *Obstet Gynecol.* (2020) 135:1492–5. doi: 10.1097/AOG.0000000000003892

3. Raguema N, Moustadraf S, Bertagnolli M. Immune and apoptosis mechanisms regulating placental development and vascularization in preeclampsia. *Front Physiol.* (2020) 11:98. doi: 10.3389/fphys.2020.00098

4. Erez O, Romero R, Jung E, Chaemsaithong P, Bosco M, Suksai M, et al. Preeclampsia and eclampsia: the conceptual evolution of a syndrome. *Am J Obstet Gynecol.* (2022) 226:S786–803. doi: 10.1016/j.ajog.2021.12.001

5. Rana S, Lemoine E, Granger JP, Karumanchi SA. Preeclampsia: pathophysiology, challenges, and perspectives. *Circ Res.* (2019) 124:1094–112. doi: 10.1161/CIRCRESAHA.118.313276

6. Chiarello DI, Abad C, Rojas D, Toledo F, Vázquez CM, Mate A, et al. Oxidative stress: normal pregnancy versus preeclampsia. *Biochim Biophys Acta Mol Basis Dis.* (2020) 1866:165354. doi: 10.1016/j.bbadis.2018.12.005

7. Taysi S, Tascan AS, Ugur MG, Demir M. Radicals, oxidative/nitrosative stress and preeclampsia. *Mini Rev Med Chem.* (2019) 19:178–93. doi: 10.2174/1389557518666181015151350

8. Zsengellér ZK, Rajakumar A, Hunter JT, Salahuddin S, Rana S, Stillman IE, et al. Trophoblast mitochondrial function is impaired in preeclampsia and correlates negatively with the expression of soluble fms-like tyrosine kinase 1. *Pregnancy Hypertens.* (2016) 6:313–9. doi: 10.1016/j.preghy.2016.06.004

9. Dadsena S, King LE, García-Sáez AJ. Apoptosis regulation at the mitochondria membrane level. *Biochim Biophys Acta Biomembr.* (2021) 1863:183716. doi: 10.1016/j.bbamem.2021.183716

10. Shen Y, Shen Z, Luo S, Guo W, Zhu YZ. The cardioprotective effects of hydrogen sulfide in heart diseases: from molecular mechanisms to therapeutic potential. *Oxid Med Cell Longev.* (2015) 2015:925167. doi: 10.1155/2015/925167

11. Lv B, Chen S, Tang C, Jin H, Du J, Huang Y. Hydrogen sulfide and vascular regulation – an update. *J Adv Res.* (2021) 27:85–97. doi: 10.1016/j.jare.2020.05.007

12. Kumar M, Sandhir R. Hydrogen sulfide in physiological and pathological mechanisms in brain. *CNS Neurol Disord Drug Targets.* (2018) 17:654–70. doi: 10.2174/1871527317666180605072018

13. Lee ZW, Deng LW. Role of H2S donors in cancer biology. *Handb Exp Pharmacol.* (2015) 230:243–65. doi: 10.1007/978-3-319-18144-8_13

14. Murphy B, Bhattacharya R, Mukherjee P. Hydrogen sulfide signaling in mitochondria and disease. *Faseb J.* (2019) 33:13098–125. doi: 10.1096/fj.201901304R

15. Guo W, Kan JT, Cheng ZY, Chen JF, Shen YQ, Xu J, et al. Hydrogen sulfide as an endogenous modulator in mitochondria and mitochondria dysfunction. *Oxid Med Cell Longev.* (2012) 2012:878052. doi: 10.1155/2012/878052

16. Sarno L, Raso GM, di Villa Bianca RD, Mitidieri E, Maruotti GM, Esposito G, et al. OS064. Contribute of the L-cysteine/ H2S pathway in placenta homeostasisin hypertensive disorders. *Pregnancy Hypertens.* (2012) 2:211–2. doi: 10.1016/j.preghy.2012.04.065

17. Rezai H, Ahmad S, Alzahrani FA, Sanchez-Aranguren L, Dias IH, Agrawal S, et al. MZe786, a hydrogen sulfide-releasing aspirin prevents preeclampsia in heme oxygenase-1 haplodeficient pregnancy under high soluble flt-1 environment. *Redox Biol.* (2021) 38:101768. doi: 10.1016/j.redox.2020.101768

18. Saif J, Ahmad S, Rezai H, Litvinova K, Sparatore A, Alzahrani FA, et al. Hydrogen sulfide releasing molecule MZe786 inhibits soluble Flt-1 and prevents preeclampsia in a refined RUPP mouse model. *Redox Biol.* (2021) 38:101814. doi: 10.1016/j.redox.2020.101814

19. Terstappen F, Clarke SM, Joles JA, Ross CA, Garrett MR, Minnion M, et al. Sodium thiosulfate in the pregnant dahl salt-sensitive rat, a model of preeclampsia. *Biomolecules.* (2020) 10:302. doi: 10.3390/biom10020302

20. Covarrubias AE, Lecarpentier E, Lo A, Salahuddin S, Gray KJ, Karumanchi SA, et al. AP39, a modulator of mitochondrial bioenergetics, reduces antiangiogenic response and oxidative stress in hypoxia-exposed trophoblasts: relevance for preeclampsia pathogenesis. *Am J Pathol.* (2019) 189:104–14. doi: 10.1016/j.ajpath.2018.09.007

21. Shen Y, Guo W, Wang Z, Zhang Y, Zhong L, Zhu Y. Protective effects of hydrogen sulfide in hypoxic human umbilical vein endothelial cells: a possible mitochondria-dependent pathway. *Int J Mol Sci.* (2013) 14:13093–108. doi: 10.3390/ijms140713093

22. Xin L, Junhua W, Long L, Jun Y, Yang X. Exogenous hydrogen sulfide protects SH-SY5Y cells from OGD/Rinduced injury. *Curr Mol Med.* (2017) 17:563–7. doi: 10.2174/1566524018666180222121643

23. Wang XL, Tang J. Focal adhesion kinase signaling is necessary for the hydrogen sulfide-enhanced proliferation, migration, and invasion of HTR8/SVneo human trophoblasts. *Reprod Dev Med.* (2022). doi: 10.1097/RD9.0000000000000047 [Epub ahead of print].

24. Qi L, Jiang J, Zhang J, Zhang L, Wang T. Curcumin protects human trophoblast HTR8/SVneo cells from H(2)O(2)-induced oxidative stress by activating Nrf2 signaling pathway. *Antioxidants (Basel).* (2020) 9:121. doi: 10.3390/antiox9020121

25. Fu J-Y, Jing Y, Xiao Y-P, Wang X-H, Guo Y-W, Zhu Y-J. Astaxanthin inhibiting oxidative stress damage of placental trophoblast cells in vitro. *Syst Biol Reprod Med.* (2021) 67:79–88. doi: 10.1080/19396368.2020.1824031

26. Zhang J, Wang X, Vikash V, Ye Q, Wu D, Liu Y, et al. ROS and ROS-mediated cellular signaling. *Oxid Med Cell Longev.* (2016) 2016:4350965. doi: 10.1155/2016/4350965

27. Zorova LD, Popkov VA, Plotnikov EY, Silachev DN, Pevzner IB, Jankauskas SS, et al. Mitochondrial membrane potential. *Anal Biochem.* (2018) 552:50–9. doi: 10.1016/j.ab.2017.07.009

28. Cereghetti GM, Stangherlin A, Martins de Brito O, Chang CR, Blackstone C, Bernardi P, et al. Dephosphorylation by calcineurin regulates translocation of Drp1 to mitochondria. *Proc Natl Acad Sci USA.* (2008) 105:15803–8. doi: 10.1073/pnas.0808249105

29. Cribbs JT, Strack S. Reversible phosphorylation of Drp1 by cyclic AMP-dependent protein kinase and calcineurin regulates mitochondrial fission and cell death. *EMBO Rep.* (2007) 8:939–44. doi: 10.1038/sj.embor.7401062

30. Holwerda K, Weedon-Fekjær S, Staff A, Nolte I, Goor H, Lely T, et al. PP013. Single nucleotide polymorphisms of the maternal cystathionine-b-synthase gene are associated with preeclampsia (PE). *Pregnancy Hypertens.* (2013) 3:72. doi: 10.1016/j.preghy.2013.04.041

31. Abbas Y, Turco MY, Burton GJ, Moffett A. Investigation of human trophoblast invasion in vitro. *Hum Reprod Update.* (2020) 26:501–13. doi: 10.1093/humupd/dmaa017

32. Fonseca TB, Sánchez-Guerrero Á, Milosevic I, Raimundo N. Mitochondrial fission requires DRP1 but not dynamins. *Nature.* (2019) 570:E34–42. doi: 10.1038/s41586-019-1296-y

33. Shen Y, White E. p53-dependent apoptosis pathways. *Adv Cancer Res.* (2001) 82:55–84. doi: 10.1016/S0065-230X(01)82002-9

frontiers | Frontiers in Cardiovascular Medicine

TYPE Original Research
PUBLISHED 08 November 2022
DOI 10.3389/fcvm.2022.1024014

OPEN ACCESS

EDITED BY
Jia Qi,
Shanghai Jiao Tong University, China

REVIEWED BY
Genmao Cao,
Second Hospital of Shanxi Medical University, China
Zhi Geng,
Shanghai Jiao Tong University, China
Xiaoqin Cheng,
Fudan University, China

*CORRESPONDENCE
Feng Wang
13816566556@163.com
Jue Wang
wangjueshiyuan@163.com

†These authors have contributed equally to this work

SPECIALTY SECTION
This article was submitted to General Cardiovascular Medicine, a section of the journal Frontiers in Cardiovascular Medicine

RECEIVED 20 August 2022
ACCEPTED 20 October 2022
PUBLISHED 08 November 2022

CITATION
Bi Q, Zhou X, Lu Y, Fu W, Wang Y, Wang F and Wang J (2022) Polymorphisms of the apolipoprotein E gene affect response to atorvastatin therapy in acute ischemic stroke. *Front. Cardiovasc. Med.* 9:1024014. doi: 10.3389/fcvm.2022.1024014

Polymorphisms of the apolipoprotein E gene affect response to atorvastatin therapy in acute ischemic stroke

QianQian Bi[1†], XiaoYu Zhou[2†], YanQin Lu[3], Wang Fu[1], YongPeng Wang[1], Feng Wang[1*] and Jue Wang[2*]

[1]Department of Neurology, Seventh People's Hospital of Shanghai University of Traditional Chinese Medicine, Shanghai, China, [2]Department of Neurology, Shanghai Tenth People's Hospital, Tongji University School of Medicine, Shanghai, China, [3]Department of Infectious Diseases, Shanghai Tenth People's Hospital, Tongji University School of Medicine, Shanghai, China

Background: Polymorphisms of the apolipoprotein E (APOE) gene are related to the efficacy of statin therapy. The biological functions of the APOE subtypes determine the metabolism of blood plasma lipids and the progression of atherosclerosis. This study aimed to explore the impact of APOE gene polymorphisms on the effect of atorvastatin on lipid regulation and plaque stabilization.

Methods: The study was a prospective cohort study that consecutively included patients with acute ischemic stroke (AIS) in the Department of Neurology, Shanghai Tenth People's Hospital, from December 2018 to December 2019. The patients were divided into E2, E3, and E4 groups according to their APOE genotype. Atorvastatin (20 mg) was administrated to all patients. Changes in blood lipid levels over 3 months and plaque size and stability over 12 months were analyzed.

Results: We enrolled 253 consecutive patients with AIS, of whom, 136 had carotid atherosclerotic plaques. Two patients with genotype E2/E4 were excluded. There were 30 patients in the E2 group (12.0%), 191 patients in the E3 group (76.0%), and 30 patients in the E4 group (12.0%). The lowest percentage reduction in low-density lipoprotein cholesterol (LDL-C) was observed in the E4 group (41.2%), while the highest percentage reduction was observed in the E2 group (17.6%). The plaques in the E2 group showed slower progression, while those in the E4 group showed more rapid progression.

Conclusion: APOE gene polymorphisms affect the biological functions of atorvastatin. Compared to the ε3 or ε4 allele, the ε2 allele exerted a greater lipid-lowering effect on LDL-C levels, enhanced the ability of atorvastatin to stabilize carotid artery plaques, and slowed carotid artery plaque progression.

KEYWORDS

apolipoprotein E, polymorphism, lipid-lowering, atherosclerosis, carotid artery plaques

Introduction

Atherosclerosis is one of the leading causes of stroke. Low-density lipoprotein cholesterol (LDL-C) is closely related to the progression of atherosclerosis (1). With every 1 mmol/L reduction in LDL-C, the relative risk of stroke decreases by 21.1%, thus showing the importance of reducing LDL-C levels for stroke prevention (2). Statins that competitively inhibit critical enzymes in cholesterol synthesis are the most widely used lipid-lowering drugs and have become one of the three cornerstones of acute ischemic stroke (AIS) treatment. However, apparent individual differences in lipid-lowering effects have been observed with the widespread use of statins. Statin metabolism is affected by a variety of genes, and gene polymorphisms are related to the lipid-lowering effects of statins. Genetic factors contribute to approximately 70% of the efficacy of statin treatment (3), and the apolipoprotein E (APOE) gene is closely related (4, 5).

APOE is mainly synthesized in the periphery of the liver. On the one hand, as a structural protein of chylomicron (CM), LDL-C, very low-density lipoprotein cholesterol (VLDL-C), and part of high-density lipoprotein cholesterol (HDL-C), APOE is beneficial in stabilizing the structure of these lipoproteins. On the other hand, as a ligand and member of the LDL receptor family, it regulates blood CM, LDL-C, VLDL-C, and HDL-C levels (6, 7). Gene polymorphisms determine the transport and regulation of blood lipids. The gene coding APOE is located on chromosome 19 and is approximately 3.7 kb in length (8). It comprises two loci, rs429358T > $C^{3,937}$ and rs7412C > $T^{4,075}$, and includes four alleles, ε2 ($T^{3,937}$–$T^{4,075}$), ε3 ($T^{3,937}$–$C^{4,075}$), ε4 ($C^{3,937}$–$C^{4,075}$), and ε3r ($C^{3,937}$–$T^{4,075}$), of which ε3r is extremely rare. To date, only two Caucasian families in Italy and one Yoruba family in Ibadan have been reported with this allele, which is why it is generally excluded from clinical studies (9). The ε3 is the most common in the general population (10) and has a frequency of 85% in Asia, 82% in North America, and 77% in South America (11). ε3 is considered "wild type" due to its high frequency in the general population, while ε2 and ε4 alleles are mutations of ε3. The three alleles comprise six common genotypes, including three homozygotes (E2/E2, E3/E3, and E4/E4) and three heterozygotes (E2/E3, E2/E4, and E3/E4).

Due to differences in protein conformations, the affinities for cholesterol receptors in people with distinct genotypes are different, affecting the efficacy of statin therapy. Some studies have shown that statins may confer reduced benefits in APOE ε4 carriers (12) and that ε2 gene carriers may experience superior lipid-lowering effects (13). However, other studies have suggested that the APOE genotype is not significantly associated with the lipid-lowering effect of statins (14). In another study, polymorphisms of the APOE gene determined baseline LDL-C levels, but not the lipid-lowering effect of statins (15). In the Chilean population, patients with the E3/E4 genotype had a smaller reduction in cholesterol levels after statin therapy than those with the E3/E3 genotype (16). However, the association between APOE gene polymorphisms and the progression of atherosclerotic plaques with statin therapy is not well described. Thus, we aimed to explore the differences in lipid-lowering effects and the progression of atherosclerotic plaques with atorvastatin in different APOE genotypes.

Materials and methods

Patients and study design

We prospectively and consecutively collected data from a cohort that included all hospitalized patients with AIS in the Department of Neurology, Shanghai Tenth People's Hospital, between December 2018 and December 2019. Patients were enrolled if they met the following criteria: (1) patients diagnosed with AIS using MRI within 7 days after stroke onset; (2) no previous history of lipid-lowering drug use, such as statins, fibrins, and PCSK9 inhibitors, or lipid-lowering drug withdrawal for more than 1 month; (3) willing to receive 20 mg atorvastatin; (4) patients gave informed consent and participated voluntarily. Exclusion criteria included (1) severe liver or kidney dysfunction or major cardiovascular or respiratory diseases; (2) allergic or intolerant to atorvastatin; (3) severe trauma or major surgery recently; (4) patients with non-compliance or poor compliance. The genotype was confirmed at the study's inception. Previous studies have indicated that the E2 and E4 mutant alleles may have opposite effects on treatment. Therefore, we excluded patients with the E2/E4 genotype. Patients were divided into three groups according to their APOE genotype: E2 (E2/E2 + E2/E3), E3 (E3/E3), and E4 (E3/E4 + E4/E4). All eligible patients received atorvastatin (atorvastatin calcium tablets, Pfizer Pharmaceuticals Limited, 20 mg*7) 20 mg daily and were followed up for 3 months. Patients with carotid plaques were followed up for 12 months. Blood lipids were tested at 3 months and carotid artery ultrasonography was performed at 12 months. The basic characteristics of every patient, including gender, age, height, weight, past medical history, and personal history, were recorded from the electronic medical records and by direct communication with the patients by two doctors at the beginning of the study, and the information was double checked by two doctors at the end.

All patients provided written informed consent to participate in this study. The Ethics Committee of Shanghai Tenth People's Hospital approved this study (No. 22k205).

Apolipoprotein E genotyping

Genomic DNA was extracted from whole blood using the whole blood DNA Extraction Kit (Beijing Jingzhun Medical

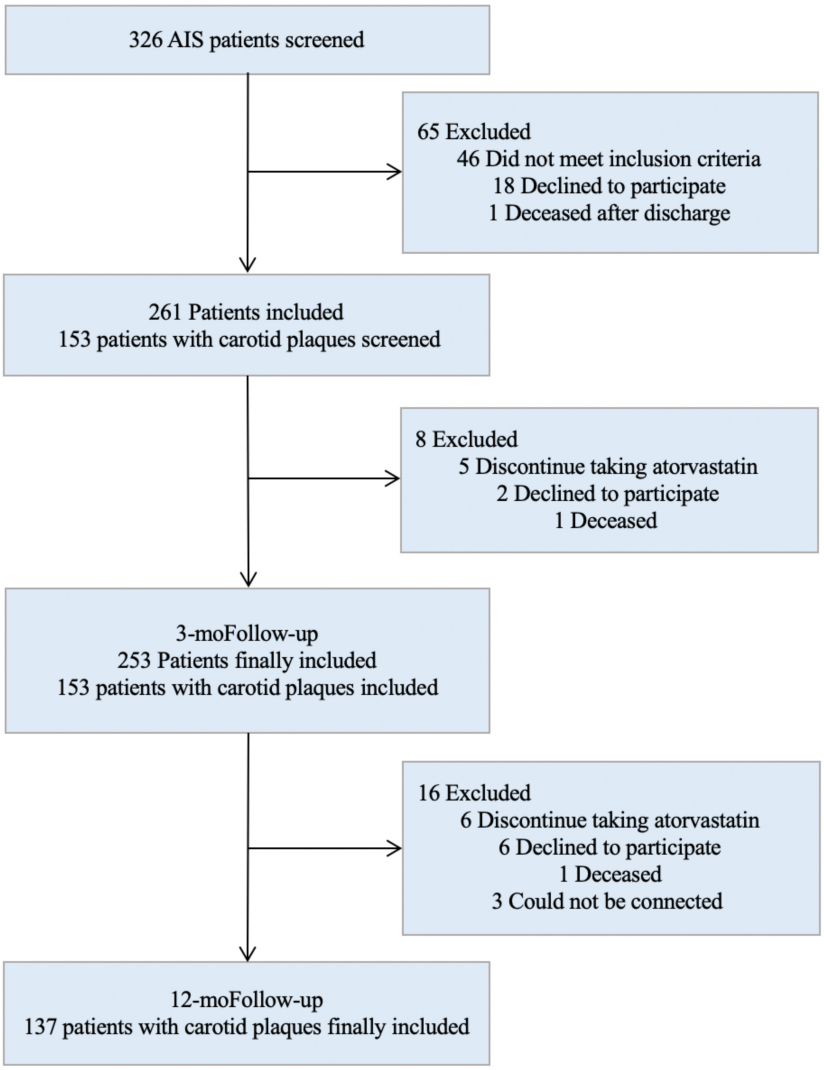

FIGURE 1
Screening flowchart.

Technology Co., Ltd.). Polymerase chain reaction [Honglong Biotechnology (Shanghai) Co., Ltd.] was used for DNA amplification, and the product fragments were subjected to capillary electrophoresis sequencing analysis. According to the peak characteristics performing APOE genotyping.

Detection and classification of plaques

Two ultrasound specialists performed carotid ultrasonography using a color Doppler ultrasound system (Logiq E9, GE, USA). Each patient was placed in a quiet supine position, with the head tilted back and turned to the opposite side. The probe was not pressurized, following the lateral border of the sternocleidomastoid muscle from bottom to top. The patient's common carotid artery trunk, common carotid artery bifurcation, and neck were observed in turn. The internal and external carotid arteries were observed and recorded for plaque length, thickness, and echogenicity. Information on the largest plaque was recorded

TABLE 1 The Hardy-Weinberg genetic balance test of the APOE gene.

Genotype	Actual frequency	Theoretical frequency	χ^2	*P*-value
E2/E2	3 (1.2%)	1.21	3.8133	0.1486
E2/E3	27 (10.7%)	30.23		
E2/E4	2 (0.8%)	2.35		
E3/E3	191 (75.5%)	188.87		
E3/E4	28 (11.1%)	29.71		
E4/E4	2 (0.8%)	1.14		

TABLE 2 Characteristics of the patients at baseline.

Variable	APOE genotype group				*P*-value
	Total group *n* = 251	E2 cases *n* = 30	E3 cases *n* = 191	E4 cases *n* = 30	
Gender, no. (%)					0.078
Male	186 (74.1)	20 (66.7)	148 (77.5)	18 (60.0)	
Female	65 (25.9)	10 (33.3)	43 (22.5)	12 (40.0)	
Age, median (IQR), y	65 (60.72)	65.5 (60.71)	66 (60.71)	65 (61.77)	0.073
Age, no. (%)					0.815
>60	181 (72.1)	22 (73.3)	136 (71.2)	23 (76.7)	
≤60	70 (27.9)	8 (26.7)	55 (28.8)	7 (23.3)	
Hypertension, no. (%)					0.120
Yes	172 (68.5)	16 (53.3)	133 (69.6)	23 (76.7)	
No	79 (31.5)	14 (46.7)	58 (30.4)	7 (23.3)	
Diabetes mellitus, no. (%)					0.124
Yes	97 (38.6)	7 (23.3)	80 (41.9)	10 (33.3)	
No	153 (61.0)	23 (76.7)	111 (58.1)	20 (66.7)	
CHD, no. (%)					0.592
Yes	33 (13.1)	5 (16.7)	23 (12.0)	5 (16.7)	
No	218 (86.9)	25 (83.3)	168 (88.0)	25 (83.3)	
AF, no. (%)					0.319
Yes	17 (6.8)	3 (10.0)	12 (6.3)	4 (13.3)	
No	234 (93.8)	27 (90.0)	179 (93.7)	26 (86.7)	
Smoking*, no. (%)					0.119
Yes	91 (36.3)	13 (43.3)	72 (37.7)	6 (20.0)	
No	160 (63.7)	17 (56.7)	119 (62.3)	24 (80.0)	
Drinking*, no. (%)					0.738
Yes	34 (13.5)	5 (16.7)	26 (13.6)	3 (10.0)	
No	217 (86.5)	25 (83.3)	165 (86.4)	27 (90.0)	
BMI, median (IQR), kg/m^2	24.5 (22.9, 26.7)	24.2 (22.9, 25.7)	24.5 (22.9, 26.7)	24.7 (22.3, 28.7)	0.397
BMI, no. (%)					0.960
>24	148 (59.0)	18 (60.0)	113 (59.2)	17 (56.7)	
≤24	103 (41.0)	12 (40.0)	78 (40.8)	13 (43.3)	

Smoking*, smoked at least 100 cigarettes or 100 g of tobacco in their lifetime; Drinking*, ≥ 1 time per month, ≥ 1 standard drink each time, one standard drink equals 10 g of pure alcohol. AF, atrial fibrillation; CHD, coronary heart disease; BMI, body mass index.

if a patient had multiple plaques simultaneously. Carotid artery intima-media thickness (CIMT) was measured in a 1 cm segment at the bulb of the common carotid artery and 1 cm each from its proximal and distal segments, and the average value of three points was taken as the final value of CIMT. The contralateral side was observed in the same way.

Atherosclerotic plaque formation is defined as a condition in which the intima-media thickness (IMT) is ≥ 1.5 mm, and it protrudes from the vascular lumen, or the localized intimal thickening is > 50% of the surrounding IMT. According to the morphology and echo characteristics of ultrasound, plaques can be divided into (I) hypoechoic lipid soft plaques, (II) fibrous flat plaques with medium echoes rich in collagen tissue, (III) hyperechoic calcifications with acoustic shadows, and (IV) ulcerative mixed plaques with varying echo intensity (17). Among them, (I), (II), and (IV) are vulnerable plaques, and (III) are stable plaques.

Statistical analysis

Statistical analyses were performed using IBM SPS Statistics (version 26.0; IBM, Armonk, NY, USA). Normally distributed measurement data are presented as mean ± standard deviation, and non-normally distributed data are expressed as median and quartile. To compare the three groups, one-way analysis of variance or the Kruskal Wallis test was used, and differences between the two groups were analyzed using the independent samples *T*-test or the Mann-Whitney *U*-test.

The count data are expressed as frequency (percentage), and differences between groups were compared using the chi-square test. To explore the factors affecting LDL-C reduction and changes in plaque length, univariate and multivariate linear regression analyses were performed. The Hardy-Weinberg genetic balance test of APOE was performed using the chi-square test. A two-tailed value of $p < 0.05$ was considered statistically significant.

Results

Polymorphisms of apolipoprotein E

A total of 253 AIS patients with complete follow-up data were included in the study (Figure 1). Six genotypes were detected: three cases with E2/E2 (1.2%), 27 cases with E2/E3 (10.7%), two cases with E2/E4 (0.8%), 191 cases with E3/E3 (75.5%), 28 cases with E3/E4 (11.1%), and two cases with E4/E4 (0.8%).

According to the Hardy-Weinberg genetic balance test, we calculated the theoretical frequency of the included population and compared it with the actual frequency in Table 1. The results indicated that the population in our study was in line with the Hardy-Weinberg genetic balance ($P = 0.1486$), which means that it had good group representation.

Two patients with the E2/E4 genotype were excluded and the remaining 251 patients were divided into three groups: 30 patients in the E2 group (12%), 191 in the E3 group (76%), and 30 in the E4 group (12%). The baseline characteristics of the patients were similar among the three groups (Table 2).

Effects on blood lipids and plaques

After 3 months of atorvastatin treatment, total cholesterol (TC), triglyceride (TG), and LDL-C levels were lower than baseline. There was a significant difference in the reduction rate of blood LDL-C level after treatment (Figure 2A); the E2 group had the highest reduction rate (41.2%), followed by the E3 group (19.8%), while the E4 group had the lowest (17.6%) ($P = 0.020$). When we stratified the cohort by gender, no differences were found in females (Table 3). We performed multiple linear regression based on univariate analysis and expertise (Tables 4, 5). The results showed that the E2 group was sensitive to atorvastatin therapy based on the LDL-C reduction rate (Table 6). The progression of carotid plaques in the E4 group was more rapid than in the E2 and E3 groups ($P = 0.011$) (Figure 2B). After 12 months of atorvastatin treatment, the percentage of vulnerable plaques decreased in the three groups, with significant plaque stabilization in the E2 group (Table 7).

Discussion

This study examined the effects of APOE genetic polymorphisms on atorvastatin therapy in regulating blood lipids and promoting plaque stabilization. Our results showed that compared to ε3 and ε4 allele carriers, ε2 allele carriers had greater lipid-lowering effect on LDL-C, enhanced carotid artery plaque stabilization by atorvastatin, and slower plaque progression.

Polymorphisms of the APOE gene change the structure and function of APOE lipoproteins, resulting in a difference in the

TABLE 3 Percentage variation in lipid concentrations after treatment with atorvastatin and stratified analyses according to gender.

	E2 $n = 30$, male = 20, female = 10	E3 $n = 191$, male = 148, female = 43	E4 $n = 30$, male = 18, female = 12	*P*-value
TC				
All	−19.3 (−36.6, −5.9)	−5.9 (−31.2, 3.1)	−4.9 (−25.2, 12.8)	0.097
Male	−19.5 (−38.2, −5.2)	−12.6 (−31.3, 2.8)	−13.9 (−27.4, 5.9)	0.312
Female	−19.4 (−21.0, −8.1)	−14.5 (−30.5, 14.7)	6.4 (−18.1, 25.4)	0.252
TG				
All	−6.2 (−35.3, 24.7)	24.7 (−25.4, 16.5)	−10.0 (−34.8, 4.6)	0.786
Male	0.0 (−31.3, 27.6)	−6.7 (−25.6, 16.5)	−10.0 (−29.6, 0.0)	0.681
Female	−12.3 (−40.3, 14.0)	−8.8 (−23.3, 19.3)	−7.5 (−39.5, 23.4)	0.921
HDL-C				
All	2.7 (−8.0, 16.8)	16.8 (−5.2, 18.5)	5.9 (0.0, 12.0)	0.847
Male	3.4 (−9.4, 23.6)	3.6 (−5.7, 17.9)	5.9 (0.0, 11.8)	0.983
Female	1.4 (−0.7, 14.4)	9.4 (0.0, 20.0)	3.7 (−19.7, 20.5)	0.493
6				
LDL-C				
All	−41.2 (−52.2, −10.4)	−19.7 (−46.7, 1.9)	−17.6 (−36.6, 14.8)	0.020
Male	−48.5 (−55.5, −9.8)	−19.7 (−46.7, 1.5)	−23.2 (−37.3, 1.2)	0.037
Female	−36.9 (−41.2, −21.5)	−20.8 (−43.8, 16.1)	0.0 (−34.0, 71.0)	0.316

Median of the individual percentage changes (IQR).

TABLE 4 Analysis of factors influencing the LDL-C reduction rate following atorvastatin therapy.

	B	B (95%CI) lower limit	B (95%CI) upper limit	*P*
Gender	−9.35	−22.31	3.61	0.157
Age	0.07	−0.46	0.60	0.794
Hypertension	4.34	−7.92	16.61	0.486
Diabetes mellitus	8.16	−3.41	19.72	0.166
CHD	12.80	−3.91	29.52	0.133
AF	38.04	16.89	59.19	<0.001
Smoking	1.87	−9.84	13.57	0.754
Drinking	−5.33	−21.68	11.02	0.521
BMI	1.25	−0.49	2.99	0.156
E2 gene carrying	−22.21	−39.501	−4.925	0.012

CI: confidence interval.

TABLE 5 Analysis of factors influencing plaque length following atorvastatin therapy.

	B	B (95%CI) lower limit	B (95%CI) upper limit	*P*
Gender	0.28	−0.25	0.81	0.292
Age	−0.27	−0.05	−0.01	0.028
Hypertension	0.47	−0.05	0.99	0.077
Diabetes mellitus	0.019	−0.47	0.51	0.930
CHD	−0.25	−0.93	0.43	0.466
AF	0.44	−0.65	1.53	0.428
Smoking	0.62	0.13	1.11	0.014
Drinking	−0.42	−1.14	0.31	0.261
BMI	0.01	−0.06	0.09	0.730
E4 gene carrying	0.95	0.29	1.61	0.005

CI, confidence interval.

affinity of different isomers for LDL receptors and leading to differences in blood lipid levels between carriers of different genotypes. Type E4 preferentially binds to the larger LDL and VLDL receptors, whereas types E2 and E3 preferentially bind to the smaller HDL receptor (18, 19). Additionally, the affinity of the E2 type for LDL receptors is more than 50 times weaker than that of the E3 type, and the binding force of the E4 type to VLDL is strong, which weakens the process of VLDL lipolysis in the peripheral blood (6, 20). Therefore, the APOE genotype may be associated with basal blood lipid levels, and the E4 allele may be associated with higher TC, LDL-C, TG, and VLDL-C and lower HDL-C levels (21). A study found that the LDL-C and TC levels of patients in the E4 carrier group tended to be higher than those of patients in the E2 and E3 groups (22), while a study by Xie et al. showed that the blood TC level of the E4 gene carrier group was significantly higher than that of the E2 and E3 groups (23). Our study also found that the median initial TC level in the E4 group was slightly higher than that in the E2 and E3 groups, suggesting that there may be a correlation between the APOE genotype and basal blood lipid level.

The lipid-lowering effect of statins is closely related to APOE gene polymorphisms. The E4 allele may attenuate the lipid-lowering effect of statins (24), while the E2 allele exerts a relatively better lipid-lowering effect (4). After 3 months of atorvastatin treatment, the effect on LDL-C reduction was highest in the E2 group, followed by the E3 and E4 groups. Although there was no significant difference between the three groups in the TC reduction rate after treatment, the reduction effect of TC was found to be in the following order: E2 group > E3 group > E4 group, indicating that E2 carriers had a higher tendency to lower lipids with statins than other carriers. Some studies have demonstrated that there are sex differences in the lipid-lowering effect of APOE on statins; that is, the E2 allele enhances the lipid-lowering effect of statins, which is more significant in male patients, but not in female patients (25); this may be related to differences in immune activation and hormone levels (26). Consistent with previous findings, our study also found that E2 allele carriers had a greater LDL-C-lowering effect on statins in males, while this difference was not apparent in females.

APOE polymorphisms can affect the occurrence and development of carotid plaques through various mechanisms. First, many previous studies have shown that APOE gene polymorphisms affect blood lipid metabolism, and dyslipidemia is a significant risk factor for the occurrence and development of atherosclerotic plaques. Therefore, APOE may affect the blood lipid metabolic pathway and carotid plaque progression. Second, APOE gene polymorphisms are associated with the development of diabetes (27), but the underlying mechanism is currently unknown. Studies have speculated that E4 carrier status may affect peripheral and central insulin metabolism (28, 29); therefore, differences in blood glucose metabolism can impact arterial plaque development. Third, studies have found that E4 carriers have higher expression of lipoprotein-related phospholipase, which can promote the body's inflammatory response and plaque instability (30, 31).

Our results provide robust evidence for personalized lipid-lowering and plaque stabilization treatments based on APOE genotypes. This precise treatment can maximize the efficacy of statins. People can achieve lower LDL-C levels, reducing the incidence and recurrence rate of stroke. However, several limitations should also be noted. First, this is a single-center study, which limited the ability to draw major conclusions for all populations. Further studies with larger sample sizes are needed to corroborate our findings. Second, we determined the properties of plaques using ultrasound based on the echo morphology of plaques, which may be less precise than using high-resolution magnetic resonance imaging.

TABLE 6 Multivariate regression analysis of factors influencing the LDL-C reduction rate.

Variables	Unadjusted		Model 1		Model 2	
	B (95%CI)	*P*-value	B (95%CI)	*P*-value	B (95%CI)	*P*-value
LDL-C	−22.21 (−39.50, −4.93)	0.012	−22.94 (−40.24, −5.64)	0.032	−22.51 (−39.47, −5.56)	<0.001
Length of plaque	0.95 (0.29, 1.61)	0.005	0.99 (0.33, 1.65)	0.002	1.06 (0.42, 1.71)	<0.001

For LDL-C, Model 1: adjusted for age and gender. Model 2: adjusted for Model 1 + hypertension, smoking. For the length of the plaque, Model 1: adjusted for age and gender. Model 2: adjusted for Model 1 + diabetes mellitus, coronary heart disease, atrial fibrillation, body mass index.

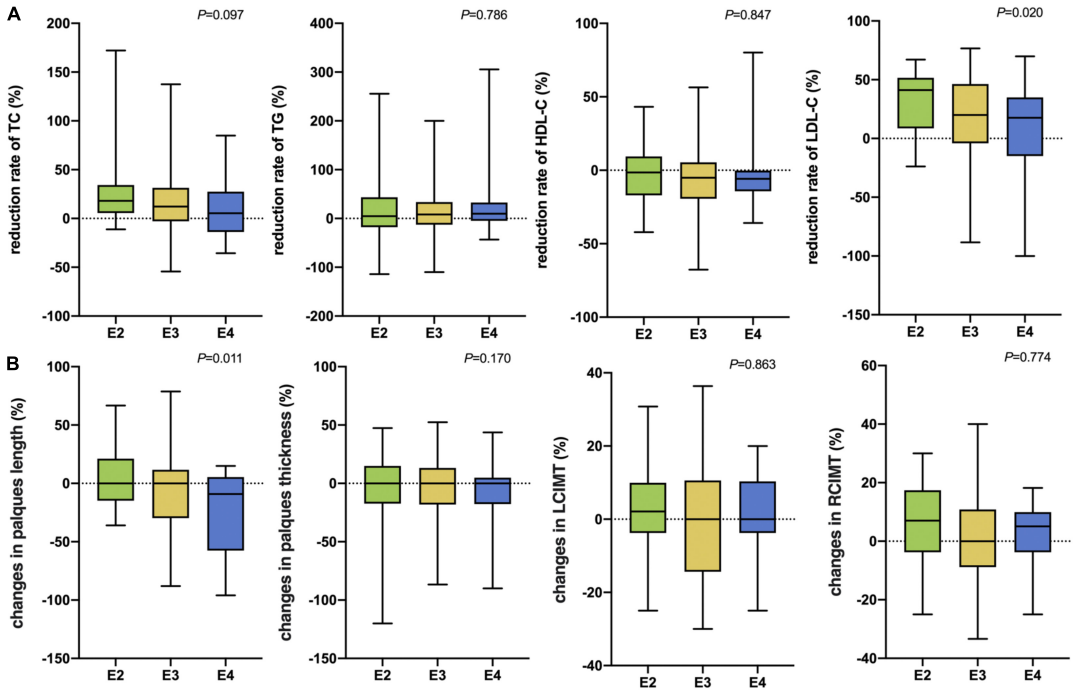

FIGURE 2
(A) The rate of reduction in blood lipids after 3 months of atorvastatin treatment in the three groups. **(B)** Changes in carotid plaque size after 12 months of atorvastatin treatment in the three groups. TC, Total cholesterol; TG, Triglyceride; HDL-C, High-density lipoprotein cholesterol; LDL-C, Low-density lipoprotein cholesterol; LCIMT, Left carotid intima-media thickness; RCIMT, Right carotid intima-media thickness.

TABLE 7 Changes in vulnerable plaques after 12 months of atorvastatin therapy.

Outcome	APOE genotype group				*P*-value
	Total group *n* = 78	E2 cases *n* = 10	E3 cases *n* = 57	E4 cases *n* = 11	
Effective, no, %. yes	28 (35.9)	7 (70.0)	19 (33.3)	2 (18.2)	0.036
No	50 (64.1)	3 (30.0)	38 (66.7)	9 (81.8)	

Conclusion

Polymorphisms of the APOE gene are related to the effects of atorvastatin on lipid lowering and the progression of carotid artery plaques. The population with the ε2 allele experienced a better lipid-lowering effect on LDL-C and slower progression of carotid artery plaques than the population with the ε3 or ε4 allele. Patients with E4 genotype need a higher statin dose or a change to another statin to achieve a better effect. A larger population is required to provide more reliable evidence to explore this relationship.

Data availability statement

The data analyzed in this study is subject to the following licenses/restrictions: The data are available from the corresponding author on reasonable request. Requests to access these datasets should be directed to biqianqian12@163.com.

Ethics statement

The studies involving human participants were reviewed and approved by the Ethics Committee of Shanghai Tenth People's Hospital. The patients/participants provided their written informed consent to participate in this study.

Author contributions

XZ and JW revised the study. QB drafted the manuscript. QB, YL, and YW analyzed and interpreted the data. QB and WF collected the data. XZ and FW contributed to the critical

revision of the manuscript. All authors read and approved the final manuscript.

Funding

This work was supported by the 2020 Health Science and Technology Project of the Pudong New Area Health Commission (No. PW2020D-5), the 2021 Scientific Research Project of Shanghai Municipal Commission of Health and Family Planning (No. 202140282), 2019 Scientific Research Project of Shanghai Science and Technology Commission (No. 19401972803), the 2019 Shanghai Municipal Key Clinical Specialty (No. shslczdzk06102), and the 2020 Science and Technology Development Fund of Pudong New Area Special Fund for People's Livelihood Scientific Research (PKJ2020-Y-15). The content was solely the responsibility of the authors.

Conflict of interest

The authors declare that the research was conducted in the absence of any commercial or financial relationships that could be construed as a potential conflict of interest.

Publisher's note

References

1. Libby P, Buring JE, Badimon L, Hansson GK, Deanfield J, Bittencourt MS, et al. Atherosclerosis. *Nat Rev Dis Primers.* (2019) 5:56. doi: 10.1038/s41572-019-0106-z

2. Amarenco P, Labreuche J. Lipid management in the prevention of stroke: review and updated meta-analysis of statins for stroke prevention. *Lancet Neurol.* (2009) 8:453–63. doi: 10.1016/S1474-4422(09)70058-4

3. Hubacek JA, Vrablik M. Effect of apolipoprotein E polymorphism on statin-induced decreases in plasma lipids and cardiovascular events. *Drug Metabol Drug Interact.* (2011) 26:13–20. doi: 10.1515/DMDI.2011.107

4. Zhang L, He S, Li Z, Gan X, Li S, Cheng X, et al. Apolipoprotein E polymorphisms contribute to statin response in Chinese ASCVD patients with dyslipidemia. *Lipids Health Dis.* (2019) 18:129. doi: 10.1186/s12944-019-1069-5

5. Kirac D, Bayam E, Dagdelen M, Gezmis H, Sarikaya S, Pala S, et al. HMGCR and ApoE mutations may cause different responses to lipid lowering statin therapy. *Cell Mol Biol.* (2017) 63:43–8. doi: 10.14715/cmb/2017.63.10.6

6. Phillips MC. Apolipoprotein E isoforms and lipoprotein metabolism. *IUBMB Life.* (2014) 66:616–23. doi: 10.1002/iub.1314

7. Marais AD. Apolipoprotein E in lipoprotein metabolism, health and cardiovascular disease. *Pathology.* (2019) 51:165–76. doi: 10.1016/j.pathol.2018.11.002

8. Borgaonkar DS, Schmidt LC, Martin SE, Kanzer MD, Edelsohn L, Growdon J, et al. Linkage of late-onset Alzheimer's disease with apolipoprotein E type 4 on chromosome 19. *Lancet.* (1993) 342:625. doi: 10.1016/0140-6736(93)91458-x

9. Seripa D, D'Onofrio G, Panza F, Cascavilla L, Masullo C, Pilotto A. The genetics of the human APOE polymorphism. *Rejuvenation Res.* (2011) 14:491–500. doi: 10.1089/rej.2011.1169

10. Farrer LA, Cupples LA, Haines JL, Hyman B, Kukull WA, Mayeux R, et al. Effects of age, sex, and ethnicity on the association between apolipoprotein E genotype and Alzheimer disease. a meta-analysis. APOE and Alzheimer Disease Meta Analysis Consortium. *JAMA.* (1997) 278:1349–56. doi: 10.1001/jama.278.16.1349

11. Huebbe P, Rimbach G. Evolution of human apolipoprotein E (APOE) isoforms: gene structure, protein function and interaction with dietary factors. *Ageing Res Rev.* (2017) 37:146–61. doi: 10.1016/j.arr.2017.06.002

12. Cai C, Wen Z, Li L. The relationship between ApoE gene polymorphism and the efficacy of statins controlling hyperlipidemia. *Am J Transl Res.* (2021) 13:6772–7.

13. Xi N, Wang Y, Zhou J, Li Y, Ruan S. [Influence of ApoE gene polymorphisms on therapeutic effects of lipid-lowering statins among patients with ischemic cerebral infarction]. *Zhonghua Yi Xue Yi Chuan Xue Za Zhi.* (2022) 39:94–8. doi: 10.3760/cma.j.cn511374-20201104-00775

14. Zintzaras E, Kitsios GD, Triposkiadis F, Lau J, Raman G. APOE gene polymorphisms and response to statin therapy. *Pharmacogenomics J.* (2009) 9:248–57. doi: 10.1038/tpj.2009.25

15. Hu M, Mak VW, Tomlinson B. Polymorphisms in apolipoprotein E and apolipoprotein A-V do not influence the lipid response to rosuvastatin but are associated with baseline lipid levels in Chinese patients with hyperlipidemia. *J Clin Lipidol.* (2012) 6:585–92. doi: 10.1016/j.jacl.2012.02.005

16. Lagos J, Zambrano T, Rosales A, Salazar LA. APOE polymorphisms contribute to reduced atorvastatin response in Chilean Amerindian subjects. *Int J Mol Sci.* (2015) 16:7890–9. doi: 10.3390/ijms16047890

17. Wang YY, Tang XB, Kou L, Wu ZM, Liu H, Wang S, et al. A comparative study of noninvasive imaging in assessing carotid atherosclerotic plaque stability. *Chin J Vasc Surg.* (2017) 2:209–17. doi: 10.1161/STROKEAHA.119.025496

18. Weisgraber KH. Apolipoprotein E distribution among human plasma lipoproteins: role of the cysteine-arginine interchange at residue 112. *J Lipid Res.* (1990) 31:1503–11. doi:

19. Huang Y, Mahley RW. Apolipoprotein E: structure and function in lipid metabolism, neurobiology, and Alzheimer's diseases. *Neurobiol Dis.* (2014) 72:3–12. doi: 10.1016/j.nbd.2014.08.025

20. Hatters DM, Peters-Libeu CA, Weisgraber KH. Apolipoprotein E structure: insights into function. *Trends Biochem Sci.* (2006) 31:445–54. doi: 10.1016/j.tibs.2006.06.008

21. Shafagoj YA, Naffa RG, El-Khateeb MS, Abdulla YL, Al-Qaddoumi AA, Khatib FA, et al. APOE Gene polymorphism among Jordanian Alzheimer's patients with relation to lipid profile. *Neurosciences.* (2018) 23:29–34. doi: 10.17712/nsj.2018.1.20170169

22. Sun Q, Zhou H, Guo LN. ApoE and SLCO1B1 gene polymorphisms and their correlation in dyslipidemia population. *J Mod Lab Med.* (2017) 2017:28–31.

23. Xie L, Hong M, Liu T, Li Q, Duan YP, Feng Y. Analysis of SLCO1B1 and ApoE gene polymorphisms in patients with hyperlipidemia and their correlation with blood lipid levels in patients. *Label Immun Clin Med.* (2019) 2019:1723–8.

24. Zhang Y, Wei DD, Yuan RR, Ge QX, Chen F, Yang SX, et al. [Effects of ApoE gene polymorphism on the efficacy of atorvastatin in the treatment of hyperlipidemia]. *Zhonghua Yi Xue Za Zhi.* (2017) 97:291–4.

25. Pedro-Botet J, Schaefer EJ, Bakker-Arkema RG, Black DM, Stein EM, Corella D, et al. Apolipoprotein E genotype affects plasma lipid response to atorvastatin in a gender specific manner. *Atherosclerosis.* (2001) 158:183–93. doi: 10.1016/s0021-9150(01)00410-5

26. Faubion SS, Kapoor E, Moyer AM, Hodis HN, Miller VM. Statin therapy: does sex matter? *Menopause.* (2019) 26:1425–35. doi: 10.1097/GME.0000000000001412

27. Gonzalez-Aldaco K, Roman S, Torres-Reyes LA, Panduro A. Association of apolipoprotein e2 allele with insulin resistance and risk of type 2 diabetes mellitus among an admixed population of Mexico. *Diabetes Metab Syndr Obes.* (2020) 13:3527–34. doi: 10.2147/DMSO.S268329

28. Rhea EM, Raber J, Banks WA. ApoE and cerebral insulin: trafficking, receptors, and resistance. *Neurobiol Dis.* (2020) 137:104755. doi: 10.1016/j.nbd.2020.104755

29. Pekkala T, Hall A, Mangialasche F, Kemppainen N, Mecocci P, Ngandu T, et al. Association of peripheral insulin resistance and other markers of type 2 diabetes mellitus with brain amyloid deposition in healthy individuals at risk of Dementia. *J Alzheimers Dis.* (2020) 76:1243–8. doi: 10.3233/JAD-200145

30. Corson MA. Phospholipase A2 inhibitors in atherosclerosis: the race is on. *Lancet.* (2009) 373:608–10. doi: 10.1016/S0140-6736(09)60378-0

31. Li B, Li W, Li X, Zhou H. Inflammation: a novel therapeutic target/direction in atherosclerosis. *Curr Pharm Des.* (2017) 23:1216–27. doi: 10.2174/1381612822666161230142931

frontiers | Frontiers in Cardiovascular Medicine

TYPE Original Research
PUBLISHED 21 November 2022
DOI 10.3389/fcvm.2022.1054208

OPEN ACCESS

EDITED BY
Jia Qi,
Shanghai Jiao Tong University, China

REVIEWED BY
Xu De En,
Nanjing Medical University, China
Li Hou,
Affiliated Hospital of Jiangsu University, China

*CORRESPONDENCE
Kan Hong
lindashao99@163.com
Xiaowei Zhu
1766990886@qq.com
Yunyun Zhang
zhangyunyun026133@126.com

†These authors have contributed equally to this work and share first authorship

SPECIALTY SECTION
This article was submitted to General Cardiovascular Medicine, a section of the journal Frontiers in Cardiovascular Medicine

RECEIVED 26 September 2022
ACCEPTED 07 November 2022
PUBLISHED 21 November 2022

CITATION
Lu S, Xu Q, Yu J, Yang Y, Wang Z, Zhang B, Wang S, Chen X, Zhang Y, Zhu X and Hong K (2022) Prevalence and possible factors of cognitive frailty in the elderly with hypertension and diabetes.
Front. Cardiovasc. Med. 9:1054208.
doi: 10.3389/fcvm.2022.1054208

Prevalence and possible factors of cognitive frailty in the elderly with hypertension and diabetes

Shourong Lu[1†], Qiao Xu[1†], Jie Yu[1], Ying Yang[1], Zhuo Wang[1], Bingshan Zhang[1], Shuqiang Wang[2], Xiaorong Chen[2], Yunyun Zhang[3*], Xiaowei Zhu[4*] and Kan Hong[1*]

[1]Department of Geriatric, The Affiliated Wuxi People's Hospital of Nanjing Medical University, Wuxi, China, [2]Department of Medicine, Wuxi Xin'an Community Health Service Center, Wuxi, China, [3]Department of General Practice, The Affiliated Wuxi People's Hospital of Nanjing Medical University, Wuxi, China, [4]Department of Endocrinology, The Affiliated Wuxi People's Hospital of Nanjing Medical University, Wuxi, China

Background: Cognitive frailty is the coexistence of physical frailty and mild cognitive impairment. Research shows that cognitive frailty is related to an increased risk of hospitalization, mortality, disability, and dementia. Diabetes and hypertension are common risk factors for physical frailty and cognitive impairment. However, the factors influencing cognitive frailty in the elderly with hypertension and diabetes are still unclear. This study aimed to investigate the possible factors influencing cognitive frailty in the elderly with hypertension and diabetes.

Methods: A cross-sectional study was conducted. We evaluated people over 60 years with hypertension and diabetes who underwent physical examination in Wuxi Xin'an Community Health Service Center. Frail scale, Montreal Cognitive Assessment-Basic and clinical dementia rating were used to assess cognitive frailty. We collected demographic characteristics, hypertension and diabetes-related laboratory indicators of the participants. We also used various scales to assess the overall health status of the elderly.

Results: Approximately 20.8% of the participants were determined to have cognitive frailty in elderly adults with hypertension and diabetes. These participants were older, had a lower monthly income, and included a higher proportion of peasants. They also had a higher level of depression ($p = 0.037$), higher risk of falls ($p = 0.000$), higher risk of malnutrition ($p = 0.002$), poorer ability to perform activities of daily living (ADL) ($p = 0.000$), and less social support ($p = 0.030$). Multivariate regression analysis was used to further assess the factors for cognitive frailty. After adjusting for possible confounders, age and ADL score emerged as risk factors, whereas high monthly income decreased the risk of cognitive frailty.

Conclusion: Cognitive frailty is correlated with age, income, and ability to perform daily living activities in the elderly with diabetes and hypertension. Closer attention to the elderly who have low income and poor self-care ability may play an important role in the early prevention of cognitive frailty and even dementia.

KEYWORDS

diabetes, hypertension, cognitive frailty, elderly, activities of daily living

Introduction

Cognitive frailty, defined as the co-existence of physical frailty and cognitive impairment, has recently attracted increasing attention. The term "cognitive frailty" was coined by experts in 2013 (1). However, its definition has never been well-established. Researchers in different regions of the world have different definitions. Assessment scales are also different. The Fried scale and Frail scale are commonly used to evaluate physical frailty. Montreal Cognitive Assessment (MoCA) scale and Mini-Mental State Examination (MMSE) scale are commonly used in cognitive assessment. Ruan et al. (2) classify cognitive frailty into two types: reversible and potentially reversible. This study considered the latter definition. It is defined by the presence of physical frailty or prefrailty and cognitive impairment, excluding dementia, caused by various reasons (2). The prevalence of cognitive frailty in community settings is 1.2 to 7.7%, which increases to 20% in nursing centers and inpatient departments (3–6).

Cognitive frailty is closely associated with a higher risk of hospitalization, death, and disability (7, 8). It is also a strong predictor of overall dementia and vascular dementia (9). Thus, early intervention for the population with cognitive frailty can help prevent dementia and other aggravations. As we all know, cognitive frailty is strongly correlated with multiple factors. Panza et al. mentioned some possible neurobiological mechanisms underlying cognitive frailty, including vascular diseases, sarcopenia, metabolic disorders, nutritional status, psychological factors and inflammatory status (10). Due to reduced ability of activities and decline of brain function, the prevalence of cognitive frailty increases with age (11). Weight loss and vitamin deficiency may lead to physical frailty. Several studies have shown that the incidence of malnutrition is extremely high among elderly people with cognitive frailty (12–14). In addition, level of education is strongly associated with cognitive decline. The longer the years of education, the slower the cognitive decline (15, 16). Older adults with depression are more likely to develop cognitive frailty (17). Liu et al. indicates that moderate physical activities for 1 year can reduce the progression of cognitive frailty in sedentary older adults (18).

Hypertension and diabetes, the most common chronic diseases worldwide (19, 20), have been considered risk factors for physical frailty (21, 22) and cognitive impairment (23, 24). Thus, more attention should be paid to older adults with hypertension and diabetes. This study aimed to investigate the risk factors of cognitive frailty in the elderly with hypertension and diabetes.

Materials and methods

Participants and data collection

A cross-sectional study was conducted in Wuxi Xin'an Community Health Service Center from April 2018 to May 2018. Participants included older adults with diabetes and hypertension.

Inclusion criteria: 1. aged over 60; 2. previous diagnosis of hypertension and diabetes.

Exclusion criteria: 1. dementia; 2. severe hepatic and renal insufficiency; 3. failure to cooperate in the assessment using various scales.

The demographic and clinical variables included age, gender, occupation, education level, income per month, smoking history, and drinking history. Serum albumin, calcium, 25- hydroxy Vitamin D, triglycerides (TG), low-density lipoprotein cholesterol (LDL), high-density lipoprotein cholesterol (HDL), homocysteine, folic acid, Vitamin B12, fasting plasma glucose, fasting insulin, and HbA1c levels were assessed by the Laboratory Center of Wuxi People's Hospital.

Assessment of cognitive function

Montreal Cognitive Assessment-Basic (MoCA-B) was used to evaluate cognitive function. MoCA-B score <26 and clinical dementia rating (CDR) = 0.5 (excluding dementia) indicated mild cognitive impairment.

Other evaluation scales

The 5-item Frail scale was used to assess physical frailty. Frail score ≥1 indicated physical frailty, with a higher score showing a higher level of frailty. The Mini-Nutrition Assessment-Short Form (MNA-SF) evaluated the nutritional status of the participants. MNA-SF scores <8, 8–11, and >11 indicated malnutrition, risk of nutrition, and no malnutrition, respectively. The Geriatric Depression Scale 15-item (GDS-15) assessed the psychological health of participants, with a higher score indicating severe depression. The 10-item Social Support Rating Scale (SSRS) evaluated support from themselves, others and society. A higher total score indicated better social support. The Morse Fall Scale (MFS) was used to assess participants' risk of falling, with MFS scores <25, 25–45, and >45 indicating low risk, medium risk, and high risk, respectively. The ability to perform activities of daily living (ADL) was assessed at two levels. The basic activities of daily living scale (BADL) assessed skills including eating, dressing, grooming, bathing, going to the toilet, and walking; the instrumental activities of daily living scale (IADL) evaluated skills such as making phone calls, shopping, preparing meals, doing housework, washing clothes, taking public transport, taking drugs, and money management. A score >14 showed functional decline, with a higher score indicating decreased ability to perform daily living activities.

Statistical analysis

All variables were tested for normal distribution. Student *t*-test, Mann-Whitney U test, and Chi-square test were conducted to compare the variables between groups. Continuous variables with normal distribution were presented as mean with standard deviation. Continuous variables with non-normal distribution were presented as median with quartile, and categorical variables as percentages. The multivariate logistic regression analysis was also performed. SPSS 22.0 software was used for data analysis, and $p < 0.05$ was considered statistically significant.

Results

A total of 154 participants were enrolled, including 91 females (59.1%), 98 with a primary level or below education (63.6%), and 122 non-drinkers (79.2%). After the assessment, 32 (20.8%) were determined to have cognitive frailty. These participants were older, had a lower monthly income, and included a higher proportion of peasants. Participants with cognitive frailty also had higher scores of GDS-15 ($p = 0.037$), higher risk of malnutrition ($p = 0.002$), higher fall risk ($p = 0.000$), higher ADL score ($p = 0.000$), poorer daily living ability ($p = 0.000$), and less social support ($p = 0.030$) (Table 1). The participants between the two groups did not differ in laboratory indexes, such as lipid levels, albumin, calcium, 25-hydroxy Vitamin D, homocysteine, folic acid, Vitamin B12, fasting plasma glucose, fasting insulin, and HbA1c level.

After adjusting for education level, status of nutrition, GDS-15, age and ADL score were risk factors for cognitive frailty. After adjusting for age, social support, ADL score, Morse Fall score, GDS-15 score, MNA-SF score, income, and occupation in Table 2, the risk of cognitive frailty increased significantly with age (OR = 1.164, 95% CI: 1.022–1.326, $p < 0.05$) and ADL score (OR = 1.308, 95% CI: 1.024–1.670, $p < 0.05$), and decreased significantly with monthly income (OR = 0.237, 95% CI: 0.059–0.955, $p < 0.05$).

Discussion

Recently, comprehensive geriatric assessment has been attracting increasing attention in China. In this study, we screened the associated factors of mild cognitive impairment and physical frailty in the elderly by reviewing relevant literature. We evaluated the nutritional status, depression level, social support, demographic and clinical characteristics, lipid levels, blood glucose levels, and other indicators of the recruited population. This was the first study to investigate the influencing factors of cognitive frailty in the elderly with hypertension and diabetes. Cognitive frailty can progress to various forms of dementia (25–27), thus increasing the risk of hospitalization, falls, and death (28–30). About 20.8% of the participants were

TABLE 1 Demographic and baseline characteristics of participants.

	Non–cognitive frailty ($n = 122$)	Cognitive frailty ($n = 32$)	P value
Demographics			
Age (years)[a]	68.0(65.0–72.0)	70.0(69.0–73.8)	**0.001**
Gender			0.212
Male (*n*, %)	53 (43.4)	10 (31.2)	
Female (*n*, %)	69 (56.6)	22 (68.8)	
Duration of hypertension			0.194
≤10 years (*n*, %)	80 (65.6)	17 (53.1)	
>10 years (*n*, %)	42 (34.4)	15 (46.9)	
Duration of diabetes			0.606
<10 years (*n*, %)	71 (58.2)	17 (53.1)	
≥10 years (*n*, %)	51 (41.8)	15 (46.9)	
Education level			0.056
Primary or below (*n*, %)	73 (59.8)	25 (78.1)	
Secondary or above (*n*, %)	49 (40.2)	7 (21.9)	
Income (RMB/month)			**0.000**
<1,000 (*n*, %)	60 (49.2)	27 (84.4)	
≥1,000 (*n*, %)	62 (50.8)	5 (15.6)	
Occupation			**0.012**
Retiree (*n*, %)	48 (39.3)	5 (15.6)	
Peasant (*n*, %)	74 (60.7)	27 (84.4)	
Smoking			0.532
Smoker (*n*, %)	21 (65.6)	11 (34.4)	
Non–smoker (*n*, %)	87 (71.3)	35 (28.7)	
Drinking			0.250
Yes (*n*, %)	23 (18.9)	9 (28.1)	
No (*n*, %)	99 (81.1)	23 (71.9)	
Scales			
MNA–SF[a]	11.0(11.0–13.0)	10.5(9.0–11.0)	**0.002**
GDS−15[a]	1.0(0.0–2.0)	2.0(0.0–4.0)	**0.037**
SSRS	39.6±7.0	36.7±5.9	**0.030**
ADL[a]	14.0(14.0–14.0)	15.0(15.0–18.0)	**0.000**
MFS[a]	35.0(35.0–35.0)	35.0(35.0–56.3)	**0.000**
Laboratory indexes			
Albumin (g/L)	45.4±2.6	44.7±3.3	0.296
Calcium (mmol/L)[a]	1.18(1.14–1.21)	1.17(1.13–1.22)	0.331
25–Vitamin D (ng/mL)[a]	20.1(15.5–24.5)	18.5(12.9–21.8)	0.120
Homocysteine (umol/L)[a]	17.9±4.1	18.5±4.0	0.507
Folic acid (nmol/L)[a]	31.4(23.7–41.9)	31.9(24.7–41.2)	0.883
Vitamin B12 (pmol/L)[a]	281.0(208.0–356.5)	285.0(174.3–400.8)	0.982
TG (mmol/L)[a]	1.46(1.11–2.36)	1.67(1.09–2.36)	0.956
LDL (mmol/L)[a]	2.16(1.75–2.86)	2.33(1.73–2.84)	0.640
HDL (mmol/L)[a]	1.05(0.85–1.34)	1.09(0.77–1.25)	0.745
FPG (mmol/L)[a]	7.9(6.8–9.1)	8.1(7.0–9.2)	0.513
FI (mU/L)[a]	10.8(7.3–16.7)	14.5(8.7–16.1)	0.181
HbA1C (%)[a]	6.7(6.0–7.9)	6.3(5.8–8.8)	0.167

MNA-SF, Mini-Nutrition Assessment-Short Form; GDS-15, Geriatric Depression Scale 15-item; SSRS, Social Support Rating Scale; ADL, Activities of Daily Living; MFS, Morse Fall Scale; TG: triglycerides, LDL, low-density lipoprotein cholesterol; HDL, high-density lipoprotein cholesterol; FPG, fasting plasma glucose; FI, fasting insulin. Data are presented as %(n), mean ±SD and median (25^{th}-75th percentile). [a]Compared by Mann-Whitney U test.
The bold values mean $p < 0.05$.

TABLE 2 Multivariate regression analysis using cognitive frailty as the dependent variable.

Model 1	Adjusted OR	P value	95% Confidence interval	
			Lower bound	Upper bound
Age	1.151	**0.021**	1.021	1.298
Education level	0.422	0.110	0.147	1.215
MNA-SF	0.832	0.214	0.623	1.112
GDS-15	1.248	**0.049**	1.001	1.557
ADL	1.434	**0.004**	1.124	1.831
Model 2				
Age	1.164	**0.022**	1.022	1.326
MNA-SF	0.867	0.360	0.640	1.176
Occupation	0.759	0.713	0.175	3.297
Income	0.237	**0.043**	0.059	0.955
MFS	1.037	0.218	0.979	1.100
SSRS	0.997	0.940	0.924	1.076
GDS-15	1.190	0.151	0.938	1.510
ADL	1.308	**0.032**	1.024	1.670

MNA-SF, Mini-Nutrition Assessment-Short Form; MFS, Morse Fall Scale; SSRS, Social Support Rating Scale; GDS-15, Geriatric Depression Scale 15-item; ADL, Activities of Daily Living. Adjusted OR, Adjusted odds ratio. Model 1: adjusted for age, education level, MNA-SF, GDS-15, ADL. Model 2: adjusted for age, MNA-SF, MFS, occupation, income, MFS, SSRS, GDS-15, ADL.
The bold values mean $p < 0.05$.

determined to have cognitive frailty in this study, a number higher than that previously reported (31). This may be explained by the fact that the participants in this study had multiple chronic diseases. Mone et al. (32) suggest that hypertension and diabetes, which are associated with endothelial dysfunction, inflammation, and oxidative stress, can lead to cognitive frailty. Furthermore, adults with cognitive frailty in this study were older, had a lower income, and were mainly peasants with a high risk of malnutrition, less social support, higher ADL score, and a high risk of falling. Moreover, age, income, and ADL score were significantly associated with cognitive frailty, even after adjusting for other possible influencing factors.

Age was found to be the most common risk factor for cognitive frailty, which is consistent with the study of Kim et al. and Mone et al. (33, 34). High-income people may have a stronger awareness of chronic disease management and could intervene in the early stage of the disease. The terms physical frailty, cognitive impairment, and cognitive frailty have partially overlapped in definitions. Several studies have investigated the effects of ADL on people with cognitive frailty, but the assessment methods of ADL in other study are different. IADL has been shown as a risk factor for physical frailty and cognitive impairment. Research also shows that physical disability, indicated by lower performance in BADL (assessed by the Katz index), is a risk factor for cognitive frailty (11, 35–37). Ma et al. (38) showed that cognitive frailty can increase the risk of BADL disability by over ten times during a 3-year follow-up in the elderly compared to robust adults. As Avila-Funes et al. (39) supported, people with cognitive frailty tended to develop ADL dependence. They used internationally recognized scales to assess BADL and IADL dependence. In the present study, the risk of ADL dependence in participants with cognitive frailty was significantly greater than in those without cognitive frailty.

There was no statistical significance in the education level between the two groups in this study, which might be associated with the distribution of education level of our individuals. More participants were primary or lower education level in our study. However, after adjusted for education level, MNA-SF, GDS-15, age and ADL score still significantly increased risk of cognitive frailty. Previous studies suggested that cognitive frailty could be improved with nutritional interventions, muscle exercise, resistance training, and fall avoidance (17, 40). Our study also suggested that improving the ability to perform daily living activities may reduce the prevalence of cognitive frailty in the elderly population. Age is an irreversible factor. With increasing age, more attention should be paid to people with hypertension and diabetes at lower income levels and lower ability of daily living.

There are several limitations of this study. First, the study had a relatively small sample size. Future research should include a bigger sample population. Second, this was a cross-sectional study, and follow-up is required to confirm the findings. Finally, the groups of physical frailty and mild cognitive impairment only should be constructed.

Furthermore, we can screen people at a high risk of cognitive frailty based on ADL assessment quickly. Future research should focus on improving the level of ADL, which may be beneficial in reducing the prevalence of cognitive frailty.

Conclusion

Cognitive frailty is correlated with age, monthly income, and ability to perform daily living activities in the elderly with hypertension and diabetes. For the elderly with low income and poor self-care ability, early intervention for cognitive frailty should be carried out. We will next investigate the effects of these interventions on early dementia.

Data availability statement

The raw data supporting the conclusions of this article will be made available by the authors, without undue reservation.

Ethics statement

The studies involving human participants were reviewed and approved by Ethics Committee of the Wuxi People's Hospital. The patients/participants provided their written informed consent to participate in this study.

Author contributions

KH, XZ, YZ, and SL designed the research. SL, QX, JY, YY, ZW, BZ, SW, and XC helped with the data collection and analysis. SL and QX wrote the first draft of the manuscript. KH, XZ, and YZ contributed to the critical revision of the manuscript. All authors contributed to the manuscript revision and approved the submitted version.

Funding

This work was funded by the Young Project of the Wuxi Health Committee (Q201914), the Top Talent Support Program for Young and Middle-Aged People of Wuxi Health (BJ2020008), and the Major Project of the Wuxi Health Committee (Z202002).

Acknowledgments

We thank the study participants and the clinical staff for their support and contribution to this study.

Conflict of interest

The authors declare that the research was conducted in the absence of any commercial or financial relationships that could be construed as a potential conflict of interest.

The reviewer XE declared a shared affiliation with the authors SL, QX, JY, YY, ZW, BZ, YZ, XZ, and KH to the handling editor at the time of review.

Publisher's note

References

1. van Kan GA, Ousset PJ, Gillette-Guyonnet S, Abellan Van Kan G, Ousset PJ, Doto ME, et al. Cognitive frailty: Rational and definition from an(IANA/IAGG) international consensus group. *J Nutr Health Aging.* (2013) 17:726–34. doi: 10.1007/s12603-013-0367-2

2. Ruan QW, Yu ZW, Chen M, Bao ZJ, Li J, He W. Cognitive frailty, a novel target for the prevention of elderly dependency. *Ageing Res Rev.* (2015) 20:1–10. doi: 10.1016/j.arr.2014.12.004

3. Shimada H, Makizako H, Lee S, Doi T, Lee S, Tsutsumimoto K, et al. Impact of cognitive frailty on daily activities in older persons. *J Nutr Health Aging.* (2016) 20:729–35. doi: 10.1007/s12603-016-0685-2

4. Rajab NF, Singh DKA, Che Din N, Mahadzir H, Ishak WS, Sahar S, et al. Incidence and predictors of cognitive frailty among older adults: a community-based longitudinal study. *Int J Environ Res Public Health.* (2020) 17:1547. doi: 10.3390/ijerph17051547

5. Roppolo M, Mulasso A, Rabaglietti E. Cognitive frailty in Italian community dwelling older adults: prevalence rate and its association with disability. *J Nutr Health Aging.* (2016) 21:631–6. doi: 10.1007/s12603-016-0828-5

6. Sugimoto T, Sakurai T, Ono R, Kimura A, Saji N, Niida S, et al. Epidemiological and clinical significance of cognitive frailty: a mini review. *Ageing Res Rev.* (2018) 44:1–7. doi: 10.1016/j.arr.2018.03.002

7. Lee WJ, Peng LN, Liang CK, Loh CH, Chen LK. Cognitive frailty predicting all-cause mortality among community-living older adults in Taiwan: a 4-year nationwide population-based cohort study. *PLoS ONE.* (2018) 13:e0200447. doi: 10.1371/journal.pone.0200447

8. St John PD, Tyas SL, Griffith LE, Menec V. The cumulative effect of frailty and cognition on mortality - results of a prospective cohort study. *Int Psychogeriatr.* (2016) 29:535–43. doi: 10.1017/S1041610216002088

9. Solfrizzi V, Scafato E, Seripa D, Lozupone M, Imbimbo BP, D'Amato A, et al. Reversible cognitive frailty, dementia, and all-cause mortality. the italian longitudinal study on aging. *J Am Med Dir Assoc.* (2017) 18:89e1–e8. 10.1016/j.jamda.2016.10.012. doi: 10.1016/j.jamda.2016.10.012

10. Panza F, Lozupone M, Solfrizzi V, Sardone R, Dibello V, Di Lena L, et al. Different cognitive frailty models and health- and cognitive-related outcomes in older age: from epidemiology to prevention. J *Alzheimers Dis.* (2018) 62:993–1012. doi: 10.3233/JAD-170963

11. Malek Rivan NF, Shahar S, Rajab NF, Singh DKA, Din NC, Hazlina M, et al. Cognitive frailty among Malaysian older adults: baseline findings from the LRGS TUA cohort study. *Clin Interv Aging.* (2019) 14:1343–52. doi: 10.2147/CIA.S211027

12. Chye L, Wei K, Nyunt MSZ, Gao Q, Wee SL, Ng TP. Strong relationship between malnutrition and cognitive frailty in the Singapore longitudinal

ageing studies (SLAS-1 and SLAS-2). *J Prev Alzheimers Dis.* (2018) 5:1–7. doi: 10.14283/jpad.2017.46

13. Dominguez LJ, Barbagallo M. The relevance of nutrition for the concept of cognitive frailty. *Curr Opin Clin Nutr Metab Care.* (2017) 20:61–8. doi: 10.1097/MCO.0000000000000337

14. Seesen M, Sirikul W, Ruangsuriya J, Griffiths J, Siviroj P. Cognitive frailty in Thai community-dwelling elderly: prevalence and its association with malnutrition. *Nutrients*. (2021) 13: 4239. doi: 10.3390/nu13124239

15. Brigola AG, Alexandre TDS, Inouye K, Yassuda MS, Pavarini SCI, Mioshi E. Limited formal education is strongly associated with lower cognitive status, functional disability and frailty status in older adults. *Dement Neuropsychol.* (2019) 13:216–24. doi: 10.1590/1980-57642018dn13-020011

16. Zahodne LB, Stern Y, Manly JJ. Differing effects of education on cognitive decline in diverse elders with low versus high educational attainment. *Neuropsychology*. (2015) 29:649–57. doi: 10.1037/neu0000141

17. Kwan RYC, Leung AYM. Yee A, Lau LT, Xu XY, Dai DLK, et al. Cognitive frailty and its association with nutrition and depression in community-dwelling older people. *J Nutr Health Aging.* (2019) 23:1–6. doi: 10.1007/s12603-019-1258-y

18. King AC, Liu CK, Manini TM. Effect of 24-month physical activity on cognitive frailty and the role of inflammation: the LIFE randomized clinical trial. *BMC Med.* (2018) 16:185. doi: 10.1186/s12916-018-1174-8

19. Draznin B, Aroda VR, Bakris G, Benson G, Brown FM, Freeman R, et al. Diabetes care in the hospital: standards of medical care in diabetes-2022. *Diab Care*. (2022)45(Suppl 1):S244–253. doi: 10.2337/dc22-S016

20. Ida S, Kaneko R, Imataka K, Murata K. Relationship between frailty and mortality, hospitalization, and cardiovascular diseases in diabetes: a systematic review and meta-analysis. *Cardiovasc Diabetol*. (2019) 18:1–13. doi: 10.1186/s12933-019-0885-2

21. Clegg A, Hassan-Smith Z. Frailty and the endocrine system. *Lancet Diabetes Endocrinol*. (2018) 6:743–52. doi: 10.1016/S2213-8587(18)30110-4

22. Pulgrossi RC, Biella MM, Izbicki R, Torres LM, Biella MM, et al. Hypertension and frailty in older adults. *J Clin Hypertens*. (2018) 20:186–92. doi: 10.1111/jch.13135

23. Ganmore I, Elkayam I, Ravona-Springer R, Lin HM, Liu X, Plotnik M, et al. Deterioration in motor function over time in older adults with type 2 diabetes is associated with accelerated cognitive decline. *Endocr Pract*. (2020) 26:1143–52. doi: 10.4158/EP-2020-0289

24. Chan YH, Lim JY, Vellas B. Slow gait, subjective cognitive decline and motoric cognitive RISK syndrome: prevalence and associated factors in community dwelling older adults. *J Nutr Health Aging.* (2021) 25:48–56. doi: 10.1007/s12603-020-1525-y

25. Muir Hunter SW, Doherty TJ, Duque G. Disentangling cognitive-frailty: results from the gait and brain study. *J Gerontol A Biol Sci Med Sci*. (2016) 71:1476–82. doi: 10.1093/gerona/glw044

26. Zheng L, Li G, Gao D, Wang S, Meng X, Wang C, et al. Cognitive frailty as a predictor of dementia among older adults: a systematic review and meta-analysis. *Arch Gerontol Geriatr*. (2020) 87:103997. doi: 10.1016/j.archger.2019.103997

27. Kojima G, Taniguchi Y, Iliffe S, Walters, K. Frailty as a predictor of Alzheimer disease, vascular dementia, and all dementia among community-dwelling older people: a systematic review and meta-analysis. *J Am MedDirect Assoc.* (2016) 17:881–8. doi: 10.1016/j.jamda.2016.05.013

28. Yu R, Morley JE, Kwok T, Leung J, Cheung O, Woo J. The effects of combinations of cognitive impairment and pre-frailty on adverse outcomes from a prospective community-based cohort study of older Chinese people. *Front Med.* (2018) 5:1–11. doi: 10.3389/fmed.2018.00050

29. Rivan NFM, Singh DKA, Shahar S, Wen GJ, Rajab NF, Din NC, et al. Cognitive frailty is a robust predictor of falls, injuries, and disability among community-dwelling older adults. *BMC Geriatr*. (2021) 21:593. doi: 10.1186/s12877-021-02525-y

30. Bu ZH, Huang AL, Xue MT, Li QY, Bai YM, Xu GH, et al. Cognitive frailty as a predictor of adverse outcomes among older adults: a systematic review and meta-analysis. *Brain Behav.* (2021) 11:e01926. doi: 10.1002/brb3.1926

31. Shimada H, Makizako H, Tsutsumimoto K, Doi T, Lee S, Suzuki T. Cognitive frailty and incidence of dementia in older persons. *J Prev Alzheimers Dis*. (2018) 5:42–8. doi: 10.14283/jpad.2017.29

32. Mone P, Gambardella J, Lombardi A, Pansini A, De Gennaro S, Leo AL, et al. Correlation of physical and cognitive impairment in diabetic and hypertensive frail older adults. *Cardiovasc Diabetol.* (2022) 21:1–6. doi: 10.1186/s12933-021-01442-z

33. Kim H, Awata S, Watanabe Y, Kojima N, Osuka Y, Motokawa K, et al. Cognitive frailty in community-dwelling older Japanese people: prevalence and its association with falls. *Geriatr Gerontol Int*. (2019) 19:647–53. doi: 10.1111/ggi.13685

34. Mone P, Gambardella J, Pansini A, de Donato A, Martinelli G, Boccalone E, et al. Cognitive impairment in frail hypertensive elderly patients: role of hyperglycemia. *Cells*. (2021) 10:2115. doi: 10.3390/cells10082115

35. Aliberti MJR, Cenzer IS, Smith AK, Lee SJ, Yaffe K, Covinsky KE. Assessing risk for adverse outcomes in older adults: The need to include both physical frailty and cognition. *J Am Geriatr Soc.* (2019) 67:477–83. doi: 10.1111/jgs.15683

36. Feng L, Zin Nyunt MS, Gao Q, Feng L, Yap KB, Ng TP, et al. Cognitive frailty and adverse health outcomes: findings from the Singapore longitudinal ageing studies (SLAS). *J Am Med Dir Assoc*. (2017) 18:252–8. doi: 10.1016/j.jamda.2016.09.015

37. Won CW, Lee Y, Kim S, Yoo J, Kim M, Ng TP, et al. Modified criteria for diagnosing "cognitive frailty". *Psychiatry Investig*. (2018) 15:839–42. doi: 10.30773/pi.2018.05.22

38. Ma YJ, Li XD, Pan Y, Zhao R, Wang X, Jiang X, et al. Cognitive frailty predicting death and disability in Chinese elderly. *Neurol Res.* (2021) 43:1–9. doi: 10.1080/01616412.2021.1939235

39. Avila-Funes JA, Amieva H, Barberger-Gateau P, Le Goff M, Raoux N, Ritchie K, et al. Cognitive impairment improves the predictive validity of the phenotype of frailty for adverse health outcomes: the three-city study. *J Am Geriatr Soc*. (2009) 57:453–61. doi: 10.1111/j.1532-5415.2008.02136.x

40. Sternberg SA, Wershof Schwartz A, Karunananthan S,Bergman H, Mark Clarfield A. The identification of frailty: a systematic literature review. *J Am Geriatr Soc*. (2011) 59:2129–38. doi: 10.1111/j.1532-5415.2011.03597.x

frontiers | Frontiers in Cardiovascular Medicine

TYPE Mini Review
PUBLISHED 21 December 2022
DOI 10.3389/fcvm.2022.1070935

OPEN ACCESS

EDITED BY
Jintao Wang,
National Heart, Lung, and Blood Institute (NIH), United States

REVIEWED BY
Yunhui Du,
Beijing Institute of Heart, Capital Medical University, China

*CORRESPONDENCE
Rodrigo Del Rio
rdelrio@bio.puc.cl

SPECIALTY SECTION
This article was submitted to General Cardiovascular Medicine, a section of the journal Frontiers in Cardiovascular Medicine

RECEIVED 15 October 2022
ACCEPTED 17 November 2022
PUBLISHED 21 December 2022

CITATION
Saavedra-Alvarez A, Pereyra KV, Toledo C, Iturriaga R and Del Rio R (2022) Vascular dysfunction in HFpEF: Potential role in the development, maintenance, and progression of the disease.
Front. Cardiovasc. Med. 9:1070935.
doi: 10.3389/fcvm.2022.1070935

Vascular dysfunction in HFpEF: Potential role in the development, maintenance, and progression of the disease

Andrea Saavedra-Alvarez[1], Katherine V. Pereyra[1], Camilo Toledo[1], Rodrigo Iturriaga[1,2,3] and Rodrigo Del Rio[1,2,3]*

[1]Laboratory of Cardiorespiratory Control, Department of Physiology, Pontificia Universidad Católica de Chile, Santiago, Chile, [2]Centro de Excelencia en Biomedicina de Magallanes (CEBIMA), Universidad de Magallanes, Punta Arenas, Chile, [3]Facultad de la Salud, Centro de Investigación en Fisiología y Medicina de Altura (MedAlt), Universidad de Antofagasta, Antofagasta, Chile

Heart failure with preserved ejection fraction (HFpEF) is a complex, heterogeneous disease characterized by autonomic imbalance, cardiac remodeling, and diastolic dysfunction. One feature that has recently been linked to the pathology is the presence of macrovascular and microvascular dysfunction. Indeed, vascular dysfunction directly affects the functionality of cardiomyocytes, leading to decreased dilatation capacity and increased cell rigidity, which are the outcomes of the progressive decline in myocardial function. The presence of an inflammatory condition in HFpEF produced by an increase in proinflammatory molecules and activation of immune cells (i.e., chronic low-grade inflammation) has been proposed to play a pivotal role in vascular remodeling and endothelial cell death, which may ultimately lead to increased arterial elastance, decreased myocardium perfusion, and decreased oxygen supply to the tissue. Despite this, the precise mechanism linking low-grade inflammation to vascular alterations in the setting of HFpEF is not completely known. However, the enhanced sympathetic vasomotor tone in HFpEF, which may result from inflammatory activation of the sympathetic nervous system, could contribute to orchestrate vascular dysfunction in the setting of HFpEF due to the exquisite sympathetic innervation of both the macro and microvasculature. Accordingly, the present brief review aims to discuss the main mechanisms that may be involved in the macro- and microvascular function impairment in HFpEF and the potential role of the sympathetic nervous system in vascular dysfunction.

KEYWORDS

inflammation, oxidative stress, heart failure, vascular dysfunction, preserved ejection fraction heart failure (HFpEF)

Introduction

Heart failure (HF) is a pathological condition affecting mainly the elderly population. A subcategory of this disease is HF with preserved ejection fraction (HFpEF), whose incidence has increased notably in recent years, particularly in the last two decades, from 48 to 57% compared with systolic HF (or reduced ejection fraction HF). Furthermore, HFpEF accounts for the death of 1 in 8 people over 65 years (1). Patients with HFpEF have a poor quality of life, high medical costs, and early death (2). Then, understanding the pathophysiology of HFpEF is relevant for future therapeutic strategies to improve HFpEF outcomes.

Patients with HFpEF display several comorbidities associated with cardiac and vascular disturbances, including but not limited to diabetes mellitus, obesity, pulmonary hypertension, coronary artery disease, chronic renal failure, and systemic inflammation (1), all of which contribute to endothelial dysfunction, cardiomyocyte hypertrophy, and cardiac fibrosis (2, 3). Furthermore, it has been described that autonomic imbalance, a hallmark of HF independent of its etiology (i.e., reduced or preserved EF), plays a key role in disease progression (4). Indeed, patients with HF showing sustained elevations in systemic circulating levels of catecholamines (i.e., norepinephrine) show higher mortality rates (5). Importantly, evidence indicates that the sympathetic nervous system (SNS) is critically influenced, at the central and peripheral levels, by the most relevant factors regulating vascular function, such as nitric oxide (NO), reactive oxygen species (ROS), endothelin 1 (ET-1), and the renin-angiotensin system (RAS). Then, a bidirectional and maladaptive relationship between endothelial function and hyperactivity of the SNS could play a role in short- and long-term vascular dysfunction in HFpEF. Indeed, autonomic imbalance in HFpEF increases sympathetic vasomotor tone (6). The latter results in increased excitatory sympathetic activity to blood vessels changing the balance between vasodilator and vasoconstrictor molecules that regulate endothelial cell function and therefore, cardiovascular integrity (7). In this review, we will focus on the main factors that may contribute to the development/maintenance of vascular cell dysfunction and their potential link to enhanced sympatho-vasomotor tone in the setting of HFpEF.

Relevance of vascular dysfunction in HFpEF

Endothelium-dependent coronary microvascular dysfunction is present in approximately 30% of patients with HFpEF (8). In addition, more than 30% of patients with HFpEF display endothelium-independent dysfunction, reflected in significant reductions in coronary flow reserve (CFR) (8). Indeed, patients with HFpEF present vascular-ventricular uncoupling and stiffness, which is associated with decreased exercise capacity (9). Accordingly, acute increases in cardiac afterload, in the setting of arterial-ventricular stiffness, lead to increases in arterial blood pressure that impairs diastolic relaxation and increases filling pressures during exercise (10). The specific mechanisms associated with the changes in arterial elastance during HFpEF are not fully elucidated, but they have been associated with blood vessels alterations in the bioavailability and responses to vasoactive molecules such as ET-1 and NO (11, 12).

In addition to systemic functional alterations in the vasculature, a reduction in myocardial microvascular density, called microvascular *rarefaction*, is observed in patients with HFpEF (13). Microvascular *rarefaction* contributes to cardiac perfusion failure by decreasing myocardial oxygen delivery in patients with HFpEF (14). Therefore, *rarefaction* of resistance vessels, including small arteries and arterioles, increases coronary microvascular resistance, resulting in reduced cardiac perfusion (15), which has been proposed as a pathogenic mechanism involved in the progressive decline in cardiac function in HFpEF (15). The precise mechanism(s) underpinning vascular *rarefaction* in HFpEF is still not completely known; however, due to the exquisite sympathetic regulation of blood vessels, and the fact that sympathoexcitation occurs in HFpEF, it is plausible that enhanced sympatho-vasomotor tone may play a role in vascular *rarefaction* by changing the vasoconstrictor to vasodilator balance in the vessel microenvironment (Figure 1).

To the best of our knowledge, there is no comprehensive literature providing mechanistic insights into macrovasculature changes in HFpEF. Macrovascular arterial stiffness results in an increase in pulse pressure and wave velocity, which impairs normal microvascular function (16). The latter is particularly relevant for the coronary and renal microvasculature since pathological alterations in pulse pressure and blood flow result in damage to the capillary network of these vascular territories (17). Indeed, coronary artery disease is considered an indicative sign of vascular dysfunction in patients with HFpEF (18). Arterial rarefaction and inadequate angiogenesis that take place during microvascular/macrovascular dysfunction may contribute to a decrease in oxygen supply to the myocardium (19). Accordingly, it has been proposed that left ventricular diastolic dysfunction in patients with HFpEF results from vascular alterations, with aortic stiffness and altered vascular endothelial function being fundamental characteristics of this process (20). Indeed, stiffness at the macrovasculature level is associated with ventricular decreases in elastance, leading to abnormal left arterio-ventricular crowning (21). Notably, ventricular stiffness occurs regardless of several comorbidities presented by patients with HFpEF (22). Besides the changes in vascular stiffness, studies in HFpEF also showed a decrease in brachial flow-mediated dilatation (FMD) and hyperemia, suggesting the presence of endothelial dysfunction at macrovascular/microvascular circulation. Lee et al. (23), proposed that macrovascular dysfunction is indeed a consequence of primary alterations at the microvascular level (23). This is in line with a previous report showing the presence of endothelial dysfunction at the microvasculature with no overt signs of vascular dysfunction in conductance vessels in experimental HFpEF models (24). Together, current evidence supports the role of microvascular/macrovascular alterations in the progression of heart disease. Whether changes/adaptations in the microvasculature/macrovasculature are a cause or consequence to support the failing heart (in the setting of heart failure) remains to be determined.

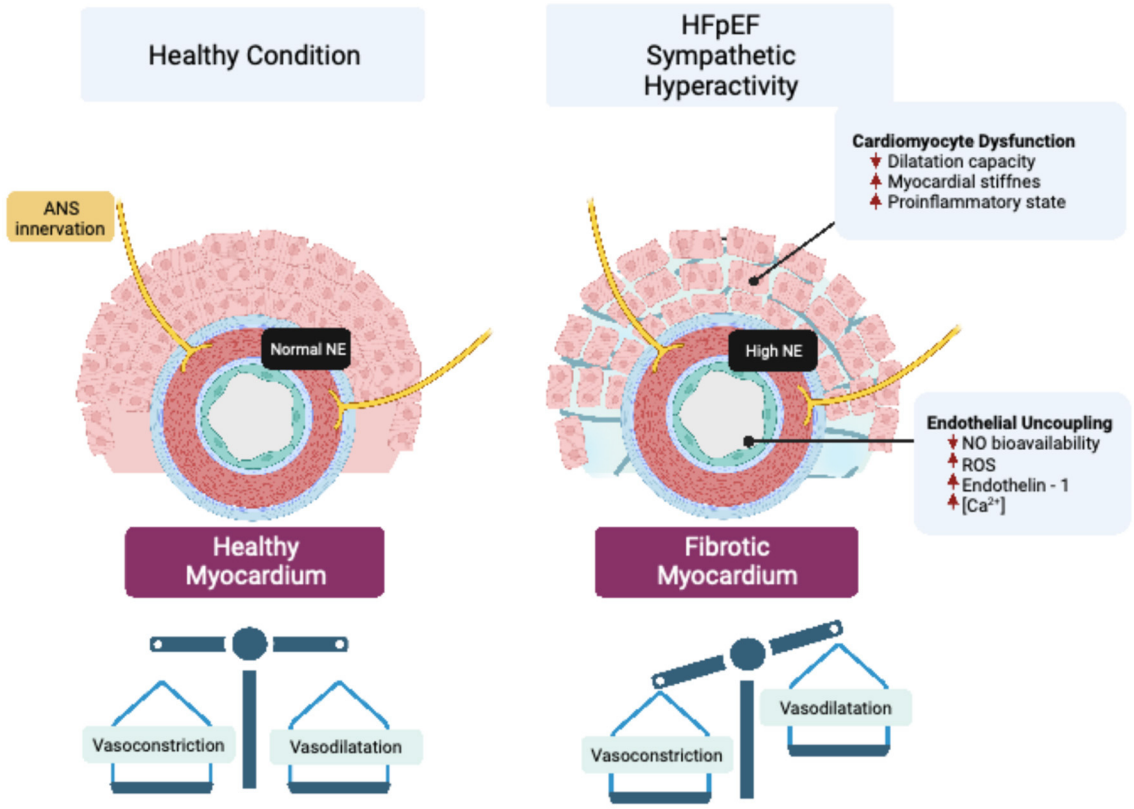

FIGURE 1
Vascular sympathetic neurotransmission and endothelial dysfunction in HFpEF. Enhanced sympathetic outflow led to increased release of norepinephrine (NE), which impair cardiovascular endothelial function by modifying peptides and signaling molecules that regulate perfusion to vascular beds. Endothelial uncoupling, in turn, can generate cardiomyocyte dysfunction that affects the structure and function of the heart through mechanisms associated with impaired myocardial dilatation capacity, stiffness, and inflammation.

Autonomic imbalance and vascular dysfunction: Main mechanisms involved

The endothelium is a highly dynamic layer that works as a barrier that separates the blood from the extravascular tissue and interacts with other cell types contributing to the physiological and homeostatic regulation of blood vessel function (25). In addition, the endothelium prevents the aggregation and adhesion of platelets and leukocytes, inhibits the proliferation of smooth muscle cells (SMC), regulates vascular tone, and plays a protective role against mechanical stimuli such as pressure or frictional stress, through the release of vasoactive substances. This is critical for the maintenance of adequate organ/tissue perfusion (26, 27). While endothelial cells (EC) are located in the most internal layer of blood vessels, SMCs are located in the medial layer and constitute the contractile elements of blood vessels, contributing to the regulation of blood vessel tone, blood pressure, and circulation (28). Then, the correct function of SMC and EC is important for vascular health since both manage vasomotor tone and vasculature integrity.

Both arms of the autonomic nervous system (ANS) (i.e., sympathetic and parasympathetic) innervate blood vessel walls and regulate wall tension (29–31). SMCs at the muscular layer of blood vessel walls receive adrenergic and cholinergic nerve projections from sympathetic and parasympathetic innervation, while ECs do not present a direct neural innervation from the ANS (29, 31). The vascular SMC layer encompasses several ANS nerve terminals. Indeed, SMC constitutively expresses β-adrenergic receptors, which modulate vasodilatation, and α_1/α_2-adrenergic receptors, which modulate vasoconstriction (29, 31). In addition, parasympathetic stimulation of muscarinic receptors within SMCs also results in blood vessel contraction. Despite not being directly innervated by the sympathetic-adrenergic system, ECs also constitutively express both β-adrenoreceptors and α_2-adrenoreceptors. While the effects of β-adrenoreceptors stimulation on EC function remain unknown, the activation of α_2-adrenoreceptors leads to the release of vasoactive molecules such as nitric oxide

(NO), which acting at SMC induces cell relaxation resulting in blood vessel vasodilation (29, 31). Besides the fine regulation of vascular function by the ANS, how autonomic imbalance could affect vasculature integrity by modulating mechanisms associated with vasoconstriction/relaxation and the vasculature environment is not completely understood, and much less is known about these mechanisms in the pathological setting of HFpEF. In this review, we discussed the potential mechanism of vascular dysfunction in HFpEF and its relation to autonomic imbalance.

Nitric oxide signaling and oxidative stress

The role of vascular NO is essential for vasodilation, inhibition of platelet aggregation, and protection of the integrity of the endothelial layer given its anti-inflammatory, proangiogenic, anti-apoptotic, and anti-fibrotic properties, reducing vascular inflammation and atherosclerosis (32, 33). At the major circulation, NO diffuses into platelets and SMC from EC, which stimulates soluble guanylate cyclase (sGC) and activates the cyclic GMP (cGMP) pathway to induce calcium release from the sarcoplasmic reticulum (SCR) in SMC, preventing platelet aggregation and producing vasodilation, respectively. At the level of cardiac microcirculation, NO can diffuse into cardiomyocytes from adjacent coronary vasculature, modulating cardiac function (7). In addition, NO signaling is involved in tissue repair by mediating the mobilization of stem and progenitor cells (34). In HFpEF, endothelial dysfunction has been linked to decreased production of cGMP and reduced activity of protein kinase G (PKG) and the L-arginine-NO synthetic pathway. Therefore, mechanisms for vasodilation are likely to be impaired in patients with HFpEF. Interestingly, vascular endothelial dysfunction in the heart shared similar mechanisms compared to those found in the systemic circulation, being alterations in sGC-cGMP signaling a common pathway affected at both levels during the progression HFpEF. More importantly, alterations in the sGC-cGMP-PKG pathway in HFpEF promote functional impairment in cardiomyocytes, as evidenced by delayed myocardial relaxation, increased myocardial stiffness, cardiac hypertrophy, and interstitial fibrosis (35). Therefore, direct interventions targeting the NO/cGMP/PKG pathway have been proposed as novel therapeutics to improve both vascular and cardiac function in HFpEF (36, 37).

How autonomic imbalance, a hallmark pathophysiological condition found in experimental and human HFpEF, affects vascular NO production is still not known. Endothelial β_2-adrenergic receptors stimulate NO synthesis by the activation of endothelial nitric oxide synthase isoform (eNOS) (32). Interestingly, overexpression or chronic activation of eNOS could be maladaptive since marked increases in intracellular oxidative stress have been reported following eNOS overexpression (38, 39). Furthermore, chronic β-adrenoreceptor activation exacerbates eNOS activity and upregulates eNOS gene expression, favoring superoxide anion generation and vascular dysfunction through reductions in NO bioavailability (38, 40). Indeed, oxygen free radicals rapidly react with NO to form reactive nitrogen species, which are known to promote a prothrombotic and proinflammatory niche within blood vessels (12, 41). Notably, the relevance of reduced NO bioavailability and increased oxidative stress to promote HFpEF pathophysiology has been demonstrated in experimental HF in which concomitant metabolic and vascular stress in mice (high-fat diet and constitutive NOS inhibition using N(omega)-nitro-L-arginine methyl ester) recapitulated the cardiovascular features of human HFpEF (12, 26). Therefore, it is plausible that hyperactivation of the sympathetic nervous system in HFpEF may lead to decreases in NO bioavailability by promoting the formation of reactive nitrogen species within blood vessels. Further investigation is needed to fully determine the contribution of enhanced sympathetic activity on NO and vascular alterations in HFpEF. In addition, HFpEF increases ROS levels and/or antioxidant enzyme suppression, leading to cardiac and endothelial dysfunction. The different risk factors for HFpEF stimulate the production of ROS (42–44). Oxidative stress by their side increases levels of hydrogen peroxide and reactive oxidative metabolites, uncoupled endothelial nitric oxide synthase, endothelial NADPH oxidase 2 (NOX2) expression, and reduced NO levels indicate the presence of myocardial oxidative stress in patients with HFpEF (45). Beyond oxidation, inhibition of NO production can reduce NO bioavailability, for example, through AGE-induced elevation of asymmetric levels of ADMA (dimethyl L-arginine), an inhibitor of eNOS (endothelial NOS), which contributes to endothelium-dependent dysfunction associated with poorer HFpEF prognosis (46). Also, autonomic dysfunction characterized by chronic activation of the SNS might contribute to oxidative stress at the EC level. Previous reports showed high contractile activity in β_2-adrenoreceptor deficient mice, and this loss of function can trigger ROS-mediated NO impairment (47). Thus, a lack of β_2 receptors increases oxidative stress in the β_2-KO mice arteries, and this change the vasoconstrictor response to phenylephrine. In addition, the above evidence suggests a crucial link between adrenergic pathways, oxidative stress, and NO bioavailability in the vasculature (47, 48). Interestingly, patients with HFpEF display not only impaired catecholamine sensitivity and β-adrenoreceptor density at the cardiac level (49, 50) but also display impaired chronotropic and vasodilatation response to exercise (51), suggesting possible desensitization of adrenergic signaling at the cardiac and vascular level. Overall, heightened SNS activity in the setting of HFpEF might contribute to creating a vicious cycle that promotes and maintains vascular dysfunction.

Inflammatory status

Risk factors in HF, such as diabetes mellitus, aging, and hypertension, among others, trigger systemic low-grade inflammation, characterized by chronic elevations in circulating immune cells, proinflammatory cytokines, and increased expression of endothelial adhesion molecules, such as vascular and intercellular cell adhesion molecules-1 (ICAM-1 and VCAM-1), and the corresponding ligands of circulating leukocytes, increasing myocardial infiltration of CD45+ and CD3+ T-lymphocytes (52). The latter further promotes the infiltration of leukocytes, especially monocytes, into the myocardial tissue, increasing the release of transforming growth factor beta (TGF-β), which ultimately leads to extracellular matrix remodeling and fibrosis (41, 43). Importantly, it has been reported that flow-mediated dilation (FMD) and reactive hyperemic index (RH) are reduced in patients with HFpEF (45), which is closely associated with elevations in inflammatory markers, such as CRP, IL-6, TNF-α, IL-1β, and NFG15 (53, 54). The increase in the inflammatory status leads to coronary microvascular endothelial dysfunction and further increases in inflammatory cytokines (55) partially mediated by the activation of the nuclear factor-kappa B (NFkB) signaling pathway (43). Thus, microvascular dysfunction is proposed to be the central mediator connecting systemic low-grade inflammation with myocardial dysfunction and remodeling in the setting of HFpEF (35).

Calcium signaling

Chronic elevation of catecholamines in HF, such as epinephrine and norepinephrine, is a hallmark and strong predictor of mortality in patients with HF (56, 57). Catecholamines activate the adenyl cyclase (AC)-cAMP-PKA pathway, leading to IP_3R1 activation and in consequence IP_3 signal to increased Ca^{2+} release and vascular tone in VSMCs during HF (58). Also, it has been found that BK potassium channels, which contribute to VSMC hyperpolarization, are downregulated in HF, promoting vasoconstriction, and synergizing with IP_3R1 for elevations in cytosolic [Ca^{2+}] (59). Since mRNA and protein levels of inositol 1,4,5 phosphate receptor 1 (IP_3R1) are upregulated in HF and increased receptor phosphorylation in HF, it has been suggested that IP_3R1 may play an important role in Ca^{2+} regulation in VSMC (60, 61). However, little is known about the contribution of intracellular calcium (Ca^{2+}) mishandling in the vasculature and subsequent acceleration of cardiac remodeling and progression of HFpEF (58). Nevertheless, alterations in the expression and function of proteins that handle Ca^{2+} and a maladaptive redistribution of intracellular calcium have been described in HF (62). Some of these proteins are RyR2, Serca2a, Na^+-Ca^{2+} exchanger (NCX), and transient receptor potential cation channels (TRPC) (63). For RyR2, there is evidence of PKA-dependent hyperphosphorylation (in S2808), causing channel dissociation, increasing Ca^{2+} leakage from the SR, decreasing Ca^{2+} transients, changing spontaneous Ca^{2+} release events, and altering cytosolic Ca^{2+} management (64). In addition, Serca2a is downregulated in HFpEF, then Ca^{2+} reuptake toward the SR affecting both active and passive cardiovascular functions (65). In addition, increased activity of NCX in HFpEF has also been described (66). Finally, the TRPC channels that participate in the entry of Ca^{2+} from the extracellular medium that allows the increase of Ca^{2+} reservoirs into the SR are increased in HFpEF, possibly as an adaptive mechanism due to a decrease in Ca^{2+} reserves in the SR (67). In addition, increased myosin heavy chain phosphorylation has also been found in the arteries of patients with HF and mice (68). The latter has been linked to VSMC remodeling and has been associated with alterations in VSMC Ca^{2+} handling (69). Therefore, alterations in the management of intracellular Ca^{2+} in the vasculature in HF may play an important role not only in vascular cell function but also in the adverse remodeling of several vascular compartments.

Conclusion

Little is known about the role of macro- and microvascular alterations during the onset, development, and progression of HFpEF. However, it is highly likely that vascular rarefaction takes place during the onset, maintenance and/or progression of HFpEF resulting in increases in microvascular resistance, reductions in tissue perfusion, and activation of vasomotor sympathetic fibers that ultimately create a feed-forward mechanism that promotes the further deterioration of vascular function by shifting the balance between vasoconstriction and vasodilation. On the contrary, proinflammatory and pro-oxidative molecules have been associated with the etiology of the disease. At the microvascular level, the decrease in the bioavailability of NO, alterations in the sGC-cGMP-PKG pathway, accumulation of ROS, and chronic low-grade inflammation are the main actions involved in the alteration of vascular function both at the systemic circulation and in the coronary territory, promoting a functional decrease in cardiomyocytes, evidenced by delayed myocardial relaxation, increased myocardial stiffness, cardiac hypertrophy, and interstitial fibrosis. The latter may have fundamental implications for the progressive decline in cardiac function during HFpEF.

To date, there are only preventive and palliative actions to deal with HFpEF, such as exercise and a healthy lifestyle, which do not imply a remission of the disease. In this article, several molecular candidates rise as potential therapeutic targets to improve both vascular and cardiac functions in HFpEF, including but not limited to NO metabolic pathway, IP3R

signaling, adrenergic pathways, and reduction of oxidative stress and vascular inflammation.

Author contributions

AS-A wrote the first draft. KP, CT, RI, and RDR contributed to manuscript formulation and revision. All authors have read and approved the final manuscript.

Funding

This study was supported by Fondo de Desarrollo Científico y Tecnológico Fondecyt (1220950) and the Basal Center of Excellence in Aging and Regeneration (AFB 170005; ACE 210009).

Conflict of interest

The authors declare that the research was conducted in the absence of any commercial or financial relationships that could be construed as a potential conflict of interest.

Publisher's note

References

1. Tsao CW, Lyass A, Enserro D, Larson MG, Ho JE, Kizer JR, et al. Temporal trends in the incidence of and mortality associated with heart failure with preserved and reduced ejection fraction. *JACC Heart Failure.* (2018) 6:678–85. doi: 10.1016/j.jchf.2018.03.006

2. Nair N. Epidemiology and pathogenesis of heart failure with preserved ejection fraction. *Rev Cardiovasc Med.* (2020) 21:531–40. doi: 10.31083/j.rcm.2020.04.154

3. Alem M. Endothelial dysfunction in chronic heart failure: assessment, findings, significance, and potential therapeutic targets. *Int J Mol Sci.* (2019) 20:3198. doi: 10.3390/ijms20133198

4. Triposkiadis F, Karayannis G, Giamouzis G, Skoularigis J, Louridas G, Butler J, et al. The sympathetic nervous system in heart failure physiology, pathophysiology, and clinical implications. *J Am Coll Cardiol.* (2009) 54:1747–62. doi: 10.1016/j.jacc.2009.05.015

5. Cohn JN. Physiologic basis of vasodilator therapy for heart failure. *Am J Md.* (1981) 71:135–9. doi: 10.1016/0002-9343(81)90276-X

6. Heusser K, Wittkoepper J, Bara C, Haverich A, Diedrich A, Levine B, et al. Sympathetic vasoconstrictor activity before and after left ventricular assist device implantation in patients with end-stage heart failure. *Eur J Heart Fail.* (2021) 23:1955–9. doi: 10.1002/ejhf.2344

7. Wang P, Wei M, Zhu X, Liu Y, Yoshimura K, Zheng M, et al. Nitric oxide down-regulates voltage-gated Na $^{+}$channel in cardiomyocytes possibly through S-nitrosylation-mediated signaling. *Sci Rep.* (2021) 11:11273. doi: 10.1038/s41598-021-90840-0

8. Yang JH, Obokata M, Reddy YNV, Redfield MM, Lerman A, Borlaug BA, et al. Endothelium-dependent and independent coronary microvascular dysfunction in patients with heart failure with preserved ejection fraction. *Eur J Heart Fail.* (2020) 22:432–41. doi: 10.1002/ejhf.1671

9. Hundley WG, Kitzman DW, Morgan TM, Hamilton CA, Darty SN, Stewart KP, et al. Cardiac cycle-dependent changes in aortic area and distensibility are reduced in older patients with isolated diastolic heart failure and correlate with exercise intolerance. *J Am Coll Cardiol.* (2001) 38:796–802. doi: 10.1016/S0735-1097(01)01447-4

10. Mohammed SF, Borlaug BA, McNulty S, Lewis GD, Lin G, Zakeri R, et al. Resting ventricular–vascular function and exercise capacity in heart failure with preserved ejection fraction: a relax trial ancillary study. *Circ Heart Fail.* (2014) 7:580–9. doi: 10.1161/CIRCHEARTFAILURE.114.001192

11. Chowdhury MA, Moukarbel GV, Gupta R, Frank SM, Anderson AM, Liu LC, et al. Endothelin 1 is associated with heart failure hospitalization and long-term mortality in patients with heart failure with preserved ejection fraction and pulmonary hypertension. *Cardiology.* (2019) 143:124–33. doi: 10.1159/000501100

12. Schiattarella G, Altamirano F, Tong D, French K, Villalobos E, Kim S, et al. Nitrosative stress drives heart failure with preserved ejection fraction. *Nature.* (2019) 568:351–6. doi: 10.1038/s41586-019-1100-z

13. Mohammed SF, Hussain S, Mirzoyev SA, Edwards WD, Maleszewski JJ, Redfield MM, et al. Coronary microvascular rarefaction and myocardial fibrosis in heart failure with preserved ejection fraction. *Circulation.* (2015) 131:550–9. doi: 10.1161/CIRCULATIONAHA.114.009625

14. Van Empel VP, Mariani J, Borlaug BA, Kaye DM. Impaired myocardial oxygen availability contributes to abnormal exercise hemodynamics in heart failure with preserved ejection fraction. *J Am Heart Assoc.* (2014) 3:e001293. doi: 10.1161/JAHA.114.001293

15. Van de Wouw J, Sorop O, van Drie RWA, van Duin RWB, Nguyen ITN, Joles JA, et al. Perturbations in myocardial perfusion and oxygen balance in swine with multiple risk factors: a novel model of ischemia and no obstructive coronary artery disease. *Basic Res Cardiol.* (2020) 115:21. doi: 10.1007/s00395-020-0778-2

16. Mitchell GF. Effects of central arterial aging on the structure and function of the peripheral vasculature: implications for end-organ damage. *J Appl Physiol.* (2008) 105:1652–60. doi: 10.1152/japplphysiol.90549.2008

17. Van de Wouw J, Broekhuizen M, Sorop O, Joles JA, Verhaar MC, Duncker DJ, et al. Chronic kidney disease as a risk factor for heart failure with preserved ejection fraction: a focus on microcirculatory factors and therapeutic targets. *Front Physiol.* (2019) 4:1108. doi: 10.3389/fphys.2019.01108

18. Gori M, Lam CS, Gupta DK, Santos AB, Cheng S, Shah AM, et al. Sex-specific cardiovascular structure and function in heart failure with preserved ejection fraction. *Eur J Heart Fail.* (2014) 16:535–42. doi: 10.1002/ejhf.67

19. Gladden JD, Linke WA, Redfield MM. Heart failure with preserved ejection fraction. *Pflugers Arch.* (2014) 466:1037–53. s00424-014-1480-8. doi: 10.1007/s00424-014-1480-8

20. Maréchaux S, Samson R, Van Belle E, Breyne J, De Monte J, Dédrie C, et al. Vascular and microvascular endothelial function in heart failure with preserved ejection fraction. *J Card Fail.* (2016) 22:3–11. doi: 10.1016/j.cardfail.2015.09.003

21. Teo LY, Chan LL, Lam CS. Heart Failure with preserved ejection fraction in hypertension. *Curr Opin Cardiol.* (2016) 31:410–6. doi: 10.1097/HCO.0000000000000292

22. Mohammed SF, Borlaug BA, Roger VL, Mirzoyev SA, Rodeheffer RJ, Chirinos JA, et al. Comorbidity and ventricular and vascular structure and function in heart failure with preserved ejection fraction. A community-based study. *Circ Heart Fail.* (2012) 5:710–19. doi: 10.1161/CIRCHEARTFAILURE.112.968594

23. Lee, J. F. Barrett-O'Keefe, Z., Garten, R. S., Nelson, A., Ryan, J., Nativi, J., Richardson, R., and Wray, D. Evidence of microvascular dysfunction in heart failure with preserved ejection fraction. *Heart.* (2016) 102:278–84. doi: 10.1136/heartjnl-2015-308403

24. Haykowsky MJ, Herrington DM, Brukaber PH, Morgan TM, Hundley WG, Kitzman DW, et al. Relationship of flow-mediated arterial dilation and exercise capacity in older patients with heart failure and preserved ejection fraction. *J Gerontol A Biol Sci Med Sci.* (2013) 68:161–7. doi: 10.1093/gerona/gls099

25. Pinto, A. R. Ilinykh,. A., Ivey, M. J., Kuwabara, J. T., D'Antoni, M. L., Debuque, R., Chandran, A., Wang, L., Arora, K., Rosenthal, N. A., and Tallquist, M. D. (2016). Revisiting cardiac cellular composition. *Circ Res*. 118, 400–409. doi: 10.1161/CIRCRESAHA.115.307778

26. Riad A, Westermann D, Van Linthout S, Mohr Z, Uyulmaz S, Becher PM, et al. Enhancement of endothelial nitric oxide synthase production reverses vascular dysfunction and inflammation in the hindlimbs of a rat model of diabetes. *Diabetologia*. (2008) 51:2325–32. doi: 10.1007/s00125-008-1159-9

27. Hayashida R, Kondo K, Morita S, Unno K, Shintani S, Shimizu Y, et al. Diallyl trisulfide augments ischemia-induced angiogenesis via an endothelial nitric oxide synthase-dependent mechanism. *Circ J*. (2017) 81:870–8. doi: 10.1253/circj.CJ-16-1097

28. Michel J, Li Z, Lacolley P. Smooth muscle cells and vascular diseases. *Cardiovasc Res*. (2012) 95:135–7. doi: 10.1093/cvr/cvs172

29. Amiya E, Watanabe M, Komuro I. The relationship between vascular function and the autonomic nervous system. *Ann Vasc Dis*. (2014) 7:109–19. doi: 10.3400/avd.ra.14-00048

30. Harris KF, Matthews KA. Interactions between autonomic nervous system activity and endothelial function: a model for the development of cardiovascular disease. *Psychosom Med*. (2004). 66:153–64. doi: 10.1097/01.psy.0000116719.95524.e2

31. Sheng Y, Zhu L. The crosstalk between autonomic nervous system and blood vessels. *Int J Physiol Pathophysiol Pharmacol*. (2018) 10:17–28.

32. Cyr AR, Huckaby LV, Shiva SS, Zuckerbraun BS. Nitric oxide and endothelial dysfunction. *Crit Care Clin*. (2019) 36:307–21. doi: 10.1016/j.ccc.2019.12.009

33. Clapp BR, Hingorani AD, Kharbanda RK, Mohamed-Ali V, Stephens JW, Vallance P, et al. Inflammation-induced endothelial dysfunction involves reduced nitric oxide bioavailability and increased oxidant stress. *Cardiovasc Res*. (2004) 64:20. doi: 10.1016/j.cardiores.2004.06.020

34. Emanueli C, Van Linthout S, Bonaria Salis M, Monopoli A, Del Soldato P, Ongini E, et al. Nitric oxide-releasing aspirin derivative, NCX 4016, promotes reparative angiogenesis and prevents apoptosis and oxidative stress in a mouse model of peripheral ischemia. *Arterioscler Thromb Vasc Biol*. (2004) 24:2082–7. doi: 10.1161/01.ATV.0000144030.39087.3b

35. Chirinos JA, Akers SR, Trieu L, Ischiropoulos H, Doulias PT, Tariq A, et al. Heart failure, left ventricular remodeling, and circulating nitric oxide metabolites. *J Am Heart Assoc*. (2016) 5:e004133. doi: 10.1161/JAHA.116.004133

36. Greene SJ, Gheorghiade M, Borlaug BA, Pieske B, Vaduganathan M, Burnett JC, et al. The cGMP signaling pathway as a therapeutic target in heart failure with preserved ejection fraction. *J Am Heart Assoc*. (2013) 2:e000536. doi: 10.1161/JAHA.113.000536

37. Wilck N, Marko L, Balogh A, Kraeker K, Herse F, Bartolomaeus H, et al. Nitric oxide-sensitive guanylyl cyclase stimulation improves experimental heart failure with preserved ejection fraction. *JCI Insight*. (2018) 3:e96006. doi: 10.1172/jci.insight.96006

38. Toblli JE, DiGennaro F, Giani JF, Dominici FP. Nebivolol: impact on cardiac and endothelial function and clinical utility. *Vasc Health Risk Manag*. (2012) 8:151–60. doi: 10.2147/VHRM.S20669

39. Suvorava T, Nagy N, Pick S, Lieven O, Rüther U, Dao VT, et al. Impact of eNOS-dependent oxidative stress on endothelial function and neointima formation. *Antioxidants Redox Signal*. (2015) 23:711–23. doi: 10.1089/ars.2014.6059

40. Ferro A, Queen LR, Priest R, Xu B, Ritter JM, Poston L, et al. Activation of nitric oxide synthase by beta 2-adrenoceptors in human umbilical vein endothelium in vitro. *Br J Pharmocol*. (1999) 126:1872–80. doi: 10.1038/sj.bjp.0702512

41. Paulus WJ, Tschope C. A novel paradigm for heart failure with preserved ejection fraction: comorbidities drive myocardial dysfunction and remodeling through coronary microvascular endothelial inflammation. *J Am Coll Cardiol*. (2013) 62:263–71. doi: 10.1016/j.jacc.2013.02.092

42. Zhazykbayeva S, Pabel S, Mügge A, Sossalla S, Hamdani N. The molecular mechanisms associated with the physiological responses to inflammation and oxidative stress in cardiovascular diseases. *Biophys Rev*. (2020) 12:947–680. doi: 10.1007/s12551-020-00742-0

43. Forrester SJ, Kikuchi DS, Hernandes MS, Xu Q, Griendling KK. Reactive oxygen species in metabolic and inflammatory signaling. *Circ Res*. (2018) 122:877–902. doi: 10.1161/CIRCRESAHA.117.311401

44. Inoguchi T, Li P, Umeda F, Yu HY, Kakimoto M, Imamura M, et al. High glucose level and free fatty acid stimulate reactive oxygen species production through protein kinase C dependent activation of NADPH oxidase in cultured vascular cells. *Diabetes*. (2000) 49:1939–45. doi: 10.2337/diabetes.49.11.1939

45. Franssen C, Chen S, Unger A, Korkmaz HI, De Keulenaer GW, Tschöpe C, et al. Myocardial microvascular inflammatory endothelial activation in heart failure with preserved ejection fraction. *JACC Heart Fail*. (2016) 4:312–24. doi: 10.1016/j.jchf.2015.10.007

46. Babes E, Babes V. ADMA and prognosis in patients with heart failure and preserved ejection fraction. *Esc Heart Fail*. (2013) 7:1491. doi: 10.1093/eurheartj/eht308.P1491

47. Davel AP, Ceravolo GS, Wenceslau CF, Carvalho MH, Brum PC, Rossoni LV, et al. Increased vascular contractility and oxidative stress in β2-adrenoceptor knockout mice: the role of NADPH oxidase. *J Vasc Res*. (2012) 49:342–52. doi: 10.1159/000337486

48. Conti V, Russomanno G, Corbi G, Izzo V, Vecchione C, Filippelli A, et al. Adrenoreceptors and nitric oxide in the cardiovascular system. *Front Physiol*. (2013) 4:321. doi: 10.3389/fphys.2013.00321

49. Bristow MR, Mann DL. Cardiac adrenergic activation in heart failure with preserved ejection fraction. *JACC Basic Transl Sci*. (2022) 7:128–30. doi: 10.1016/j.jacbts.2022.01.003

50. van Veldhuisen DJ, Cohen-Solal A, Böhm M, Anker SD, Babalis D, Roughton M, et al. Beta-blockade with nebivolol in elderly heart failure patients with impaired and preserved left ventricular ejection fraction: data from seniors (study of effects of nebivolol intervention on outcomes and rehospitalization in seniors with heart failure). *J Am Coll Cardiol*. (2009) 53:2150–8. doi: 10.1016/j.jacc.2009.02.046

51. Borlaug BA, Melenovský V, Russell SD, Kessler K, Pacak K, Becker L, et al. Impaired chronotropic and vasodilator reserves limit exercise capacity in patients with heart failure and a preserved ejection fraction. *Circulation*. (2006) 114:2138–47. doi: 10.1161/CIRCULATIONAHA.106.632745

52. Westermann D, Lindner D, Kasner M, Zietsch C, Savvatis K, Escher F, et al. Cardiac inflammation contributes to changes in the extracellular matrix in patients with heart failure and normal ejection fraction. *Circ Heart Fail*. (2011) 4:44–52. doi: 10.1161/CIRCHEARTFAILURE.109.931451

53. Collier P, Watson CJ, Voon V, Phelan D, Jan A, Mak G, et al. Can emerging biomarkers of myocardial remodeling identify asymptomatic hypertensive patients at risk for diastolic dysfunction and diastolic heart failure. *Eur J Heart Fail*. (2011) 13:1087–95. doi: 10.1093/eurjhf/hfr079

54. DuBrock HM, AbouEzzeddine OF, Redfield MM. High-sensitivity C-reactive protein in heart failure with preserved ejection fraction. *PLoS ONE*. (2018) 13:e0201836. doi: 10.1371/journal.pone.0201836

55. Bishu K, Deswal A, Chen HH, LeWinter MM, Lewis GD, Semigran MJ, et al. Biomarkers in acutely decompensated heart failure with preserved or reduced ejection fraction. *Am Heart J*. (2012) 164:763–70. doi: 10.1016/j.ahj.2012.08.014

56. Lymperopoulos A, Rengo G, Koch WJ. Adrenergic nervous system in heart failure: pathophysiology and therapy. *Circ Res*. (2013) 113:739–53. doi: 10.1161/CIRCRESAHA.113.300308

57. Santulli G, Iaccarino G. *A*drenergic signaling in heart failure and cardiovascular aging. *Maturitas*. (2016) 93:65–72. doi: 10.1016/j.maturitas.2016.03.022

58. Dridi H, Santulli G, Gambardella J, Jankauskas S, Yuan Q, Yang Q, et al. IP3 receptor orchestrates maladaptive vascular responses in heart failure. *J Clin Invest*. (2022) 132:e152859. doi: 10.1172/JCI152859

59. Jackson WF. Potassium channels in regulation of vascular smooth muscle contraction and growth. *Adv Pharmacol*. (2016) 78:89–144. doi: 10.1016/bs.apha.2016.07.001

60. Lin Q, Zhao G, Fang X, Peng X, Tang H, Wang H, et al. IP3 receptors regulate vascular smooth muscle contractility and hypertension. *JCI Insight*. (2016) 1:e89402. doi: 10.1172/jci.insight.89402

61. Gambardella J, Lombardi A, Morelli MB, Ferrara J, Santulli G. Inositol 1,4,5-trisphosphate receptors in human disease: a comprehensive update. *J Clin Med*. (2020) 9:1096. doi: 10.3390/jcm9041096

62. Guo A, Zhang C, Wei S, Chen B, Sheng Song L. Emerging mechanisms of T-tubule remodelling in heart failure. *Cardiovasc Res*. (2013) 98:204–15. doi: 10.1093/cvr/cvt020

63. Zhao J, Xu T, Zhou Y, Zhou Y, Xia Y, Li D, et al. B-type natriuretic peptide and its role in altering Ca2+-regulatory proteins in heat failure-mechanistic insights. *Heart Fail Rev*. (2020) 25:861–71. doi: 10.1007/s10741-019-09883-1

64. Bovo E, Huke S, Blatter LA, Zima AV. The effect of PKA-mediated phosphorylation of ryanodine receptor on SR Ca^{2+} leak in ventricular myocytes. *J Mol Cell Cardiol*. (2017) 104:9–16. doi: 10.1016/j.yjmcc.2017.01.015

65. Li L, Louch W, Niederer S, Aronsen J, Christensen G, Sejersted O, et al. Sodium accumulation in SERCA Knockout-induced heart failure. *Biophys J*. (2012) 102:2039–48. doi: 10.1016/j.bpj.2012.03.045

66. Bers DM. Cardiac sarcoplasmic reticulum calcium leak: basis and roles in cardiac dysfunction. *Annu Rev Physiol*. (2014) 76:107–27. doi: 10.1146/annurev-physiol-020911-153308

67. Eder P, Molkentin JD. TRPC channels as effectors of cardiac hypertrophy. *Circ Res*. (2011) 108:265–72. doi: 10.1161/CIRCRESAHA.110.225888

68. He WQ, Peng YJ, Zhang WC, Lv N, Tang J, Chen C, et al. Myosin light chain kinase is central to smooth muscle contraction and required for gastrointestinal motility in mice. *Gastroenterology*. (2008) 135:610–20. doi: 10.1053/j.gastro.2008.05.032

69. Heusch G, Libby P, Gersh B, Yellon D, Böhm M, Lopaschuk G, et al. Cardiovascular remodeling in coronary artery disease and heart failure. *Lancet*. (2014) 383:1933–43. doi: 10.1016/S0140-6736(14)60107-0

frontiers | Frontiers in Cardiovascular Medicine

TYPE Original Research
PUBLISHED 10 January 2023
DOI 10.3389/fcvm.2022.1063078

OPEN ACCESS

EDITED BY
Jia Qi,
Shanghai Jiao Tong University, China

REVIEWED BY
Xin Cheng,
Fudan University, China
Yueqi Zhu,
Shanghai Jiao Tong University, China

*CORRESPONDENCE
Feng Wang
✉ 13816566556@163.com
Quanbin Zhang
✉ quanbinzhang@aliyun.com

†These authors have contributed equally to this work and share first authorship

SPECIALTY SECTION
This article was submitted to General Cardiovascular Medicine, a section of the journal Frontiers in Cardiovascular Medicine

RECEIVED 06 October 2022
ACCEPTED 12 December 2022
PUBLISHED 10 January 2023

CITATION
Xu Y, Fu W, Wang Y, Bi Q, Wang Q, Yang L, Zhang Q and Wang F (2023) Endovascular treatment for acute M2 occlusion stroke within 6 hours-a retrospective real-world evidence. *Front. Cardiovasc. Med.* 9:1063078. doi: 10.3389/fcvm.2022.1063078

Endovascular treatment for acute M2 occlusion stroke within 6 hours-a retrospective real-world evidence

Yi Xu[1†], Wang Fu[2†], Yongpeng Wang[2], Qianqian Bi[2], Qiwei Wang[2], Lu Yang[2], Quanbin Zhang[1*] and Feng Wang[2*]

[1]Department of Neurosurgery, Shanghai Tenth People's Hospital, Tongji University School of Medicine, Shanghai, China, [2]Department of Neurology, Seventh People's Hospital of Shanghai University of Traditional Chinese Medicine, Shanghai, China

Background: We compared the efficacy and safety of endovascular therapy (EVT), intravenous (IV) thrombolysis and conservative treatment in M2 segment occlusion stroke based on a real-world database.

Methods: We retrospectively analyzed the database of admitted patients with M2 segment occlusion between January 2018 and December 2020. The patients who were eligible for reperfusion treatment were assigned to EVT, IV thrombolysis or conservative treatment according to the exact management proceeding. The primary outcome was a score of 0 and 1 on the modified Rankin scale (mRS) at 90 days. The odds ratio (OR) for the primary outcome was adjusted for age, baseline National Institute of Health Stroke Scale score, and door-to-treatment time. The secondary outcomes were based on a mRS score from 0 to 2 at 90 days and the safety outcomes including symptomatic intracranial hemorrhage, and all-cause mortality. The data were analyzed by the logistical regression model, including baseline adjustments.

Results: A total of 109 patients were included. Among them, 42 (38.5%) patients received EVT, 45 (42.5%) received IV thrombolysis and 22 (20.8%) received conservative treatment. The primary outcome based on a mRS score of 0 and 1, occurred in 66.7% of patients in the EVT group and 40% in the IV thrombolysis group (adjusted OR, 1.79; 95% confidence interval [CI], 1.19-2.68; $P = 0.01$). Symptomatic intracranial hemorrhage occurred in 1 patient (2.3%) in the EVT group and in 2 patients (4.4%) in the IV thrombolysis group (adjusted OR = 0.71, 95% CI: 0.13-4.07).

Conclusion: EVT showed better functional outcomes than IV thrombolysis and conservative treatment in moderate to severe acute stoke patients with M2 occlusion. There was no significant difference in the three groups concerning the incidence of symptomatic intracranial hemorrhage.

KEYWORDS

acute ischemic stroke, M2 occlusion, endovascular therapy, intravenous thrombolysis, stroke

1. Introduction

Based on the recent landmark trials, current guidelines recommend endovascular therapy (EVT) as the standard care for acute ischemic stroke with an occlusion of the distal internal carotid artery or proximal middle cerebral artery (1). These trials concluded that the combination of EVT with intravenous (IV) thrombolysis improves the 90-day outcomes of ischaemic stroke with internal carotid artery (ICA) or M1 segment of the middle cerebral artery (MCA) occlusion, within 6 hours from the stroke onset. However, occlusion of M2 segment has been underestimated in these trials and therefore the treatment of M2 segment remains controversial (2–4).

Previous study indicated that occlusion at a more distal MCA might be associated with unsuccessful recanalization (5). The PROMISE study compared the angiographic and clinical outcomes of aspiration thrombectomy in M1 and M2 occlusion, indicated that the M2 segment had similar outcomes to M1. These were represented by a comparable rate of recanalization, device-related severe adverse events, and post-treatment symptomatic intracranial hemorrhage (sICH) (6).

In addition, very few studies analyzed the different outcomes between EVT, IV treatment and conservative treatment in acute M2 segment occlusion. Only one sub-analysis of RESCUE-Japan Registry 2 compared the EVT and non-EVT treatment (including IV thrombolysis and conservative therapy). Although showing the same likelihood of sICH, the study showed that EVT might increase mortality (7).

In recent years, EVT and IV thrombolysis are increasingly being performed in our country. More acute stroke units tend to proceed with EVT for vessel occlusion but also for the middle-sized ones, particularly for the M2 segment. Whether EVT is safer and more beneficial than IV thrombolysis in treating M2 occlusion patients are becoming critical questions that need addressing. To support the clinical decision-making, this study aimed to investigate the efficacy and safety of EVT, IV thrombolysis and conservative therapy in patients with acute ischaemic stroke resulting from acute occlusion of the middle cerebral artery M2 segment. Meanwhile, we defined M2 segment according to Tomsick's study (8).

2. Materials and methods

2.1. Study design and setting

This study is a multicentre, retrospective, cohort study in Shanghai, China. As a developed major city, Shanghai has more than 70,000 ischaemic stroke per year. There are more than 30 hospitals that provide 24/7 thrombolysis services, two of which (Tenth People's Hospital and the Seventh People's Hospital) are tertiary neurovascular centers in North and East Shanghai that are equipped to provide EVT. Both centers have a stroke team and an acute stroke unit that use a same acute stroke intervention protocol. The acute stroke patients are recognized by trained ambulance staff who informs the hospital-based triage nurse and acute stroke team before arriving at the emergency department (ED). On the patient's arrival, the acute stroke team is ready to initiate the Code Stroke that consists in proceeding with the stroke imaging protocol including non-contrast CT brain, CT perfusion (CTP), CT angiogram (CTA) and informing the on-call interventional neuroradiologist to remotely access the stroke imaging and prepare for the EVT if required. By using the acute stroke protocol, the recorded average time of door-to-needle (from patients entering the hospital to the needle) was 41 min, and the average door-to-puncture (from patients entering the hospital to the puncture) was 78 min. We provide continuous stroke management from acute phase to post-discharge for up to 3 months. The collected data from these two metropolitan hospitals are from the same database.

2.2. Participants

The data were selected from the shared Stroke Database of the Tenth People's Hospital and the Seventh People's Hospital in Shanghai. An eligible dataset was included if the patient: (1) was recorded by the Stroke Database between 1st January 2018 and 31st December 2020; (2) was diagnosed with an acute ischaemic stroke resulting from M2 occlusion (the diagnostic selection criteria is as below); (3) received IV thrombolysis within 4.5 h or EVT within 6 h after onset; (4) had complete series of CT perfusion, CT angiogram or DSA images before treatment; (5) completed the follow-up review in 90 days post-stroke. Those who received bridged treatments, including EVT + IV thrombolysis were included in the EVT group. Those who were assessed to be eligible but refused to proceed with either EVT or IV thrombolysis treatment, were assigned to the conservative treatment group where they promptly received standard anti-platelet therapy. Meanwhile, patients with contraindication of thrombolysis or EVT would also receive conservative treatment.

Those who did not have analyzable images or did not complete the modified Rankin scale (mRS) assessment at 90 days after stroke, were excluded. This study was approved by the Tenth People's Hospital Research Ethics Committee (approval number: 21k253) and the Seventh People's Hospital Research Ethics Committee (approval number: 2021-B151). The informed consent was waived due to the retrospective nature.

In this study, we used the functional-anatomical M1-M2 classification to define the M2 occlusion. Arsing from M1, adjacent to ATA but larger or giving origin to ATA and distributing to the mid- and posterior temporal lobe were termed "posterior temporal M2 branch" and "holotemporal

M2 branch". The single vessel continuation of M1 beyond the posterior temporal or holotemporal M2 branches was termed "M2 trunk" (8).

It suggested that the filling of at least one M2 branch, including the existence of holotemporal artery or posterior temporal artery, was considered as M2 occlusion when using CTA, CTP with or without DSA. The imaging for each patient was reviewed by a neurologist and a neuroradiological specialist and a consensus opinion was reached to assert the presence of an M2 segment occlusion. Those without agreement were reviewed by an interventional neuroradiologist to determine a consensus.

2.3. Imaging protocol

According to the stroke care protocol at both hospitals, all patients with acute ischemic stroke received a multimodal CT assessment which included non-contrast CT brain, CTA and CTP, with or without a following DSA. Iodinated contrast (40-mL iohexol 350 mg/ml, Omnipaque 350; GE Healthcare, Milwaukee, WI, USA) was injected at 8 mL/s, and 40 images were acquired per second (total acquisition time, 44 s). The images were processed using a commercial version of RAPID automated software.

2.4. Interventions

Patients were managed according to the acute stroke treatment guideline and hospital acute stroke protocol of EVT and IV thrombolysis. When the patients were within the time window of 4.5 h, IV thrombolysis was performed. The IV thrombolysis combined with EVT was used when the CTP mismatched while the large vessel occlusion was diagnosed. On the other hand, when the patients were within the time window of 4.5-6 h, the EVT was used when the CTP mismatched while the large vessel occlusion was diagnosed. Or the patient would receive conservative treatment. Patients with contraindication of thrombolysis or EVT would also receive conservative treatment.

The performance of EVT was as follows: 8F or 6F guide tube was advanced at the end of C1 segment, then the micro wire (Boston Science, USA) was slowly advanced through the M2 occluded section, and the Navien catheter (EV3, USA) was advanced at the C4 segment over the micro wire. The micro wire was advanced across the occluded segment followed by the micro catheter (EV3, USA) which was confirmed to be in the true lumen by angiography. The Solitaire thrombectomy stent (Solitaire FR, Medtronic) was sent through the microcatheter and placed in distal true lumen of the occluded segment. After accurate positioning, the stent was released. After 5 minutes, the stent and microcatheter were withdrawn together for thrombectomy. The final angiography was performed to evaluate the lesions.

The IV thrombolysis was performed using tissue plasminogen activator at a concentration of 0.9 mg/kg and with a maximum of 90 mg. The patients received first a 10% of the total dose via intravenous bolus injection and then a continuous infusion within 1 h to finish the total dosage. The patient received retrieval therapy that may have been preceded by an IV t-PA. Conservative treatment was used for patients who were contraindicated to IV thrombolysis therapy and who failed to receive EVT for whatever reason.

2.5. Outcomes

The primary outcome was a score of 0 or 1 on the mRS at 90 days (indicating an excellent functional outcome with a return to all usual activities). Data were obtained by telephone or outpatient interview. The odds ratio (OR) for the primary outcome was adjusted for age, clinical severity of stroke (National Institute of Health Stroke Scale, [NIHSS] score) at baseline, and time from onset to treatment. The secondary outcomes were scored from 0 to 2 on the mRS at 90 days (indicating functional independence); the score (0 to 6) on the mRS at 90 days (with the distribution of scores in each trial group used in an ordinal analysis to assess functional improvement); safety assessment, including the sICH (defined according to the SITS-MOST definition (9) and all-cause mortality. An independent neurologist, who was blind to the treatment method, was responsible for the evaluation of mRS at 90 days by telephone consult or outpatient interview.

2.6. Data collection

Baseline characteristics included age, gender, vascular risk factors, pre-event mRS score, and NIHSS at presentation. In this study, the onset-to-CT time (measured in minutes) was used to represent the onset-to- ED (time from the onset to entering the ED) time due to a better accuracy of the CT recording time. The average time between ED-admission and CT performance was 38 min. Stroke onset time was evaluated according to the patients or the witness. For an unknown-onset stroke, the time when the patients were last noticed as unaffected, was considered to represent the onset.

2.7. Statistical analysis

The statistical analysis was performed using SPSS version 20.0 for Windows (IBM Co., Armonk, NY, USA). Continuous variables were presented as mean ± standard deviation (SD), and categorical variables were presented as frequencies and percentages. Fisher exact test was used to compare the difference at baseline between categorical variables, and Wilcoxon-Mann-Whitney test was used for continuous variables. The logistic

regression model was used to compare the 90-day mRS, sICH, and mortality in the different treatment cohorts, that were adjusted by age, NIHSS score at baseline, and time from onset to treatment. In the analysis, EVT group was set as the reference, which was used to compare the IV group and conservative group. A p-value of less than 0.05 was considered statistically significant.

3. Results

Between the 1st of January 2018 and the 31st of December 2020, 2761 patients with acute ischemic stroke were screened, of which 109 had an M2-occlusion. The mean age of the study population was 69.4 ± 12.0 years, and 45.0% of them were females. All participants received the brain-scan within 6 hours after the onset. Forty-two (38.5%) participants underwent EVT, of which, 24 received thrombolysis beforehand (57.1% of all EVT cases), 45 received IV thrombolysis alone (41.3%), and 22 underwent conservative treatment (20.2%). The baseline characteristics of the three groups were detailed in **Table 1**. The conservative group, which was comprised of older patients, had a prolonged waiting time for CT scan in ED (door-to-CT time 54 min vs. 35.8 min for EVT and 32.5 min for thrombolysis). Although the conservative group had a relatively lower percentage of being well function at baseline (mRS ≤ 2: 77.2%), the baseline mRS did not show a statistical significance across the groups (p = 0.34). The patients who received EVT showed a longer time from emergency arrival to recanalization due to the time that was spent in preparation for the operation compared with IV thrombolysis (65 vs. 43 min). Otherwise, no significant difference was observed between EVT and IV thrombolysis at baseline.

3.1. Efficacy

The primary outcome of the mRS score of 0 or 1 was attained by 66.7% of the patients in the EVT group, by 44.3% in the IV thrombolysis group and by 22.7% in the conservative treatment group. The adjusted OR of EVT to IV thrombolysis was 1.67, showing a significant difference between the groups (95% confidence interval [CI]: 1.10-2.53, p = 0.01). Given the door-to-puncture time being longer than that of the door-to-needle (65 min vs. 43 min), the adjusted OR became more significant by 1.79 (95% CI 1.19-2.68). Only 22.7% of the patients who received conservative treatment could achieve a mRS score of 0 or 1, which was significantly lower than that in the EVT group (adjusted OR: 3.04; 95% CI 1.37-6.74; p = 0.001) (**Table 2**).

Regarding the secondary outcomes, a mRS score of 0 to 2 was attained by 76.2% of the patients in the EVT group, 53.3% in the IV thrombolysis group (adjusted RR: 1.52; 95% CI 1.11-2.07; p = 0.04), and 27.2% in the conservative treatment group (adjusted OR: 2.84; 95% CI 1.41-5.73; p < 0.001) (**Table 2**). A shift analysis of the distribution of scores for each group, mRS did not show statistical significance between the groups' difference in functional improvement at 90 days, due to the small sample size (**Figure 1**).

3.2. Safety assessment

The safety of the different treatments was assessed by sICH and mortality at 90 days. There was only one case in the EVT group and two cases in the IV thrombolysis cohort developed sICH. Given the small sample side, no statistical significances were observed (sICH 2.3 vs. 4.4%, p > 0.99; adjusted OR = 0.71; 95% CI: 0.13-4.07) (**Table 3**). No patients died in this study cohort.

4. Discussion

In this study, we retrospectively enrolled 109 patients. Among them, 42 (38.5%) patients received EVT, 45 (42.5%) received IV thrombolysis and 22 (20.8%) received conservative treatment. EVT showed its superiority in functional outcomes (attain of a mRS score ≤ 1) and safety compared with the other two kinds of treatments.

Due to the more distal position of M2, the tissue loss was conceptually smaller than M1 occlusion. Hence the potential improvement of functional status after treatment may be not significant as that in M1 (10). Furthermore, M2 segment branches were characterized by thinner vessel walls and a narrower lumen, making the procedure technically more difficult and the vessel wall more prone to perforation, increasing the risk of complications and early re-occlusion (11). Despite all this, previous studies found M2 occlusions involving the eloquent cortex may cause significant neurological impairment, and these patients may benefit from reperfusion therapy compared with medical therapy (12). Meanwhile, Rai et al found 56% of patients with M2 occlusions had poor clinical outcomes and a mortality rate of 27% (13). Lima et al concluded that the 6-month mortality similar to patients with M1 occlusions, indicating the necessity of treatment of M2 segment (14). Sarraj et al also found patients managed with ECR had significantly better 90-day clinical outcomes (62.8 vs. 35.4%, P = 0.001) and although the ECR group did show higher frequency of sICH compared to those treated by medicine (15).

Recent meta-analysis studies also demonstrated that mechanical thrombectomy in M2 segment may have similar outcomes in hemorrhagic transformation, functional independence and motility compared to M1 segment occlusion (16–18). However, the definition of M2 segment was various. The most common definition was the vertical portion of MCA in the Sylvian fissure, extending from the genu to the

TABLE 1 Baseline characteristics for study groups.

Characteristic	EVT (*n* = 42)	IV thrombolysis (*n* = 45)	Conservative treatment (*n* = 22)	*P*-value
Age — years (mean, SD)	67.4 (13.0)	68.7 (10.9)	74.71 (8.3)	0.046
Gender (Male) — N (%)	19 (45.2)	21 (46.7)	9 (40.9)	0.90
Medical history — N (%)				
Hypertension	29 (69.0)	34 (75.6)	16 (72.7)	0.79
Hyper-lipidemia	7 (16.7)	10 (22.2)	6 (27.3)	0.60
Diabetes Mellitus	10 (23.8)	12 (26.7)	4 (18.2)	0.75
Atrial fibrillation	14 (33.3)	18 (10.0)	12 (54.5)	0.26
Previous stroke/TIA	15 (35.7)	10 (22.2)	3 (13.6)	0.12
Ischaemic heart disease	9 (21.4)	10 (22.2)	4 (18.2)	0.93
Smoker (current)	11 (26.2)	14 (31.1)	6 (27.3)	0.87
Pre-onset mRS $\leq$ 2 — N (%)	38 (90.4)	39 (86.7)	17 (77.2)	0.34
Onset NIHSS (mean, SD)	13.1 (3.9)	11.7 (3.2)	13.1 (2.7)	0.07
Door to CT time (mean, SD)	35.8 (10.6)	32.5 (8.9)	54.0 (12.8)	<0.001
Door to puncture or needle time (Median, IQR)	65 (56-300)	43 (26-58)	NA	<0.001

EVT, endovascular treatment; IV, intravenous; tPA, tissue-type plasminogen activator; TIA, transient ischemic attack; NIHSS, National Institutes of Health Stroke Scale; mRS, modified Rankin scale. Door to CT time and door to puncture or needle time was calculated by minutes.

TABLE 2 Multivariable logistic regression analysis for the 90-days follow-up mRS across three groups.

	EVT (*n* = 42) *N* (%)	IV-tPA (*n* = 45)				Conservative treatment (n = 22)			
		N (%)	*p*	OR (95% CI)		*N* (%)	*p*	OR (95% CI)	
				Unadjusted	Adjusted*			Unadjusted	Adjusted#
mRS $\leq$ 1	28 (66.7)	18 (40.0)	0.01	1.67 (1.10-2.53)	1.79 (1.19-2.68)	5 (22.7)	0.001	2.93 (1.32-6.52)	3.04 (1.37-6.74)
mRS $\leq$ 2	32 (76.2)	24 (53.3)	0.04	1.43 (1.04-1.97)	1.52 (1.11-2.07)	6 (27.2)	<0.001	2.79 (1.38-5.64)	2.84 (1.41-5.73)

OR, odds ratio. The OR was adjusted for age, onset NIHSS score, pre-onset mRS, hypertension, diabetes, hyper-lipidemia, current smoker, time from door to CT. *Comparison between EVT and IV-tPA; #Comparison between EVT and conservative treatment.

apex of the circular sclcus, which may lead to a disparity during treatment decision making. Tomsick et al proposed the functional-anatomical M1-M2 classification to define the M2 occlusion and concluded it was closely related to patient's prognosis after endovascular therapy (8). In this study, we used the novel definition of M2 segment and compared the safety and clinical outcomes of EVT, IV thrombolysis and conservative treatment in M2 segment occlusion stroke based on a real-world database. This study provided real-world evidence of the beneficial superiority and non-of EVT safety compared with IV thrombolysis and conservative treatment among the patients with acute ischaemic stroke associated with M2 occlusion in two centers. The EVT indicated a significantly higher potential of post-stroke function maintenance at 90 days with a mRS $\leq$ 1 being 66.7% and a mRS $\leq$ 2 being 76.2%, while IV thrombolysis maintaining a mRS $\leq$ 1 by 44.3% and mRS $\leq$ 2 by 53.3%. In an ordinal analysis of the distribution of mRS scores at 90 days, the small sample size in each subscale did not provide sufficient power to detect the differences between the groups. Findings for the sICH showed no significant difference between EVT and IV thrombolysis in absolute number. Due to lack of deceased cases in the study cohorts, we were unable to conduct analysis for mortality.

In this study, the classification of M2 occlusion was different from that of previous studies. The lack of consensus brings challenges in selecting an appropriate M2-segment occlusion population for intervention. One of the more common methods to define the M2 segment relies on the use of anatomic boundaries, in which the M2 segment originates from the genu of the MCA as it takes a vertical turn in the Sylvian fissure. Another widely accepted theory adopted the branching pattern and identified post-bifurcation branches of MCA as M2 segment (19). Due to the high frequency of early bifurcation MCA anatomy, these two methods may obtain inconsistent results (20). In this study, we used a mixing strategy to differentiate M2 from M1 using the functional-anatomical method. It defines

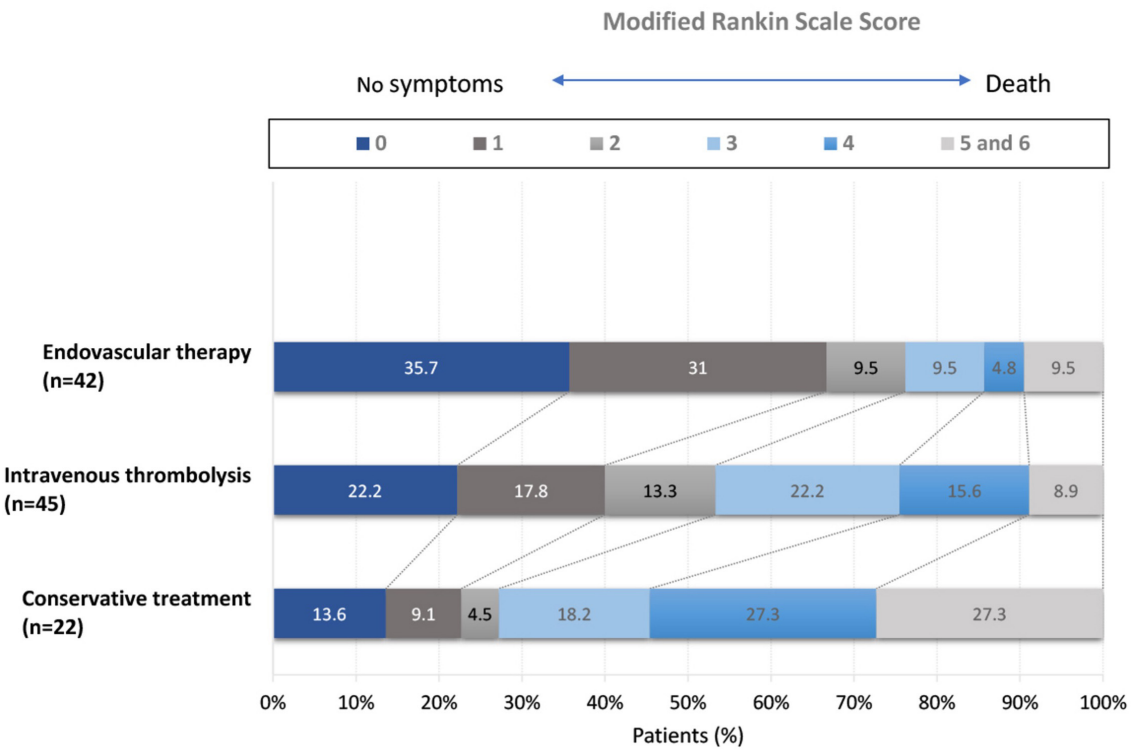

FIGURE 1
The mRS scores at 90 days among patients receiving endovascular therapy, intravenous thrombolysis, and conservative treatment.

TABLE 3 The safety assessment of the treatments: Symptomatic ICH and mortality.

	EVT (*n* = 42) *N* (%)	IV thrombolysis (*n* = 45) *N* (%)	*P*-value	OR (95% CI)	
				Unadjusted	Adjusted
Symptomatic ICH	1 (2.3)	2 (4.4)	>0.99	0.54 (0.05-5.69)	0.71 (0.13-4.07)

ICH, intracranial hemorrhage. The OR was adjusted for age, baseline NIHSS score and door-to-puncture or needle time by minutes.

M2 occlusion as having at least one filling of the classic M2 branch. Unlike those definitions which rely on "bifurcation" as a key component, the functional-anatomical method reduces the confusion from anatomic variation and may reasonably include holo-temporal artery and posterior temporal artery, which extend out before MCA bifurcates as M2 branches.

Our results showed that the EVT group achieve a higher percentage in maintaining a mRS $\leq$ 0-2 at 90 days (73%), a lower sICH (2.3%) and mortality (no decease case) compared with the results of recent meta-analysis (mRS of 0-2: 59%, sICH: 4.9-10%, mortality: 7.7-16%) (8, 9). The success of EVT may be due to the selection criteria that used functional-anatomical M2 identification which was introduced in this study. The improvement of the EVT technique also escalated the benefit of post-stroke outcomes by successfully achieving a better recanalization and by shortening the door-to-treatment time.

However, this study had several limitations. Firstly, it is a retrospective cohort study that was conducted in a metropolitan city, where the selection bias needs to be considered. Meanwhile, patients in the EVT group may have higher NHISS scores and the retrospective design of the study with unknown confounding factors unable to be adjusted also had potential effect on the results. Secondly, the exclusion of patients by neuro-interventionists, due to the difficulty in clot retrieval performance may decrease adverse outcomes and mortality. Thirdly, some of the patients receiving EVT were refereed and transferred from other hospitals where they may have received intravenous treatment before admission. For those patients, it was difficult to track the initial treatment which may have an impact on the results. Finally, the small sample size increased type II error and reduced the significance of the results.

5. Conclusion

This study provided real-world evidence of the benefit and safety in EVT, IV thrombolysis and conservative treatment in

moderate to severe acute stroke patients with M2 occlusion. EVT showed its superiority in functional outcomes and safety compared with the other two treatments. The results in this study may support the design of a treatment strategy for acute ischemic stroke with M2 occlusion. Additional large data analysis across different cities involving more hospitals, is required to broaden the results, especially in safety assessment.

Data availability statement

The raw data supporting the conclusions of this article will be made available by the authors, without undue reservation.

Ethics statement

The studies involving human participants were reviewed and approved by Tenth People's Hospital Research Ethics Committee (approval number: 21k253) and the Seventh People's Hospital Research Ethics Committee (approval number: 2021-B151). The patients/participants provided their written informed consent to participate in this study.

Author contributions

YX and WF: conception, design, data collection, data analysis, and write and revise the manuscript. YW, QB, QW, and LY: conception, design, patient follow-up, literature review, and revise the manuscript. QZ and FW: conception, design, data analysis, result interruption, and revise the manuscript. All authors have final approval of the manuscript.

Funding

This research was funded by the 2021 Scientific Research Project of Shanghai Municipal Commission of Health and Family Planning (202140282), 2020 Health Science and Technology Project of Pudong New Area Health Commission (PW2020D-5), Outstanding Leaders Training Program of Pudong Health Bureau of Shanghai (PWR12020-03), 2020 Science and Technology Development Fund of Pudong New Area Special Fund for People's Livelihood Scientific Research (PKJ2020-Y-15), and the Key Discipline in Pudong New Area Health Commission (PWZxq2022-01).

Conflict of interest

The authors declare that the research was conducted in the absence of any commercial or financial relationships that could be construed as a potential conflict of interest.

Publisher's note

All claims expressed in this article are solely those of the authors and do not necessarily represent those of their affiliated organizations, or those of the publisher, the editors and the reviewers. Any product that may be evaluated in this article, or claim that may be made by its manufacturer, is not guaranteed or endorsed by the publisher.

References

1. Powers W, Rabinstein A, Ackerson T, Adeoye O, Bambakidis N, Becker K, et al. Guidelines for the early management of patients with acute ischemic stroke: 2019 update to the 2018 guidelines for the early management of acute ischemic stroke: a guideline for healthcare professionals from the American heart association/American stroke association. *Stroke.* (2019) 50:e344–418. doi: 10.1161/STR.0000000000000211

2. Mönch S, Boeckh-Behrens T, Maegerlein C, Berndt M, Wunderlich S, Zimmer C, et al. Mechanical thrombectomy of the middle cerebral artery – neither segment nor diameter matter. *J Stroke Cerebrovasc Dis.* (2020) 29:104542. doi: 10.1016/j.jstrokecerebrovasdis.2019.104542

3. Compagne KCJ, van der Sluijs PM, van den Wijngaard IR, Roozenbeek B, Mulder MJHL, van Zwam WH, et al. Endovascular treatment: the role of dominant caliber m2 segment occlusion in ischemic stroke. *Stroke.* (2019) 50:419–27. doi: 10.1161/STROKEAHA.118.023117

4. Goebel J, Stenzel E, Wanke I, Paech D, Koehrmann M, Kleinschnitz C, et al. Effectiveness of endovascular recanalization treatment for M2 segment occlusion: comparison between intracranial ICA, M1, and M2 segment thrombectomy. *Acad Radiol.* (2019) 26:e298–304. doi: 10.1016/j.acra.2018.11.019

5. Goda T, Oyama N, Kitano T, Iwamoto T, Yamashita S, Takai H, et al. Factors associated with unsuccessful recanalization in mechanical thrombectomy for acute ischemic stroke. *Cerebrovasc Dis Extra.* (2019) 9:107–13. doi: 10.1159/000503001

6. Navia P, Schramm P, Fiehler J. ADAPT technique in ischemic stroke treatment of M2 middle cerebral artery occlusions in comparison to M1 occlusions: post hoc analysis of the promise study. *Interv Neuroradiol.* (2020) 26:178–86. doi: 10.1177/1591019919894800

7. Miura M, Yoshimura S, Sakai N, Yamagami H, Uchida K, Nagao Y, et al. Endovascular therapy for middle cerebral artery M2 segment occlusion: subanalyses of RESCUE-Japan registry 2. *J Neurointerv Surg.* (2019) 11:964–9. doi: 10.1136/neurintsurg-2018-014627

8. Tomsick T, Carrozzella J, Foster L, Hill M, von Kummer R, Goyal M, et al. Endovascular therapy of M2 occlusion in IMS III: role of M2 segment definition and location on clinical and revascularization outcomes. *AJNR Am J Neuroradiol.* (2017) 38:84–9. doi: 10.3174/ajnr.A4979

9. Wahlgren N, Ahmed N, Dávalos A, Ford G, Grond M, Hacke W, et al. Thrombolysis with alteplase for acute ischaemic stroke in the safe implementation of thrombolysis in stroke-monitoring study (SITS-MOST): an observational study. *Lancet.* (2007) 369:275–82. doi: 10.1016/S0140-6736(07)60149-4

10. Chen C, Wang C, Buell T, Ding D, Raper D, Ironside N, et al. Endovascular mechanical thrombectomy for acute middle cerebral artery M2 segment occlusion: a systematic review. *World Neurosurg.* (2017) 107:684–91. doi: 10.1016/j.wneu.2017.08.108

11. Protto S, Sillanpaa N, Pienimaki J, Matkaselka I, Seppanen J, Numminen H. Stent retriever thrombectomy in different thrombus locations of anterior cerebral circulation. *Cardiovasc Intervent Radiol.* (2016) 39:988–93. doi: 10.1007/s00270-016-1315-4

12. Sarraj A, Parsons M, Bivard A, Hassan A, Abraham M, Wu T, et al. Endovascular thrombectomy versus medical management in isolated M2 occlusions: pooled patient-level analysis from the EXTEND-IA trials, INSPIRE, and SELECT studies. *Ann Neurol.* (2022) 91:629–39. doi: 10.1002/ana.26331

13. Rai A, Domico J, Buseman C, Tarabishy A, Fulks D, Lucke-Wold N, et al. A population-based incidence of M2 strokes indicates potential expansion of large vessel occlusions amenable to endovascular therapy. *J Neurointerv Surg.* (2018) 10:510–5. doi: 10.1136/neurintsurg-2017-013371

14. Lima F, Furie K, Silva G, Lev M, Camargo E, Singhal A, et al. Prognosis of untreated strokes due to anterior circulation proximal intracranial arterial occlusions detected by use of computed tomography angiography. *JAMA Neurol.* (2014) 71:151–7. doi: 10.1001/jamaneurol.2013.5007

15. Sarraj A, Sangha N, Hussain M, Wisco D, Vora N, Elijovich L, et al. Endovascular therapy for acute ischemic stroke with occlusion of the middle cerebral artery M2 segment. *JAMA Neurol.* (2016) 73:1291–6. doi: 10.1001/jamaneurol.2016.2773

16. Wang J, Qian J, Fan L, Wang Y. *Efficacy and safety of mechanical thrombectomy for M2 segment of middle cerebral artery: a systematic review and meta-analysis. J Neurol.* (2021) 268:2346–54. doi: 10.1007/s00415-020-09710-w

17. Saber H, Narayanan S, Palla M, Saver J, Nogueira R, Yoo A, et al. Mechanical thrombectomy for acute ischemic stroke with occlusion of the M2 segment of the middle cerebral artery: a meta-analysis. *J Neurointervent Surg.* (2018) 10:620–4. doi: 10.1136/neurintsurg-2017-013515

18. Li G, Huang R, Li W, Zhang X, Bi G. Mechanical thrombectomy with second-generation devices for acute cerebral middle artery M2 segment occlusion: a meta-analysis. *Interv Neuroradiol.* (2020) 26:187–94. doi: 10.1177/1591019919886405

19. Goyal M, Menon B, Krings T, Patil S, Qazi E, McTaggart R, et al. What constitutes the M1 segment of the middle cerebral artery? *J Neurointerv Surg.* (2016) 8:1273–7. doi: 10.1136/neurintsurg-2015-012191

20. Nicola Morelli M. 2; Eugenia rota, MD1; Emanuele Michieletti, MD2. Not all middle cerebral artery M2 segments are the same. *JAMA Neurol.* (2017) 74:2. doi: 10.1001/jamaneurol.2016.6171

frontiers | Frontiers in Cardiovascular Medicine

TYPE Review
PUBLISHED 13 February 2023
DOI 10.3389/fcvm.2023.1067732

OPEN ACCESS

EDITED BY
Maria Monsalve,
Autonomous University of Madrid, Spain

REVIEWED BY
Manikandan Panchatcharam,
Louisiana State University Health Shreveport, United States
Ting Yuan,
Goethe-Universität Frankfurt, Germany

*CORRESPONDENCE
Jia Qi
✉ qijia@xinhuamed.com.cn
Jian Zhang
✉ zhangjian@xinhuamed.com.cn

SPECIALTY SECTION
This article was submitted to General Cardiovascular Medicine, a section of the journal Frontiers in Cardiovascular Medicine

RECEIVED 12 October 2022
ACCEPTED 30 January 2023
PUBLISHED 13 February 2023

CITATION
Zhu T, Hu Q, Yuan Y, Yao H, Zhang J and Qi J (2023) Mitochondrial dynamics in vascular remodeling and target-organ damage. *Front. Cardiovasc. Med.* 10:1067732. doi: 10.3389/fcvm.2023.1067732

Mitochondrial dynamics in vascular remodeling and target-organ damage

Tong Zhu[1], Qingxun Hu[2,3], Yanggang Yuan[4], Huijuan Yao[1], Jian Zhang[1]* and Jia Qi[1]*

[1]Department of Pharmacy, Xinhua Hospital Affiliated to Shanghai Jiao Tong University School of Medicine, Shanghai, China, [2]Institute of Geriatrics (Shanghai University), Affiliated Nantong Hospital of Shanghai University, School of Medicine, Shanghai University, Shanghai, China, [3]Shanghai Engineering Research Center of Organ Repair, School of Medicine, Shanghai University, Shanghai, China, [4]Department of Nephrology, The First Hospital Affiliated to Nanjing Medical University, Nanjing, China

Vascular remodeling is the pathological basis for the development of many cardiovascular diseases. The mechanisms underlying endothelial cell dysfunction, smooth muscle cell phenotypic switching, fibroblast activation, and inflammatory macrophage differentiation during vascular remodeling remain elusive. Mitochondria are highly dynamic organelles. Recent studies showed that mitochondrial fusion and fission play crucial roles in vascular remodeling and that the delicate balance of fusion-fission may be more important than individual processes. In addition, vascular remodeling may also lead to target-organ damage by interfering with the blood supply to major body organs such as the heart, brain, and kidney. The protective effect of mitochondrial dynamics modulators on target-organs has been demonstrated in numerous studies, but whether they can be used for the treatment of related cardiovascular diseases needs to be verified in future clinical studies. Herein, we summarize recent advances regarding mitochondrial dynamics in multiple cells involved in vascular remodeling and associated target-organ damage.

KEYWORDS

mitochondrial dynamics, vascular remodeling, cardiovascular diseases, target-organ damage, fusion, fission

Introduction

Cardiovascular disease (CVD) remains the leading cause of morbidity and mortality in developing countries, cardiovascular disease accounted for about 31 percent of global deaths in 2015 (1, 2). According to the statistics of the global burden of disease (GBD), from 2009 to 2019, the global deaths caused by CVD and vascular diseases were respectively related to ischemic heart disease (IHD, 16.17%), stroke (11.59%), cardiomyopathy and myocarditis (0.6%), other cardiovascular and circulatory diseases (0.49%), and chronic kidney disease (2.53%) [(IHME), (3)]. Vascular remodeling (VR) is an important process in various cardiovascular diseases. The vessel wall is an active and integrated organ composed of endothelial cells (ECs), smooth muscle cells (SMCs) as well as vascular fibroblasts (VAFs), and these cells can interact with each other (4). VR represents changes in vascular structure and arrangement, usually accompanied by activation of endothelial cells, migration and apoptosis of smooth muscle cells, degradation of the extravascular matrix (ECM), and disruption of the structural integrity of the vessel (4). Macrophages and inflammation also promote the development of vascular

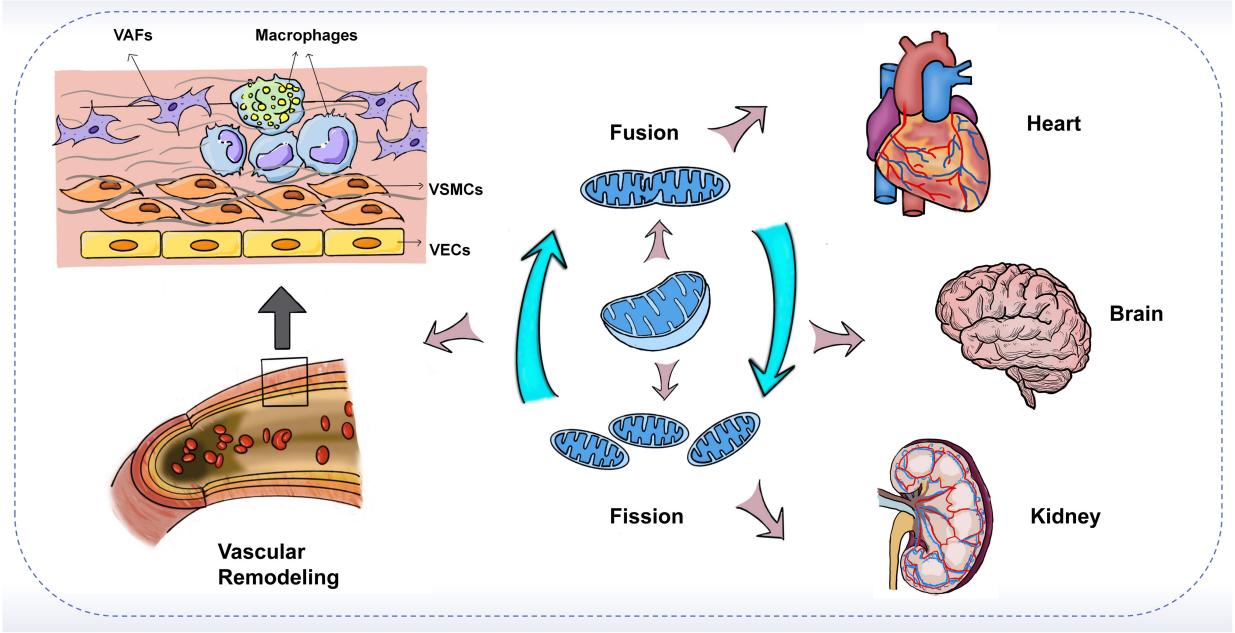

GRAPHICAL ABSTRACT
The imbalance of mitochondrial fusion and fission plays an important role in vascular remodeling and target-organ damage.

remodeling (5). Mitochondrial dysfunction is one of the important mechanisms mediating vascular remodeling and affects cellular homeostasis mainly by affecting cellular energy, reactive oxygen species (ROS) production, intracellular calcium levels, and apoptotic protein production (6). The vascular system is a tissue that does not require a lot of energy, thus the mitochondria here play the role of sensors, signaling hubs, and regulators of apoptosis, despite their role in energy metabolism (7, 8). In recent years, a growing number of studies have shown that defects in mitochondrial dynamics play a crucial role in the pathogenesis of several cardiovascular diseases (6). Mitochondrial dynamics is thought to have important functions in the growth, death, and migration of vascular endothelial and smooth muscle cells, and may also be involved in regulating the production or degradation of extracellular matrix, all of which contribute to vascular remodeling in cardiovascular diseases (9).

Abbreviations: CVD, cardiovascular disease; VR, vascular remodeling; ECs, endothelial cells; SMCs, smooth muscle cells; VAFs, vascular fibroblasts; ECM, extravascular matrix; ROS, reactive oxygen species; OM, outer membrane; OMM, outer mitochondrial membrane; IM, inner membrane; IMM, inner mitochondrial membrane; IMS, intermembrane space; MtDNA, mitochondrial DNA; OXPHOS, oxidative phosphorylation; Mfns, mitofusins Opa1, Optic atrophy protein 1; Drp1, dynamin-related protein 1; DLP1, dynamin-like protein 1; Mfn1/2, mitofusin 1/2; HR1, heptad repeat 1; TMs, transmembrane structural domains; CL, cardiolipin; MTS, mitochondrial targeting sequence; MPP, matrix processing protease; ER, endoplasmic reticulum; INF2, inverted formin 2; ApoE, apolipoprotein E; PI(4)P, phosphatidylinositol 4-phosphate; MIEF1/2, mitochondrial elongation factors 1/2; AFs, adventitial fibroblasts; MFs, myofibroblasts; HG, high-glucose; HUVECs, human umbilical vein endothelial cells; PKM2, pyruvate kinase myozyme 2; VR-EPCs, vascular-resident endothelial progenitor cells; ATX, astaxanthin; MCECs, mouse coronary artery endothelial cells; VCAM-1, vascular cell adhesion molecule-1; PASMCs, pulmonary artery smooth muscle cells; PDGF, platelet-derived growth factor-BB; GLP-1, glucagon-like peptide-1; CaMKII, calmodulin-dependent kinase II; CN, calcineurin; Klf5, Krüppel-like factor 5; HSP90, heat shock protein 90; TAB, transverse aortic banding; TGF-β1, transforming growth factor-β1; MCAO, mouse middle cerebral artery occlusion; I/R, ischemia/reperfusion; AKAP1, A-kinase anchoring protein 1; CKD, chronic kidney disease; VC, vascular calcification.

Mitochondria originated from a eukaryotic ancestor unified with an alpha-proteobacterium (10). Mitochondria have two relatively independent and functionally distinct membranes, the outer membrane (OM) and the inner membrane (IM) (11), which divide the mitochondria into two compartments. Located between the two mitochondrial membranes is the intermembrane space (IMS), and wrapped by the inner membrane are the matrix compartments (11). A small amount of DNA is present in the mitochondrial matrix, called mitochondrial DNA (mtDNA), which encodes a series of proteins critical to mitochondrial respiration (12). Despite the long evolutionary history before being perceived as eukaryotic organelles, the important role of mitochondria in eukaryotic cell function is deeply ingrained (13). As is known to all that mitochondria are the "powerhouses" of cells, responsible for producing most of the ATP in cells through oxidative phosphorylation (OXPHOS). In addition, mitochondrial electron transport chains are also vital to the regulation of mitochondrial calcium (14). Mitochondria can be the main source of ROS during electron transport to produce ATP, which can both promote cell death and act as signaling molecules. Therefore, mitochondria are also key regulators of cell death (15). To achieve these functions, mitochondria have become organelles that exhibit remarkable dynamics (16). Mitochondria regulate their morphology and control their number and size through fusion and fission, a continuous cycle of fission and fusion is also known as mitochondrial dynamics (17). Mitochondrial dynamics is closely related to mitochondrial function. The balanced fusion and fission events of mitochondria maintain the health of mitochondria and their host cells and organisms (15, 17). There is evidence that an imbalance of mitochondrial dynamics plays a crucial role in the pathogenesis of many cardiovascular diseases (6). This review summarizes recent progress in the understanding of the role of mitochondrial dynamics in vascular remodeling and related target-organ damage.

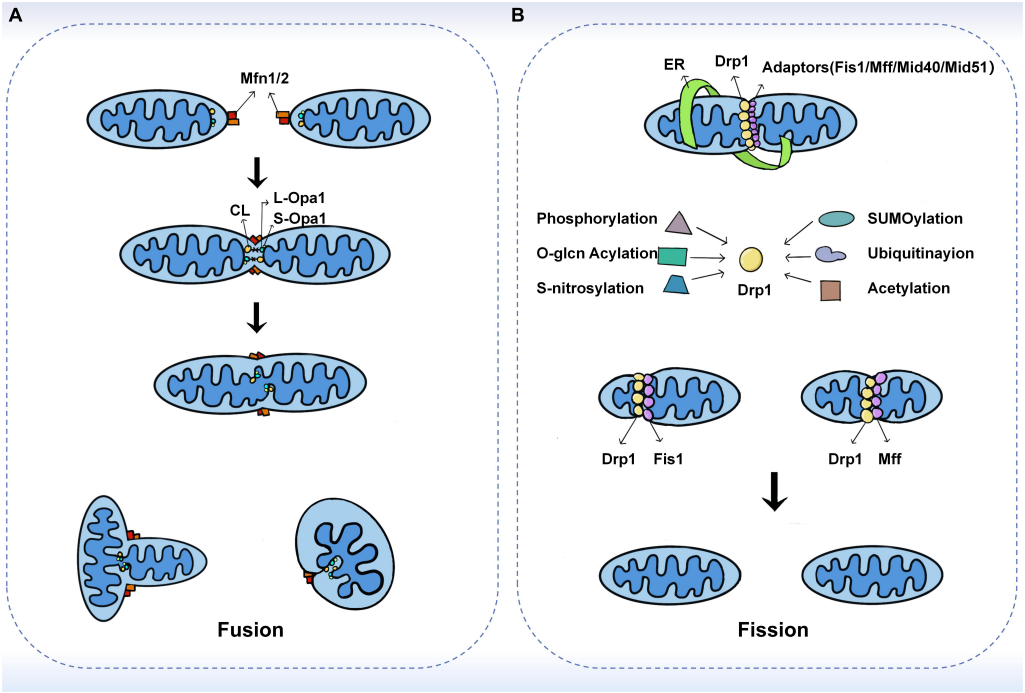

FIGURE 1
The fusion and fission machinery. **(A)** The mechanisms of mitochondrial fusion. Mfn1/2 mediate outer membrane fusion. Opa1 mediates inner membrane fusion and maintains cristae structure. Under stress, L-Opa1 is activated and S-Opa1 can regulate the fusion activity of L-Opa1. **(B)** The mechanisms of mitochondrial fission. Drp1 plays a central role in mitochondrial fission. Several kinds of post-translational modifications of Drp1 may affect the recruitment of Drp1 from the cytoplasm. The adaptors including Fis1, Mff, MiD49, and MiD51 also have substantial roles in the recruitment of Drp1 to mitochondria.

Mitochondrial fusion and fission

Mitochondrial fusion

Mitochondrial fusion refers to the integration of the outer and inner membranes of two adjacent mitochondria into one, resulting in a fibrous extension and network structure of mitochondria (18). Mitochondrial fusion has been shown to occur through a sequential event of the outer mitochondrial membrane (OMM) and inner mitochondrial membrane (IMM) fusion, with Mitofusins (Mfns) and Optic atrophy protein 1 (Opa1) mediating the fusion of the outer and inner membranes, respectively (19, 20). In a typical mitochondrial fusion reaction, the endpoints of two mitochondria collide, with the outer membrane fusing first and then the inner membrane fusing at the collision site. Fusion events can also occur between ends and sides, or within a single mitochondrion to form a ring structure (16). As a result of fusion, the content is mixed and the matrix is exchanged, but mtDNA exchange is limited despite being in the matrix (21). In addition to complete fusion, mitochondrial fusion can take different forms, such as instantaneous fusion, the so-called "kiss-and-run" encounter, in which no obvious merger or structural rearrangement occurs (22) (**Figure 1A**).

Regulators of mitochondrial fusion

Mitochondria primarily mediate fusion through three membrane GTPases of the dynamin-related protein (DRP) superfamily, including Mitofusin 1 (Mfn1), Mitofusin 2 (Mfn2), and Optic atrophy protein 1 (Opa1). Among them, Mfn1/2 is located on the outer mitochondrial membrane and its main function is to facilitate mitochondrial docking and fusion (18). The mitochondrial fusion mechanism of Mfns has been investigated based on its topology (23). In the past, Mfns were thought to be inserted into the OMM through two transmembrane structural domains (TMs). TMs are separated by a short loop containing GTPase and coil-coil heptad repeat 1 (HR1) structural domain at the N-terminal end, while the C-terminal end carries the HR2 structural domain (24, 25). It has been proposed that Mfns establish a linkage between paralogous mitochondria *via* dimeric antiparallel *trans* interactions at their HR2 structural domains, followed by GTP hydrolysis to produce an OMM fusion (23). However, a recent study showed that only one transmembrane structural domain exists in human Mfns, which places the N-terminal GTPase and HR1 structural domains in the cytoplasm and the C-terminal HR2 structural domain in the mitochondrial membrane gap (26). Several studies have proposed that the bolting of the two OMMs occurs through oligomerization of the GTPase structural domains in the Mfns. Upon GTP binding and hydrolysis, the GTPase structural domain undergoes a conformational change leading to its oligomerization, which facilitates the docking and subsequent fusion of the two mitochondria at the two outer membranes (27, 28). Mattie et al. demonstrated that with increasing levels of oxidized glutathione, the two cysteine residues located in the HR2 structural domain can be oxidized, leading to the formation of disulfide bonds between Mfn molecules and then oligomerization occurs (26). This new mechanism suggests that redox signaling plays a crucial role in OMM fusion. Furthermore, studies in cells have shown that Mfn1 and Mfn2 have different functions. For example, Mfn1 has a higher

GTPase activity than Mfn2 and therefore promotes mitochondrial fusion more efficiently (29). Opa1-mediated fusion is also dependent on Mfn1 rather than Mfn2 (30). This explains that overexpression of either Mfns leads to perinuclear mitochondrial aggregation but with different results. Mfn1 induces mitochondrial fragmentation, while Mfn2 exhibits swollen spherical mitochondria (31).

Mitochondrial endosomal fusion is mediated by the direct action of optic atrophy 1 (Opa1) and cardiolipin (CL), a specific component localized to the inner mitochondrial membrane (24). Unlike Mfns, only one of the two opposing mitochondria needs to carry Opa1 for endosomal fusion to occur (16). Ban et al. showed that Opa1 mediates endosomal fusion *via* heterotrimeric Opa1-cardiolipin interactions. Similarly, when cardiolipin was not present, membrane fusion was not observed even when L-Opa1 was present on both sides of the membrane (32). The encoding of Opa1 forms eight isoforms during transcription by differential splicing in exons 4, 4b, and 5b. All isoforms contain an N-terminal mitochondrial targeting sequence (MTS) and a generic exon 5 encoding the S1 protein hydrolysis site (33). The MTS is removed by matrix processing protease (MPP) during N-terminal entry into the matrix, while the retention or not of the S1 site determines the isoforms of Opa1 (34). If the S1 site remains intact, a long isoform of Opa1 (L-Opa1) is produced that is anchored to the endosomal membrane. In the steady state, approximately half of Opa1 exists as L-Opa1. In contrast, if the S1 site is cleaved by the Oma1 protease, short isoforms of Opa1 (S-Opa1) are produced, and they form a complex through the L-Opa1 isoform to regulate fusion activity. It was shown that the addition of S-Opa1 enhanced the membrane fusion activity of L-Opa1 *in vitro* (32, 34). Alternatively, variant S-Opa1 can be produced by the shearing of S2 proteins by the Yme1L protease (34, 35). Previous and recent studies have shown that fusion requires the co-action of long and short isoforms under basal conditions (36, 37). However, several different findings also exist. For instance, some studies have shown that L-Opa1 alone promotes IMM fusion (34, 38). Moreover, S-Opa1 has been proposed to promote fission (39).

Mitochondrial fission

Mitochondrial fission is the division of one mitochondrion into two smaller mitochondria, usually asymmetrically, resulting in the formation of two unequal-sized daughter mitochondria (16, 40). The core reaction of mitochondrial division is the contraction and rupture of the two mitochondrial membranes, which is driven by the recruitment of Drp1 to the mitochondria *via* its receptor protein located on the outer membrane and is regulated at multiple levels (40–42). During the life cycle of mitochondria, fission can both produce new mitochondria and eliminate dysfunctional mitochondria through mitochondrial phagosomes (43, 44). Previous studies have shown that fission is the basis of mitochondrial proliferation and degradation (43). However, recent studies have found that the regulation of organelle levels, that is, the localization of fission sites, may be a key morphological feature leading to different mitochondrial fates (45). Super-resolution microscopy was used to analyze the mitochondrial division and then two spatially different types of division were defined in this study. Midzone division occurs at the center of the organelle (within the central 50%), whereas peripheral division occurs at both ends of the mitochondria (less than 25% from the tip). Division in the outer region contributes to the shedding of damaged material into smaller mitochondria for mitochondrial phagocytosis, while division in the middle region causes the mitochondrial proliferation (45) (**Figure 1B**).

Regulators of mitochondrial fission

The central reaction of mitochondrial division is the contraction and rupture of two mitochondrial membranes (46). Recently, Kraus et al. introduced the concept of "mitochondrial divisome." That is, in eukaryotic cells, the core components of the division include dynamin-related protein 1 (Drp1) and its adapters, while other organelles such as the endoplasmic reticulum (ER), actin, contact sites between organelles, and specific lipids on the outer membrane are classified as accessory components, which together regulate and control mitochondrial division (47).

Drp1 is a cytoplasmic protein that acts as a key GTPase in mitochondrial fission (18). Once recruited from the cytoplasmic pool to the outer mitochondrial membrane, it forms helical oligomers that induce membrane contraction and fracture. In contrast, the deletion of Drp1 blocks mitochondrial division, causing mitochondria to lengthen or expand (40). Whether Drp1 can independently mediate mitochondrial division has not been fully demonstrated (48, 49). It has been suggested that Dynamin 2 (DNM2) is also recruited to the mitochondrial division site and is involved in the final membrane break event, and that knockdown of DNM2 inhibits mitochondrial fission, revealing its functional importance in fission (48). However, the necessity of DNM2 in mitochondrial fission has been challenged by many new studies. Drp1 itself has been shown to sever membrane tubules (50). Moreover, the loss of all conventional kinesins, including DNM1, DNM2, and DNM3, did not lead to mitochondrial inhibition of fission (51). These suggest that Drp1 can independently lead to mitochondrial fission. Nonetheless, DMN2 was also observed at the mitochondrial fission site on both sides of Drp1 (48), so it may play a non-essential role in fission. Post-translational modifications, such as phosphorylation, further regulate Drp1-mediated mitochondrial fission (52). MAPK1 can stimulate the phosphorylation of Ser616, which enhances Drp1 activity and leads to increased mitochondrial fission. On the other hand, PKA-induced phosphorylation of Ser637 inhibits Drp1 GTPase activity and fission, whereas Ca^{2+}-activated dephosphorylation triggers fission (18). Recently, the mitochondrial phosphatase PGAM5 has also been found to be involved in Ser637 dephosphorylation, the loss of which impairs mitochondrial fission and increases cellular senescence (53). In addition, o-glcn acylation, SUMOylation, s-nitrosylation, and ubiquitination can also regulate Drp1 activity (18). O-glcn acylation and s-nitrosylation of Drp1 increase its fission activity (54, 55), while mitochondria-associated protein ligase (MAPL)-mediated SUMOylation contributes to the stabilization of Drp1 function (56). Parkin can degrade the mitochondrial splitting protein Drp1 by ubiquitination (57). Apart from the above, recent studies have shown that excess lipid supply can create an intracellular environment in mice that promotes Drp1 acetylation, which in turn increases its activity and mitochondrial translocation, leading to cardiomyocyte dysfunction and death (58). It has been reported that low doses of methylmercury (MeHg) induced depolymerization of Drp1 at Cys624-S(n)H, leading to filamin-dependent activation of Drp1 and mitochondrial hyperfission, which increased cardiac fragility to mechanical load. In contrast, cilnidipine, a blocker of Drp1 and filamin-A interaction, inhibited mitochondrial

hyperfission in neonatal rat cardiomyocytes induced by low-dose MeHg exposure (59).

Adapters for Drp1 include four extramembrane proteins, Fis1, Mff, MiD49, and MiD51. Each adapter can independently recruit Drp1 into mitochondria, and there are also indications of interactions between MiDs and Mff (60, 61). In yeast, Fis1 plays a central role in mitochondrial fission, but in mammals, cells lacking Fis1 show little or no fission deficiency (41). Mff, MiD49, and MiD51 appear to have a more important role in mammalian Drp1 recruitment. Mff deficiency results in a reduced recruitment of Drp1 to mitochondria and disrupts fission, whereas Mff overexpression enhances mitochondrial fragmentation (61). MiDs are more complex, as their low protein expressions lead to enhanced mitochondrial fission, but overexpression leads to significant mitochondrial elongation (62). However, a recent study by Kleele et al. showed that there is more than one type of mitochondrial division and that Fis1 and Mff play different roles in the different forms of mitochondrial division (45). When mitochondria are damaged or stressed, Fis1-mediated peripheral division is increased, predicting mitochondrial autophagy. In contrast, Mff has no role in the peripheral division but plays a role in the midzone division. Mid-region division is usually increased in situations that stimulate cell proliferation (45). This study also raises exciting questions, such as whether other factors are specifically involved in a peripheral division or midzone division. In this regard, MiD51 and MiD49 are of particular interest because this new study does not provide conclusive results regarding their role.

In the complex environment of living cells, accessory components of the "mitochondrial divisome," such as the endoplasmic reticulum (ER) and lysosomes, as well as actin, cytoskeleton-related binding proteins inverted formin 2 (INF2) and Spire1C, which are required for initiation and control of mitochondrial fission (47). The contact site between mitochondria and the ER is important for coordination between the two organelles and may be the site where the first step of the division process occurs (63). Before Drp1 is recruited, ER-bound INF2 cooperates with mitochondria-anchored Spire1C to regulate mitochondrial contraction to a size that allows Drp1-oligomeric loop formation at the contact site between the two organelles (64). This process may also be related to the motor protein myosin II (65). However, it has also shown that Ca^{2+}-dependent inner membrane (IMM) contraction represents the initiating event of mitochondrial fission (66). IMM contraction occurs before outer membrane contraction and is regulated by Opa1, a kinetic protein that controls mitochondrial fusion. Opa1 interacts with the MICOS complex that connects the outer and inner membranes and promotes inner membrane contraction (66). Interestingly, endosome contraction is enhanced in the absence of Drp1, suggesting that cells can compensate for the absence of mitochondrial division by increasing endosome contraction (67).

Contact of lysosomes and *trans*-Golgi networks with mitochondria is also associated with fission. Lysosomes bind at the site of mitochondrial contraction before fission (68). The mitochondria-localized GTPase-activating protein TBC1D15 is involved in fission along with the lysosome-associated RAB7. Recently, phosphatidylinositol 4-phosphate [PI(4)P] *trans*-Golgi vesicles and ARF1 were discovered to co-localize at Drp1-positive mitochondrial fission sites, which are also labeled by lysosomes (69). The deletion of ARF1 or PI(4)P increased mitochondrial length but not Drp1 recruitment, suggesting that loss of PI(4)P delayed the late phase of Drp1-mediated fission.

Mitochondrial lipids are also involved in the regulation of mitochondrial fission and have different roles. In addition to its role in fusion, cardiolipin binds to Drp1, drives Drp1 oligomerization, and stimulates its GTPase activity (70). In contrast, phosphatidic acid interacts with Drp1 and inhibits its function (71). The mitochondrial phospholipase MitoPLD can act as a key regulator in the conversion of stimulatory cardiolipin and inhibitory phosphatidic acid. Interestingly, Drp1 can form a complex with DMitoPLD to generate phosphatidic acid from cardiolipin (72). It will be exciting to further decipher how the interactions of Drp1, the actin cytoskeleton, phospholipids, and other organelles coordinate to control mitochondrial division.

Balance of fusion and fission

Nearly 100 years ago, mitochondrial motility and fission were first observed with light microscopy (73), and by the 1980s and 1990s, the study of mitochondrial dynamics continued to advance with the development of technology. First with phase-contrast microscopy, then with vital dyes, and finally with targeted fluorescent proteins, it was confirmed that mitochondria are in a constant process of division and fusion (74–76). The fact that mitochondrial fission and fusion are considered to be critical processes for mitochondrial and cellular health has not been fully appreciated until recent years (46, 77). Fission is important to ensure the number and distribution of mitochondria in daughter cells, and fusion allows content exchange between fused mitochondria to ensure optimal mitochondrial activity (18). Mitochondrial fusion and fusion usually occur simultaneously in a balanced manner within the cell, and the net balance between fusion and fission controls the size, number, shape, and activity of mitochondria (40). Disruption of homeostasis leads to imbalances in mitochondrial function, ultimately leading to a variety of diseases, including cardiovascular disease, neurodegenerative diseases, and cancer (78). An increase in fission or a decrease in fusion will result in more short or small mitochondria. In some cells, the shape itself has important functional consequences. In neurons, for example, the transport of small mitochondria to nerve terminals may be more efficient compared to long mitochondria (16). In addition, the size of mitochondria is crucial for their degradation by mitochondrial phagocytosis (41). However, the proper balance of fusion and fission seems to be more important compared to the absolute level of each process. For example, mice lacking Mff show severely reduced mitochondrial fission, significantly reduced OXPHOS activity in cardiomyocytes, and extensive fibrosis in cardiac tissue. In contrast, these defects can be completely rescued by concomitant loss of Mfn1 (79). A new study shows that mitochondrial elongation factors 1 and 2 (MIEF1/2) regulate mitochondrial fusion through direct interaction with the fusion proteins Mfn1 and Mfn2, in addition to their role in the fission machinery. MIEF1/2 competitively reduces the interaction of hFis1 with Mfn1 and Mfn2, alleviating hFis1-induced mitochondrial fragmentation and contributing to mitochondrial fusion (80). Furthermore, there is evidence that cellular feedback mechanisms can rebalance mitochondrial dynamics in part through compensatory responses when fission is disturbed. For instance, when Drp1 was deleted, the levels of Mfn1 and Mfn2 decreased by approximately 50% (81, 82). Based on the above, it can be argued that the delicate balance between mitochondrial fusion and fission plays an integral role in maintaining the mitochondria functions and determining cell fate. In fact, the reciprocal regulation of fission

and fusion is thought to be an emerging trend in the remodeling of mitochondrial networks, where multiple regulatory pathways influence both processes (83).

Mitochondrial dynamics and mechanism of vascular remodeling

In the arterial wall, endothelial cells (ECs), vascular smooth muscle cells (VSMCs), fibroblasts (VAFs), and macrophages are all important players in the process of vascular remodeling (VR). Mitochondrial dynamics are essential for the proper function of all key cell types involved in the development of vascular remodeling. Endothelial dysfunction is often considered a marker of atherosclerosis (84). Inhibition of Drp1 in apolipoprotein E (ApoE) knockout diabetic mice reduces endothelial dysfunction and atherosclerosis (85). Mfn2 expression is reduced in atherosclerosis models, and conversely, Mfn2 overexpression reduces atherosclerotic lesions in rabbits (86, 87). In addition, endothelial cells from patients with reduced vascular function exhibit increased expression of Fis1 and mitochondrial fragments, a phenomenon that can be rescued by *in vitro* fission inhibition (88). On the other hand, vascular smooth muscle cells (VSMCs) also proliferate and migrate during vascular reconstitution. Reduction of Mfn2 is associated with the activation of VSMCs by platelet-derived growth factor (PDGF), while inhibition of fission attenuates VSMCs proliferation (89). In an *in vitro* aortic ring assay, inhibition of Drp1 significantly reduced the proliferation and migration of VSMCs and decreased neovascularization in a rat carotid balloon injury model (90). Furthermore, macrophage-mediated inflammation is thought to accelerate the process of vascular remodeling. Blocking Drp1 reduces the accumulation of inflammatory macrophages in injured vessels and inhibits the growth and migration of VSMCs (91). In conclusion, these findings suggest that the expression of mitochondrial dynamin proteins plays an integral role in the development of vascular remodeling. Modulation of the balance of mitochondrial fission and fusion is expected to be an effective therapeutic strategy to slow the progression of vascular remodeling (**Figure 2**).

Vascular endothelial cells (ECs)

All arterial vessels from the heart to the capillaries have a continuous layer of endothelial cells (ECs), which constitute the innermost layer of the vessel wall and are in direct contact with blood flow (92). ECs provide an impermeable barrier between blood and tissues, ready to sense the environment and signal the regulation of vascular function. Therefore, alterations in endothelial function are often considered to be the beginning of vascular remodeling (92). On the other hand, mediators released by ECs can modulate the function of VSMCs and thus exert a decisive influence on vascular remodeling (93). Endothelial cells derive most of their energy from anaerobic glycolysis, and ATP production from oxidative phosphorylation reactions represents only a small fraction of the total energy they obtain. Compared to energy production, endothelial cell mitochondria seem to play a more dominant role in cellular homeostasis and activation of signaling cascades (94, 95). In addition to the traditional functions of regulating ROS, maintaining Ca^{2+} concentration, and integrating apoptotic stimuli, intact mitochondrial dynamics have an important role in regulating apoptosis, angiogenesis, and the pro-inflammatory state of the endothelium (96).

A series of studies have confirmed the involvement of the imbalance of mitochondrial fusion and division in the regulation of endothelial cell function. Lugus et al. demonstrated that Mitofusins have an important role in endothelial cell survival and angiogenic function (96). In VEGFA-induced human umbilical vein endothelial cells (HUVECs), knockdown of any of the Mfns resulted in disruption of the mitochondrial network and reduction of the mitochondrial membrane potential (96). At the same time, the ablation of Mfns impaired endothelial cell viability and increased apoptosis. Knockdown of Mfn2 alone results in reduced reactive oxygen species production, whereas knockdown of Mfn1 alone selectively reduces VEGF-stimulated Akt-eNOS signaling (96). Thus, Mfn1 and Mfn2 regulate endothelial cell migration, differentiation, and survival by affecting different aspects of angiogenic signaling. A recent study also showed that reduced Mfn2 expression leads to the uncoupling of endoplasmic reticulum-mitochondrial contacts, which in turn leads to enhanced mitochondrial fission, mitochondrial fragmentation, and as a result, increased ECs death (97). Several other studies in recent years have also shown an important role of mitochondrial fission and fusion in endothelial cell angiogenesis (98, 99). By activating pyruvate kinase myozyme 2 (PKM2), glycolytic and mitochondrial fusion events are significantly enhanced, thereby promoting angiogenesis in vascular-resident endothelial progenitor cells (VR-EPCs). Conversely, inhibition of PKM2 activity leads to a decrease in glycolysis and a significant promotion of mitochondrial fission, resulting in reduced expression of angiogenesis-related genes (98). Another study showed that increased phosphorylation of Drp1 in HUVECs enhances its activity in regulating mitochondrial fission and induces endothelial cell migration through the AMPK signaling pathway (99). The same results were obtained in a mouse model.

An increasing number of studies have found morphological alterations, loss of mitochondrial networks, and increased expression of fission proteins in mitochondria in endothelial cells under diabetic conditions. Makino et al. found in *in vitro* experiments that decreased levels of Drp1 in high-glucose (HG)-treated mouse coronary artery endothelial cells (MCECs) led to increased mitochondrial elongation, while increased levels of Drp1 may lead to mitochondrial fracture. This increases mitochondrial fragmentation and exhibits disruption of normal endothelial cell functions (100). In this study, similar results were obtained in animal experiments. Levels of Opa1 were significantly reduced in MCECs from diabetic mice, and levels of Drp1 were significantly increased, ultimately leading to an increase in mitochondrial fission (100). However, alterations in the levels of other fusion or fission-related proteins, such as Mfn1/2 and Fis1, were not confirmed in the present study. Similarly, Trudeau et al. discovered increased mitochondrial fragmentation in rat retinal endothelial cells cultured in an HG medium, which may underlie retinal endothelial cell apoptosis in diabetic retinopathy (101). A recent study showed that mitochondrial fission genes Fis1 and Drp1 were overexpressed under HG conditions, and that downregulation of Fis1 and Drp1 preserved the normal morphology of mitochondria, inhibited mitochondrial fission, and reduced apoptosis in retinal endothelial cells (102). Emerging evidence suggests that altered mitochondrial fusion-fission homeostasis is divided into a compensatory phase, an equilibrium shift phase, and a loss of compensatory phase (103). Initially, Mfn1 and Mfn2 exhibit a significant decrease while Drp1 and Fis1 are elevated, and mitochondrial fusion/fission

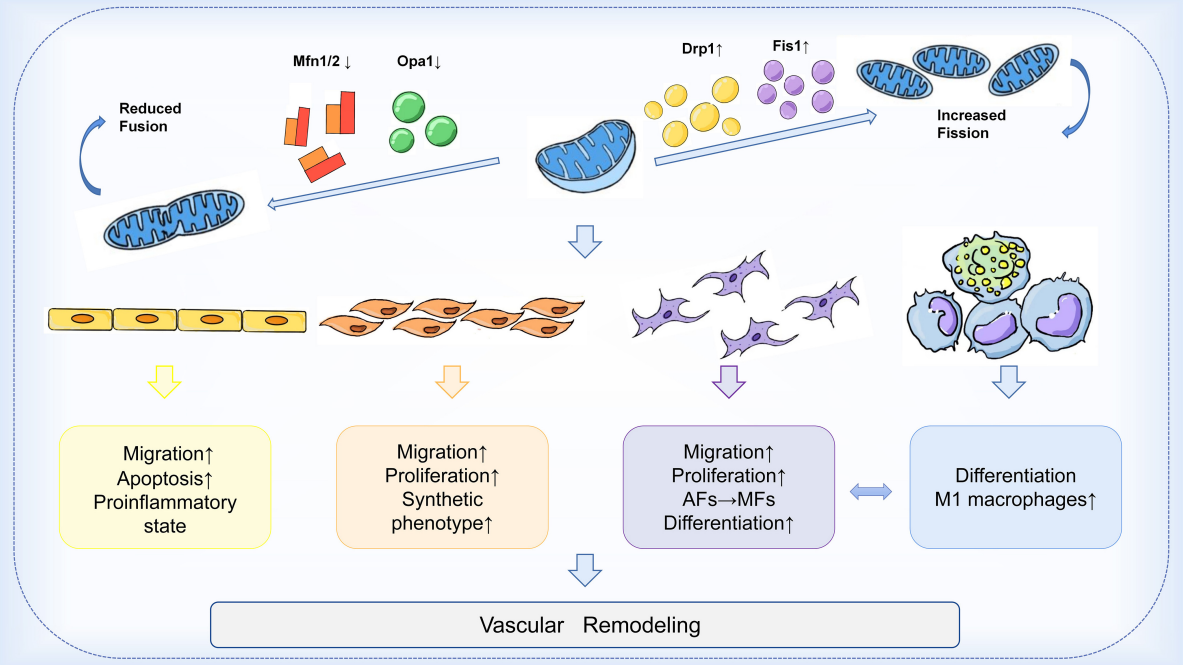

FIGURE 2
Mechanism of mitochondrial dynamics in vascular remodeling. During vascular remodeling, multiple cells of the vessel wall are regulated by mitochondrial dynamics. Mitochondrial division and fusion play an important role in regulating the migration, apoptosis, and pro-inflammatory state of endothelial cells, and are also involved in the transformation of the synthetic phenotype of VSMCs and the process of phenotypic changes from adventitial fibroblasts (AFs) to myofibroblasts (MFs). Mitochondrial kinetic imbalance is also an important factor in the proliferation and migration of VSMCs and AFs. In addition to these, the delicate balance between mitochondrial fission and fusion seems to be involved in regulating macrophages and the interactions between VSMCs and macrophages, thus affecting vascular remodeling.

homeostasis is disturbed, but normal mitochondrial membrane potential (MMP) can still be maintained. Then, with prolonged high glucose exposure, mitochondrial fusion/fission imbalance and mitochondrial fragmentation occurred. Finally, Opa1 expression decreased and mitochondrial fragmentation triggered endothelial cell apoptosis (103). Notably, Fis1 expression initially increased and decreased at the end, so Fis1 may be a predictor of changes in mitochondrial fusion-fission homeostasis during vascular injury. Both *in vitro* and *in vivo* results consistently showed that altered mitochondrial fusion-fission homeostasis could trigger high-glucose-induced vascular endothelial injury. The mechanism responsible for this outcome may be related to the AMPK signaling pathway.

The pro-inflammatory state associated with mitochondrial fission is also a factor contributing to vascular endothelial cell injury. Drp1-mediated mitochondrial fission plays a fundamental role in the regulation of inflammation (6). For example, mRNA transcript levels of inflammatory factors such as IL-1β, IFNγ, and TNFα are higher in Drp1-deficient mice (104). A recent study identified a unifying mechanism linking impaired mitochondrial dynamics to endothelial inflammation. The activity of Drp1 was shown to be necessary for the induction of inflammation by the proinflammatory proteome in endothelial cells. Drp1 and its receptor Mff are involved in mediating endothelial Inflammatory NF-κB activation and vascular cell adhesion molecule-1 (VCAM-1) induction (104). In cultured endothelial cells, inhibition of Drp1 activity or expression inhibits not only mitochondrial fission but also NF-κB activation, VCAM-1 induction, and leukocyte adhesion induced by these proinflammatory factors. On the other hand, attenuation of inflammatory leukocyte adhesion was also observed in Drp1 heterozygous-deficient mice and endothelial-type Drp1-silenced mice. Interestingly, this study also demonstrated that inhibition of the typical NF-κB signaling pathway could also in turn inhibit endothelial cell and mitochondrial fission. Thus, there may be interdependence between the typical NF-κB cascade activation and mitochondrial fission pathways in endothelial cells, which together regulate endothelial cell inflammation. In addition, it was shown that the classical anti-inflammatory drug salicylate could also maintain mitochondrial fission-fusion homeostasis by inhibiting NF-κ B.

Although the mitochondrial content of vascular endothelial cells is relatively low, mitochondria are a key site of ROS production (105). Chronic accumulation of mitochondria-derived ROS (mROS) contributes to vascular fibrosis and remodeling secondary to endothelial cell apoptosis (106). mROS-induced oxidative stress accelerates endothelial cell senescence, particularly by impairing the endothelial cell migration response, reducing paracrine capacity, and increasing endothelial permeability. These characteristic alterations impede endothelial regeneration and angiogenesis (105). Moreover, disruption of mitochondrial redox homeostasis in ECs can cause chronic inflammation, which in turn disrupts vascular endothelial homeostasis (107). Mitochondrial fusion and fission are directly or indirectly associated with mitochondrial energy metabolism (108). When Drp1 activity is inhibited, mitochondrial ROS production and ATP levels are subsequently reduced (109). Studies have consistently shown that mitochondrial respiration and energetics are also inhibited in cardiac-specific Drp1-KO mice (110). It was shown that silencing of Fis1 or Drp1 under high glucose conditions may maintain endothelial NOs (eNOs) activity and NO bioavailability by decreasing mitochondrial ROS (88). Overall,

fusion-fission imbalance in endothelial mitochondria can lead to loss of mitochondrial function and increased ROS production, while excessive accumulation of ROS in turn further disrupts normal mitochondrial function and morphology. This vicious cycle promotes the initiation of vascular remodeling (111).

Vascular smooth muscle cells (VSMCs)

Vascular smooth muscle cells (VSMCs) are key components of the medial layer of arteries and major determinants of vascular tone (112). VSMCs have significant phenotypic plasticity and can respond to functional demands and external stimuli by transitioning from a contractile to a synthetic phenotype (113). In the contractile state, VSMCs, together with ECs, regulate vascular homeostasis by controlling blood flow. On the other hand, in response to vascular injury, VSMCs lose contractile markers and switch to a synthetic phenotype, becoming dedifferentiated and with enhanced proliferation and migration capacity (114, 115). Phenotypically modified VSMCs play important roles in vascular remodeling (116). Recent findings suggest that the phenotype switching of VSMCs is associated with dysfunctional mitochondrial dynamics (117). Notably, VSMCs are energy-dense cells that are susceptible to organelle dysfunction. Thus, mitochondrial dysfunction caused by fusion-fission imbalance may also aggravate vascular remodeling by causing the calcification of VSMCs (118).

In previous studies, mitochondrial fission has been shown to have a crucial role in pulmonary artery smooth muscle cells (PASMCs) hyperproliferation (119). In addition, VSMCs exposed to platelet-derived growth factor-BB (PDGF) showed mitochondrial fragmentation and a significant decrease in Mfn2, accompanied by a decrease in glucose oxidation and an increase in fatty acid oxidation (89). In contrast, Mdivi-1 inhibited Drp1-mediated mitochondrial division and exhibited anti-VSMCs proliferation and migration activity in both cellular and animal experiments (89). These results suggest that changes in mitochondrial morphology and energetics underlie the overproliferation of the VSMCs synthetic phenotype. A recent study has shown that astaxanthin (ATX) can inhibit mitochondrial fission and thus VSMCs proliferation by reducing Drp1 phosphorylation, exhibiting potential for therapeutic vascular remodeling (120). Mitochondrial fusion has also been shown to be associated with VSMCs proliferation. Glucagon-like peptide-1 (GLP-1) stimulates mitochondrial fusion through the PKA/Drp1 signaling pathway, increasing mitochondrial activity and reducing VSMCs dedifferentiation (121). *In vitro* and *in vivo* experiments suggest that GLP-1 can inhibit vascular remodeling through a mitochondrial dynamics-dependent pathway. In addition, Mfn2 is an important inhibitor of VSMC proliferation (122). Studies showed that in VSMCs, the specific site of Mfn2 could be phosphorylated by PKA, leading to an inhibitory effect on the proliferation of VSMCs. Also, an inhibitory effect on endothelial proliferation and restenosis was demonstrated in a rat balloon injury model. Interestingly, although PKA-specific phosphorylation plays a key role in Mfn2-mediated VSMCs growth inhibition, it is not related to its role in the regulation of mitochondrial morphology. It can be considered a non-canonical action of mitochondrial dynamics proteins (123). Another study showed that overexpression of Mfn2 triggered vascular smooth muscle apoptosis, whereas silencing Mfn2 prevented vascular smooth muscle apoptosis (124). Similarly, this is an independent way of mitochondrial fusion.

Altered mitochondrial dynamics also have important influences on PDGF-induced VSMCs migration, which leads to VSMCs migration by regulating calmodulin-dependent kinase II (CaMKII) (114). Indeed, altered mitochondrial morphology leading to metabolic dysfunction, damage to mitochondrial components, and mitochondria-mediated ROS generation are also mediators involved in VSMCs proliferation and migration, a potential mechanism promoting cardiovascular disease (112). A related study showed that PDGF induces mitochondrial shortening *via* DLP1 in VSMCs in mice and that perturbing mitochondrial fission by silencing Drp1 significantly reduces VSMCs migration (125). This suggests that mitochondrial fission is an indispensable process for VSMCs migration. In DLP1-K38A transgenic mice, mitochondrial fission was reduced *in vivo*, leading to a restricted development of endothelial proliferation induced by arterial injury. This study demonstrates that inhibition of mitochondrial fission results in a significant reduction in PDGF-induced VSMCs migration and line injury-induced intimal hyperplasia. Moreover, the correlation between altered mitochondrial morphology, such as mitochondrial shortening, and cell migration was verified in this study. Recent findings show that Krüppel-like factor 5 (Klf5), a transcription factor important for vascular remodeling, was shown to be associated with mitochondrial fission. knockdown of Klf5 was enhanced, while Klf5 overexpression inhibited mitochondrial fission (126). Furthermore, activation of the p38 MAPK pathway can promote VSMCs proliferation and arteriogenesis *in vitro* in response to Mfns through PGC1α-dependent mitochondrial dynamics (127). Overall, the above findings suggest that mitochondrial dynamics plays a key role in VSMCs proliferation and migration.

Vascular smooth muscle cells phenotypic switching and its driven calcification process play a key role in regulating vascular wall remodeling. As the studies were explored in depth, the process of calcification exhibiting mitochondrial dysfunction was gradually exposed (115, 118). An excessive increase in mitochondrial fission was observed in VSMCs treated with phosphate and a similar disruption of mitochondrial structural integrity was found in a rat model of adenine-induced aortic calcification (128). Drp1 is involved in the transformation of VSMCs into an osteoblast-like phenotype by regulating mitochondrial fission. Increased mitochondrial fragmentation and enhanced Drp1 expression can be observed during calcification events (128), while further studies have shown that inhibition of Drp1 attenuates cardiovascular calcification under some degree of oxidative stress (129). It has been confirmed that melatonin can attenuate β-glycerophosphate (β-GP)-induced VSMCs calcification *via* the AMPK/Drp1 signaling pathway. In this process, melatonin also attenuates mitochondrial fragmentation and reduces apoptosis to protect VSMCs from calcification (130). On the other hand, in contrast to fission that exacerbates calcification, activation of Opa1-associated mitochondrial fusion can reverse this. In β-GP-induced calcification of VSMCs, activation of mitochondrial fusion and reduction of mitochondrial fission ameliorates VSMCs calcification (131).

As is the case in many cells, excessive mitochondrial fission generates large amounts of mitochondrial fragments that cause oxidative stress and disrupt normal mitochondrial respiration and ATP production. Thus, in addition to dysfunction, the calcification process is often accompanied by the reprogramming of mitochondrial energy metabolism due to low mitochondrial activity under pathological conditions (132, 133). Similar to the Warburg effect in cancer cells (134), mitochondria were found

to decrease glucose oxidation and increase fatty acid oxidation during VSMC phenotypic transition (89). VSMCs may need to undergo this process during osteogenic differentiation and vascular calcification to obtain energy and produce the necessary biosynthetic precursors (135).

Vascular fibroblasts (VAFs)

For a long time, endothelial cells and smooth muscle cells have received much attention as the major cellular components of the intima and interlayer of the vasculature, respectively. However, the adventitia has been considered solely as a structure that provides support and nutrition to the vasculature, and its role in vascular remodeling has been largely overlooked. The vascular adventitia is composed of a variety of cells, nerves, and connective tissue, with the most abundant cell type being fibroblasts (136). There is increasing evidence that the vascular adventitia is a key regulator of vessel wall structure and function, and the contribution of adventitial fibroblasts (AFs) to vascular remodeling has received considerable attention (137, 138). The vascular adventitia exhibited epigenetic thickening, an increased number of fibroblasts, and phenotypic alteration of AFs to myofibroblasts (MFs) in vascular remodeling (139). The transformed MFs exhibit enhanced proliferative and migratory activities and the presence of α-smooth muscle actin (α-SMA) (140). Recent studies have suggested that the switch for this phenotypic transition in fibroblasts may be related to mitochondrial function (141, 142).

It has been shown that mitochondrial fission contributes to the phenotypic switching of AFs (141). In AngII-treated primary mouse AFs, calcium-regulated phosphatase (CN)-dependent dephosphorylation of Drp1 induced mitochondrial fission, which stimulated AFs proliferation, migration, and phenotypic switching. In contrast, inhibition of heat shock protein 90 (HSP90) ameliorated CN expression and subsequent Drp1 activation, which ultimately attenuated vascular AngII-induced vascular adventitia remodeling. This demonstrates the involvement of HSP90 as a molecular chaperone of CN in the mitochondrial kinetic mechanism of AFs phenotypic transformation. Consistent with *in vitro* experiments, in an animal model of AngII-induced vascular outer membrane remodeling, inhibitors of HSP90 significantly reduced mitochondrial fission mediated by the CN/Drp1 signaling pathway, which in turn ameliorated AFs phenotypic conversion, vessel wall thickening, and aortic outer membrane fibrosis. In a recent study, Drp1 phosphorylation as well as fragmented mitochondria were significantly increased in transforming growth factor-β1 (TGF-β1)-treated primary AFs, leading to proliferation, migration, and phenotypic transformation of AFs. Moreover, inhibition of Drp1 by gene silencing could prevent this effect (142). Mechanistically, *in vitro* experiments demonstrated that hydrogen sulfide (H_2S), a gas signaling molecule that regulates various cardiovascular functions, can block mitochondrial fission and improve TGF-β1-induced phenotypic conversion of AFs to MFs by regulating Rho-associated protein kinase 1-dependent Drp1 phosphorylation. This study reveals a novel mechanism of AFs phenotypic transformation and extravascular membrane remodeling involving mitochondrial dynamics.

Interesting observations by Lemmons et al. suggest that fibroblasts exhibit distinct metabolic phenotypes under both resting and proliferating conditions (143). Even under resting conditions, fibroblasts exhibit high metabolic activity compared to other cells (144). Fibroblasts could rapidly respond to hypoxic stress, and the ability of fibroblasts to proliferate, differentiate, and migrate under hypoxic conditions appears to be unique. However, chronic hypoxia still leads to phenotypic changes in fibroblasts (145). Studies indicated that the pulmonary artery adventitia harbors activated fibroblasts (PH-Fibs) show the characteristics of hyperproliferation, antiapoptotic, and proinflammatory phenotype in experimental hypoxic pulmonary hypertension (PH) and human PH (146). In response to vascular injury, fibroblasts can respond to environmental demands by rapidly altering their metabolic network. Therefore, one study explored the state of mitochondrial metabolism in PH-fibroblasts (147). In PH-Fibs, it was observed that pyruvate dehydrogenase was significantly inhibited, leading to increased glycolysis, which is consistent with a Warburg-like phenotype. The pro-oxidative state was further enhanced by increased mitochondrial superoxide production due to less efficient ATP synthesis. In addition, mitochondrial bioenergetics was suppressed in PH-Fibs and mitochondrial fragmentation was increased. Most importantly, the activity of complex I was greatly reduced. Conversely, acute and chronic hypoxia-induced increases in glycolysis in vascular fibroblasts were not accompanied by a lack of complex I (147). This evidence suggests that in the mechanism of vascular remodeling in PH, fibroblast mitochondrial metabolism may be altered differently from the effects of hypoxia, which in turn drives unique changes in cellular behavior.

Macrophages

During atherosclerosis, macrophages retain the ability to phagocytose modified LDL and progressively transform into lipid-rich foam cells, which amplify and exacerbate the disease. It is widely believed that monocyte/macrophage-mediated inflammation accelerates the process of vascular remodeling (91). In the vascular system, monocytes differentiate into a heterogeneous population of macrophages, including M1 macrophages associated with pro-inflammatory processes and M2 macrophages associated with regression and repair (148).

The function of these polarized macrophages depends on the reprogramming of metabolism, which is essential for energy homeostasis (149). Indeed, mitochondrial dynamics are important for macrophage polarization and effector functions and are controlled by metabolic changes (150). For example, mitochondrial organization shifts to a hyperperfused state from a tubular and filamentous appearance and presents increased OXPHOS during nutrient starvation. Conversely, in the presence of nutrient overload, mitochondria are also hyperperfused, but in this way, they undergo altered OXPHOS associated with glycolytic metabolic characteristics (5). A recent study highlighted that mitochondrial dynamics are also associated with activation states during macrophage polarization *in vitro* (151). M1 macrophages have smaller mitochondrial networks, shorter branch lengths, lower mitochondrial membrane potential, and higher mitochondrial fission rates. This is due to the activation of Drp1 causing mitochondrial fragmentation in cells with enhanced glycolysis to support pro-inflammatory function. In contrast, the mitochondria of M2 macrophages are organized in larger networks, have longer branch lengths, and show higher fusion rates. This feature leads to better ETC and OXPHOS efficiency, supporting their anti-inflammatory and repair properties (151).

A recent study showed that macrophage Drp1 regulates this selective differentiation of macrophages (91). Macrophage-selective Drp1-deficient mice were created and were subjected to femoral artery wire injury. Drp1 deficiency also attenuated macrophage proliferation and accumulation in the damaged arteries of mice compared to control mice with attenuated intimal thickening and negative remodeling after vascular injury. Morphologically, inflammatory macrophages (M1) induced mitochondrial fission, whereas non-inflammatory/repair macrophages (M2) induced mitochondrial fusion. *In vitro* experiments showed that Drp1 induced the expression of molecules associated with inflammatory macrophages, while inhibition or knockdown of Drp1 reduced mitochondrial reactive oxygen species and chemotactic activity in cultured macrophages (91). These results suggest that in acute vascular injury, macrophage Drp1 deficiency can lead to reduced accumulation of inflammatory macrophages into injured vessels. Interestingly, macrophage mitochondrial fission may play a protective role in advanced atherosclerosis (152). In macrophage-enriched mouse atherosclerotic lesion areas, Drp1 levels were downregulated and Mfn2 levels were upregulated as the lesion progressed. A study conducted by Wang et al. demonstrated that Drp1-mediated mitochondrial fission has an important role in efferocytosis in atherosclerotic lesions in hyperlipidemic mice. Impaired efferocytosis induces the formation of large necrotic cores and leads to plaque vulnerability. This suggests that long-term blockade of Drp1 may be detrimental to cardiovascular events (153). Thus, how the delicate balance of mitochondrial fission and fusion regulates the role of macrophages in vascular remodeling is a question worth investigating.

Furthermore, co-culture experiments with macrophages and VSMCs showed that deletion of Drp1 in macrophages reduced macrophage-derived soluble factors, which in turn inhibited VSMCs growth and migration. This suggests that mitochondrial division inhibition may slow the process of atherosclerosis and vascular remodeling by disrupting the interaction between VSMCs and macrophages (91, 154).

Mitochondrial dynamics and target-organ damage of vascular disease

Myocardial hypertrophy and heart failure

Atherosclerosis is the pathological basis of various cardiovascular diseases, ultimately leading to cardiac insufficiency (155). Mitochondrial dynamics imbalance is also known to have an important place in cardiac diseases such as cardiac hypertrophy and heart failure. In transverse aortic banding (TAB)-treated mouse hearts, a phosphorylation-mediated increase in the number and loss of function of Drp1 mitochondria was found. The inhibitor mdivi-1 reduced the TAB-induced hypertrophic response and prevented PE-induced hypertrophic growth in rat neonatal cardiomyocytes (156). Treatment of neonatal rat cardiomyocytes with norepinephrine, a hypertrophic agonist, promotes mitochondrial fission characterized by a decrease in mean volume and an increase in relative number and leads to a decrease in mitochondrial function. Inhibition of Drp1 not only prevented mitochondrial fission but also blocked the hypertrophic growth of cardiomyocytes in response to norepinephrine. In the same study, inhibition of the fusion protein Mfn2 was also found to increase mitochondrial fission and stimulate the hypertrophic response (157). In addition, a reduced ratio of Mfn2 to Drp1 was observed in heart failure, while Mdivi-1 treatment normalized this ratio and thus improved cardiac function (158). Reduced expression of the fusion proteins Mfn2 and Opa1 was also observed *in vitro* in hypertrophic cardiomyocytes and a rat model of heart failure (159, 160). Interestingly, in a rat model of hypertension with cardiac insufficiency, promoting glucagon-like peptide-1 (GLP-1) production enhanced mitochondrial fusion in the heart and improved cardiac function (161). In a recent study, the oligopeptide Szeto-Schiller compound 31 (SS31) was found to significantly improve cardiac function, reduce myocardial interstitial fibrosis, and increase expression of optic atrophy-associated protein 1 (Opa1) in mice with pressure-overload heart failure by modulating mitochondrial fusion (162).

It is generally accepted that fused mitochondria are more efficient than fragmented mitochondria in the production of ATP and also compensate for the long-term accumulation of mitochondrial mutations (163). Therefore, many studies have been carried out based on the presence of mitochondrial fission or sensitivity to Drp1 chemical inhibitors, including Mdivi-1. Excessive mitochondrial fission has been proposed as a potential mechanism of cardiac dysfunction. Although dysregulated activation of Drp1 in response to stress may be detrimental to the heart, sustained inhibition of Drp1 is also detrimental because it eliminates the homeostatic function of Drp1 (164). Sustained inhibition of Drp1 through genetic deletion or repeated application of Mdivi-1 in the heart has been shown to exacerbate myocardial I/R injury (110). Taken together, it can be concluded that the balance between mitochondrial fusion and fission is a key factor in the onset and progression of myocardial hypertrophy and heart failure. Since Drp1 may have a fission-independent function (165), and given that inhibitors of Drp1 also appear to have some Drp1-independent effects (166), further studies are needed to clarify whether cardiac insufficiency is predominantly induced by excessive fission and whether fission inhibitors, such as Mdivi-1, can be used clinically for the treatment of cardiac disease.

Ischemic stroke

Indeed, mitochondrial dynamics also play an important role in cell death and survival during cerebral ischemia. In the mouse middle cerebral artery occlusion (MCAO) I/R model, the emergence of mitochondrial fission was found to precede neuronal injury and neuronal cell death. Notably, NO-induced neuronal cell death could be alleviated by Mfn1 and dominant-negative Drp1, whereas overexpression of Drp1 or Fis1 caused cleavage and increased neuronal loss. Thus, sustained mitochondrial fission may play a causal role in NO-mediated neurotoxicity (167). Similarly, when Mdivi-1 was given as an inhibitor of Drp1 prior to cerebral ischemia, it attenuated ischemia-induced brain injury, reduced infarct volume, and improved neurological function. When given after ischemia and before reperfusion, Mdivi-1 also prevents brain injury by inhibiting mitochondrial fission-induced mitochondria-mediated apoptosis (168). A recent systematic review analyzed the effects of Mdivi-1 on mitochondria-mediated apoptosis and mitochondrial dysfunction in neuronal cells in the ischemia/reperfusion (I/R) injury after stroke model. The results suggest that Mdivi-1 protects mitochondrial function in neuronal cells by attenuating mitochondrial division,

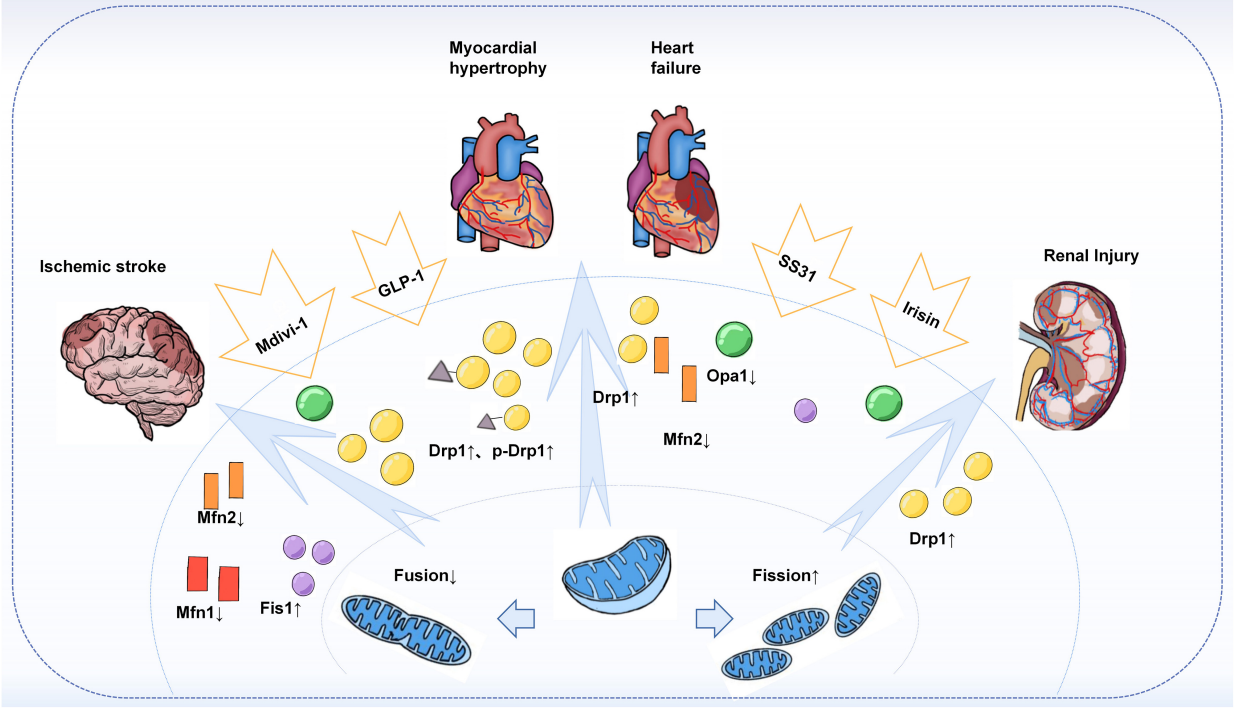

FIGURE 3
Mitochondrial dynamics in target-organ injury. Increased Drp1 and phosphorylated Drp1 were observed in an animal or *in vitro* models of cardiac hypertrophy, heart failure, stroke, and acute and chronic types of kidney injury, leading to enhanced mitochondrial division and increased fragmented mitochondria. At the same time, the expression of fusion proteins Mfns, especially Mfn2, and Opa1 was found to be reduced. Treatment with Mdivi-1, an inhibitor of Drp1, restored the Drp1 to Mfn2 ratio and improved cardiac function, attenuated brain injury, and reduced apoptosis in the kidney. In addition, others such as GLP-1, SS31, and Irisin have also been found to have a role in regulating mitochondrial dynamics, thereby reducing target organ damage.

thereby attenuating I/R-induced brain injury and apoptosis (169). However, the specificity and efficacy of the pharmacological Drp1 inhibitor used, Mdivi-1, has now been questioned. A new study provides new possible mechanisms for the role of mitochondrial fission in neuronal injury (170). Deregulation of Drp1 repression by knocking down the mitochondrial A-kinase anchoring protein 1 (AKAP1) leads to increased stroke injury in mice. The evidence suggests that AKAP1 may protect against cerebral ischemic stroke by inhibiting Drp1-dependent mitochondrial fission, providing a new idea to resolve the current controversy about the role of mitochondrial fission in neuronal injury. Furthermore, Mfn2 was also found to be downregulated in the permanent MCAO model (171). Considering these evidences, increased mitochondrial fission should be considered an important factor contributing to ischemic stroke and brain injury.

Renal injury

Similar to organs such as the arteries, heart, and brain, a series of studies have identified mitochondrial dynamics in kidney injury. CVD is a major cause of mortality and morbidity in patients with chronic kidney disease (CKD), and vascular calcification (VC) is an independent predictor of cardiovascular mortality in CKD (172). A recent study found that in a chronic kidney disease model, Irisin restored mitochondrial function and reduced fission ameliorated CKD-associated vascular calcification, resulting in reduced serum creatinine, urea, and phosphorus levels in CKD mice. Mechanistically, Irisin restored mitochondrial function and alleviated mitochondrial fission *via* the AMPK/Drp1 signaling pathway, which further reduced CKD-associated vascular calcification (173). In addition, Drp1-induced mitochondrial fragmentation was observed in experimental models of renal ischemia/reperfusion and cisplatin-induced nephrotoxicity, demonstrating altered mitochondrial dynamics during acute kidney injury. Moreover, both acute kidney injury and apoptosis could be attenuated by the Drp1 inhibitor Mdivi-1 (174). Similar results were shown in a model of ischemic acute kidney injury (175). It was found that inhibition of Drp1-mediated mitochondrial fission plays an important role in ischemic preconditioning (IPC)-mediated renal protection (**Figure 3**).

Conclusion remarks

In this review, we discussed recent advances in mitochondrial fusion, fission, and the delicate balance between them, focusing on the role of mitochondrial dynamics in several cells that make up the vascular wall in the involvement of vascular remodeling. We also discuss the function of mitochondrial fusion and division in target-organs of cardiovascular diseases. Related studies and applications of mitochondrial dynamics regulators, such as Mdivi-1, are also reviewed.

The dynamic balance of mitochondrial fission-fusion is the basis for maintaining normal mitochondrial morphology, number, distribution as well as the functional integrity of mitochondria. In mammalian cells, mitochondrial fusion is mainly controlled by Mfn1/2 and Opa1; while mitochondrial fission is controlled by Drp1, Fis1, Mff, and MiD49/51. However, this is not absolute, because

some components regulating fusion, such as S-Opa1 and cardiolipin, are also involved in the mitochondrial division mechanism. In addition, MIEF1/2 is also involved in both fission and fusion. Recent findings also suggest that cells in different states my have different ways of mitochondrial division, which would also lead to different fate directions of the cells. Furthermore, the absence of either mitochondrial division or fusion alone can lead to abnormal cellular function, while division and fusion are also regulated by mitochondria and show a tendency to compensate for each other, suggesting that the delicate balance between division and fusion may be more important than the processes of division or fusion alone.

The typical vessel wall has a three-layer structure. The innermost layer consists of a tightly connected layer of endothelial cells (ECs), the endothelium, which is in direct contact with blood flow. The middle layer is mainly composed of smooth muscle cells (VSMCs) and elastic fibrous tissue. Fibroblasts, together with nerves and collagen, make up the outer membrane of the artery. The major cells in the three structural layers of the vessel wall all involved in vascular remodeling and are regulated by mitochondrial dynamics. Alterations in endothelial function are often considered to be the beginning of arterial remodeling, and mitochondrial division and fusion in ECs have important roles in regulating apoptosis, angiogenesis, and proinflammatory states. VSMCs have significant phenotypic plasticity, transforming to a synthetic phenotype after the loss of contractile markers, exhibiting dedifferentiation and increased proliferation and migration. Mitochondrial dynamics are involved in the regulation of this transition process. In addition, an imbalance of mitochondrial fusion and division may lead to VSMCs calcification, which is one of the important influences of vascular remodeling. The role of the arterial outer membrane and its major component, fibroblasts, in vascular remodeling has long been overlooked. There is increasing evidence that phenotypic changes from extravascular fibroblasts (AFs) to myofibroblasts (MFs) are important for the vascular remodeling process. Although there are still relatively few relevant studies, it is well-established that this phenotypic transition process is regulated by mitochondrial dynamics. Interestingly, how the delicate balance between mitochondrial fission and fusion regulates the role of macrophages in vascular remodeling is also worthy of further study.

The pathogenesis of cardiovascular disease, a leading cause of morbidity and mortality in developing countries, has been widely studied and focused on. Vascular remodeling associated with an imbalance in mitochondrial dynamics is an important player in several cardiovascular diseases. The heart, brain, and kidneys are all potential targets of vascular remodeling. Excessive mitochondrial division or reduced mitochondrial fusion has been found in diseases such as atherosclerosis, cardiac insufficiency, ischemic stroke, as well as acute and chronic kidney injury. In contrast, restoration of mitochondrial dynamics homeostasis by silencing related genes, using division inhibitors or fusion promoters may provide some protection. This suggests that inhibiting mitochondrial division or promoting mitochondrial fusion to maintaining mitochondrial kinetic homeostasis is promising new targets for the treatment of vascular remodeling and its associated cardiovascular diseases. However, how to finely regulate the activity of mitochondrial dynamics proteins while reducing the possible side effects is one of the main challenges at hand.

Since Cassidy-Stone et al. reported in 2008 that Mdivi-1 inhibits excessive mitochondrial fission and enhances mitochondrial fusion activity, which can protect cells from toxic injury, a large number of studies on the regulation of mitochondrial dynamics have emerged. In the last decades, some progress has been made in the development of mitochondrial fission inhibitors such as Mdivi-1, P110 and Dynasore. Inhibitors of mitochondrial fission may be promising therapeutic targets in neurodegenerative disease disorders such as Alzheimer's disease (AD) and Huntington's disease (HD). However, no drug formulations have been reported that are available for use in humans. In mechanistic studies of cardiovascular disease, beneficial effects of mitochondrial dynamic modulators have been reported at both the cellular and animal levels. Overall, mitochondrial kinetic modulators have good research prospects for the treatment of human diseases and may provide new therapeutic approaches for cardiovascular diseases in the future. Considering the differences in mitochondrial energy requirements and functions in different cell types, especially between cardiomyocytes and other cells, selective modulation of mitochondrial dynamics in cells is also worth considering. Therefore, whether the mitochondrial dynamics modulators used in basic experiments, such as Mdivi-1, an inhibitor of Drp1, and P110, an adapter-specific inhibitor of Drp1/Fis1 interaction discovered in recent years, can be used for the treatment of related cardiovascular diseases still needs to be verified by numerous clinical studies, and their related toxicological and pharmacokinetic characteristics still need to be further investigated. This will be a new direction for future research.

Author contributions

TZ, JQ, and JZ structured the manuscript and contributed to the figures. QH, YY, and HY revised the manuscript and confirmed the final revision. All authors contributed to the manuscript preparation and approved the submitted version.

Funding

This work was supported by the Shanghai Science and Technology Commission of China (21ZR1441300) and the National Natural Science Foundation of China (81302768, 81870469, and 82170699).

Conflict of interest

The authors declare that the research was conducted in the absence of any commercial or financial relationships that could be construed as a potential conflict of interest.

Publisher's note

References

1. Benjamin EJ, Virani SS, Callaway CW, Chamberlain AM, Chang AR, Cheng S, et al. Heart disease and stroke statistics-2018 update: a report from the American Heart Association. *Circulation.* (2018) 137:e67–492. doi: 10.1161/CIR.0000000000000573

2. Libby P, Buring JE, Badimon L, Hansson GK, Deanfield J, Bittencourt MS, et al. Atherosclerosis. *Nat Rev Dis Primers.* (2019) 5:56. doi: 10.1038/s41572-019-0106-z

3. IHME. *VizHub – GBD Compare (healthdata.org)*. Seattle: IHME (2019).

4. Gibbons GH, Dzau VJ. The emerging concept of vascular remodeling. *N Engl J Med.* (1994) 330:1431–8. doi: 10.1056/NEJM199405193302008

5. Dumont A, Lee M, Barouillet T, Murphy A, Yvan-Charvet L. Mitochondria orchestrate macrophage effector functions in atherosclerosis. *Mol Aspects Med.* (2021) 77:100922. doi: 10.1016/j.mam.2020.100922

6. Jin JY, Wei XX, Zhi XL, Wang XH, Meng D. Drp1-dependent mitochondrial fission in cardiovascular disease. *Acta Pharmacol Sin.* (2021) 42:655–64. doi: 10.1038/s41401-020-00518-y

7. Dromparis P, Michelakis ED. Mitochondria in vascular health and disease. *Annu Rev Physiol.* (2013) 75:95–126. doi: 10.1146/annurev-physiol-030212-183804

8. Diebold LP, Gil HJ, Gao P, Martinez CA, Weinberg SE, Chandel NS. Mitochondrial complex III is necessary for endothelial cell proliferation during angiogenesis. *Nat Metab.* (2019) 1:158–71. doi: 10.1038/s42255-018-0011-x

9. He J, Bao Q, Yan M, Liang J, Zhu Y, Wang C, et al. The role of Hippo/yes-associated protein signalling in vascular remodelling associated with cardiovascular disease. *Br J Pharmacol.* (2018) 175:1354–61. doi: 10.1111/bph.13806

10. Gray MW, Burger G, Lang BF. The origin and early evolution of mitochondria. *Genome Biol.* (2001) 2:REVIEWS1018.

11. Frey TG, Mannella CA. The internal structure of mitochondria. *Trends Biochem Sci.* (2000) 25:319–24. doi: 10.1016/S0968-0004(00)01609-1

12. Yan C, Duanmu X, Zeng L, Liu B, Song Z. Mitochondrial DNA: Distribution, Mutations, and Elimination. *Cells.* (2019) 8:379. doi: 10.3390/cells8040379

13. Evans A, Neuman N. The mighty mitochondria. *Mol Cell.* (2016) 61:641.

14. Nunnari J, Suomalainen A. Mitochondria: in sickness and in health. *Cell.* (2012) 148:1145–59. doi: 10.1016/j.cell.2012.02.035

15. Murphy E, Ardehali H, Balaban RS, Dilisa F, Dorn GW 2nd, Kitsis RN, et al. Mitochondrial Function, Biology, and Role in Disease: A Scientific Statement From the American Heart Association. *Circ Res.* (2016) 118:1960–91. doi: 10.1161/RES.0000000000000104

16. Chan DC. Mitochondrial dynamics and its involvement in disease. *Annu Rev Pathol.* (2020) 15:235–59.

17. Wai T, Langer T. Mitochondrial Dynamics and Metabolic Regulation. *Trends Endocrinol Metab.* (2016) 27:105–17. doi: 10.1016/j.tem.2015.12.001

18. Adebayo M, Singh S, Singh AP, Dasgupta S. Mitochondrial fusion and fission: the fine-tune balance for cellular homeostasis. *FASEB J.* (2021) 35:e21620. doi: 10.1096/fj.202100067R

19. Meeusen S, Mccaffery JM, Nunnari J. Mitochondrial fusion intermediates revealed in vitro. *Science.* (2004) 305:1747–52. doi: 10.1126/science.1100612

20. Malka F, Guillery O, Cifuentes-Diaz C, Guillou E, Belenguer P, Lombes A, et al. Separate fusion of outer and inner mitochondrial membranes. *EMBO Rep.* (2005) 6:853–9. doi: 10.1038/sj.embor.7400488

21. Gilkerson RW, Schon EA, Hernandez E, Davidson MM. Mitochondrial nucleoids maintain genetic autonomy but allow for functional complementation. *J Cell Biol.* (2008) 181:1117–28. doi: 10.1083/jcb.200712101

22. Liu X, Weaver D, Shirihai O, Hajnoczky G. Mitochondrial 'kiss-and-run': interplay between mitochondrial motility and fusion-fission dynamics. *EMBO J.* (2009) 28:3074–89. doi: 10.1038/emboj.2009.255

23. Koshiba T, Detmer SA, Kaiser JT, Chen H, Mccaffery JM, Chan DC. Structural basis of mitochondrial tethering by mitofusin complexes. *Science.* (2004) 305:858–62. doi: 10.1126/science.1099793

24. Tilokani L, Nagashima S, Paupe V, Prudent J. Mitochondrial dynamics: overview of molecular mechanisms. *Essays Biochem.* (2018) 62:341–60. doi: 10.1042/EBC20170104

25. Santel A, Fuller MT. Control of mitochondrial morphology by a human mitofusin. *J Cell Sci.* (2001) 114:867–74. doi: 10.1242/jcs.114.5.867

26. Mattie S, Riemer J, Wideman JG, Mcbride HM. A new mitofusin topology places the redox-regulated C terminus in the mitochondrial intermembrane space. *J Cell Biol.* (2018) 217:507–15. doi: 10.1083/jcb.201611194

27. Qi Y, Yan L, Yu C, Guo X, Zhou X, Hu X, et al. Structures of human mitofusin 1 provide insight into mitochondrial tethering. *J Cell Biol.* (2016) 215:621–9.

28. Cao YL, Meng S, Chen Y, Feng JX, Gu DD, Yu B, et al. MFN1 structures reveal nucleotide-triggered dimerization critical for mitochondrial fusion. *Nature.* (2017) 542:372–6. doi: 10.1038/nature21077

29. Ishihara N, Eura Y, Mihara K. Mitofusin 1 and 2 play distinct roles in mitochondrial fusion reactions via GTPase activity. *J Cell Sci.* (2004) 117:6535–46. doi: 10.1242/jcs.01565

30. Song Z, Ghochani M, Mccaffery JM, Frey TG, Chan DC. Mitofusins and OPA1 mediate sequential steps in mitochondrial membrane fusion. *Mol Biol Cell.* (2009) 20:3525–32. doi: 10.1091/mbc.e09-03-0252

31. Eura Y, Ishihara N, Yokota S, Mihara K. Two mitofusin proteins, mammalian homologues of FZO, with distinct functions are both required for mitochondrial fusion. *J Biochem.* (2003) 134:333–44. doi: 10.1093/jb/mvg150

32. Ban T, Ishihara T, Kohno H, Saita S, Ichimura A, Maenaka K, et al. Molecular basis of selective mitochondrial fusion by heterotypic action between OPA1 and cardiolipin. *Nat Cell Biol.* (2017) 19:856–63. doi: 10.1038/ncb3560

33. Delettre C, Griffoin J-M, Kaplan J, Dollfus H, Lorenz B, Faivre L, et al. Mutation spectrum and splicing variants in the OPA1 gene. *Hum Genet.* (2001) 109:584–91.

34. Ishihara N, Fujita Y, Oka T, Mihara K. Regulation of mitochondrial morphology through proteolytic cleavage of OPA1. *EMBO J.* (2006) 25:2966–77.

35. Mishra P, Carelli V, Manfredi G, Chan DC. Proteolytic Cleavage of Opa1 Stimulates Mitochondrial Inner Membrane Fusion and Couples Fusion to Oxidative Phosphorylation. *Cell Metab.* (2014) 19:630–41. doi: 10.1016/j.cmet.2014.03.011

36. Song Z, Chen H, Fiket M, Alexander C, Chan DC. OPA1 processing controls mitochondrial fusion and is regulated by mRNA splicing, membrane potential, and Yme1L. *J Cell Biol.* (2007) 178:749–55. doi: 10.1083/jcb.200704110

37. Ge Y, Shi X, Boopathy S, Mcdonald J, Smith AW, Chao LH. Two forms of Opa1 cooperate to complete fusion of the mitochondrial inner-membrane. *eLife.* (2020) 9:e50973. doi: 10.7554/eLife.50973

38. Tondera D, Grandemange S, Jourdain A, Karbowski M, Mattenberger Y, Herzig S, et al. SLP-2 is required for stress-induced mitochondrial hyperfusion. *EMBO J.* (2009) 28:1589–600.

39. Anand R, Wai T, Baker MJ, Kladt N, Schauss AC, Rugarli E, et al. The i-AAA protease YME1L and OMA1 cleave OPA1 to balance mitochondrial fusion and fission. *J Cell Biol.* (2014) 204:919–29. doi: 10.1083/jcb.201308006

40. Pagliuso A, Cossart P, Stavru F. The ever-growing complexity of the mitochondrial fission machinery. *Cell Mol Life Sci.* (2018) 75:355–74. doi: 10.1007/s00018-017-2603-0

41. Murata D, Arai K, Iijima M, Sesaki H. Mitochondrial division, fusion and degradation. *J Biochem.* (2020) 167:233–41.

42. Tamura Y, Itoh K, Sesaki H. SnapShot: mitochondrial dynamics. *Cell.* (2011) 145:1158.

43. Twig G, Elorza A, Molina AJ, Mohamed H, Wikstrom JD, Walzer G, et al. Fission and selective fusion govern mitochondrial segregation and elimination by autophagy. *EMBO J.* (2008) 27:433–46. doi: 10.1038/sj.emboj.7601963

44. Burman JL, Pickles S, Wang C, Sekine S, Vargas JNS, Zhang Z, et al. Mitochondrial fission facilitates the selective mitophagy of protein aggregates. *J Cell Biol.* (2017) 216:3231–47. doi: 10.1083/jcb.201612106

45. Kleele T, Rey T, Winter J, Zaganelli S, Mahecic D, Perreten LH, et al. Distinct fission signatures predict mitochondrial degradation or biogenesis. *Nature.* (2021) 593:435–9.

46. Lee H, Yoon Y. Mitochondrial fission and fusion. *Biochem Soc Trans.* (2016) 44:1725–35.

47. Kraus F, Roy K, Pucadyil TJ, Ryan MT. Function and regulation of the divisome for mitochondrial fission. *Nature.* (2021) 590:57–66. doi: 10.1038/s41586-021-03214-x

48. Lee JE, Westrate LM, Wu H, Page C, Voeltz GK. Multiple dynamin family members collaborate to drive mitochondrial division. *Nature.* (2016) 540:139–43. doi: 10.1038/nature20555

49. Legesse-Miller A, Massol RH, Kirchhausen T. Constriction and Dnm1p recruitment are distinct processes in mitochondrial fission. *Mol Biol Cell.* (2003) 14:1953–63. doi: 10.1091/mbc.e02-10-0657

50. Kamerkar SC, Kraus F, Sharpe AJ, Pucadyil TJ, Ryan MT. Dynamin-related protein 1 has membrane constricting and severing abilities sufficient for mitochondrial and peroxisomal fission. *Nat Commun.* (2018) 9:5239. doi: 10.1038/s41467-018-07543-w

51. Fonseca TB, Sanchez-Guerrero A, Milosevic I, Raimundo N. Mitochondrial fission requires DRP1 but not dynamins. *Nature.* (2019) 570:E34–42.

52. Chang CR, Blackstone C. Dynamic regulation of mitochondrial fission through modification of the dynamin-related protein Drp1. *Ann N Y Acad Sci.* (2010) 1201:34–9.

53. Yu B, Ma J, Li J, Wang D, Wang Z, Wang S. Mitochondrial phosphatase PGAM5 modulates cellular senescence by regulating mitochondrial dynamics. *Nat Commun.* (2020) 11:2549. doi: 10.1038/s41467-020-16312-7

54. Gawlowski T, Suarez J, Scott B, Torres-Gonzalez M, Wang H, Schwappacher R, et al. Modulation of dynamin-related protein 1 (DRP1) function by increased O-linked-beta-N-acetylglucosamine modification (O-GlcNAc) in cardiac myocytes. *J Biol Chem.* (2012) 287:30024–34. doi: 10.1074/jbc.M112.390682

55. Cho DH, Nakamura T, Fang J, Cieplak P, Godzik A, Gu Z, et al. S-nitrosylation of Drp1 mediates beta-amyloid-related mitochondrial fission and neuronal injury. *Science.* (2009) 324:102–5. doi: 10.1126/science.1171091

56. Prudent J, Zunino R, Sugiura A, Mattie S, Shore GC, McBride HM. MAPL SUMOylation of Drp1 stabilizes an ER/mitochondrial platform required for cell death. *Mol Cell.* (2015) 59:941–55. doi: 10.1016/j.molcel.2015.08.001

57. Wang H, Song P, Du L, Tian W, Yue W, Liu M, et al. Parkin ubiquitinates Drp1 for proteasome-dependent degradation: implication of dysregulated mitochondrial dynamics in Parkinson disease. *J Biol Chem.* (2011) 286:11649–58. doi: 10.1074/jbc.M110.144238

58. Hu Q, Zhang H, Gutierrez CN, Wu D, Wang P, Zhang J, et al. Increased Drp1 Acetylation by Lipid Overload Induces Cardiomyocyte Death and Heart Dysfunction. *Circ Res.* (2020) 126:456–70. doi: 10.1161/CIRCRESAHA.119.315252

59. Nishimura A, Shimoda K, Tanaka T, Toyama T, Nishiyama K, Shinkai Y, et al. Depolysulfidation of Drp1 induced by low-dose methylmercury exposure increases cardiac vulnerability to hemodynamic overload. *Sci Signal.* (2019) 12:aaw1920. doi: 10.1126/scisignal.aaw1920

60. Loson OC, Song Z, Chen H, Chan DC. Fis1, Mff, MiD49, and MiD51 mediate Drp1 recruitment in mitochondrial fission. *Mol Biol Cell.* (2013) 24:659–67.

61. Osellame LD, Singh AP, Stroud DA, Palmer CS, Stojanovski D, Ramachandran R, et al. Cooperative and independent roles of the Drp1 adaptors Mff, MiD49 and MiD51 in mitochondrial fission. *J Cell Sci.* (2016) 129:2170–81. doi: 10.1242/jcs.185165

62. Otera H, Miyata N, Kuge O, Mihara K. Drp1-dependent mitochondrial fission via MiD49/51 is essential for apoptotic cristae remodeling. *J Cell Biol.* (2016) 212:531–44. doi: 10.1083/jcb.201508099

63. Friedman JR, Lackner LL, West M, Dibenedetto JR, Nunnari J, Voeltz GK. ER tubules mark sites of mitochondrial division. *Science.* (2011) 334:358–62.

64. Korobova F, Ramabhadran V, Higgs HN. An actin-dependent step in mitochondrial fission mediated by the ER-associated formin INF2. *Science.* (2013) 339:464–7. doi: 10.1126/science.1228360

65. Korobova F, Gauvin TJ, Higgs HN. A role for myosin II in mammalian mitochondrial fission. *Curr Biol.* (2014) 24:409–14.

66. Cho B, Cho HM, Jo Y, Kim HD, Song M, Moon C, et al. Constriction of the mitochondrial inner compartment is a priming event for mitochondrial division. *Nat Commun.* (2017) 8:15754. doi: 10.1038/ncomms15754

67. Chan DC. Fusion and fission: interlinked processes critical for mitochondrial health. *Annu Rev Genet.* (2012) 46:265–87. doi: 10.1146/annurev-genet-110410-132529

68. Wong YC, Ysselstein D, Krainc D. Mitochondria-lysosome contacts regulate mitochondrial fission via RAB7 GTP hydrolysis. *Nature.* (2018) 554:382–6.

69. Nagashima S, Tabara LC, Tilokani L, Paupe V, Anand H, Pogson JH, et al. Golgi-derived PI(4)P-containing vesicles drive late steps of mitochondrial division. *Science.* (2020) 367:1366–71. doi: 10.1126/science.aax6089

70. Bustillo-Zabalbeitia I, Montessuit S, Raemy E, Basanez G, Terrones O, Martinou JC. Specific interaction with cardiolipin triggers functional activation of Dynamin-Related Protein 1. *PLoS One.* (2014) 9:e102738. doi: 10.1371/journal.pone.0102738

71. Adachi Y, Itoh K, Yamada T, Cerveny KL, Suzuki TL, Macdonald P, et al. Coincident phosphatidic acid interaction restrains Drp1 in mitochondrial division. *Mol Cell.* (2016) 63:1034–43. doi: 10.1016/j.molcel.2016.08.013

72. Adachi Y, Iijima M, Sesaki H. An unstructured loop that is critical for interactions of the stalk domain of Drp1 with saturated phosphatidic acid. *Small GTPases.* (2018) 9:472–9. doi: 10.1080/21541248.2017.1321614

73. Lewis MR, Lewis WH. Mitochondria (and other cytoplasmic structures) in tissue cultures. *Am J Anat.* (1915) 17:339–401.

74. Johnson LV, Walsh ML, Bockus BJ, Chen LB. Monitoring of relative mitochondrial membrane potential in living cells by fluorescence microscopy. *J Cell Biol.* (1981) 88:526–35.

75. Bereiter-Hahn J, Voth M. Dynamics of mitochondria in living cells: shape changes, dislocations, fusion, and fission of mitochondria. *Microsc Res Tech.* (1994) 27:198–219. doi: 10.1002/jemt.1070270303

76. Rizzuto R, Brini M, De G, Rossi R, Heim R, Tsien RY, et al. Double labelling of subcellular structures with organelle-targeted GFP mutants in vivo. *Curr Biol.* (1996) 6:183–8. doi: 10.1016/s0960-9822(02)00451-7

77. van der Bliek A, Shen Q, Kawajiri S. Mechanisms of mitochondrial fission and fusion. *Cold Spring Harb Perspect Biol.* (2013) 5:a011072.

78. Vasquez-Trincado C, Garcia-Carvajal I, Pennanen C, Parra V, Hill JA, Rothermel BA, et al. Mitochondrial dynamics, mitophagy and cardiovascular disease. *J Physiol.* (2016) 594:509–25.

79. Chen H, Ren S, Clish C, Jain M, Mootha V, Mccaffery JM, et al. Titration of mitochondrial fusion rescues Mff-deficient cardiomyopathy. *J Cell Biol.* (2015) 211:795–805. doi: 10.1083/jcb.201507035

80. Yu R, Liu T, Jin SB, Ankarcrona M, Lendahl U, Nister M, et al. MIEF1/2 orchestrate mitochondrial dynamics through direct engagement with both the fission and fusion machineries. *BMC Biol.* (2021) 19:229. doi: 10.1186/s12915-021-01161-7

81. Ishihara N, Nomura M, Jofuku A, Kato H, Suzuki SO, Masuda K, et al. Mitochondrial fission factor Drp1 is essential for embryonic development and synapse formation in mice. *Nat Cell Biol.* (2009) 11:958–66. doi: 10.1038/ncb1907

82. Wakabayashi J, Zhang Z, Wakabayashi N, Tamura Y, Fukaya M, Kensler TW, et al. The dynamin-related GTPase Drp1 is required for embryonic and brain development in mice. *J Cell Biol.* (2009) 186:805–16. doi: 10.1083/jcb.200903065

83. Sabouny R, Shutt TE. Reciprocal Regulation of Mitochondrial Fission and Fusion. *Trends Biochem Sci.* (2020) 45:564–77.

84. Forte M, Schirone L, Ameri P, Basso C, Catalucci D, Modica J, et al. The role of mitochondrial dynamics in cardiovascular diseases. *Br J Pharmacol.* (2021) 178:2060–76.

85. Wang Q, Zhang M, Torres G, Wu S, Ouyang C, Xie Z, et al. Metformin suppresses diabetes-accelerated atherosclerosis via the inhibition of Drp1-mediated mitochondrial fission. *Diabetes.* (2017) 66:193–205. doi: 10.2337/db16-0915

86. Liu C, Ge B, He C, Zhang Y, Liu X, Liu K, et al. Mitofusin 2 decreases intracellular lipids in macrophages by regulating peroxisome proliferator-activated receptor-gamma. *Biochem Biophys Res Commun.* (2014) 450:500–6. doi: 10.1016/j.bbrc.2014.06.005

87. Guo YH, Chen K, Gao W, Li Q, Chen L, Wang GS, et al. Overexpression of Mitofusin 2 inhibited oxidized low-density lipoprotein induced vascular smooth muscle cell proliferation and reduced atherosclerotic lesion formation in rabbit. *Biochem Biophys Res Commun.* (2007) 363:411–7. doi: 10.1016/j.bbrc.2007.08.191

88. Shenouda SM, Widlansky ME, Chen K, Xu G, Holbrook M, Tabit CE, et al. Altered mitochondrial dynamics contributes to endothelial dysfunction in diabetes mellitus. *Circulation.* (2011) 124:444–53. doi: 10.1161/CIRCULATIONAHA.110.014506

89. Salabei JK, Hill BG. Mitochondrial fission induced by platelet-derived growth factor regulates vascular smooth muscle cell bioenergetics and cell proliferation. *Redox Biol.* (2013) 1:542–51.

90. Lim S, Lee SY, Seo HH, Ham O, Lee C, Park JH, et al. Regulation of mitochondrial morphology by positive feedback interaction between PKCdelta and Drp1 in vascular smooth muscle cell. *J Cell Biochem.* (2015) 116:648–60. doi: 10.1002/jcb.25016

91. Umezu R, Koga JI, Matoba T, Katsuki S, Wang L, Hasuzawa N, et al. Macrophage (Drp1) Dynamin-Related Protein 1 Accelerates Intimal Thickening After Vascular Injury. *Arterioscler Thromb Vasc Biol.* (2020) 40:e214–26. doi: 10.1161/ATVBAHA.120.314383

92. Davidson SM, Duchen MR. Endothelial mitochondria: contributing to vascular function and disease. *Circ Res.* (2007) 100:1128–41.

93. Heusch G, Libby P, Gersh B, Yellon D, BöHM M, Lopaschuk G, et al. Cardiovascular remodelling in coronary artery disease and heart failure. *Lancet.* (2014) 383:1933–43.

94. Quintero M, Colombo SL, Godfrey A, Moncada S. Mitochondria as signaling organelles in the vascular endothelium. *Proc Natl Acad Sci U.S.A.* (2006) 103:5379–84. doi: 10.1073/pnas.0601026103

95. Culic O, Gruwel ML, Schrader J. Energy turnover of vascular endothelial cells. *Am J Physiol.* (1997) 273:C205–13. doi: 10.1152/ajpcell.1997.273.1.C205

96. Lugus JJ, Ngoh GA, Bachschmid MM, Walsh K. Mitofusins are required for angiogenic function and modulate different signaling pathways in cultured endothelial cells. *J Mol Cell Cardiol.* (2011) 51:885–93. doi: 10.1016/j.yjmcc.2011.07.023

97. Rao G, Murphy B, Dey A, Dwivedi SKD, Zhang Y, Roy RV, et al. Cystathionine beta synthase regulates mitochondrial dynamics and function in endothelial cells. *FASEB J.* (2020) 34:9372–92. doi: 10.1096/fj.202000173R

98. Ren R, Guo J, Shi J, Tian Y, Li M, Kang H. PKM2 regulates angiogenesis of VR-EPCs through modulating glycolysis, mitochondrial fission, and fusion. *J Cell Physiol.* (2020) 235:6204–17. doi: 10.1002/jcp.29549

99. Wang LT, He PC, Li AQ, Cao KX, Yan JW, Guo S, et al. Caffeine promotes angiogenesis through modulating endothelial mitochondrial dynamics. *Acta Pharmacol Sin.* (2021) 42:2033–45. doi: 10.1038/s41401-021-00623-6

100. Makino A, Scott BT, Dillmann WH. Mitochondrial fragmentation and superoxide anion production in coronary endothelial cells from a mouse model of type 1 diabetes. *Diabetologia.* (2010) 53:1783–94. doi: 10.1007/s00125-010-1770-4

101. Trudeau K, Molina AJ, Guo W, Roy S. High glucose disrupts mitochondrial morphology in retinal endothelial cells: implications for diabetic retinopathy. *Am J Pathol.* (2010) 177:447–55.

102. Kim D, Sankaramoorthy A, Roy S. Downregulation of Drp1 and Fis1 inhibits mitochondrial fission and prevents high glucose-induced apoptosis in retinal endothelial cells. *Cells.* (2020) 9:1662. doi: 10.3390/cells9071662

103. Zheng Y, Luo A, Liu X. The Imbalance of Mitochondrial Fusion/Fission Drives High-Glucose-Induced Vascular Injury. *Biomolecules.* (2021) 11:1779. doi: 10.3390/biom11121779

104. Forrester SJ, Preston KJ, Cooper HA, Boyer MJ, Escoto KM, Poltronetti AJ, et al. Mitochondrial Fission Mediates Endothelial Inflammation. *Hypertension.* (2020) 76:267–76. doi: 10.1161/HYPERTENSIONAHA.120.14686

105. Wang J, Toan S, Zhou H. New insights into the role of mitochondria in cardiac microvascular ischemia/reperfusion injury. *Angiogenesis.* (2020) 23:299–314. doi: 10.1007/s10456-020-09720-2

106. Goh KY, He L, Song J, Jinno M, Rogers AJ, Sethu P, et al. Mitoquinone ameliorates pressure overload-induced cardiac fibrosis and left ventricular dysfunction in mice. *Redox Biol.* (2019) 21:101100. doi: 10.1016/j.redox.2019.101100

107. Li Z, Li Q, Wang L, Li C, Xu M, Duan Y, et al. Targeting mitochondria-inflammation circle by renal denervation reduces atheroprone endothelial phenotypes and atherosclerosis. *Redox Biol.* (2021) 47:102156. doi: 10.1016/j.redox.2021.102156

108. Galloway CA, Lee H, Yoon Y. Mitochondrial morphology-emerging role in bioenergetics. *Free Radic Biol Med.* (2012) 53:2218–28. doi: 10.1016/j.freeradbiomed.2012.09.035

109. Wang P, Fernandez-Sanz C, Wang W, Sheu SS. Why don't mice lacking the mitochondrial Ca(2+) uniporter experience an energy crisis? *J Physiol.* (2020) 598:1307–26. doi: 10.1113/JP276636

110. Ikeda Y, Shirakabe A, Maejima Y, Zhai P, Sciarretta S, Toli J, et al. Endogenous Drp1 mediates mitochondrial autophagy and protects the heart against energy stress. *Circ Res.* (2015) 116:264–78. doi: 10.1161/CIRCRESAHA.116.303356

111. Kluge MA, Fetterman JL, Vita JA. Mitochondria and endothelial function. *Circ Res.* (2013) 112:1171–88.

112. Huynh DTN, Heo KS. Role of mitochondrial dynamics and mitophagy of vascular smooth muscle cell proliferation and migration in progression of atherosclerosis. *Arch Pharm Res.* (2021) 44:1051–61. doi: 10.1007/s12272-021-01360-4

113. Campbell JH, Campbell GR. Smooth muscle phenotypic modulation–a personal experience. *Arterioscler Thromb Vasc Biol.* (2012) 32:1784–9. doi: 10.1161/ATVBAHA.111.243212

114. Shi N, Chen SY. Smooth muscle cell differentiation: model systems, regulatory mechanisms, and vascular diseases. *J Cell Physiol.* (2016) 231:777–87. doi: 10.1002/jcp.25208

115. Jaminon A, Reesink K, Kroon A, Schurgers L. The Role of Vascular Smooth Muscle Cells in Arterial Remodeling: Focus on Calcification-Related Processes. *Int J Mol Sci.* (2019) 20:5694. doi: 10.3390/ijms20225694

116. Shi N, Mei X, Chen SY. Smooth muscle cells in vascular remodeling. *Arterioscler Thromb Vasc Biol.* (2019) 39:e247–52. doi: 10.1161/ATVBAHA.119.312581

117. Shi J, Yang Y, Cheng A, Xu G, He F. Metabolism of vascular smooth muscle cells in vascular diseases. *Am J Physiol Heart Circ Physiol.* (2020) 319:H613–31. doi: 10.1152/ajpheart.00220.2020

118. Li M, Zhu Y, Jaiswal SK, Liu NF. Mitochondria homeostasis and vascular medial calcification. *Calcif Tissue Int.* (2021) 109:113–20. doi: 10.1007/s00223-021-00828-1

119. Marsboom G, Toth PT, Ryan JJ, Hong Z, Wu X, Fang YH, et al. Dynamin-related protein 1-mediated mitochondrial mitotic fission permits hyperproliferation of vascular smooth muscle cells and offers a novel therapeutic target in pulmonary hypertension. *Circ Res.* (2012) 110:1484–97. doi: 10.1161/CIRCRESAHA.111.263848

120. Chen Y, Li S, Guo Y, Yu H, Bao Y, Xin X, et al. Astaxanthin attenuates hypertensive vascular remodeling by protecting vascular smooth muscle cells from oxidative stress-induced mitochondrial dysfunction. *Oxid Med Cell Longev.* (2020) 2020:4629189.

121. Torres G, Morales PE, Garcia-Miguel M, Norambuena-Soto I, Cartes-Saavedra B, Vidal-Pena G, et al. Glucagon-like peptide-1 inhibits vascular smooth muscle cell dedifferentiation through mitochondrial dynamics regulation. *Biochem Pharmacol.* (2016) 104:52–61. doi: 10.1016/j.bcp.2016.01.013

122. Zhou W, Chen KH, Cao W, Zeng J, Liao H, Zhao L, et al. Mutation of the protein kinase A phosphorylation site influences the anti-proliferative activity of mitofusin 2. *Atherosclerosis.* (2010) 211:216–23. doi: 10.1016/j.atherosclerosis.2010.02.012

123. Wang W, Fernandez-Sanz C, Sheu SS. Regulation of mitochondrial bioenergetics by the non-canonical roles of mitochondrial dynamics proteins in the heart. *Biochim Biophys Acta Mol Basis Dis.* (2018) 1864:1991–2001. doi: 10.1016/j.bbadis.2017.09.004

124. Guo X, Chen KH, Guo Y, Liao H, Tang J, Xiao RP. Mitofusin 2 triggers vascular smooth muscle cell apoptosis via mitochondrial death pathway. *Circ Res.* (2007) 101:1113–22. doi: 10.1161/CIRCRESAHA.107.157644

125. Wang L, Yu T, Lee H, O'Brien DK, Sesaki H, Yoon Y. Decreasing mitochondrial fission diminishes vascular smooth muscle cell migration and ameliorates intimal hyperplasia. *Cardiovasc Res.* (2015) 106:272–83.

126. Ma D, Zheng B, Liu HL, Zhao YB, Liu X, Zhang XH, et al. Klf5 down-regulation induces vascular senescence through eIF5a depletion and mitochondrial fission. *PLoS Biol.* (2020) 18:e3000808. doi: 10.1371/journal.pbio.3000808

127. Sahun-Espanol A, Clemente C, Jimenez-Loygorri JI, Sierra-Filardi E, Herrera-Melle L, Gomez-Duran A, et al. p38 MAPK priming boosts VSMC proliferation and arteriogenesis by promoting PGC1alpha-dependent mitochondrial dynamics. *Sci Rep.* (2022) 12:5938. doi: 10.1038/s41598-022-09757-x

128. Cui L, Li Z, Chang X, Cong G, Hao L. Quercetin attenuates vascular calcification by inhibiting oxidative stress and mitochondrial fission. *Vascul Pharmacol.* (2017) 88:21–9. doi: 10.1016/j.vph.2016.11.006

129. Rogers MA, Maldonado N, Hutcheson JD, Goettsch C, Goto S, Yamada I, et al. Dynamin-related protein 1 inhibition attenuates cardiovascular calcification in the presence of oxidative stress. *Circ Res.* (2017) 121:220–33. doi: 10.1161/CIRCRESAHA.116.310293

130. Chen WR, Zhou YJ, Sha Y, Wu XP, Yang JQ, Liu F. Melatonin attenuates vascular calcification by inhibiting mitochondria fission via an AMPK/Drp1 signalling pathway. *J Cell Mol Med.* (2020) 24:6043–54. doi: 10.1111/jcmm.15157

131. Chen WR, Zhou YJ, Yang JQ, Liu F, Wu XP, Sha Y. Melatonin attenuates calcium deposition from vascular smooth muscle cells by activating mitochondrial fusion and mitophagy via an AMPK/OPA1 Signaling Pathway. *Oxid Med Cell Longev.* (2020) 2020:5298483. doi: 10.1155/2020/5298483

132. Yu E, Mercer J, Bennett M. Mitochondria in vascular disease. *Cardiovasc Res.* (2012) 95:173–82. doi: 10.1093/cvr/cvs111

133. Yu E, Calvert PA, Mercer JR, Harrison J, Baker L, Figg NL, et al. Mitochondrial DNA damage can promote atherosclerosis independently of reactive oxygen species through effects on smooth muscle cells and monocytes and correlates with higher-risk plaques in humans. *Circulation.* (2013) 128:702–12.

134. Koppenol WH, Bounds PL, Dang CV. Otto Warburg's contributions to current concepts of cancer metabolism. *Nat Rev Cancer.* (2011) 11:325–37.

135. Leem J, Lee IK. Mechanisms of vascular calcification: the pivotal role of pyruvate dehydrogenase kinase 4. *Endocrinol Metab.* (2016) 31:52–61. doi: 10.3803/EnM.2016.31.1.52

136. Stenmark KR, Yeager ME, El Kasmi KC, Nozik-Grayck E, Gerasimovskaya EV, Li M, et al. The adventitia: essential regulator of vascular wall structure and function. *Annu Rev Physiol.* (2013) 75:23–47.

137. Coen M, Gabbiani G, Bochaton-Piallat ML. Myofibroblast-mediated adventitial remodeling: an underestimated player in arterial pathology. *Arterioscler Thromb Vasc Biol.* (2011) 31:2391–6. doi: 10.1161/ATVBAHA.111.231548

138. Fu C, Liu P, Li P, Liu W, Huang X, Liang Y. FSP1 promotes the biofunctions of adventitial fibroblast through the crosstalk among RAGE. JAK2/STAT3 and Wnt3a/beta-catenin signalling pathways. *J Cell Mol Med.* (2019) 23:7246–60. doi: 10.1111/jcmm.14518

139. Che Z-Q, Gao P-J, Shen W-L, Fan C-L, Liu J-J, Zhu D-L. Angiotensin II-Stimulated collagen synthesis in aortic adventitial fibroblasts is mediated by connective tissue growth factor. *Hypertens Res.* (2008) 31:1233–40. doi: 10.1291/hypres.31.1233

140. Guo SJ, Zhang P, Wu LY, Zhang GN, Chen WD, Gao PJ. Adenovirus-Mediated Overexpression of Septin 2 Attenuates alpha-Smooth Muscle Actin Expression and Adventitial Myofibroblast Migration Induced by Angiotensin II. *J Vasc Res.* (2016) 53:309–16.

141. Huang G, Cong Z, Wang X, Yuan Y, Xu R, Lu Z, et al. Targeting HSP90 attenuates angiotensin II-induced adventitial remodelling via suppression of mitochondrial fission. *Cardiovasc Res.* (2020) 116:1071–84. doi: 10.1093/cvr/cvz194

142. Lu ZY, Guo CL, Yang B, Yao Y, Yang ZJ, Gong YX, et al. Hydrogen Sulfide Diminishes Activation of Adventitial Fibroblasts Through the Inhibition of Mitochondrial Fission. *J Cardiovasc Pharmacol.* (2022) 79:925–34.

143. Lemons JM, Feng XJ, Bennett BD, Legesse-Miller A, Johnson EL, Raitman I, et al. Quiescent fibroblasts exhibit high metabolic activity. *PLoS Biol.* (2010) 8:e1000514. doi: 10.1371/journal.pbio.1000514

144. Zhang H, Wang D, Li M, Plecita-Hlavata L, D'Alessandro A, Tauber J, et al. Metabolic and proliferative state of vascular adventitial fibroblasts in pulmonary hypertension is regulated through a MicroRNA-124/PTBP1 (Polypyrimidine Tract Binding Protein 1)/Pyruvate Kinase Muscle Axis. *Circulation.* (2017) 136:2468–85. doi: 10.1161/CIRCULATIONAHA.117.028069

145. Stenmark KR, Gerasimovskaya E, Nemenoff RA, Das M. Hypoxic activation of adventitial fibroblasts: role in vascular remodeling. *Chest.* (2002) 122:326S–34S.

146. Li M, Riddle SR, Frid MG, El KKC, Mckinsey TA, Sokol RJ, et al. Emergence of fibroblasts with a proinflammatory epigenetically altered phenotype in severe hypoxic pulmonary hypertension. *J Immunol.* (2011) 187:2711–22. doi: 10.4049/jimmunol.1100479

147. Plecita-Hlavata L, Tauber J, Li M, Zhang H, Flockton AR, Pullamsetti SS, et al. Constitutive Reprogramming of Fibroblast Mitochondrial Metabolism in Pulmonary Hypertension. *Am J Respir Cell Mol Biol.* (2016) 55:47–57. doi: 10.1165/rcmb.2015-0142OC

148. Moore KJ, Tabas I. Macrophages in the pathogenesis of atherosclerosis. *Cell.* (2011) 145:341–55.

149. Mehta MM, Weinberg SE, Chandel NS. Mitochondrial control of immunity: beyond ATP. *Nat Rev Immunol.* (2017) 17:608–20. doi: 10.1038/nri.2017.66

150. Rambold AS, Pearce EL. Mitochondrial Dynamics at the Interface of Immune Cell Metabolism and Function. *Trends Immunol.* (2018) 39:6–18.

151. Li Y, He Y, Miao K, Zheng Y, Deng C, Liu TM. Imaging of macrophage mitochondria dynamics in vivo reveals cellular activation phenotype for diagnosis. *Theranostics.* (2020) 10:2897–917. doi: 10.7150/thno.40495

152. Yarbro JR, Emmons RS, Pence BD. Macrophage Immunometabolism and Inflammaging: Roles of Mitochondrial Dysfunction, Cellular Senescence, CD38, and NAD. *Immunometabolism.* (2020) 2:e200026. doi: 10.20900/immunometab20200026

153. Wang Y, Subramanian M, Yurdagul A JR., Barbosa-Lorenzi VC, Cai B, de Juan-Sanz J, et al. Mitochondrial Fission Promotes the Continued Clearance of Apoptotic Cells by Macrophages. *Cell.* (2017) 171:e22. doi: 10.1016/j.cell.2017.08.041

154. Beck-Joseph J, Lehoux S. Molecular interactions between vascular smooth muscle cells and macrophages in atherosclerosis. *Front Cardiovasc Med.* (2021) 8:737934. doi: 10.3389/fcvm.2021.737934

155. Li D, Yang S, Xing Y, Pan L, Zhao R, Zhao Y, et al. Novel insights and current evidence for mechanisms of atherosclerosis: mitochondrial dynamics as a potential therapeutic target. *Front Cell Dev Biol.* (2021) 9:673839. doi: 10.3389/fcell.2021.673839

156. Chang YW, Chang YT, Wang Q, Lin JJ, Chen YJ, Chen CC. Quantitative phosphoproteomic study of pressure-overloaded mouse heart reveals dynamin-related protein 1 as a modulator of cardiac hypertrophy. *Mol Cell Proteomics.* (2013) 12:3094–107. doi: 10.1074/mcp.M113.027649

157. Pennanen C, Parra V, Lopez-Crisosto C, Morales PE, Del Campo A, Gutierrez T, et al. Mitochondrial fission is required for cardiomyocyte hypertrophy mediated by a Ca2+-calcineurin signaling pathway. *J Cell Sci.* (2014) 127:2659–71. doi: 10.1242/jcs.139394

158. Givvimani S, Pushpakumar S, Veeranki S, Tyagi SC. Dysregulation of Mfn2 and Drp-1 proteins in heart failure. *Can J Physiol Pharmacol.* (2014) 92:583–91. doi: 10.1139/cjpp-2014-0060

159. Fang L, Moore XL, Gao XM, Dart AM, Lim YL, Du XJ. Down-regulation of mitofusin-2 expression in cardiac hypertrophy in vitro and in vivo. *Life Sci.* (2007) 80:2154–60. doi: 10.1016/j.lfs.2007.04.003

160. Chen L, Gong Q, Stice JP, Knowlton AA. Mitochondrial OPA1, apoptosis, and heart failure. *Cardiovasc Res.* (2009) 84:91–9.

161. Naruse G, Kanamori H, Yoshida A, Minatoguchi S, Kawaguchi T, Iwasa M, et al. The intestine responds to heart failure by enhanced mitochondrial fusion through glucagon-like peptide-1 signalling. *Cardiovasc Res.* (2019) 115:1873–85. doi: 10.1093/cvr/cvz002

162. Suo M, Qi Y, Liu L, Zhang C, Li J, Yan X, et al. SS31 alleviates pressure overload-induced heart failure caused by Sirt3-Mediated Mitochondrial Fusion. *Front Cardiovasc Med.* (2022) 9:858594. doi: 10.3389/fcvm.2022.858594

163. Westermann B. Bioenergetic role of mitochondrial fusion and fission. *Biochim Biophys Acta.* (2012) 1817:1833–8. doi: 10.1016/j.bbabio.2012.02.033

164. Tong M, Zablocki D, Sadoshima J. The role of Drp1 in mitophagy and cell death in the heart. *J Mol Cell Cardiol.* (2020) 142:138–45. doi: 10.1016/j.yjmcc.2020.04.015

165. Zhang H, Wang P, Bisetto S, Yoon Y, Chen Q, Sheu SS, et al. A novel fission-independent role of dynamin-related protein 1 in cardiac mitochondrial respiration. *Cardiovasc Res.* (2017) 113:160–70. doi: 10.1093/cvr/cvw212

166. Bordt EA, Clerc P, Roelofs BA, Saladino AJ, Tretter L, Adam-Vizi V, et al. The putative Drp1 inhibitor mdivi-1 is a reversible mitochondrial complex i inhibitor that modulates reactive oxygen species. *Dev Cell.* (2017) 40:e6. doi: 10.1016/j.devcel.2017.02.020

167. Barsoum MJ, Yuan H, Gerencser AA, Liot G, Kushnareva Y, Graber S, et al. Nitric oxide-induced mitochondrial fission is regulated by dynamin-related GTPases in neurons. *EMBO J.* (2006) 25:3900–11. doi: 10.1038/sj.emboj.7601253

168. Ma X, Xie Y, Chen Y, Han B, Li J, Qi S. Post-ischemia mdivi-1 treatment protects against ischemia/reperfusion-induced brain injury in a rat model. *Neurosci Lett.* (2016) 632:23–32. doi: 10.1016/j.neulet.2016.08.026

169. Nhu NT, Li Q, Liu Y, Xu J, Xiao SY, Lee SD. Effects of Mdivi-1 on Neural Mitochondrial Dysfunction and Mitochondria-Mediated Apoptosis in Ischemia-Reperfusion Injury After Stroke: A Systematic Review of Preclinical Studies. *Front Mol Neurosci.* (2021) 14:778569. doi: 10.3389/fnmol.2021.778569

170. Flippo KH, Gnanasekaran A, Perkins GA, Ajmal A, Merrill RA, Dickey AS, et al. AKAP1 protects from cerebral ischemic stroke by inhibiting Drp1-Dependent Mitochondrial Fission. *J Neurosci.* (2018) 38:8233–42. doi: 10.1523/JNEUROSCI.0649-18.2018

171. Peng C, Rao W, Zhang L, Wang K, Hui H, Wang L, et al. Mitofusin 2 ameliorates hypoxia-induced apoptosis via mitochondrial function and signaling pathways. *Int J Biochem Cell Biol.* (2015) 69:29–40. doi: 10.1016/j.biocel.2015.09.011

172. Zununi Vahed S, Mostafavi S, Hosseiniyan KSM, Shoja MM, Ardalan M. Vascular Calcification: An Important Understanding in Nephrology. *Vasc Health Risk Manag.* (2020) 16:167–80.

173. Wang PW, Pang Q, Zhou T, Song XY, Pan YJ, Jia LP, et al. Irisin alleviates vascular calcification by inhibiting VSMC osteoblastic transformation and mitochondria dysfunction via AMPK/Drp1 signaling pathway in chronic kidney disease. *Atherosclerosis.* (2022) 346:36–45. doi: 10.1016/j.atherosclerosis.2022.02.007

174. Brooks C, Wei Q, Cho SG, Dong Z. Regulation of mitochondrial dynamics in acute kidney injury in cell culture and rodent models. *J Clin Invest.* (2009) 119:1275–85. doi: 10.1172/JCI37829

175. Wang J, Zhu P, Li R, Ren J, Zhou H. Fundc1-dependent mitophagy is obligatory to ischemic preconditioning-conferred renoprotection in ischemic AKI via suppression of Drp1-mediated mitochondrial fission. *Redox Biol.* (2020) 30:101415. doi: 10.1016/j.redox.2019.101415

Frontiers in
Cardiovascular Medicine

Innovations and improvements in cardiovascular treatment and practice

Focuses on research that challenges the status quo of cardiovascular care, or facilitates the translation of advances into new therapies and diagnostic tools.

Discover the latest Research Topics

See more →

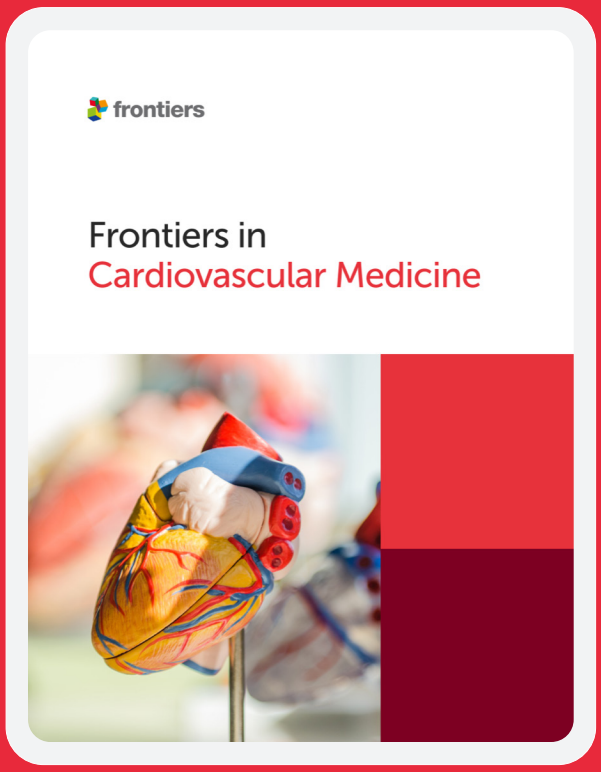

Frontiers

Avenue du Tribunal-Fédéral 34
1005 Lausanne, Switzerland
frontiersin.org

Contact us

+41 (0)21 510 17 00
frontiersin.org/about/contact